Investigating the role of the cell wall in cold acclimation and freezing tolerance in Arabidopsis thaliana

NATHAN JAMES RAMSAY

Investigating the role of the cell wall in cold acclimation and freezing tolerance in *Arabidopsis thaliana*

Nathan Ramsay

A thesis presented for the degree of

Doctor of Philosophy

Department of Biosciences

University of Durham

United Kingdom

February 2023

ABSTRACT

Many plants are susceptible to freezing stress, including crops necessary for the production of staple foods. Climate change is predicted to increase the occurrence of early autumn and late spring frosts, striking at times when plants are especially vulnerable. Most perennial plants can undergo cold acclimation, wherein freezing tolerance is increased through exposure to low, non-freezing temperatures. Encapsulating every plant cell is a thin, dynamic layer of complex polysaccharides and proteins – the cell wall. It offers structural rigidity, extensibility, a means of water transport, and protection from pathogens. The cell wall undergoes significant structural, compositional and physical remodelling during cold acclimation; it is therefore increasingly thought to have a role in freezing tolerance, perhaps by acting as a physical barrier to ice propagation and providing mechanical reinforcement against freezing-induced dehydration, though this remains unconfirmed.

In the present study, the potential role of the cell wall in both cold acclimation and basal freezing tolerance was explored further. An increase in freezing tolerance in cold-acclimated *Arabidopsis* was shown to be correlated with both reduced cell-wall porosity and enhanced cell-wall mechanical integrity. These properties are thought to limit the nucleation and spread of ice through plant tissues and protect against cellular dehydration and collapse during freezing, respectively. Comprehensive microarray polymer profiling revealed a number of compositional changes that occur in the *Arabidopsis* cell wall during cold acclimation. Most notably, there was an accumulation of extensins, a family of important structural proteins, and a shift towards the demethylesterified form of pectin, a reorganisation which can have considerable impacts on the physical properties of the cell wall by facilitating the formation of cross-links between pectic backbones. Mutants deficient in either extensin or demethylesterified pectin were shown to have impaired freezing tolerance, cell-wall porosity and mechanical properties.

In wild-type cell walls, the pectic polysaccharide rhamnogalacturonan-II (RG-II) exists predominantly as a dimer centred on a borate-ester cross-link. The freezing-sensitive *sfr8* mutant, which lacks RG-II dimerisation, was also found to have compromised wall porosity and mechanics. These defects were partially reversed when RG-II dimerisation was restored by boron supplementation, as was its freezing sensitivity, suggesting that RG-II cross-linking is critical to full freezing tolerance. A number of other mutants with defective cell walls, including those with structurally- or compositionally-impaired cellulose, hemicellulose, or pectins, were screened for freezing sensitivity and aberrant physical properties. The data largely support the idea that plant freezing tolerance is dependent on the porosity and mechanical properties of the cell wall, themselves dependent on the structure, composition, and organisation of its constituent polymers.

Contents

Acknowledgements

First and foremost, I owe my sincere gratitude to my primary supervisor, Prof. Heather Knight[1], for her unwavering support, friendship and mentorship, and from whom I learned so much these past four years. I could not have asked for a better academic supervisor.

Much of the thesis is built on the pioneering work of Dr. Paige Panter[2], to whom I am thankful for her ideas, for teaching me many of the basics of plant science when I started at Durham, and for keeping me busy during lockdown by providing stomatal micrographs for analysis. Special thanks are also owed to Prof. Marc Knight[1], my brilliant second supervisor, for his guidance, humour and invaluable contributions to my work.

I am grateful to our many collaborators and individuals who have graciously lent us their hands and minds, and without whom it would not have been possible to complete much of the work: Joanne Robson[1] and Dr. Tim Hawkins[1], for introducing me to the world of bioimaging and supporting me through my microscopy experiments; Prof. William Willats[3], for allowing me to make use of his microarraying facilities at Newcastle University, and Dr. Catherine Tétard-Jones[3], Dr. Cassie Bakshani[3], Dr. Paulina Focht[3] and Abi Smith[3], for supporting me through the microarraying experiments; Dr. Max Brown[1,4], for building the extensometer from scratch, teaching me how it works and kindly allowing me to use it; Dr. Ankush Prashar[3], for allowing us to loan his infrared camera before we acquired our own; Prof. David P. Livingston III[5,6] and Dr. Ian R. Willick[7], whom I met virtually in Gather Town during the 12th International Plant Cold Hardiness Seminar, for their useful input on the infrared video thermography experiments;

Dr. Johannes Liesche[8], for advising me on the cell-wall porosity experiments and for providing seed material when the pandemic made it difficult to do so; Prof. Daniel J. Cosgrove[9], whom I met at the IX Cell Wall Research Conference in Michigan, for his practical advice on extensometry; Dr. Alexis Peaucelle[10], Dr. Herman Höfte[10] and Dr. Kalina Haas[10], all of whom ran the exceptional 2022 Saclay Plant Sciences Summer School in Versailles, which I had the pleasure of attending, for their useful suggestions and interpretations of my data; Dr. Julien Sechet[10], Dr. Jérôme Pelloux[11], Prof. Peter Urwin[12], Dr. Catherine Lilley[12], and Prof. Charles T. Anderson[9], for kindly donating seeds for various mutants and transgenic lines; Prof. Martin Cann[1], Prof. John Gatehouse[1], Dr. Junli Liu[1] and Dr. Stephen Chivasa[1], for their contributions as members of my progress committee; and Matthew Capewell[13], for his expert opinion on statistical analysis.

Finally, I would like to thank all past and present members of the lab for their kindness, friendship, and for making Lab 19 an enjoyable place to work, in particular: Bryony Jacobs, Morgan Lee, Dr. Tracey Stevenson, Dr. Irabonosi Obomighie, Dr. Fieka Sukiran, Rico Habeahan, Maeve Dale and Rebecca Manning.

I am eternally grateful to everyone named above. Without you, this thesis would not have seen the light of day.

---

[1] *Department of Biosciences, Durham University, Durham, County Durham, UK*
[2] *Department of Cell and Developmental Biology, John Innes Centre, Norwich, Norfolk, UK*
[3] *School of Natural and Environmental Sciences, Newcastle University, Newcastle upon Tyne, Tyne and Wear, UK*
[4] *Proctor & Gamble Ltd, Newcastle upon Tyne, Tyne and Wear, UK*
[5] *Agricultural Research Service, United States Department of Agriculture, Washington, D.C., USA*
[6] *Department of Crop Science, North Carolina State University, Raleigh, North Carolina, USA*
[7] *Kentville Research and Development Centre, Agriculture and Agri-Food Canada, Kentville, Nova Scotia, Canada*
[8] *College of Life Sciences, Northwest Agriculture and Forestry University, Xianyang, Shaanxi, China*
[9] *Department of Biology, The Pennsylvania State University, University Park, Pennsylvania, USA*
[10] *Institut Jean-Pierre Bourgin, Université Paris-Saclay, Versailles, Île-de-France, France*
[11] *Biologie des Plantes et Innovation, Université de Picardie, Amiens, Hauts-de-France, France*
[12] *School of Biology, University of Leeds, Leeds, West Yorkshire, UK*
[13] *Department of Data Science, On the Beach Ltd, Manchester, Greater Manchester, UK*

Declaration

The work in this thesis is based on research carried out at the Department of Biosciences, University of Durham, Durham, UK, and the School of Natural and Environmental Sciences, University of Newcastle upon Tyne, Newcastle upon Tyne, UK. No part of this thesis has been submitted elsewhere for any other degree or qualification, and it is the sole work of the author unless stated otherwise in the text.

The work in this thesis was funded by the Biotechnology and Biological Sciences Research Council, part of UK Research and Innovation, through a Newcastle-Liverpool-Durham Doctoral Training Partnership studentship (award ref. BB/M011186/1).

Figures & Tables

Figures

Tables

Terminology

Standard scientific convention for gene and protein name formatting has been used: gene names are italicised, protein names are not; wild-type gene and protein names are capitalised, mutant gene and protein names are not.

Standard scientific units and their abbreviations have been used for measures of weight, length, volume, concentration, amount, molarity, force, rotational speed, electrical current, power, voltage, conductivity, temperature and time.

Standard chemical element symbols from the periodic table of elements have been used.

ABA	Abscisic acid
AFM	Atomic force microscopy
AGP	Arabinogalactan protein
AIR	Alcohol-insoluble residue
ANOVA	Analysis of variance
BCIP	5-bromo-4-chloro-3'-indolyphosphate
BHQ3	Black Hole Quencher 3
bp	Base pairs
CA	Cold-acclimated
CAM	Crassulacean acid metabolism
CBF	C-repeat/DRE Binding Factor
cDNA	Complementary DNA
CDTA	Diamino-cyclo-hexane-tetra-acetic acid
CESA	Cellulose synthase
Col-0	Columbia-0 (ecotype)

CoMPP	Comprehensive microarray polymer profiling
COR	Cold-on Regulated
CRT	C-repeat
CSC	Cellulose synthase complex
CSL	Cellulose-synthase like
CZF	Cold-induced Zinc Finger
dH_2O	Deionised water
DMSO	Dimethyl sulfoxide
DNA	Deoxyribonucleic acid
DRE	Drought-responsive element
dRG-II	Dimerised RG-II
dSTORM	Direct stochastic optical reconstruction microscopy
EDTA	Ethylenediaminetetraacetic acid
EMS	Ethyl methanesulfonate
EV	Empty vector
EXT	Extensin
F	Fluorescence after quenching
F_0	Fluorescence before quenching
FRAP	Fluorescence redistribution after photobleaching
FM 4-64	N-(3-Triethylammoniumpropyl)-4-(6-(4-(Diethylamino)Phenyl) Hexatrienyl) Pyridinium Dibromide (membrane dye)
GalA	Galacturonic acid
GC	Guanine-cytosine (content)
gDNA	Genomic DNA
GPC	Gel permeation chromatography
HG	Homogalacturonan
HOS	High Expression of Osmotically Responsive
hp	Hairpin (DNA)
HRGP	Hydroxyproline-rich glycoprotein
HSFC	Heat-shock factor C
ICE	Inducer of CBF Expression
IR	Infrared

IRVT	Infrared video thermography
ISX	Isoxaben
JIM	John Innes Monoclonal (antibody)
LD	Light:dark (cycle)
LM	Leeds Monoclonal (antibody)
$\boldsymbol{LT_{50}}$	Lethal temperature at which 50% of plants are killed
mAb	Monoclonal antibody
MES	2-(N-morpholino)ethanesulfonic acid
MG	Malachite green
MP	Milk powder (skimmed)
mRG-II	Monomerised RG-II
MS	Murashige & Skoog
MUR	Murus
NA	Non-acclimated
NBT	Nitro-blue tetrazolium
NFW	Nuclease-free water
NRT	No reverse transcriptase
ns	Non-significant
NTC	No template control
ODEPA	Chilean Office of Agricultural Studies and Policies
PAE	Pectin acetylesterase
PAGE	Polyacrylamide gel electrophoresis
PBS	Phosphate-buffered saline
PCR	Polymerase chain reaction
PED	Perforated-tape Epidermal Detachment
PG	Polygalacturonase
PL	Pectate lyase
PME	Pectin methylesterase
PMEI	Pectin methylesterase inhibitor
qPCR	Quantitative PCR
RG-I	Rhamnogalacturonan-I
RG-II	Rhamnogalacturonan-II

Rha	Rhamnose
RNA	Ribonucleic acid
ROI	Region of interest
ROS	Reactive oxygen species
RT-PCR	Reverse transcription PCR
SDS	Sodium dodecyl sulphate
SFR	Sensitive to freezing
SUMO	Small ubiquitin-related modifier
TB	Trypan blue
TBE	Tris-borate-EDTA
TBS	Tris-buffered saline
TBST	Tris-buffered saline + Tween-20
TE	Tris-EDTA
TEMED	Thermo Scientific Pierce Tetramethylethylenediamine
Tris	2-amino-2-(hydroxymethyl)-1,3-propanediol
T-DNA	Transfer DNA
UK	United Kingdom
USA	United States of America
UV	Ultraviolet
XTH	Xyloglucan endotransglucosylase/hydrolase
ZAT	Zinc Finger of *Arabidopsis*

Chapter 1

Introduction

Freezing is a significant environmental stress in plants. Many crops of economic importance are vulnerable to freezing damage, which can have severe consequences on agricultural economies: the citrus industry in the south-east of the USA was repeatedly devastated by frost in the latter half of the 20th century, resulting in crop losses upwards of $1 billion (Cooper *et al.* 1964, Martsolf *et al.* 1984, Okie *et al.* 1998). In 2007, the same regions experienced a week-long spring frost which caused losses of wheat, apple, peach and pecan totalling over $2 billion (Wolf 2008). Between 1999 and 2011, over one-third of all insured crop losses in Greece were caused by freezing damage (Papagiannaki *et al.* 2014). In 2013, a spring frost in central Chile caused the loss of over half a million tons of fruits and vegetables, the equivalent of approximately $350 million (ODEPA 2013). These incidents can have profound socioeconomic consequences for growers, processors, distributors, rural communities and local governments.

Such losses can be compounded by climate change, which is increasing the severity and frequency of spring frosts in certain regions (Zheng *et al.* 2012) but decreasing them in others (Müller *et al.* 2017). Spring frosts are of particular consequence to crop productivity as perennial crops will gradually de-harden, or de-acclimate, in response to warming spring temperatures, increasing the risk of damage from later freezing events. For annual crops, planting will have normally occurred by this point, meaning spring frosts would strike when plants are at an early, vulnerable stage of development. Anomalously warm temperatures in late winter will encourage premature de-acclimation, leading to a "false spring" wherein crops begin their annual development early and are left vulnerable to subsequent frosts (Pagter

& Arora 2013, Parker *et al.* 2021). Warmer winters have already been shown to decrease spring freezing tolerance in temperate forest communities, with reduced chilling delaying leafout, thus extending the period of greatest risk for freezing injury (Chamberlain & Wolkovich 2021). They are also associated with reduced snowfall; as snow cover is an effective insulator, low-lying plants may be left exposed to significantly lower air temperatures than they otherwise would have been (Hincha & Zuther 2014). Climate change is predicted to increase the incidence of such erratic temperature fluctuations during the winter-spring period.

Understanding how plants can withstand freezing temperatures, therefore, remains a key goal of agricultural biotechnology. It necessitates the identification of freezing-tolerance associated genes and a thorough understanding of the molecular mechanisms underpinning freezing tolerance. Pursuing such endeavours may not only offer protection to susceptible crops, but also increase the geographical limits of the growing regions of others, such as wheat, which are otherwise limited by temperature (Barlow *et al.* 2015). Both outcomes could ultimately help to protect local economies and preserve global food security.

This study aims to elucidate the role of the plant cell wall in both freezing tolerance and cold acclimation. The extent to which the components, structure and physical properties of the cell wall can protect the plant from freezing injury are explored.

1.1 Ice Formation & Freezing Damage

1.1.1 Ice formation *in planta*

In order to understand the mechanisms of plant freezing tolerance, it is first necessary to comprehend the various routes through which freezing injury may occur. Cellular damage typically occurs following ice crystal formation, when water molecules bind together to form a stable ice nucleus. The formation of an ice nucleus can be homogeneous (spontaneous) or heterogeneous (catalysed by other molecules).

1.1.1.1 Ice nucleation

Homogeneous nucleation consists of the spontaneous formation of an ice nucleus from molecules of pure water. Small volumes of water must reach a critical

nucleation temperature of -38.5°C for this process to occur readily; above this temperature, the volume of water required for the formation of a single homogeneous ice nucleus is enormous (3.8 x 10^{11} kg at -30°C, increasing further with temperature) and so the process rarely occurs in nature (Franks 1985). Supercooling in plants to sub-zero temperatures is possible, therefore, without any physiological damage from freezing (Fuller & Wisniewski 1998). Instead, ice crystal formation in plant tissues occurs more readily through heterogeneous nucleation, which involves the catalysis of ice nucleus formation by molecular agents other than water. Ice-nucleating agents in plants include organic and inorganic debris, ice-nucleation active bacteria and other biological molecules (Lindow *et al.* 1982, Pearce 2001). In the presence of such agents, ice crystals are able to form at more modest sub-zero temperatures; *Pseudomonas syringae*, for example, produces a protein which can nucleate ice at -2°C (Ashworth & Davis 1986, Pearce & Fuller 2001). Nucleators may be present within plant tissues or, more commonly, on the plant surface; in either case, the nucleators must be in contact with molecules of water. There is evidence suggesting that the initial formation of ice in plants can begin either in the xylem vessels (Asahina 1956, Single & Marcellos 1981, Sakai & Larcher 1987), where the larger diameter and relatively lower concentration of solutes can facilitate ice nucleation, or in extracellular components, such as the cell wall and intercellular spaces (Wisniewski *et al.* 1997, Pearce & Fuller 2001).

1.1.1.2 Intracellular ice formation

Although intracellular ice formation has been observed experimentally, it typically only occurs following a rapid cooling event. As the air temperature in nature decreases, at most, by a few degrees per hour, plants are unlikely to experience this in the field (Weiser & White 1964, Weiser 1970). Nevertheless, the phenomenon has been observed in a variety of species in the laboratory, with freezing following a flash-like, cell-by-cell pattern (Chambers & Hale 1932, Brown & Reuter 1974, Brown *et al.* 1974). Intracellular ice formation is almost always lethal, either due to mechanical damage of cellular components resembling desiccation stress (Hubel *et al.* 2007, Saragusty *et al.* 2009) or membrane damage (Steponkus *et al.* 1993). However, Wesley-Smith *et al.* (2014) observed that cells of *Acer saccharinum* seeds

could survive intracellular ice formation if the crystals were small and localised to the cytoplasm, though cells that subsequently thawed incurred considerable damage.

In studies of single cells or cell cultures, there can be a "U-shaped" survival curve in response to cooling rate, with lower mortality for both slow (0.001-0.1°C per sec) and fast (100-10000°C per sec) rates of cooling, and both intracellular ice formation and mortality occurring at rates in between (Mazur & Koshimoto 2002, Dumont *et al.* 2004, Seki & Mazur 2012). It appears that very rapid cooling facilitates supercooling and subsequent vitrification (Franks 1985) whereas slow cooling enables freeze-desiccation: the migration of water to and freezing in extracellular spaces, decreasing cellular water concentration (Mazur 1984).

1.1.1.3 Extracellular ice formation and propagation

As mentioned, extracellular ice formation occurs far more readily in nature than intracellular ice formation due to the rate at which air tends to cool, but it may also reflect the higher freezing point of the intercellular fluid. The higher freezing point is likely due to a lower solute concentration and, possibly, a higher concentration of nucleating agents (Pearce & Ashworth 1992). Extracellular freezing may also represent a strategy employed by plants to tolerate ice formation in their tissues, facilitating ice build-up in the intercellular spaces in order to protect living cells (Neuner 2014). Although ice can nucleate on the leaf surface and enter plants through open stomata (Wisniewski & Fuller 1999), this is probably not a major route of ice entry into plant tissues given that the stomata of non-CAM plants close at night which, in many climates, is when the majority of ice formation occurs (Pearce 2001). Ice crystal formation begins at specific nucleation sites in the extracellular space; the lower water potential of the ice crystal draws water out of nearby cells through osmosis, thereby further growing the ice mass and reducing the solute concentration within the cells, leading to further cellular freezing-point depression (Beck *et al.* 2007). Chambers & Hale (1932) showed that the hydrophobic cell membrane will prevent growth of the extracellular ice crystal into the cell, thus protecting cellular contents. This is probably due to the lipid nature of the plasma membrane: Lusena & Cook (1953) showed that even non-living

membranes, which are permeable to liquid water, may be completely impermeable to a growing ice mass. However, it has been theorised that, if ice forms rapidly enough and at a sufficiently low temperature, the crystals may be small enough to permeate through the plasma membrane and induce intracellular freezing (Mazur 1963). This would almost certainly be as damaging as spontaneous intracellular ice formation. Additionally, ice is even unlikely to extend its growth into the cell wall if the pores of the cell wall are sufficiently small: Moor (1960) calculated that the water present in the cell wall with microcapillaries <0.1 µm in diameter will have its freezing point lowered to the extent that it has the propensity to supercool. Consequently, ice will spread only in the intercellular spaces, forming from water vapour in the air and from the surface films of cell walls. Even then, ice can be restricted from entering vulnerable tissues via structural barriers within the intercellular spaces, a strategy that can be used to protect flower buds (Wisniewski *et al.* 2014) and fruit (Workmaster *et al.* 1999).

Luyet & Gehenio (1937) first observed what is now known as the "double freezing point" in plant tissues, in which extracellular freezing occurs in two stages, by measuring exotherms. In this context, exotherms are small increases in temperature caused by heat of fusion. As ice nucleation is an exothermic process, freezing can be observed by measuring these temperature increases. More recently, infrared video thermography (IRVT) has been used to further elucidate the double freezing point (Pearce & Fuller 2001). The initial spread of ice is very rapid (4-40 mm per sec) but only involves the freezing of a relatively low proportion of a plant's water content. The second freezing event, which is characterised by a more prolonged and intense freeze, involves drawing water from cells to compound the extracellular freezing. Most freezing damage occurs as a result of the second freezing event.

1.1.2 Mechanisms of freezing damage

Plants vary in their susceptibility to low temperature (chilling or freezing) injury. Tropical and subtropical plants can undergo severe physiological impairment at chilling temperatures as high as 10-12°C, inducing symptoms such as wilting, reduced vigour, chlorosis and, occasionally, plant death (Lyons 1973). Other species, such as rye, however, can survive freezing temperatures below -20°C (Webb

et al. 1994). Temperate plants, including *Arabidopsis*, are generally chilling-tolerant but vary in their degrees of freezing tolerance. At the cellular level, the plasma membrane is believed to be the main site of freezing damage in plants (Steponkus 1984).

1.1.2.1 Freezing-induced cellular dehydration

Extracellular ice formation causes cellular dehydration, which is one of the most significant symptoms of freezing injury in plants (Steponkus 1984). Ice has a lower water potential than that of liquid water, so the presence of extracellular ice draws water from the cell, dehydrating the protoplast, growing the ice crystals outside of the cell and initiating the second freezing event (Steponkus & Lynch 1989). As temperature continues to decrease, so too does the water potential of ice, thus dehydration of the cell becomes progressively more severe as the temperature drops: at -10°C, over 90% of a cell's water can be drawn out through the plasma membrane (Gusta *et al.* 1975, Thomashow 1999). Such water loss, beyond depriving cells of water for maintaining turgor and performing basic cellular processes, can cause structural damage to various cell membranes. The plasma membrane is particularly susceptible, and its injury is quantifiable by measuring electrolyte leakage from cells (Stout *et al.* 1980, Steponkus 1984, Pearce & Willison 1985). As has been reported since the 19th century, osmotic shock can cause the plasma membrane to retract from the cell wall (plasmolysis), thus decreasing the volume of the cell, and even collapse of the cell wall (cytorrhysis). As sufficiently large retractions of the plasma membrane are irreversible (the retractions involve removal of membrane components), leading to a permanent reduction in the size of the protoplast, cell lysis can occur when extracellular ice thaws and water re-enters the cell in a process known as expansion-induced lysis (Gordon-Kamm & Steponkus 1984). Even small, reversible reductions in protoplast volume can cause expansion-induced lysis after thawing: as the plasma membrane shrinks in size, excess lipids are withdrawn in endocytotic vesicles in order to maintain cellular tension. When water re-enters the cell, the lipid vesicles often cannot be reincorporated into the membrane at a rate sufficient to keep up with osmotic expansion (Wiest & Steponkus 1978).

More severe freezing injury may also be associated with fracture-jump lesions, which involve the localised fusion of the plasma membrane with other organellar membranes. Fracture-jump lesions can form as a result of the close apposition of cellular membranes following freezing-induced dehydration and shrinkage of the protoplast (Fujikawa 1995). One consequence of fracture-jump lesions is lamellar-to-hexagonal-II phase transitions within membrane lipids, reducing the osmotic responsiveness of the cell, leading to further expansion-induced lysis after thawing (Gordon-Kamm & Steponkus 1984). Steponkus *et al.* (1977) have shown that the thylakoid membrane is also susceptible to freezing damage; this may be one cause of the chlorosis, and therefore reduction in photosynthetic capacity, which occurs in affected plants.

1.1.2.2 Non-membrane effects

Numerous other cellular components and processes can be impaired during freezing. Sub-zero temperatures can reduce the conformational stability of important proteins, eventually leading to their denaturation (Guy *et al.* 1998). Freezing can cause the accumulation of reactive oxygen species (ROS; Zhang & Kirkham 1994, Allen 1995, Baek & Skinner 2012). ROS are normally produced as by-products of biological pathways or as signal transducers (Zelko *et al.* 2002, Halliwell & Gutteridge 2007), but excessive production and insufficient removal by antioxidant enzymes, which can occur during freezing, can cause oxidative stress (Fridovich 1991). The effects of oxidative stress include denaturation of critical enzymes, scission of DNA strands, peroxidation of unsaturated fatty acids in membranes, and destruction of the integrity of chloroplast membranes (Monk *et al.* 1989, Scandalios 1993, Liu *et al.* 2018).

Clearly, it is necessary for plants to have mechanisms through which they can prevent or tolerate ice formation in their tissues and negate the plethora of detrimental effects it has on their normal functioning. Many plants can only employ such mechanisms after undergoing the process of cold acclimation.

1.2 Cold Acclimation & Freezing Tolerance

As plants are sessile organisms, there are three main strategies at their disposal for surviving freezing injury during the winter. Many herbaceous annual plants survive by freezing *avoidance* rather than freezing *tolerance*: they endure winter months as seeds or roots buried in the soil to avoid freezing air temperatures (Hincha & Zuther 2014). Other species, such as cold-hardy trees, prevent ice nucleation in their tissues by undergoing supercooling (Kuroda *et al.* 2003). Most perennial plants, however, cannot avoid ice nucleation at sub-zero temperatures and so they must tolerate extracellular ice formation in their tissues. Many achieve this by first undergoing cold acclimation. If a plant is capable of cold acclimation, it will occur when it is exposed to low, non-freezing temperatures between 0 and 5°C over an extended period of time. In practice, this usually occurs in the colder autumn months during the approach to winter. It has been established for well over a century that cold acclimation can produce a significant increase in a plant's freezing tolerance (Lidforss 1896, 1907), but the broader suite of biochemical, metabolic and physiological changes, induced by widespread transcriptional reprogramming, was not elucidated until much later (reviewed in Hincha *et al.* 2012). The overarching outcome is that cold-acclimated plants are more able to tolerate freezing temperatures and ice build-up in their tissues than non-acclimated plants of the same species: cold-acclimated rye, for example, can survive temperatures below -20°C, whereas non-acclimated rye is killed at just -5°C (Webb *et al.* 1994). In *Arabidopsis*, just 24 h of cold acclimation can decrease the LT_{50} (lethal temperature at which 50% of plants are killed) from -3 to -6°C (Gilmour *et al.* 1988), though most plants must undergo approximately two weeks of cold acclimation in order to benefit from the maximum degree of freezing tolerance. Some plants, including *Arabidopsis,* however, can become fully acclimated within just four days of continuous acclimating conditions (Gilmour *et al.* 1988); the LT_{50} of *Arabidopsis* decreases below -8°C after this point. Some species can increase their freezing tolerance even further by exposure to mild, non-damaging freezing temperatures, known as sub-zero acclimation (Olien 1984, Livingston 1996, Herman *et al.* 2006, Takahashi *et al.* 2019). In either case, plants must first be able to perceive low temperatures in order to begin acclimating.

1.2.1 Low-temperature perception

The mechanisms by which plants perceive low temperatures, and activate relevant signalling pathways in response, remains poorly understood (Knight & Knight 2012). Murata & Los (1997) suggested that biological membranes have a central role in this process. In their hypothetical model, cell membranes become more rigid in response to lower temperatures, and such a reduction in fluidity can be detected and used as a signal to begin cold acclimation. Indeed, induction or prevention of cold-acclimation specific gene expression can be tightly controlled by temperature-independent increases in membrane rigidity or fluidity, respectively (Örvar *et al.* 2000). Activating mechanosensitive Ca^{2+} channels is also important for activation of downstream signalling cascades leading to increased freezing tolerance (Ding & Pickard 1993, Plieth *et al.* 1999). Although a Ca^{2+} channel which acts directly as a primary sensor of cold is yet to be identified, Ca^{2+} is clearly involved in low-temperature perception and signal transduction as Ca^{2+} channel proteins have been shown to accumulate in response to low temperatures (Shao *et al.* 2008) and cytosolic influx of Ca^{2+} occurs shortly after exposure (Knight *et al.* 1996). A plausible candidate for a cold-sensing protein in rice (*Oryza sativa*) is the plasma membrane G-protein COLD1 (Ma *et al.* 2015); candidates in other species include glutamate receptors (Meyerhoff *et al.* 2005), cyclic-nucleotide gated channels (Finka *et al.* 2012) and phytochrome B proteins (Shi *et al.* 2015).

1.2.2 CBF-mediated cold acclimation

A number of gene families are upregulated in response to the perception of low temperatures. The most well understood of these is the *CBF* gene family of transcription factors, which regulate expression of Cold-on Regulated (*COR*) genes. There are thousands of *COR* genes in *Arabidopsis* and they are rapidly upregulated in response to cold: treating plants at 4°C for just 24 h induces the expression of approximately 4,000 *COR* genes (Zhao *et al.* 2016). The products of *COR* gene expression are varied but many have been shown to function in cold acclimation and the acquisition of freezing tolerance. They include transcription factors, protein kinases, chloroplast proteins, lipid-metabolism associated proteins, hormone-

response associated proteins, cell-wall modifying enzymes, and osmoprotectant-synthesising enzymes (Liu *et al.* 2019c).

Baker *et al.* (1994) identified a region of the promoter of one *COR* gene, *COR15A*, involved in the regulation of gene expression central to both cold and drought tolerance. It contains the *cis*-acting drought-responsive element (DRE, also known as the C-repeat or CRT) which was later found in the promoters of many other genes that are regulated by low temperatures. The *trans*-acting factors, later named DRE Binding Factor 1 (DREB1, also known as the C-box Binding Factors, C-repeat Binding Factors, or simply CBFs) and DRE Binding Factor 2 (DREB2), were then found to bind to CRT/DRE motifs in *Arabidopsis,* regulating expression of cold- and drought-responsive genes, respectively (Stockinger *et al.* 1997, Liu *et al.* 1998). The *CBF* gene family in *Arabidopsis* consists of *CBF1, 2* and *3,* sometimes referred to as *DREB1B,* C and A, respectively (Gilmour *et al.* 1998). *CBF4,* a more distantly related member of the *CBF* family, is involved in the expression of drought- and abscisic acid (ABA)-responsive genes, but not cold-responsive genes (Haake *et al.* 2002). CBF1 was the first factor shown to bind to CRT/DRE motifs, and it was found that overexpression of *CBF1* conferred enhanced freezing tolerance in non-acclimated *Arabidopsis*, suggesting that it may have an important role in cold acclimation (Jaglo-Ottosen *et al.* 1998). Although it has been suggested that *CBF1, 2* and *3* have largely redundant roles in cold acclimation (Gilmour *et al.* 2004), it has since been found that *CBF2* may have a slightly different function than the other *CBF* family members (Novillo *et al.* 2007), including involvement in the regulation of *CBF1* and *CBF3* (Novillo *et al.* 2004). Furthermore, analysis of single, double and triple *cbf* mutants indicated that *CBF2* may be more important to achieving full cold acclimation than *CBF1* or *CBF3* (Zhao *et al.* 2016).

CBFs accumulate at low temperatures, partly due to the instability of their transcripts at ambient temperatures, but also due to positive regulation by the transcription factors Inducer of CBF Expression 1 and 2 (ICE1 and ICE2), which are themselves regulated through post-translational modifications (Zarka *et al.* 2003). ICE1 is stabilised through sumoylation (ligation to small ubiquitin-like

modifiers, or SUMOs) by the E3 ligase SIZ1, facilitating its binding to *CBF* promoters and subsequent cold-acclimation related gene expression; consequently, *siz1* mutants, which lack SUMO activity, have both reduced expression of cold-responsive genes and overall freezing tolerance (Miura *et al.* 2007). ICE1 is ubiquitinated by the E3 ligase High Expression of Osmotically Responsive Gene 1 (HOS1), which causes its degradation at ambient temperatures and thus prevents expression of cold-responsive genes when their transcripts are not needed (Dong *et al.* 2006). CBFs are also regulated at the hormonal level, with expression induced by the abiotic-stress related plant hormone ABA (Knight *et al.* 2004). CBFs are subjected to negative regulation by another transcription factor, MYB15, which binds to specific sites in *CBF* promoters to prevent transcription; unsurprisingly, *myb15* knock-out mutants show increased *CBF* expression and freezing tolerance (Agarwal *et al.* 2006). CBFs are also regulated by photoperiod, light quality and the circadian clock at ambient temperatures (Kidokoro *et al.* 2009, Lee & Thomashow 2012, Jiang *et al.* 2017); mutants lacking expression of two transcription factors that are core components of the clock were found to have reduced expression and circadian regulation of *CBFs* (Dong *et al.* 2011). Such controlled, multi-faceted, regulation of CBFs is necessary for striking the balance between expression (and subsequent cold acclimation) and growth: both *CBF* overexpression and cold acclimation have been shown to significantly reduce plant growth as well as decrease the production of several growth-related hormones (Hannah *et al.* 2005, Oakenfull *et al.* 2013). Indeed, CBF1 has been shown to directly reduce the production of gibberellin, leading to an accumulation of growth-repressing DELLA proteins (Achard *et al.* 2011). Although exposure to cold generally slows down biochemical processes and restricts growth due to a decreased metabolic rate (Stitt & Hurry 2002), it has been suggested that DELLA-mediated growth repression is beneficial to plants undergoing abiotic stress and therefore DELLA accumulation may directly contribute to freezing tolerance (Achard *et al.* 2006).

1.2.3 CBF-independent cold acclimation

In *Arabidopsis,* CBF1, 2 and 3 only regulate approximately 10% of all *COR* genes (Park *et al.* 2015) and 38% of *COR* genes lack a CRT motif in their promoter (Zhao *et al.* 2016). Therefore, cold acclimation and the acquisition of freezing tolerance is achieved partially independent of the *CBF* pathway. For example, *COR* gene expression is regulated by the cold-inducible transcription factors HSFC1 (Heat-Shock Factor C1), ZAT12 (Zinc Finger of *Arabidopsis* 12) and CZF1 (Cold-induced Zinc Finger protein 1), whose expressions are unaffected in *cbf* triple mutants (Park *et al.* 2015, Jia *et al.* 2016, Zhao *et al.* 2016, Shi *et al.* 2017). ESK1 (Eskimo 1), a negative regulator of cold acclimation, controls the expression of genes that have little overlap with *CBF*-induced genes (Xin & Browse 1998, Xin *et al.* 2007).

1.2.4 Effects of cold acclimation *in planta*

The products of *COR* gene expression contribute to enhanced freezing tolerance through various mechanisms. As discussed earlier, cell membranes often suffer the most damage during freezing, and so protecting them is a key aspect of cold acclimation. Therefore, membrane-stabilising and membrane-protective proteins accumulate in response to cold, including enzymes responsible for fatty acid biosynthesis and lipid remodelling, membrane-specific COR-proteins, and antifreeze proteins (Ishizaki-Nishizawa *et al.* 1996, Sakamoto & Murata 2002, Hundertmark & Hincha 2008, Zhou *et al.* 2018). One important example of such a protein is COR15am, a cryoprotective protein which lowers the temperature at which lamellar-to-hexagonal-II phase transitions begin to occur by remodelling the inner membrane of the chloroplast (Steponkus *et al.* 1998). Similarly, SFR2, an outer-chloroplast galactolipid-remodelling enzyme discovered while screening mutants for freezing sensitivity (Warren *et al.* 1996), also stabilises membranes during freezing stress (Moellering *et al.* 2010). Other examples include dehydrins, which stabilise the membrane against water loss (Kosová *et al.* 2007), and synaptotagmins, which repair the membrane following freezing-induced lysis (Reddy *et al.* 2001, Yamazaki *et al.* 2008). To effect further stabilisation, cold acclimation can induce significant lipid remodelling in the plasma membrane. Its proportions of the phospholipids

phosphatidylcholine and phosphatidylethanolamine are increased, while the amount of free sterols are decreased (Uemura *et al.* 1995). Such compositional changes increase the proportion of unsaturated fatty acids present in the membrane, which has been associated with improved freezing tolerance in both plants and bacteria, possibly by protecting against expansion-induced lysis after thawing (Wada *et al.* 1990, Murata *et al.* 1992). Plants have also been shown to alter lipid-to-protein ratios and decrease fatty acid chain length during cold acclimation (Sakai & Larcher 1987, Takahashi *et al.* 2013).

Cold acclimation induces the accumulation of sugars such as sucrose (Juurakko *et al.* 2021), which has been shown to stabilise membranes and reduce their permeability during freezing stress *in vitro* (Strauss & Hauser 1986, Anchordoguy *et al.* 1987). Accumulation of other compatible solutes, including raffinose, galactinol and proline, can lower water potential and help resist freezing-induced cellular dehydration (Nanjo *et al.* 1999, Taji *et al.* 2002). Sugars are a particularly useful compatible solute to accumulate as they can also contribute to freezing-point depression in tissues (Hagiwara *et al.* 2006, Walters *et al.* 2009). A secondary benefit of compatible solute accumulation is that it prepares plants for other abiotic stresses that are sometimes associated with sub-zero temperatures, including drought or salt stress (Fujita *et al.* 2006).

The expression of chaperone proteins, which protect other freezing-sensitive proteins from denaturation in sub-zero temperatures, can also be increased during cold acclimation (Guy & Li 1998). Another family of proteins which increase in abundance in response to cold are the antifreeze proteins (Griffith *et al.* 1992), which function by binding to ice nuclei and depressing the freezing point of potential subsequent ice crystals, thus limiting ice growth in tissues (Jia & Davies 2002). As discussed earlier, sufficient freezing and dehydration of the cell is sometimes associated with ROS accumulation, so cold-acclimated plants also produce more enzymatic scavengers of ROS, such as glutathione reductase and monodehydroascorbate reductase, thus helping to alleviate potential oxidative damage (Tao *et al.* 1998).

More recently, the plant microbiome has been identified as conferring freezing tolerance to the host plant as part of a symbiotic relationship. Cold temperatures have been shown to induce changes in the composition of the plant microbiome, thus symbiotic microbes could potentially contribute to plant cold acclimation and freezing tolerance (Etemadi *et al.* 2018, Acuña-Rodríguez *et al.* 2020, Liu *et al.* 2020). This may be in the form of facilitating nutrient uptake (Hill *et al.* 2019), contributing to the protection of cell membranes (Su *et al.* 2015), increasing the accumulation of compatible solutes (Yooyongwech *et al.* 2013) or enhancing ROS scavenging (Subramanian *et al.* 2015).

1.2.5 Supercooling

Cold acclimation is primarily used by plants as a means of freezing *tolerance* rather than *avoidance*. As mentioned, one method of freezing avoidance is supercooling, which is the capacity for cellular contents to be cooled below their freezing point without actually freezing. Supercooling may be particularly important when freezing occurs during a period of high metabolic or developmental demand, where resources cannot be spared to sufficiently cold-acclimate (Sakai & Larcher 1987). However, as described above, cold acclimation can increase a plant's propensity to supercool through compatible-solute mediated freezing-point depression and antifreeze protein production. Substantial (deep) supercooling is mainly associated with woody plants: xylem parenchyma in some trees have been shown to supercool to around -40°C, at which point the critical nucleation temperature of water is surpassed and freezing occurs homogeneously (Burke *et al.* 1976). Although *Arabidopsis* has historically been described as a freezing tolerant species, Reyes-Díaz *et al.* (2006) have shown that it can avoid freezing by supercooling. IRVT can be used to study supercooling by monitoring the temperature of plant tissues during freezing (Fuller & Wisniewski 1998). As ice nucleation is an exothermic process, the freezing point of tissue water can be identified by a sharp increase in temperature following cooling to sub-zero temperatures (Zaragotas *et al.* 2016). The degree of supercooling, therefore, is represented by the fall in temperature below 0°C before freezing has occurred (**Figure 1.1**).

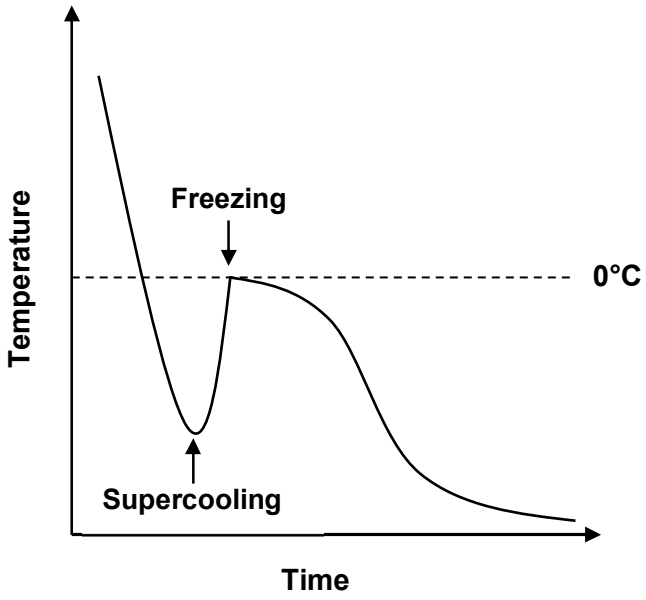

Figure 1.1: Graphical illustration of the process of supercooling. Shown is a mock freezing curve that could have been obtained by recording the temperature of plant tissues during freezing. As the temperature falls below 0°C, plant tissue water does not necessarily freeze immediately. Many species can avoid ice nucleation by "supercooling" water in their tissues: maintaining it in a liquid phase despite being subjected to sub-zero temperatures. The degree of supercooling is represented by how far below its freezing point tissue water can get before ice nucleation. As nucleation is an exothermic process, the freezing point can be identified by a sharp increase in temperature following supercooling.

1.2.6 Cold acclimation and climate change

Cold acclimation depends on a plant's ability to perceive changes in temperature and light. In the field, this typically occurs during autumn months when there are detectable decreases in both temperature and photoperiod (Rapacz *et al.* 2014, Maurya & Bhalerao 2017). As discussed above, *CBF* expression is regulated by photoperiod, light quality and the circadian clock, as well as temperature. As climate change causes autumn months in temperate regions to become warmer, low-temperature perception and subsequent signal transduction will not occur as readily. This may disrupt or delay the process of cold acclimation, leading to decreased freezing tolerance during winter. For example, some species of grass show reduced freezing tolerance in winter when cold acclimation during the preceding autumn occurred at higher temperatures (Dalmannsdottir *et al.* 2017). Another consequence of climate change is more variable, erratic winter temperatures. Unusually warm spells during or after cold acclimation can cause "de-acclimation" (Vyse *et al.* 2019), wherein plants reverse their acclimated state and either completely or partially lose their acquired freezing tolerance, making them vulnerable to a subsequent, sudden onset of frost (Kovi *et al.* 2016). For these reasons, a warming climate may, somewhat unintuitively, exacerbate crop losses due to freezing damage.

1.3 The Plant Cell Wall

While the physical properties and environmental interactions of animal cells are determined by their cytoskeletal network, plant cells are instead encapsulated in a cell wall: a thin (0.1-1 µm), extensible layer of complex polysaccharides and structural proteins. Although flexible enough to allow for cell movement and expansion, it is rigid enough to provide the cell with a stiff structural integrity. It also has important roles in intercellular communication, cell differentiation and water movement, and it can act as a physical barrier to pathogens (Cosgrove 2005). Up to 15% of the genome of *Arabidopsis* is responsible for the construction, maintenance, and metabolism of its cell wall (Carpita *et al.* 2001, Cosgrove 2015).

1.3.1 Structure and composition

The plant cell wall typically consists of three distinct layers: the primary cell wall, middle lamella, and secondary cell wall (**Figure 1.2A**). The primary cell wall consists predominantly of cellulose microfibrils, which are linked together by hemicellulosic polysaccharides (such as xyloglucan) and are embedded in a matrix of pectin (**Figure 1.2B**). The middle lamella, a pectin-rich layer, is secreted outside of the primary cell wall and forms the interface between adjacent cells. Both of these layers are formed during the initial growth and expansion phases of the plant cell. After growth ceases, a secondary cell wall is sometimes secreted in cases where the cell requires additional structural reinforcement (Clarke 1938).

1.3.1.1 Cellulose and hemicellulose

Cellulose microfibrils are perhaps the most abundant biopolymers on the planet, making up between 20 and 30% of the dry mass of the primary cell walls of higher plants (McNeil *et al.* 1984) whilst also being present in the cell walls of some species of algae (Domozych *et al.* 1980), tunicates (Kimura & Itoh 1995), oomycetes (Lin & Aronson 1970) and bacteria (Römling 2002). They are groups of linear, unbranched polysaccharides consisting of a repeating backbone of β(1,4)-linked glucose residues. Up to 100 cellulose chains bundle together to form a microfibril: a long, rigid structure that can span the entire circumference of a cell (McNeil *et al.* 1984). To add further structural rigidity, cellulose microfibrils are cross-linked by hemicelluloses, polysaccharides whose backbones resemble those of cellulose but branches and other modifications prevent them from forming microfibrils of their own (Cosgrove 2005). Common hemicelluloses include xyloglucan, arabinoxylan, callose and mannan, each differing in their monosaccharide composition and structure. For example, the backbone of xyloglucan is similar to that of cellulose but it features regular additions of xylose residues, which themselves can be decorated with galactose and fucose residues (Hayashi 1989). Depending on their side-chain monosaccharide composition, xyloglucans can form varying amounts of hydrogen bonds with cellulose microfibrils to form a potentially heavily cross-linked network (McCann *et al.* 1990, Levy *et al.* 1997); the cellulose-hemicellulose framework, therefore, is the primary element of the cell wall providing structural

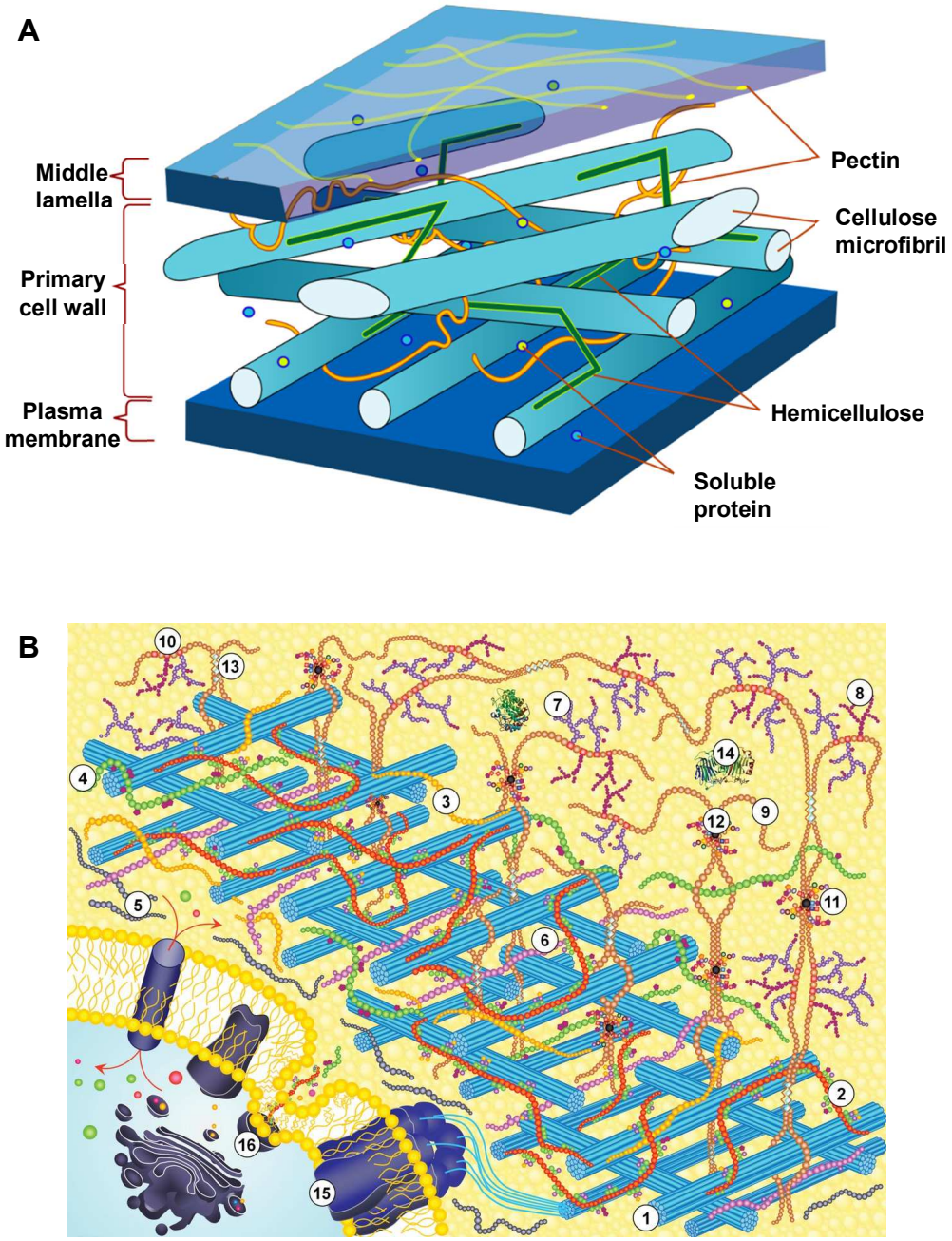

Figure 1.2: Schematic overview of plant cell wall architecture. A) Two of the three integral layers of the plant cell wall, the middle lamella and primary cell wall, as well as some of the major groupings of polysaccharides and proteins. Adapted from Sticklen (2008). **B)** Polysaccharide composition of a typical plant cell wall. 1: cellulose microfibrils. 2: xyloglucan. 3: mixed-linkage glucan. 4: xylan. 5: callose. 6: mannan. 7: galactan. 8: arabinan. 9: homogalacturonan. 10: rhamnogalacturonan-I. 11: rhamnogalacturonan-II. 12: boron cross-link. 13: "egg-box" with calcium cross-links. 14: enzymes and structural proteins. 15: cellulose synthase complex. 16: transport vesicles. Note that components 2-6 are hemicelluloses, 7-11 are pectins and 14-16 are non-polysaccharide components. Pectins are linked together following the generally accepted "linear" model of pectin arrangement (Albersheim *et al.* 1996). Adapted from Franková & Fry (2013).

integrity and load-bearing capacity (Nishiyama 2009).

Cellulose is synthesised by large membrane complexes known as cellulose synthase complexes (CSCs; Kimura *et al.* 1999). Although CSCs were visualised as early as the 1970s (Dobberst & Kiermaye 1972), cellulose synthase (*CESA*) genes were not identified until much later (Pear *et al.* 1996, Arioli *et al.* 1998). CSCs were found to be hexameric, symmetrical arrangements of six rosette subunits, with each subunit consisting of six CESA proteins (**Figure 1.3**; Mueller & Brown 1980). Although there are ten genes in the *CESA* family of *Arabidopsis* (Richmond & Somerville 2000), only three are required to synthesise a functional CSC (Burn *et al.* 2002, Taylor *et al.* 2003), and the required genes differ between the primary (*CESA1, 3* and *6*) and secondary (*CESA4, 7* and *8*) cell walls (Arioli *et al.* 1998, Fagard *et al.* 2000). There is, however, some overlap: CESA7 can partially rescue the phenotype of *cesa3* mutants, and CESA1 can partially rescue the phenotype of a *cesa8* mutant (Carroll & Specht 2012). Furthermore, CESA6 appears to be partially redundant with CESA2, 5 and 9 (Desprez *et al.* 2007, Persson *et al.* 2007). Each individual CESA protein synthesises a single β(1,4)-linked glucose chain, several micrometres in length, which bundles together with chains from the same CSC to form the cellulose microfibril (**Figure 1.3**; Doblin *et al.* 2002).

The *CESA* gene family is part of a larger superfamily known as *CELLULOSE SYNTHASE LIKE* (*CSL*), which includes a further eight gene families (Richmond & Somerville 2000). CSLs are localised to the Golgi and some have been shown to be involved in the synthesis of the glycan backbones of hemicelluloses (Pauly *et al.* 2013). Activated nucleotide sugars may be added to the hemicellulose backbone via the action of glycosyltransferase enzymes, including fucosyltransferases (Perrin 2003) and xylosyltransferases (Pauly & Keegstra 2016). After secretion to the cell wall, hemicelluloses form networks with newly synthesised cellulose microfibrils, potentially through spontaneous surface binding (Fry 1989, Hayashi 1989), or by becoming "entrapped" in the microfibril during its formation, leaving one end free to bind other microfibrils or polysaccharides, thus creating a strongly-tethered linkage to the microfibril (Baba *et al.* 1994, Hayashi *et al.* 1994). It has also been

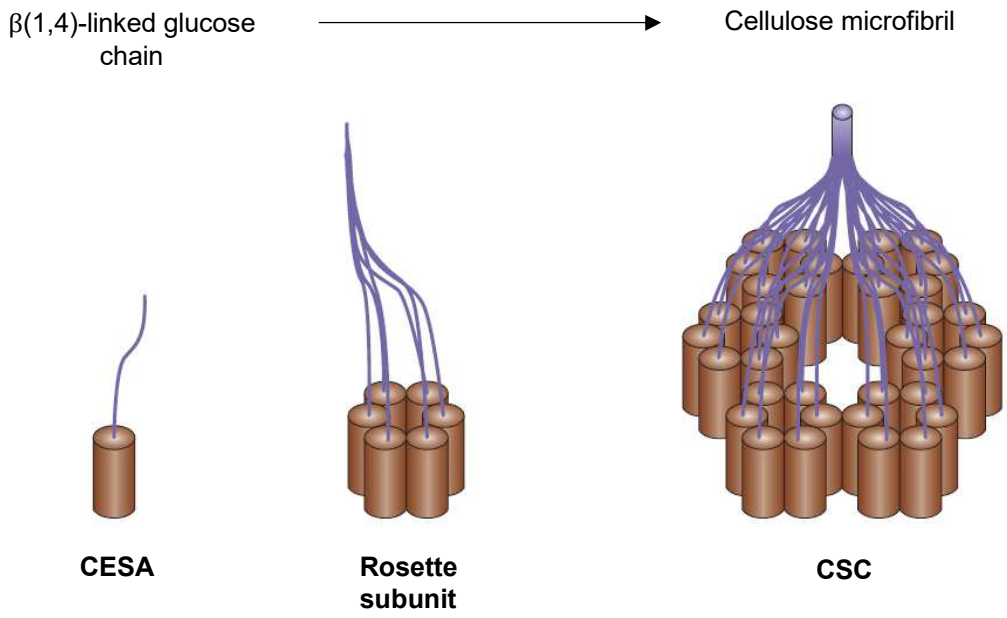

Figure 1.3: Synthesis of cellulose microfibrils by the cellulose synthase (CESA) complex (CSC). Six CESA proteins aggregate hexamerically to form a rosette subunit and six rosette subunits aggregate to form the CSC. Each individual CESA protein is capable of synthesising a single β(1,4)-linked glucose chain. Chains from the same CSC bundle together to form a strong, tightly-packed cellulose microfibril. Adapted from Kurek *et al.* (2002).

suggested that xyloglucan can bind to pectins (Thompson & Fry 2000, Cumming *et al.* 2005).

1.3.1.2 Pectins

The three major pectic polysaccharides present in the plant cell wall are homogalacturonan (HG), rhamnogalacturonan-I (RG-I) and rhamnogalacturonan-II (RG-II), and it is thought that these three domains can be covalently linked to form a complex layer throughout the primary cell wall and middle lamella (Caffall & Mohnen 2009). Alongside hemicelluloses, pectins are the other major group of polysaccharides making up the matrix in which cellulose microfibrils are embedded. They are complex and diverse, typically enriched in galacturonic acid (GalA), rhamnose (Rha), arabinose and galactose (Harholt *et al.* 2010). The roles of pectins are numerous: they form hydrated gels that separate cellulose microfibrils during growth and lock them together after growth ceases, they are significant determinants of cell-wall porosity and thickness, and they form a major part of the middle lamella, an adhesive layer that serves as an interface between adjacent cells (Willats *et al.* 2001a, Vincken *et al.* 2003). They are also the primary target of attack by pathogens and thus can modify their structure to help defend against pathogen invasion (Lionetti *et al.* 2012).

1.3.1.2.1 Homogalacturonan

HG is a linear polymer of α(1,4)-linked-D-GalA, with each chain containing 100-200 GalA residues (Thibault *et al.* 1993), making up 65% of cell-wall pectin content and approximately 23% of the primary cell-wall mass in *Arabidopsis* (Zablackis *et al.* 1995, Caffall & Mohnen 2009). It is synthesised in the Golgi (Mouille *et al.* 2007) and transported to the cell wall in a highly esterified form: up to 80% of GalA residues have methyl-esters on their C6 carboxyl groups immediately after synthesis (Mohnen 1999). Removal of methyl-ester groups by action of pectin methylesterase (PME) enzymes allows HG to be cross-linked by calcium ions (Pelloux *et al.* 2007), resulting in a supramolecular "egg-box" structure wherein two HG chains become dimerised (**Figure 1.2B**, point 13). PME activity, and thus HG cross-linking, is controlled by a group of proteinaceous enzyme inhibitors called PME inhibitors (PMEIs) which function to suppress PME activity (Wormit &

Usadel 2018). C3 carboxyl groups of HG can also be *O*-acetylated to prevent cross-linking, though *O*-acetylation is not as common as methylesterification (Pauly & Scheller 2000). *O*-acetyl groups can be removed by action of pectin acetylesterase (PAE) enzymes (Philippe *et al.* 2017).

The PME family of enzymes in *Arabidopsis* is extensive and PME isoforms can be broadly divided into two categories depending on their pattern of action: block-wise or non-block-wise (random) demethylesterification (**Figure 1.4**; Catoire *et al.* 1998). Block-wise demethylesterification involves removal of methyl-ester groups from lines of adjacent GalA residues, resulting in long stretches of demethylesterified HG backbones. Most plant PMEs are thought to act in a block-wise manner and this pattern is most conducive to efficient calcium cross-linking (Jarvis 1984). Non-block-wise demethylesterification is typically associated with PMEs produced by plant pathogens, whereby single methyl-ester groups are removed seemingly at random (Catoire *et al.* 1998). This appears to be a strategy adopted by plant pathogens to facilitate colonisation, as it leads to an increased susceptibility of plant cell-wall HG to degradation by fungal enzymes such as polygalacturonases (PGs), which hydrolyse glycosidic bonds between GalA residues, and pectate lyases (PLs) (**Figure 1.4**; Raiola *et al.* 2011). Indeed, overexpression of PMEIs in *Arabidopsis* can restrict fungal infection by decreasing native PME activity, thus reducing the extent of HG demethylesterification and, therefore, HG susceptibility to degradation by fungal PGs (Lionetti *et al.* 2007). By the same logic, *pmei* mutants can have increased susceptibility to infection by the same fungus (Lionetti *et al.* 2017). Paradoxically, fungal infection can also increase the expression of some *PME* genes to aid the immune response. For example, PME17 is highly induced in response to infection by *Botrytis* (Del Corpo *et al.* 2020). PME17 was found to perform a block-wise pattern of demethylesterification, facilitating calcium-cross-linking, which may prevent recognition by fungal PGs (Del Corpo *et al.* 2020). Another possibility is that increased demethylesterification could increase the production of demethylesterified oligogalacturonides, as well as the release of methanol, both of which are able to trigger the plant immune response (Osorio *et al.* 2008, Dorokhov *et al.* 2012, Hann

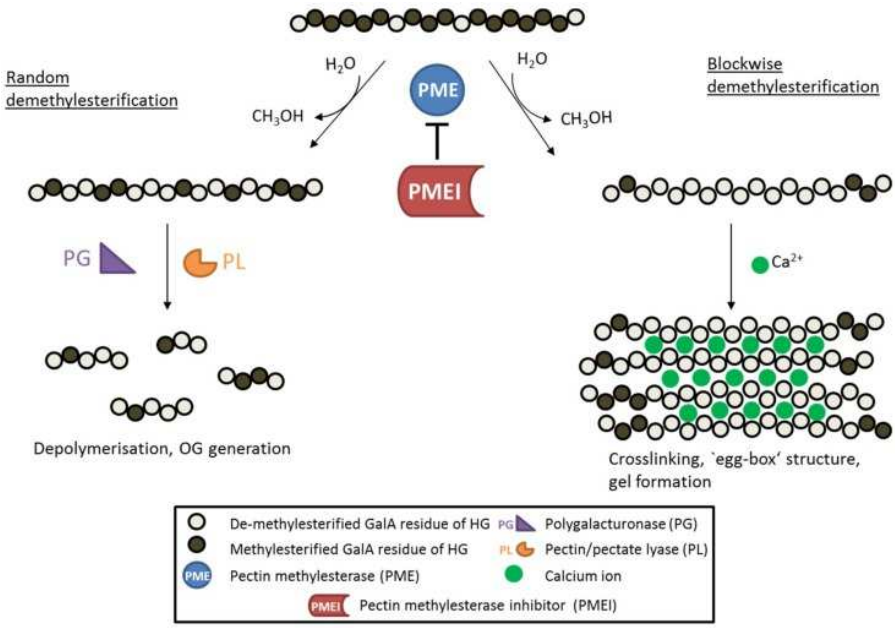

Figure 1.4 Patterns of homogalacturonan (HG) demethylesterification and its effect on pectin structure. HG is highly methylesterified upon synthesis and can be demethylesterified by the action of pectin demethylesterase (PME) enzymes. Most plant PMEs remove methyl groups in a "block-wise" pattern, allowing calcium cross-linking and "egg-box" formation between separate HG backbones. Pathogen PMEs remove methyl groups in a non-block-wise, or random, pattern, causing HG to become susceptible to pectin-degrading enzymes such as polygalacturonase (PG) and pectate lyase (PL). PME activity is regulated by PME inhibitors (PMEIs). Adapted from Wormit & Usadel (2018).

et al. 2014). Similarly, PME31 is also induced in response to infection by both fungal and bacterial pathogens, with a concomitant decrease in pectin methylesterification (Bethke *et al.* 2014). *pme31* was shown to be more susceptible to pathogen invasion but, crucially, a decrease in total PME activity was not observed in the mutants, suggesting that immunity is not correlated with overall PME activity. Instead, it is likely to be the effect of upregulation of specific PMEs such as patterns or degrees of methylesterification. Anti-pectin monoclonal antibodies can be used to detect regions of varying levels of demethylesterification; F24, for example, recognises calcium cross-links (and therefore regions of block-wise demethylesterification), whereas JIM5 and JIM7 recognise differing degrees of methylesterification (Willats *et al.* 2001a).

HG biosynthesis remains poorly understood, partly because it is highly complex, involving at least 53 enzymes (Mohnen 1999). Mutants lacking expression of a putative glycosyltransferase, *QUA1*, have reduced cell adhesion and cell-wall GalA, suggesting that the enzyme is involved in HG biosynthesis (Bouton *et al.* 2002). More recently, a galacturonosyltransferase was identified that transfers GalA residues directly to the Golgi for HG backbone synthesis (Sterling *et al.* 2018); mutants of genes in the same family show significant reductions in cell-wall GalA (Sterling *et al.* 2006), implicating the gene family in HG biosynthesis.

1.3.1.2.2 Rhamnogalacturonan-I

RG-I is a pectic domain consisting of a backbone of (1,2)α-$_{L}$-Rha-(1,4)-α-$_{D}$-GalA repeating units (O'Neill *et al.* 1990). Up to 80% of Rha residues are substituted at C4 for side-chains of arabinofuranosyl, galactopyranosyl or various other branched and linear glycosyl residues (Albersheim *et al.* 1996, Ridley *et al.* 2001), resulting in a complex and diverse family of pectins that makes up 20-35% of cell-wall pectin content and approximately 11% of the primary cell-wall mass in *Arabidopsis* (Zablackis *et al.* 1995). Unlike HG, methylesterification of GalA in RG-I is uncommon and has only been reported in a few plant species (Kaczmarska *et al.* 2022). It is generally accepted that there is a contiguous, linear chain of cell-wall pectins, with sections of HG interspersed with RG-I (Albersheim *et al.* 1996). However, more recent atomic force microscopy (AFM) analysis has shown that

almost complete removal of Rha residues from the pectin backbone does not change its length, contradicting the linear model of pectins (Round *et al.* 2010). An alternative hypothetical model suggests that HG is actually one of the side-chains of RG-I, though no physical evidence has been forthcoming (Vincken *et al.* 2003, Coenen *et al.* 2007). Due to its highly variable side-chains and potential for backbone polymerisation, RG-I has important functions in cell-wall integrity and polymer interactions in both the cell wall and middle lamella, which can influence fruit firmness and ripening (Peña & Carpita 2004, Moore *et al.* 2008a). As with the other pectins, RG-I is synthesised in the Golgi and transported to the cell wall in membrane vesicles (Mohnen 2008).

1.3.1.2.3 Rhamnogalacturonan-II

RG-II makes up approximately 10% of cell-wall pectin and 8% of the primary cell-wall mass in *Arabidopsis* (Zablackis *et al.* 1995). Despite its name, RG-II is structurally dissimilar to RG-I, with a backbone of repeating GalA residues much like HG. In fact, RG-II is released when plant cell walls are treated with PGs (Darvill *et al.* 1978), suggesting that it may be covalently linked and interspaced with HG along a GalA backbone. The RG-II backbone has six side-chains (A-F) made up of 13 different monosaccharides (**Figure 1.5A**), making it the most structurally complex polysaccharide present in the plant cell wall (Ndeh *et al.* 2017).

A significant feature of RG-II is its ability to dimerise by means of borate-ester cross-linking (**Figure 1.5B**). Boron is essential for plant growth and survival; an adequate supply of soil boron is necessary for both high crop yield and high crop quality, and symptoms of boron excess or deficiency include shortened stems and roots, the death of growing points and rough or brittle tissues (Warington 1923, Blevins & Lukaszewski 1998, Aquea *et al.* 2012, Wimmer & Eichert 2013). Until recently, the primary function of boron in plants was unknown. O'Neill *et al.* (1996) found that it binds apiose residues in side-chain A of RG-II, catalysing its dimerisation through formation of a borate-ester bond between two monomers.

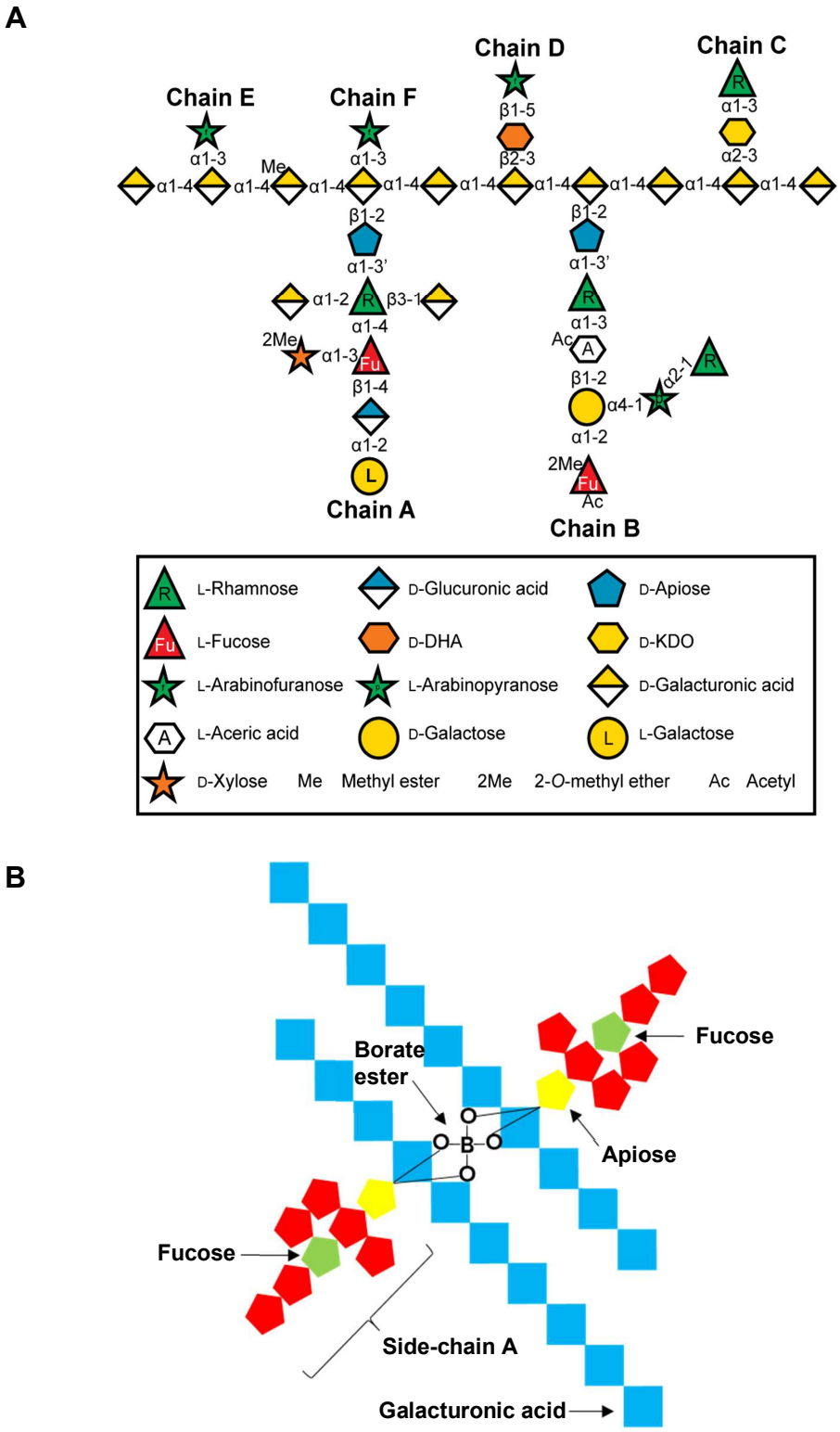

Figure 1.5: Structure of rhamnogalacturonan-II (RG-II) in *Arabidopsis*. A) Monomerised RG-II glycosyl composition showing all six side-chains. Monosaccharides are represented using Symbol Nomenclature for Glycans (Varkie *et al.* 2015). D-KDO: 3-deoxy-D-manno-octulosonic acid; D-DHA: 2-keto-3-deoxy-D-lyxo-heptulosaric acid. Adapted from Ndeh *et al.* (2017). **B)** Dimerised RG-II. The borate-ester cross-link forms between two apiose residues on side-chain A of adjacent RG-II monomers. Note that a simplified structure with only side-chain A is shown.

This cross-linking is conserved throughout the plant kingdom, with more than 95% of RG-II molecules present in the cell wall existing as covalently linked dimers (Matoh *et al.* 1996). Like many cell-wall processes, RG-II cross-linking is pH-dependent, and only occurs on the more stable side-chain A, despite the presence of apiose residues on side-chain B (Mazeau & Perez 1998, Ishii *et al.* 1999). This likely contributes to its stability. Dimerisation likely occurs during the synthesis of RG-II and before its transport to the cell wall; it is not thought that RG-II monomers are able to dimerise after secretion (Chormova *et al.* 2014). Cell-wall mutants that have impaired RG-II cross-linking can underline its importance to cell-wall structure and overall plant growth. Reiter *et al.* (1993) identified *mur1*, a mutant deficient in cell-wall fucose with a drastically altered phenotype: *mur1* is dwarfed, shows a reduction in petiole and internode length, has reduced apical dominance, smaller, rounder leaves, and a reduction in the force required to break inflorescence stems. Unsurprisingly, the *mur1* mutation was mapped to a gene encoding an enzyme involved in the first step of fucose biosynthesis, GDP-D-mannose-4,6-dehydratase (Bonin *et al.* 1997). After synthesis, fucose is incorporated into a number of cell-wall polymers including xyloglucans (Zablackis *et al.* 1995), glycoproteins (Zhang *et al.* 2018), and side-chains A and B of RG-II (Ndeh *et al.* 2017). Mutants of a xyloglucan-specific fucosyltransferase, *mur2*, exhibit none of the morphological characteristics of *mur1*, suggesting that fucose-deficient xyloglucan is not responsible for the phenotype of *mur1* (Vanzin *et al.* 2002). Similarly, mutants with fucose-deficient glycoproteins do not share the phenotype of *mur1* (von Schaewen *et al.* 1993), suggesting that a lack of fucose in RG-II domains must be responsible. Indeed, RG-II dimerisation is reduced to approximately 50% in *mur1* compared to 95% in wild-type plants, as the rate of dimer formation and the stability of the cross-link is greatly reduced in the mutant (O'Neill *et al.* 2001). This is despite galactose replacing the lost fucose residues on RG-II side-chains, indicating that the lack of fucose itself, and the truncation that it causes, hinders the formation and stability of the borate-ester cross-link between RG-II monomers (Zablackis *et al.* 1996). Furthermore, fucose supplementation of *mur1* plants both rescues the aforementioned morphological deficiencies (Reiter *et al.* 1993) and partially restores RG-II cross-linking closer to wild-type levels

(O'Neill *et al.* 2001). Interestingly, supplementing plants with boron has the same rescuing effect as fucose on morphology and RG-II cross-linking in *mur1*, despite the glycosyl composition of RG-II remaining unchanged and the side-chains still lacking fucose (O'Neill *et al.* 2001, Ryden *et al.* 2003). More recently, mutants of boron transporters, which are deficient in cell-wall boron but suffer no impairment in fucose synthesis, were also shown to have reduced RG-II cross-linking (Panter *et al.* 2019). Given that the majority of cell-wall boron is associated with RG-II complexes (Matoh *et al.* 1996), this is further evidence that the phenotype of *mur1* is caused by a reduction in RG-II cross-linking. It has been suggested that a lack of fucose may cause side-chain A of RG-II to become truncated, affecting the rate of formation of the borate-ester bond on the adjacent apiose residue and reducing the stability of the dimeric molecule (Pabst *et al.* 2013). Supplementary boron appears to compensate for the reduced binding efficiency of RG-II for boron to form the ester cross-link. Interestingly, *Arabidopsis* plants with reduced galactosylation of RG-II also have reduced RG-II dimerisation, though not to the same extent as *mur1* plants (Sechet *et al.* 2018). Like *mur1,* however, plants deficient in RG-II galactosylation have a dwarf phenotype that is rescued by boron supplementation, suggesting that truncated RG-II side-chains generally have the effect of reducing the stability of the borate-ester cross-link.

1.3.1.3 Proteins

Although structural proteins make up just one-fifth of the total mass of the cell wall (Burke *et al.* 1974), they are essential, as complete loss of the cell-wall protein network in *Arabidopsis* is lethal (Hall & Cannon 2002). One major group of cell-wall proteins is the hydroxyproline-rich glycoprotein (HRGP) superfamily, which is primarily made up of the extensins (EXTs) and the arabinogalactan proteins (AGPs).

1.3.1.3.1 Extensins

EXTs make up the majority of the HRGPs. There are at least 59 genes encoding EXTs and EXT-related glycoproteins in *Arabidopsis* (Showalter *et al.* 2010), which are generally defined as wall-located, self-assembling, basic, hydroxyproline-rich structural glycoproteins with alternating hydrophobic and hydrophilic motifs

(Lamport *et al.* 2011). An EXT scaffold is essential for formation of the plant cell wall (Cannon *et al.* 2008), but EXTs first require a number of post-translational modifications before becoming functional; these include hydroxylation, *O*-glycosylation, and cross-linking to other EXTs (Velasquez *et al.* 2011, Marzol *et al.* 2018). It has been suggested that tyrosine residues on adjacent EXTs form a highly cross-linked network that strengthens the cell wall (Schnabelrauch *et al.* 1996, Merkouropoulos *et al.* 1999), while also providing a barrier to pathogen invasion (Esquerré-Tugayé *et al.* 1979, Showalter *et al.* 1985, Castilleux *et al.* 2021). EXTs are essential for cell plate formation during cell division, as shown by the aberrant phenotype of the *ext3* mutant in *Arabidopsis* (Hall & Cannon 2002). Interestingly, EXTs may form important structural links with pectin, either through acid-base interactions (Smith *et al.* 1984, Cannon *et al.* 2008), or even through the formation of covalent cross-links (Qi *et al.* 1995, Nuñez *et al.* 2009), suggesting that EXTs may be required for efficient assembly of pectin in the cell plate (Lamport *et al.* 2011). It has also been suggested that EXTs may "wrap" around cellulose microfibrils, locking them into place after their synthesis (Lamport 1986).

1.3.1.3.2 Arabinogalactan proteins

Another well studied member of the HRGP family, AGPs are also heavily glycosylated and widespread amongst land plants and algae. They are defined by a core, protein backbone that is *O*-glycosylated by complex carbohydrates containing arabinose and galactan (Gaspar *et al.* 2001). AGPs are thought to have numerous, varied functions in the cell wall, including in cell division and death, embryonic pattern formation, pollen tube guidance, cell expansion, secondary cell wall deposition, and in the modulation of certain cell-wall mechanical properties (Seifert & Roberts 2007).

1.3.2 Physical properties

Plant cell walls possess remarkable physical properties. Despite lacking contractile muscles, they are able to move, deform, extend, and actuate force, all while acting as a sturdy scaffold for the cell, leading the wider scientific and engineering community to classify them as smart materials (Gershlak *et al.* 2017, Zurlo &

Truskinovsky 2017). This study will focus on two important physical properties: porosity and mechanics.

1.3.2.1 Porosity

In material science, porosity may be defined as the presence of voids within a material (Bidhendi & Geitmann 2019). Similarly, in the context of the plant cell wall, porosity describes the capacity for molecular movements within the wall and is dependent on the spacing (voids) between wall polysaccharides and other polymeric networks (Liu *et al.* 2019b). How porous a plant's cell wall is can impact significantly on several important processes: it affects the kinetics and efficiency of leaf water uptake (Boanares *et al.* 2018), it is correlated with cell-wall digestibility and capacity for saccharification (Himmel *et al.* 2007), and it can limit mesophyll CO_2 conductance, meaning that it influences overall photosynthetic capacity (Ellsworth *et al.* 2018). As mentioned, the cell wall physically separates the plant cell from its external environment, and so it must also limit its pore sizes in order to restrict entry of toxins and pathogens into the cell, whilst remaining large enough to allow free movement of nutrients and hormones (Carpita *et al.* 1979).

Attempts at measuring or quantifying cell-wall porosity have been numerous and varied in their methodologies over the decades. Scherrer & Gerhardt (1971) measured the cell-wall permeabilities of bacteria and yeast using a method based on gel permeation chromatography (GPC). They used GPC fractionation of a polydisperse probing solution before and after its equilibration with isolated microbial cell walls, followed by calculation of weight percent uptake values for each probing solution. By using probing molecules of a known molecular weight, a limiting measure of porosity could be calculated. Similarly, Carpita *et al.* (1979) used a solute exclusion technique to measure pore diameter in a range of plant species. It relied on two principles: 1) an external solute consisting of molecules small enough to penetrate cell-wall pores and permeate to the plasma membrane will cause plasmolysis (the retraction of the membrane away from the cell wall), and 2) an external solute consisting of high molecular-weight molecules that are too large to penetrate the cell-wall pores will draw water from the cell, leading to cytorrhysis (the collapse of the cell wall around the shrinking protoplasm). The

authors added solutes of varying, known molecular weights to a solution in which the plant cells were immersed and observed whether plasmolysis or cytorrhysis occurred, thus inferring the maximum pore diameter from the diameter of the largest molecule able to cause plasmolysis. Baron-Epel *et al.* (1988) used non-invasive fluorescence redistribution after photobleaching (FRAP) to quantify cell-wall porosity in soybean (*Glycine max*) root cell suspension cultures. Diffusion of fluorescent dextrans and proteins of differing molecular weights across isolated cell walls was monitored by measuring the distribution of macromolecular fluorescence using microscopy; using this method, the authors were able to determine the exclusion size of substances from the cell wall. Woehlecke & Ehwald (1995), Titel *et al.* (1997) and Fleischer *et al.* (1999) used size-exclusion chromatography (SEC) to determine cell-wall pore size in plant suspension cultures. This technique also relied on a polydisperse probing solution containing molecules with a range of molecular weights, and the mean size limit of probing molecules that were able to permeate through cell walls was calculated by comparing the elution profiles of different samples. Other methods of measuring cell-wall porosity include transmission electron microscopy (Cohen & Voyle 1987), measuring the chemically-induced release of UV-absorbing cellular compounds from the cell wall (De Nobel *et al.* 1990), cryo-electron microscopy (Derksen *et al.* 2011), and gas adsorption assays (Adani *et al.* 2011). However, each of these techniques either involves harsh sample preparation, potentially introducing artefacts, or have limited resolving power. More recently, Liu *et al.* (2019b) developed a fluorescence quenching assay to indirectly quantify cell-wall porosity in bacteria, yeast, and various plant species and tissues, including mutants of *Arabidopsis*. The assay measures the quenching efficiency of an extracellular quenching solution on a membrane-specific fluorescent dye, assuming that access to the membrane by the quenching molecules would depend on cell-wall pore size. Therefore, quantifying the reduction in relative fluorescence after addition of the quenching agent gives a measure of cell-wall porosity. This method has the advantages of non-invasive sample preparation and the use of live tissues (or organisms) to better reflect cell-wall porosity *in vivo*.

Cell-wall porosity is a dynamic physical property and dependent on many factors. In a hydrated, non-growing plant cell, osmotic equilibrium is reached when outward

turgor pressure against the wall is counterbalanced by inward pressure from wall stress (Cosgrove 2015). In order for the cell to expand, wall "loosening" must occur to make it more extensible (Cosgrove 2005). Wall-loosening enzymes, such as expansins, endoglucanases and endotransglycosylases, act at specific junctions of the cell wall to induce stress relaxation by rearranging (yielding) the load-bearing cellulose microfibril network (Zhang *et al.* 2019). Cell turgor pressure is reduced as a result, allowing water to enter the cell via osmosis, thus elastically expanding the cell and restoring the counterbalancing turgor pressure and wall stress (Cosgrove 2015). From one of their fluorescence quenching experiments, Liu *et al.* (2019b) concluded that increased porosity is a consequence of, not a precondition for, cell expansion, as loosening of the cell wall is accompanied by an increase in the physical distance between wall components. Increased cell-wall porosity of cells in the growth phase compared to the stationary phase has been reported previously (Titel *et al.* 1997). Indeed, it had already been suggested that cell-wall expansion does not necessarily require the addition of new polymers: when an enzymatically-loosened wall increases in surface area due to water uptake, the existing polymers may become pulled apart along the plane of the wall, increasing the physical space between them (Cosgrove 2015).

Porosity can also be affected by pectin structure. The pore size of pectin-rich dicot cell walls is increased by pectin-specific PG treatment or β-elimination, but not by proteinase or cellulysin treatment (Baron-Epel *et al.* 1988, Ehwald *et al.* 1991, 1992). In Japanese bunching onion, enhanced HG cross-linking was induced by calcium supplementation, and this was associated with decreased cell-wall permeability and a ten-fold reduction in the total number of cell-wall pores (Liu *et al.* 2022). Suspension-cultured *Chenopodium album* grown on a boron-deficient medium had both reduced RG-II dimerisation and increased cell-wall porosity (Fleischer *et al.* 1999). Addition of boron to the growth medium quickly resulted in both an increase in RG-II dimerisation and a reduction in cell-wall porosity, indicating that boron-mediated RG-II dimerisation produces a more thoroughly cross-linked pectin network that contributes to a less porous cell wall. Furthermore, PME17 has been shown to be induced by bacterial infection (Zhang *et al.* 2015). Although PME17 may play an important role in inducing a wider immune response,

increased pectin cross-linking (and the subsequent reduction in cell-wall porosity) through PME activity could also physically limit entry of bacterial cells into plant tissues. Interestingly, *Arabidopsis* plants overexpressing an extensin gene, *EXT1,* were better able to limit bacterial infection in their tissues (Wei & Shirsat 2006). Transgenic plants had significantly smaller lesions, accumulated a bacterial load 100-times smaller and exhibited reduced chlorosis compared to wild-type plants. Conversely, *Arabidopsis* mutants with impaired EXT structure show increased vulnerability to pathogen colonisation of their tissues (Castilleux *et al.* 2021). As discussed above, a heavily cross-linked EXT network may provide a barrier to pathogen or toxin ingress, and this could be part of a broader strategy used by plants to reduce cell-wall porosity, thereby slowing the spread of the pathogen or its toxins, before activation of the full immune response. Indeed, *EXT* genes are upregulated in response to pathogen invasion in a range of species, including *Arabidopsis* (Esquerré-Tugayé *et al.* 1979, Mouly *et al.* 1992, Davies *et al.* 1997, Merkouropoulos & Shirsat 2003) and, in pepper plants, formation of a HRGP matrix around bacterial cells was found to restrict bacterial colony development (Brown *et al.* 1995). It must be noted, however, that other theories of EXT-mediated immunity exist, including proposals that EXTs may immobilise pathogens by binding them directly (Mazau *et al.* 1987).

1.3.2.2 Mechanics

Mechanics is the branch of science that deals with how forces act on bodies and how the bodies move, deform or interact with one another as a result. Cell mechanics, therefore, is the study of forces applied to (or generated by) cells, or their microenvironment, and the resulting deformations (Bidhendi & Geitmann 2019). Plant cell walls exhibit tensile mechanical strength, which is the capacity of a material or structure to withstand elongating forces. In the literature, mechanical strength and mechanical stiffness (or rigidity) are sometimes used interchangeably. They broadly describe the same properties (that is, a material that is mechanically strong is generally mechanically stiff), but with subtle differences. Here, mechanical strength will be defined as resistance to breaking pressure, or the maximum stress that a material can withstand before fracture (where "stress" is an applied force,

such as elongation or compression). Mechanical stiffness will be defined as resistance to deformation, and can be quantified by applying a set force and measuring the resulting deformation.

The mechanical properties of the plant cell wall depend almost entirely on its composition of individual wall polymers and the interactions between them (Vogler *et al.* 2015). As the main load-bearing structures of the cell wall, the organisation and density of the cellulose microfibrils are the primary contributors to cell-wall mechanical properties (Probine & Preston 1961, Whitney *et al.* 1999). However, other components are also necessary to form a mechanically strong cell wall, some of which have been discovered by studying the mechanical properties of *Arabidopsis* mutants that have various cell-wall defects. For instance, *mur1* plants, which lack fucosylation and dimerisation of RG-II, have reduced mechanical strength compared to wild-type plants, a defect that is reversed when plants are supplemented with fucose (Reiter *et al.* 1993) or boron (Ryden *et al.* 2003), thus indicating that borate-complexed RG-II dimers contribute to cell-wall mechanical strength. Mutants deficient in xyloglucan (*xxt1 xxt2,* a double xylosyltransferase knock-out) have drastically reduced cell-wall mechanical strength (Cavalier *et al.* 2008), as does *mur3,* a mutant with an impaired xyloglucan-specific galactosyltransferase that lacks xyloglucan galactosylation (Peña *et al.* 2004). Interestingly, Peña *et al.* (2004) also tested *mur2*, a mutant with a defective xyloglucan-specific fucosyltransferase, but found that its mechanical properties were far less affected. This suggests that galactosylation, more so than fucosylation, of xyloglucan side-chains is required for maintaining cell-wall mechanical strength, whereas fucosylation is important in the case of RG-II. HG methylesterification has been linked to both increased (Peaucelle *et al.* 2011, Kierzkowski *et al.* 2012, Wolf & Greiner 2012, Braybrook & Peaucelle 2013) and decreased (Zerzour *et al.* 2009, Chebli *et al.* 2012, Hongo et al. 2012, Vogler *et al.* 2013) cell-wall stiffness depending on tissue and growth stage. However, just like with immunity, it may also be partly explained by the modes of action of different PMEs, specifically whether they act in a block-wise or non-block-wise pattern (Bidhendi & Geitmann 2016). There is evidence to suggest that block-wise demethylesterification of HG, leading to enhanced calcium cross-linking, is associated with increased mechanical stiffness of

the cell wall (Willats *et al.* 2001a, Li *et al.* 2012, Wolf & Greiner 2012, Xi *et al.* 2015). Additionally, acetylation or substitution of GalA can occur in regions of low methylesterification (Atmodjo *et al.* 2013), facilitating linkages with cellulose microfibrils which can further stiffen the cell wall (Phyo *et al.* 2017). Conversely, non-block-wise demethylesterification, beyond being less conducive to calcium cross-linking, may increase the susceptibility of HGs to degradation by PGs, further decreasing cell-wall mechanical stiffness (Willats *et al.* 2001a, Wakabayashi *et al.* 2003, Brummell 2006). The contribution of RG-I to overall cell-wall mechanical properties remains unclear but its side-chain composition, specifically the degrees of galactosylation and arabinosylation, are likely to be involved (McCartney *et al.* 2000, Ulvskov *et al.* 2005). Arabinose in particular may prevent Ca^{2+}-mediated HG cross-linking and subsequent cell-wall stiffening (Harholt *et al.* 2010).

Measuring the mechanical properties of the plant cell wall is inherently difficult as applying forces and measuring deformations at such small scales requires precise, meticulous experimental setups. Nano- and micro-indentation techniques, which involve indenting tissue with a rigid probe and measuring the force required to do so, have proven to be useful tools for studying mechanical properties with cellular resolution. AFM is one such technique that has revealed valuable information about plant cell-wall mechanical properties. Milani *et al.* (2011) used AFM to measure mechanical stiffness at the cellular and subcellular level of the *Arabidopsis* meristem, and found differences in stiffness values even along the plane of the same cell wall. Peaucelle *et al.* (2011) used AFM to elucidate how pectin demethylesterification is key to the changes in cell-wall mechanics that precede organ initiation in *Arabidopsis*. Feng *et al.* (2018) used AFM to show that salt stress weakens the cell wall (reduces its mechanical stiffness) by disrupting pectin cross-linking. However, as indentation techniques require force to be applied perpendicular to the plane of the cell wall and the direction of growth, they are generally only appropriate for studying the mechanical properties arising from cell-wall pectins, which are isotropic (Cosgrove 2015). Other components of the cell wall, such as the cellulose-hemicellulose framework, are highly anisotropic, and it is not clear if AFM or other indentation techniques provide useful data on the mechanical properties arising from these components (Cosgrove 2015). Methods

that apply force parallel to the plane of the cell wall and direction of growth are, therefore, required to measure these mechanical properties. Extensometry has proven to be a useful method of doing so (Robinson *et al.* 2017). It involves clamping a tissue sample, then either applying a set force (or "stretch") and measuring the deformation (thus measuring mechanical stiffness), or stretching the tissue until breakage and recording the force required to do so (thus measuring mechanical strength). Although generally offering lower resolution than AFM, extensometry can provide a better tissue-level picture of cell-wall mechanics, and can even be modified to provide cellular resolution (Robinson *et al.* 2017). Most notably, extensometry was used in the discovery of the cell-wall modifying protein expansin, which was found to induce cell-wall extension (McQueen-Mason *et al.* 1992).

1.3.3 The role of the cell wall in plant freezing tolerance

Historically, efforts to engineer freezing tolerance in plants have focused on the plasma membrane and somewhat neglected the cell wall. This is likely due to the plasma membrane being the primary site of injury during freezing and several early studies indicating that the cell wall is either irrelevant to cellular freezing tolerance (Siminovitch 1979, Singh 1979), or even detrimental to the cell during freezing (Tao *et al.* 1983, Murai & Yoshida 1998). However, there is now considerable, growing evidence that the cell wall is central to cold acclimation and the acquisition of overall freezing tolerance. This is unsurprising, as it has long been established that the cell wall is key to abiotic stress resistance beyond freezing, including resistance to drought, desiccation, salt, flooding, light, air, heat and cold stresses, as well as micronutrient and heavy metal toxicity (Yang *et al.* 2006, Moore *et al.* 2008b, Krzesłowska 2011, Le Gall *et al.* 2015, Tenhaken 2015, Housten *et al.* 2016, Feng *et al.* 2018, Wu *et al.* 2018, Parrotta *et al.* 2019, Oliveira *et al.* 2020, Zhu & Li 2021, Khan *et al.* 2022). Perhaps the biggest indicators that the cell wall is involved in freezing tolerance are the many modifications it undergoes during cold acclimation.

1.3.3.1 Cell-wall modifications during cold acclimation

Cold acclimation has profound effects on the abundance and organisation of individual cell-wall components as well as the physical properties of the cell wall generally. Cold-induced increases in total pectin (or the proportion of pectin) and pectin side-chain components have been observed in oilseed rape (Kubacka-Zębalska & Kacperska 1999, Solecka *et al.* 2008), pea (Baldwin *et al.* 2014), *Arabidopsis* (Takahashi *et al.* 2019) and *Nidularium minutum* (Carvalho *et al.* 2013). Paradoxically, the degree of pectin demethylesterification, PME activity, or pectin cross-linking has been found to both increase (Wisniewski & Davis 1995, Solecka *et al.* 2008, Qu *et al.* 2011, Lee *et al.* 2017, Liu *et al.* 2022) and decrease (Thonar *et al.* 2006, Baldwin *et al.* 2014, Willick *et al.* 2018, Takahashi *et al.* 2019) during cold acclimation depending on species and tissue type, again highlighting the complex role of pectin structure in response to abiotic stress. PMEIs have also been shown to be induced by cold acclimation, thus reducing the activity of certain PMEs (Chen *et al.* 2018). Changes to pectin structure may also be accompanied by hemicellulose modifications (Kubacka-Zębalska & Kacperska 1999, Willick *et al.* 2018, Takahashi *et al.* 2021a). Cold acclimation increases *EXT* gene transcription in pea seedlings (Weiser *et al.* 1990) and oilseed rape (Kozbial *et al.* 2002); in pea, this was also associated with an increase in arabinosyl and hydroxyproline content, both of which are major components of EXTs. Unsurprisingly, various cell-wall modifying enzymes show differential regulation during cold acclimation, including expansins and PGs (Domon *et al.* 2013, Baldwin *et al.* 2014, Tenhaken 2015, Zhao *et al.* 2016, Willick *et al.* 2018, Takahashi *et al.* 2019). In a transcriptomic analysis of pea, specific cell-wall modifying enzymes were found to be upregulated in a freezing-tolerant cultivar but not in a freezing-sensitive one, indicating that the cell-wall modifications that they catalyse are necessary for enhanced freezing tolerance (Lucau-Danila *et al.* 2012).

In a range of species and tissues, cold acclimation has been shown to increase the mass or thickness of the cell wall (Huner *et al.* 1981, Griffith & Brown 1982, Griffith *et al.* 1985, Tanino *et al.* 1990, Weiser *et al.* 1990, Kubacka-Zębalska & Kacperska 1999, Stefanowska *et al.* 1999, Solecka *et al.* 2008, Carvalho *et al.* 2013, Domon *et*

al. 2013, Tanino *et al.* 2013, Takahashi *et al.* 2019, Liu *et al.* 2022), as well as its mechanical stiffness or strength (Rajashekar & Lafta 1996, Solecka *et al.* 2008, Scholz *et al.* 2012, Arias *et al.* 2015). Decreased cell-wall porosity is also associated with cold acclimation and has been observed in several species, including in an early study of peach (Wisniewski *et al.* 1987). The limiting cell-wall pore size of suspension-cultured apple and grape cells decreased by 24% and 37%, respectively, after cold acclimation (Rajashekar & Lafta 1996) and, more recently, it was shown that cold acclimation significantly reduces the cell permeability of Japanese bunching onion, and this is likely due to reductions in pore numbers and diameters in the wall (Liu *et al.* 2022).

1.3.3.2 Cell-wall mediated freezing tolerance

Clearly, cold acclimation typically leads to increased mechanical strength or stiffness and reduced porosity of the cell wall. Even in cases where these properties were not measured directly, many of the compositional changes that occurred during cold acclimation were interpreted as mechanisms to both enhance cell-wall mechanical properties and decrease porosity, both of which may help to protect against freezing damage. In the case of porosity, it has long been suggested that the cell wall is an intrinsic barrier to ice nucleation and propagation (Olien 1974, Wisniewski 1995, Yamada *et al.* 2002, McCully *et al.* 2004). More specifically, it has been theorised that the freezing point of minute volumes of water in confined, porous material should be lower than that of free, bulk water (Mazur 1963, Homshaw 1980), which would be conducive to supercooling in the pores of the cell wall. Ashworth & Abeles (1984) developed a model system to test this theory which involved nucleating ice in glass particles with defined pore sizes; it was found that water in pores of diameter less than 100 nm froze at a lower temperature than bulk water, and ice formation in pores of diameter 4 nm could only occur below -15°C. Given that cell-wall pores are measured on a nanometre scale, it was concluded that water in smaller cell-wall pores would lower the freezing temperature of tissue water, facilitating supercooling and impeding the nucleation and propagation of extracellular ice. Smaller pores may also play a role in establishing a vapour pressure equilibrium between supercooled intracellular water and the extracellular

ice mass, a phenomenon called the "ink bottle effect" which reduces the water potential of intracellular water to prevent freezing-induced dehydration (George & Burke 1976).

The effects of reduced porosity during freezing have also been observed *in vivo*. Deep-supercooling woody perennials develop tissues that lack large extracellular spaces, instead developing a continuous network of cell walls with small pores (Sakai & Larcher 1987). Rajashekar & Lafta (1996) reported significant reductions in cell-wall pore size in cold-acclimated apple and grape cells and, during subsequent freezing, this resulted in a reduction in the presence of intracellular ice which was found in 37.6% of non-acclimated cells but just 4.3% of cold-acclimated cells. It was concluded that small cell-wall pores play an important role in excluding ice from the cell. Pectin structure is likely key to doing so. In stem sections of flowering dogwood and in peach xylem ray parenchyma cells, treatment with pectinase resulted in greater pore size and an impaired propensity to supercool (Wisniewski *et al.* 1991, Wisniewski & Davis 1995). Calcium cross-linking of HG was shown to inhibit ice propagation in both peach parenchyma cells (Wisniewski & Davis 1995) and overwintering buds of Norway spruce (Kuprian *et al.* 2017). In Japanese bunching onion, cold acclimation was associated with the following: an increase in freezing tolerance, a 70-fold reduction in tissue permeability, increased PME activity, and a reduction in HG methylesterification (Liu *et al.* 2022). Furthermore, non-acclimated cells supplemented with exogenous calcium to facilitate HG cross-linking had reduced cell-wall porosity and, crucially, a reduction in the lethal intracellular ice nucleation temperature to levels seen in cold-acclimated cells. Taken together, the results of these studies support the hypothesis of pectin cross-linking impeding ice propagation and facilitating supercooling by reducing cell-wall porosity. However, other cell-wall modifications induced by cold acclimation likely contribute to reducing porosity alongside pectins. As discussed, EXT transcripts accumulate in response to cold, and EXT accumulation in the cell wall has been shown to restrict pathogen invasiveness in *Arabidopsis* (Wei & Shirsat 2006). It is possible, therefore, that EXTs contribute to the ice barrier in the cell wall by accumulating and forming extensive, cross-linked networks during cold acclimation, as seen when contributing to the plant immune response.

The other major physical change observed in the cell wall during cold acclimation is the increase in its mass and thickness, which is likely a mechanism for increasing its mechanical stiffness (Rajashekar & Burke 1996). A mechanically stiff cell wall is better able to resist freezing-induced cellular dehydration and will therefore be less prone to deformation or collapse (Pearce 1988, Fujikawa *et al.* 1999, Yamada *et al.* 2002). It has been suggested that cell-wall deformation, or contraction, is required for extracellular ice to draw water from inside the cell down the water potential gradient (Rajashekar 1997). A cell wall of sufficient stiffness will resist this deformation, placing the cell under tension, or "negative pressure", wherein the liquid contents of the cell are at a lower pressure relative to outside of the cell and the water potential gradient is reduced (Rajashekar & Burke 1986, Hansen & Beck 1988, Zhu *et al.* 1989, Zhu & Beck 1991, Yang *et al.* 2017). The creation of such tension means that there is an energetic penalty for water being drawn out of the cell, with a stiffer cell wall associated with a higher penalty. An equilibrium is established between extracellular ice drawing water from the cell and water remaining in the cell due to the lower pressure; at this equilibrium, further water cannot be lost from the cell as the cell wall will not deform in response. Conversely, a non-stiff cell wall would have less resistance to deformation and would not be capable of establishing sufficient cell tensions and negative pressures. As a result, there would be a smaller energetic penalty for extracellular ice to draw water from the cell, meaning the cell would be more prone to severe dehydration. Therefore, a mechanically stiff cell wall can resist freezing-induced dehydration, the primary symptom of freezing injury. However, cells under negative pressure are more prone to cavitation through the formation of vapour bubbles or dissolved gases coming out of solution, which can nucleate intracellular ice (Tyree & Dixon 1986, Tyree & Sperry 1989). It appears, therefore, that there must be a trade-off in cell-wall stiffness to avoid both severe freezing-induced dehydration and lethal intracellular cavitation. It has been suggested that cold-acclimated cells show increased viscosity and greater interaction of water with hydrophilic materials, both of which may reduce the incidence of cavitation (Rajashekar & Lafta 1996).

Cell-wall stiffness, strength or thickness has repeatedly been linked to enhanced freezing tolerance *in vivo*. A freezing-tolerant cultivar of *Solanum* has a significantly

thicker cell wall than a freezing-sensitive one (Chen *et al.* 1977). In *Citrus* leaves, it was hypothesised that enhanced cell-wall stiffness contributed to freezing tolerance by resisting cell collapse and dehydration during extracellular freezing (Anderson *et al.* 1983). Salt-adapted tobacco cells were shown to have weaker cell walls than non-adapted cells, with non-adapted cells accumulating more hydroxyproline-rich proteins than adapted cells (Iraki *et al.* 1989). The authors attributed the increased cell-wall strength to a cellulose-EXT matrix containing isodityrosine linkages, which provide a rigid network in cell walls. Therefore, the accumulation of EXTs in pea and oilseed rape, observed by Weiser *et al.* (1990) and Kozbial *et al.* (2002), respectively, may be another mechanism by which plants increase their cell-wall stiffness and resistance to collapse during freezing. In palm leaves, it was suggested that supercooling was facilitated by the deposition of silica which was thought to stiffen the cell wall (Larcher *et al.* 1991). Concomitant with the reduction in porosity in apple and grape cells, there was a 12% and 54% increase in cell-wall resistance to breaking pressure, respectively, after cold acclimation, a result of increased accumulation of cell-wall materials (Rajashekar & Lafta 1996). In leaves of broadleaf evergreen species, cold acclimation resulted in higher cell tensions during extracellular freezing compared to non-acclimated leaves, suggesting an increased ability to resist dehydration and cell-wall deformation in acclimated leaves (Rajashekar & Lafta 1996). In riverbank grape stem tissue, oak leaves and cranberry leaves, extracellular freezing was associated with the development of cell tensions and an increase in cell-wall stiffness resulted in a decrease in cellular dehydration during freezing (Rajashekar & Burke 1996). In oilseed rape, cold acclimation resulted in increased freezing tolerance, leaf tensile stiffness, cell-wall mass and pectin content, as well as PME activity and demethylesterified pectins (Solecka *et al.* 2008). This suggests that, as with porosity, pectins may contribute to freezing tolerance by stiffening the cell wall through increased cross-linking, thereby providing enhanced resistance to dehydration and cell collapse. This is supported by the finding that overexpression of *PMEI13* in *Arabidopsis* led to a fall in PME activity and an increase in the degree of pectin methylesterification linked to a freezing-sensitive phenotype (Chen *et al.* 2018). Numerous other studies have found a link between pectin cross-linking

and cell-wall stiffness and have been discussed in **Section 1.3.2.2**. The existence of a cell-wall pectin-EXT network has even been proposed, which would presumably contribute substantially to cell-wall mechanical properties (Nuñez *et al.* 2009). In green algae, extracellular freezing was associated with reinforcement of the cell wall by the deposition of additional wall layers; cells that were allowed to recover from freezing lost these additional layers, suggesting that it is a dynamic adaptation to freezing stress (Steiner *et al.* 2020). In *Arabidopsis*, both cold acclimation and sub-zero acclimation were associated with enhanced freezing tolerance and a significant increase in cell-wall mass, which was interpreted as an increase in the mechanical strength of the cell wall against deformation during extracellular ice formation (Takahashi *et al.* 2019). A freezing-tolerant Alpine population of *Arabidopsis* was shown to have higher total leaf thickness, palisade parenchyma thickness and spongy parenchyma thickness than a more freezing-sensitive foothill population (Bertel *et al.* 2022). In conifer mesophyll cells, a higher cell-wall thickness to cell-size ratio (indicative of increased cell-wall strength) and smaller intercellular spaces were associated with decreased freezing-induced dehydration (Stegner *et al.* 2022).

An ethyl methanesulfonate (EMS) screen for *Arabidopsis* mutants that are freezing-sensitive, even after cold acclimation, identified *sensitive-to-freezing* (*sfr*) mutations 1-7 (Warren *et al.* 1996). Genetic mapping of these mutations led to the functional characterisation of the *SFR* genes and their roles in freezing tolerance. For example, *SFR2* expression is important for protecting the chloroplast membrane during freezing (Fourrier *et al.* 2008, Moellering *et al.* 2010), whereas *SFR6* codes for a subunit of the plant Mediator complex, a transcriptional coactivator complex that regulates cold-responsive gene expression (Hemsley *et al.* 2014). After the initial EMS screen, *sfr8* and *sfr9* were subsequently identified (Thorlby *et al.* 1999). In both acclimated and non-acclimated states, *sfr8* plants exhibit almost complete chlorosis and failure to recover after freezing (whereas wild-type plants show signs of recovery and retain substantial green tissue), and leaves of *sfr8* plants have significantly higher leakage of electrolytes compared to wild-type after exposure to a range of sub-zero temperatures, indicating that it has endured more severe freezing injury (Panter 2018). The *sfr8* mutation was mapped to *MUR1* and, like other *mur1* mutant alleles, *sfr8* has significantly reduced cell-wall fucose and

RG-II dimerisation (Panter *et al.* 2019). *mur1* mutants were also shown to be freezing-sensitive, and *sfr8* mutants complemented with a *MUR1* coding sequence showed restored levels of cell-wall fucose, RG-II dimerisation and overall freezing tolerance, confirming that *SFR8* and *MUR1* are allelic (Panter *et al.* 2019). As discussed above, *mur1* plants have reduced mechanical strength compared to wild-type, and this may be one reason for their sensitivity to freezing. Indeed, boron deficiency in squash and bean roots has been shown to reduce the elastic modulus (a measure of stiffness) of the cell wall, although this was only a short-term effect (Findeklee & Goldbach 1996, Findeklee *et al.* 1997). It was recently hypothesised that xyloglucan-modifying enzymes, endotransglucosylases, can promote cell-wall stiffening (Cosgrove 2022). Indeed, an *Arabidopsis* mutant lacking expression of a xyloglucan endotransglucosylase/hydrolase (XTH) gene, *XTH21*, was shown to be freezing-sensitive, whereas overexpression of *XTH21* resulted in increased freezing tolerance (Shi *et al.* 2014). Similarly, knock-out mutants for a different cold-inducible XTH, *XTH19,* were shown to be freezing-sensitive after cold acclimation (Takahashi *et al.* 2021a). In *xth19* mutants, cell-wall xyloglucan content was reduced under cold-acclimating conditions but not under non-acclimating conditions, indicating that this specific xyloglucan-modifying enzyme is required for full cold acclimation. Taken together, the results of these studies provide compelling evidence for the link between freezing tolerance (specifically, reduced freezing-induced dehydration) and cell-wall mechanical properties. However, further studies that involve assessing cold acclimation, freezing tolerance, and cell-wall physical properties in the same species are necessary to solidify this proposed relationship, as it is likely that different species (and even different tissues) employ different mechanisms to enhance their freezing tolerance, and it is difficult to draw comparisons between species and differing experimental setups.

Cold acclimation may induce cell-wall modifications that have purposes beyond changing the porosity and stiffness of the cell wall, but still contribute to freezing tolerance. For example, Takahashi *et al.* (2019) reported an increase in pectic arabinose content during cold acclimation, and it was speculated that this may prevent the formation of irreversible linkages between pectin backbones during extracellular freezing, thereby facilitating the recovery of cell-wall components after

thawing. Furthermore, increased pectin-associated arabinans may be necessary to maintain cell-wall flexibility during severe dehydration (Moore *et al.* 2008a), which may help frozen plant cells avoid expansion-induced lysis after thawing and reuptake of water (Takahashi *et al.* 2021b). Pectin also has considerable water-binding properties and may be important in direct protection against drought and desiccation stress in plants and algae (Piro *et al.* 2003, Konno *et al.* 2008, Leucci *et al.* 2008, Einhorn-Stoll *et al.* 2012, Karim *et al.* 2012, Abdel-Motagally & El-Zohri 2018, Herburger *et al.* 2019). Additionally, reduced methylesterification has been associated with a higher water-binding capacity of HG (Willats *et al.* 2001b) and calcium- or boron-mediated pectin cross-linking has been linked to reduced water loss *in vitro* (Forand *et al.* 2022). *Arabidopsis* mutants lacking a boron transporter, *bor1*, have a significant water-loss phenotype (Forand *et al.* 2022), as do *sfr8* and *mur1* mutants (Panter 2018). Therefore, in addition to establishing negative pressures by reinforcing the wall, heavily cross-linked pectins may also form hydrated gels that directly reduce dehydration through the binding of water molecules (Leucci *et al.* 2008).

1.4 Summary & Aims

There is growing evidence to suggest that the plant cell wall undergoes significant modifications during cold acclimation which are necessary to protect the cell from freezing damage. The degree of protection that the cell wall can provide depends on its polysaccharide and protein compositions and structures and the physical properties that they confer. However, to the best of my knowledge, a broad profile of the compositional changes that occur in the cell wall of a single species during cold acclimation, as well as their specific effects on freezing tolerance, has not been reported. Studies linking specific components of the cell wall to changes in both cell-wall physical properties and freezing tolerance are also lacking. With that in mind, this investigation had the following aims:

1. Elucidate the compositional changes that occur in the cell wall of *Arabidopsis* during cold acclimation and what effects they have, if any, on cell-wall physical properties and freezing tolerance.

2. Pursue the link between RG-II cross-linking and freezing tolerance by further exploring the freezing-sensitive and water-loss phenotypes of *sfr8*.

3. Investigate other, non-cold-responsive components of the *Arabidopsis* cell wall and how they may contribute to cell-wall physical properties and freezing tolerance.

Chapter 2

Materials & Methods

2.1 Plant Growth Methods & Conditions

Arabidopsis thaliana ecotype Columbia-0 (Col-0) was used throughout. Mutants and transgenic lines are listed in **Table 2.1**.

2.1.1 Seedlings

Seeds were surface-sterilised by submerging in 70% ethanol and shaking vigorously for 5 mins. Sterilised seeds were transferred to clean filter paper and allowed to dry in a laminar flow cabinet before being sown on petri dishes (9 cm diameter) half-filled with growth medium. Growth medium consisted of 4.4 g/l of Murashige and Skoog (MS) medium (Murashige & Skoog 1962) with additional vitamins (Duchefa Biochemie; https://www.duchefa-biochemie.com) and 8 g/l of plant cell culture agar (Sigma-Aldrich; https://www.sigmaaldrich.com) for 1X MS. 1X MS was used unless otherwise stated. pH was adjusted to 5.8 with 0.1 M potassium hydroxide (KOH) before autoclaving at 120°C for 20 mins. Plates were sealed with micropore tape and sown seeds were stratified at 4°C in the dark for 48-72 h to allow uniform germination. Plates were then transferred to a Percival CU-36L5D growth chamber (CLF PlantClimatics; https://www.plantclimatics.de) with a light:dark (LD) cycle of 16:8 h, a light intensity of 150 μmol/m^2/s and a temperature of 20°C for 7-10 days before experimentation.

For boron supplementation, seeds were sown on 0.5X MS supplemented with 0.1 mM potassium tetraborate tetrahydrate (KBO; Sigma-Aldrich). pH was adjusted to 5.8 with 0.1 M hydrochloric acid (HCl). Control seedlings were sown on 0.5X

Table 2.1: List of cell-wall mutants and transgenic lines. Given is the name of each mutant or transgenic line, the associated gene and AGI code, the NASC or ABRC seed stock ID (if applicable), and a reference.

Mutant/transgenic	Gene (Accession)	Stock ID	Reference
cesa3^{S211A}	*CEV1* (AT5G05170)	N/A	Chen *et al.* (2016)
ext18	*EXT18* (AT1G26250)	SALK_201747C	Choudhary *et al.* (2015)
hp*GGLT1*	*GGLT1* (AT1G76340)	N/A	Sechet *et al.* (2018)
msr1-2	*MSR1* (AT3G21190)	SALK_075245C	Wang *et al.* (2013)
mur2	*FUT1* (AT2G03220)	N8565	Reiter *et al.* (1997)
mur3	*MUR3* (AT2G20370)	N8566	
PGX2^{AT}	*PGX2* (AT1G78400)	N/A	Xiao *et al.* (2016)
pme17	*PME17* (AT2G45220)	SALK_059908	Sénéchal *et al.* (2014)
pme31	*PME31* (AT3G29090)	SALK_074820	Yan *et al.* (2018)
pme41	*PME41* (AT4G02330)	SALK_008958C	Qu *et al.* (2011)
pmr5	*PMR5* (AT5G58600)	N6579	Chiniquy *et al.* (2019)
prc1	*CESA6* (AT5G64740)	N6203	Fagard *et al.* (2000)
rwa2	*RWA2* (AT3G06550)	SALK_078630	Nafisi *et al.* (2015)
sfr8	*MUR1* (AT3G51160)	N/A	Panter *et al.* (2019)
xxt1 xxt2	*XXT1* (AT3G62720)	N16349	Cavalier *et al.* (2008)
	XXT2 (AT4G02500)		

MS supplemented with 0.1 mM potassium chloride (KCl). pH was adjusted to 5.8 with 0.1 M KOH.

2.1.2 Mature plants

10-day old seedlings were transferred to individual peat pellets (44 mm diameter; LBS Horticulture; https://www.lbsbuyersguide.co.uk) in plastic trays. Trays were wrapped in cling film to preserve high levels of humidity and transferred to a purpose-built growth room with an LD cycle of 12:12 h, a temperature of 20°C and a maximum relative humidity of 70%. Cling film was removed after 2 days and plants were allowed to grow for a further 20-26 days so that, upon experimentation, mature plants were 5 weeks (± 3 days) old. Plants were watered with tap water (unless otherwise stated) twice per week throughout this period.

For cold acclimation, mature plants were transferred to an MLR-351 environmental test chamber (Sanyo) with an LD cycle of 10:14 h and a temperature of 5°C for 24 h or 2 weeks as necessary.

For boron supplementation, plants were grown as above but watered twice per week with deionised water (dH2O) containing 0.1 mM KBO. Control plants were watered with dH2O containing 0.1 mM KCl.

For isoxaben (ISX) treatment, plants were grown as above but sprayed with 5 nM ISX, initially dissolved in dimethyl sulfoxide (DMSO) and diluted further in dH2O, twice per week beginning two weeks before experimentation. Control plants were sprayed with an equivalent amount of diluted DMSO.

2.2 Freezing Assays

2.2.1 Freezing recovery assay

Plants were grown as previously described. At five weeks old (or longer for acclimated plants), plants were randomly positioned onto a large tray and placed into an MIR-254 Incubator (Sanyo) at a previously determined freezing temperature in the dark for 24 h. Plants were then transferred to an MLR-351 environmental test chamber (Sanyo) with a LD cycle of 10:14 h and a temperature of 5°C for 24 h to allow for defrosting. Plants were then transferred to a purpose-

built growth room with an LD cycle of 12:12 h, a temperature of 20°C and a maximum relative humidity of 70%, and watered as necessary, with recovery assessed after 5-7 days.

2.2.2 Electrolyte leakage assay

For quantitative assessment of freezing sensitivity by measurement of leaf electrolyte leakage, six mature plants (grown as previously described) per experimental group per temperature were used in an assay adapted from Gilmour *et al.* (1988). Individual biological replicates consisted of three 8-mm discs prepared from individual leaves using a cork borer. In cases where leaves were too small to prepare leaf discs from, whole leaves were used across the experiment. In both cases, leaves were matched as closely as possible for size and age. Leaf material was transferred to individual test tubes which had been cooled on ice. Leaf material was washed with 5 ml of cold dH_2O. Water was removed from the tubes after 15 mins and tubes were placed randomly into a freezing bath (Clifton) set at -2°C. After 1 h, a small (1-2 mm) ice chip made from dH_2O was placed into each tube to initiate freezing. Tubes were left at -2°C for a further 2 h. The freezing bath was then set to the first test temperature and, 1 h after reaching temperature, six tubes per experimental group were removed and placed on ice. The bath was set to the second test temperature and, after 1 h, six more tubes per experimental group were removed and placed on ice. Finally, the bath was set to the final test temperature and, after 1 h, the final six tubes per experimental group were removed and placed on ice. All tubes were held at 5°C so that samples could thaw overnight. The following morning 5 ml of dH_2O was added to each tube and tubes were shaken at 200 rpm at room temperature for 3 h. The liquid from each tube was decanted into clean, respective tubes and a handheld conductivity meter (Mettler Toledo; https://www.mt.com/gb/en/home.html) was used to measure the conductivity (µS) of each sample. The tubes containing leaf material were frozen at -80°C for 1 h to allow complete leakage of electrolytes. After thawing, the liquid from each new tube was decanted back into its original tube, still containing leaf material, and the tubes were shaken again at 200 rpm at room temperature for 3 h. Leaf material was removed from each tube and the conductivity measured again. Percentage

electrolyte leakage was calculated for each sample by expressing the first reading as a percentage of the second reading.

A video tutorial of the electrolyte leakage assay can be viewed here: https://drive.google.com/file/d/1zmdof63T4rtxuNF4hQ3H_Zsq5BoNvdqg/view?usp=share_link.

2.2.3 Infrared video thermography of plant freezing

Plants were grown as previously described. At five weeks old (or longer for acclimated plants), plants were transferred to a Fitotron Modular Plant Growth Chamber (Weiss Technik; https://www.weiss-technik.co.uk/en) programmed to run a gradual freezing protocol. Plants were imaged from above during freezing using a FLIR A700-EST infrared (IR) camera with a 24° kit lens and at a rate of 1 frame per second. (Teledyne FLIR; https://www.flir.co.uk/). The camera was mounted and fixed to a shelf inside of the chamber using a Manfrotto Magic Arm and Super Bracket (**Figure 2.1**; Manfrotto; https://www.manfrotto.com/). The camera was operated remotely from outside of the chamber using FLIR Research Studio (https://www.flir.co.uk/products/flir-research-studio/). IR images were processed and analysed also using FLIR Research Studio.

2.3 Cell-Wall Analysis

2.3.1 Comprehensive microarray polymer profiling

Changes in cell-wall composition during cold acclimation were analysed using an adaptation of the comprehensive microarray polymer profiling (CoMPP) method described by Moller *et al.* (2007).

2.3.1.1 Plant material

Mature plants were cold-acclimated as above for either 24 h or 2 weeks. For control groups, plants were grown at ambient temperature for an equivalent amount of time. Six plants per experimental group were used. Entire rosettes from each plant were harvested and flash-frozen in liquid nitrogen. Frozen leaf tissue was ground into a fine powder using a mortar and pestle and each sample was weighed and stored at -80°C in separate 1.5-ml centrifuge tubes.

Figure 2.1: Infrared video thermography (IRVT) experimental setup. A FLIR A700-EST was mounted on a Manfrotto Magic Arm and Super Bracket. The mounted camera was clamped onto a shelf inside a Weiss Technik Fitotron Modular Plant Growth Chamber. Trays of plants were placed onto the floor of the chamber directly under the camera lens for imaging.

2.3.1.2 Preparation of alcohol-insoluble residue

To each tube of frozen, ground leaf tissue was added 15 µl of 70% ethanol per mg of tissue, along with a glass bead to aid pellet resuspension. Samples were vortexed thoroughly, ensuring complete resuspension of ground tissue, then centrifuged at 14,000 rpm for 10 mins. The supernatant was discarded and replaced by 15 µl of 1:1 methanol:chloroform per mg of tissue. Samples were vortexed and centrifuged as above. The supernatant was discarded and replaced by 15 µl of acetone per mg of tissue. Samples were vortexed and centrifuged as above. The supernatant was discarded and tubes were left to air-dry until alcohol-insoluble residue (AIR) formed as a dry, white powder.

2.3.1.3 Cell-wall extraction

Approximately 10 mg of AIR was added to a 2-ml screw-cap microfuge tube, along with a small glass bead, for each sample. To each tube was then added 30 µl of 50 mM, 7.5 pH diamino-cyclo-hexane-tetra-acetic acid (CDTA) per mg of AIR. Samples were shaken at 27 Hz for 2 mins and then 10 Hz for a further 2 h using a TissueLyser II (QIAGEN; https://www.qiagen.com/gb). Samples were centrifuged at 14,000 rpm for 10 mins. Supernatants were decanted into clean 1.5-ml centrifuge tubes and refrigerated for later use. 30 µl of 4 M NaOH + 0.1% $NaBH_4$ per mg of AIR was added to each tube containing the pellets. Samples were shaken and centrifuged as above. Supernatants were then decanted and refrigerated as above, so that there were two separate cell-wall extractions per sample.

2.3.1.4 Sample printing

CDTA and NaOH cell-wall extractions were serially diluted 2-, 10-, 50- and 250-fold in phosphate-buffered saline (PBS; 140 mM NaCl, 2.7 mM KCl, 10 mM Na_2HPO_4, 1.7 mM KH_2PO_4, pH 7.5). A total of 40 µl of each dilution was added to individual wells on a 384-well microtiter plate (Starlab; https://www.starlabgroup.com). India calligraphy ink was used as a marker for the outline of the arrays; 40 µl (diluted 20-fold with PBS) was added to the appropriate wells. The microtiter plate was spun down to remove bubbles from wells and loaded into a Marathon Argus Inkjet Microarrayer (Arrayjet;

https://www.arrayjet.co.uk), along with a nitrocellulose membrane, and the samples were printed as microarrays.

2.3.1.5 Monoclonal antibody probing of microarrays

After printing, the membrane was cut into individual arrays. Arrays were incubated in 5% (w/v) milk protein (MP; skimmed milk powder) in Tris-buffered saline (TBS) + Tween-20 (TBST; 20 mM Tris-HCl, 140 mM NaCl, 0.1% Tween-20 (v/v), pH 7.5) for 1 h at room temperature to block all binding sites. Meanwhile, 6-well plates were prepared containing various primary monoclonal antibodies (mAbs; http://www.plantprobes.net/index.php) diluted 10-fold in MP/TBST (one mAb per well). **Table 2.1** lists the mAbs used in this experiment. Arrays were incubated in primary mAb for 2 h whilst rocking gently at room temperature. Arrays were then rinsed with cold tap water and washed extensively in TBST (placed in a well containing TBST and rocked gently for 30 mins at room temperature, replacing TBST halfway through). Arrays were incubated in a secondary antibody (anti-rat lgG coupled to alkaline phosphatase) diluted 1,000-fold in MP/TBST. Arrays were then placed in wells containing tap water and rocked gently at room temperature for 30 mins. Arrays were developed by submerging in alkaline-phosphatase developing solution (1:1 mixture of nitro-blue tetrazolium (NBT) and 5-bromo-4-chloro-3'-indolyphosphate (BCIP) diluted 100-fold in TBS, prepared immediately prior to use). Alkaline phosphatase catalyses the production of a black-purple indoxyl precipitate from NBT and BCIP; at this point, or after 30 mins, the reaction was stopped by submerging arrays in cold tap water. Arrays were then left on paper towels to dry overnight.

2.3.1.6 Analysis of microarrays

Arrays were scanned using a CanoScan 9000F Mark II digital scanner (Canon; https://www.canon.co.uk) at the highest resolution (1,200 dpi) and the images were saved as 16-bit .tif files. The images were uploaded to Array-Pro Analyzer 6.3.1 microarray analysis software. Spot areas were defined using the grid tool and .GAL files were produced by the microarrayer during printing. Each signal spot was quantified and data was exported to Microsoft Excel for further processing. Raw

Table 2.2: List of monoclonal antibodies used in cell-wall profiling of cold-acclimation induced cell-wall modifications. Given is the probe code (LM: Leeds Monoclonal; JIM: John Innes Monoclonal), its specificity, and a reference.

Probe	Specificity	Reference
JIM5	Partially demethylesterified homogalacturonan	Clausen *et al.* (2003) Verhertbruggen *et al.* (2009a)
LM18		
LM19		
LM20	Partially methylesterified homogalacturonan	
JIM7		
LM5	Rhamnogalacturonan-I galactan	Willats *et al.* (1999)
LM15	Xyloglucan XXXG motif	Marcus *et al.* (2008)
LM11	Heteroxylan	McCartney *et al.* (2005)
LM28		Cornuault *et al.* (2015)
LM21	Heteromannan	Marcus *et al.* (2010)
LM1	Extensin	Smallwood *et al.* (1995)
JIM11		Smallwood *et al.* (1994)
JIM12		
JIM20		
LM2	Arabinogalactan protein	Yates *et al.* (1996)
LM14		Moller *et al.* (2008)

intensity values were normalised as a percentage of the highest value from the entire data set.

2.3.2 Polyacrylamide gel electrophoresis

2.3.2.1 Preparation of alcohol-insoluble residue

Seedlings were grown as above. At 10 days old, 6-8 seedlings were collected in a 1.5-ml microcentrifuge tube and flash-frozen in liquid nitrogen. Frozen seedlings were ground to a fine powder using an electronic micropestle (Cole-Palmer; https://www.coleparmer.co.uk). AIR was then prepared as above.

2.3.2.2 Cell-wall digestion

1 mg of AIR from each sample was incubated overnight in 350 µl of 1 M Na_2CO_3 at 4°C. Samples were centrifuged at 14,000 rpm for 3 mins and the supernatant discarded. Samples were washed with 100 µl of ethanol/acetic acid (75%/0.5%), then with 70% ethanol, and then 3-4 times with dH_2O, centrifuging as above and discarding the supernatant each time. Samples were then shaken at 200 rpm at room temperature overnight in 100 µl of 10 U/ml polygalacturonase (PG) from *Aspergillus aculeatus* (Megazyme; https://www.megazyme.com) in pyridine/acetic acid/0.5% chlorobutanol (1:1:98; pH 4.7).

2.3.2.3 Gel electrophoresis

Cell-wall rhamnogalacturonan-II (RG-II) content was analysed by polyacrylamide gel electrophoresis (PAGE). A 26.4% polyacrylamide gel was prepared by combining the following reagents in a 50-ml centrifuge tube: 1.251 ml of 1.5 M 2-amino-2-(hydroxymethyl)-1,3-propanediol (Tris) buffer + HCl (pH 8.8), 4.995 ml of AccuGel (a 40% solution of 29:1 acrylamide/bis acylamide (National Diagnostics; https://www.nationaldiagnostics.com)), 70.05 µl of 10% ammonium persulfate (APS), and 5.85 µl of tetramethylethylenediamine (TEMED; Thermo Fisher; https://www.thermofisher.com). The reagents were mixed by pipetting and then pipetted into the gel apparatus using a 10-ml tip. After the gel had dried, the apparatus was placed into a gel tank which was filled with an electrode buffer (50 mM Tris/38 mM glycine in dH_2O). Samples were centrifuged at 14,000 rpm for 3 mins and 10 µl of the supernatant was combined with 2 µl of loading buffer (0.63

M Tris + HCl/0.25% w/v bromophenol blue/50% glycerol). Samples were loaded into gel wells and electrophoresed at 200 V, 50 W, 80 mA at room temperature for 120 mins. The gel was removed from the tank and fixed in ethanol/acetic acid/dH_2O (4:1:5), shaking gently for 30 mins, before washing three times with dH_2O for 1 min per wash. The gel was treated with 400 µM sodium thiosulphate for 1 min and then washed with dH_2O a further three times. The gel was stained with 6 mM $AgNO_3$/10 mM formaldehyde for 20 mins and then washed with dH_2O twice for 20 secs per wash. To develop colour, the gel was treated with 0.28 M Na_2CO_3/8 µM sodium thiosulphate/64 mM formaldehyde whilst shaking gently until the desired colour strength was reached. Colour development was stopped by treating the gel with a stopping solution (0.33 M Tris/2% acetic acid). Finally, the gel was scanned with a Perfection 3490 Photo digital scanner (Epson; https://www.epson.co.uk) for analysis.

2.3.3 Analysis of cell-wall porosity

Cell-wall porosity of leaf tissue was quantified using an adaptation of a fluorescence quenching assay as described by Liu *et al.* (2019a). Briefly, epidermal peels were stained with a fluorescent membrane dye and either imaged immediately or treated with a fluorescence quencher before imaging. Average fluorescence intensity values were calculated for both sets of images. As the quenching solution consists of relatively large molecular quenchers, it can be prevented from accessing the fluorescently-stained membrane based on how porous the cell wall is. The reduction in fluorescence after quenching, therefore, can be used as a quantification of cell-wall porosity.

2.3.3.1 Preparation of epidermal peels

Mature plants were grown for 5 weeks as described above. Epidermal peels were prepared from harvested leaves using an adaptation of the Perforated-tape Epidermal Detachment (PED) method as described by Ibata *et al.* (2013). Briefly, a 1.5-mm hole-punch was used to perforate Scotch Magic Tape (3M; https://www.3m.co.uk) at regular intervals along its length. This tape was cut into strips so that each smaller strip was perforated with a single, 1.5-mm hole towards one edge. The adaxial surface of a harvested leaf was then attached to a piece of

electrical tape (PandaFix; https://pandafix.uk). A perforated strip of Scotch Magic Tape was used to detach the abaxial epidermis from the leaf by gently attaching it to the lower epidermal surface, then slowly pulling it away from the leaf. This resulted in the leaf tissue within the hole detaching along with the surrounding tissue that was firmly affixed to the Scotch Magic Tape. The epidermal peel was then immediately processed for experimentation.

2.3.3.2 FM 4-64 staining of epidermal peels

0.5 ml of 20 µM FM™ 4-64 Dye (N-(3-Triethylammoniumpropyl)-4-(6-(4-(Diethylamino) Phenyl) Hexatrienyl) Pyridinium Dibromide; hereafter referred to as FM 4-64; Thermo Fisher) was added to a 1.5-ml microcentrifuge tube which was cooled on ice before experimentation. An epidermal peel still attached to its Scotch Magic Tape strip was submerged in the tube containing FM 4-64, still on ice, for 3 mins. The peel was then transferred consecutively to two wells of a 6-well plate containing ice-cold dH_2O for 1 min each to remove excess dye. The PED method and staining procedure are illustrated in **Figure 2.2**.

2.3.3.3 Confocal imaging and fluorescence quenching of stained peels

A strip of Scotch Magic Tape approximately the same length as a glass microscope slide was cut in half length-ways and each half stuck to the top of the slide along each length, resulting in two slightly raised edges spanning the length of the slide, and a chamber in the middle. 4-5 smaller squares of Scotch Magic Tape were stacked on top of each other at one end of the slide. A few droplets of dH_2O were pipetted into the chamber in the middle of the three areas covered by tape. The epidermal peel was placed into the chamber and oriented parallel to the length of the slide, with the 1.5-mm perforation furthest away from the stack of tape squares. A glass coverslip was placed over the peel, resting on the two long strips of tape, and pushed back against the stack of tape squares to prevent further movement. By doing so, a small gap was created between the glass slide and coverslip to facilitate the removal and addition of solutions. A drop of Immersol (ZEISS; https://www.zeiss.co.uk) immersion oil was added to the coverslip in the region above the 1.5-mm perforation. The eyepiece was used to locate the region of interest

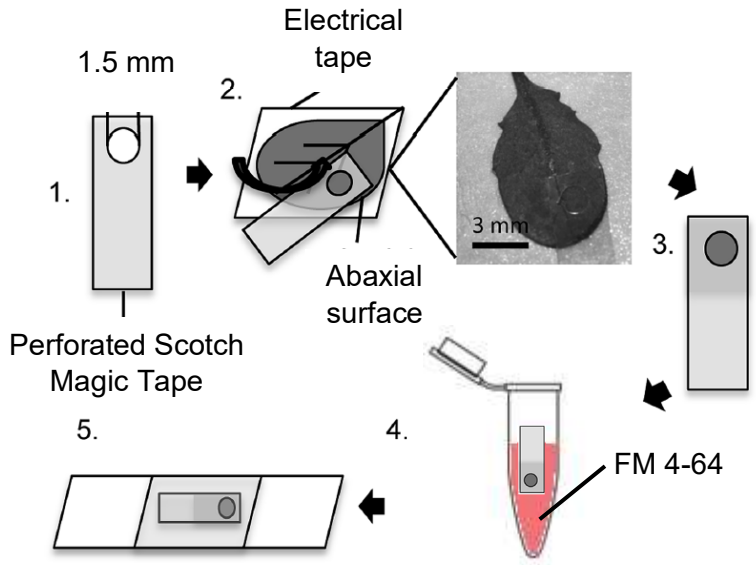

Figure 2.2: Illustration of the Perforated-tape Epidermal Detachment (PED) method and FM 4-64 staining procedure. 1. A 1.5-mm hole-punch is used to perforate a strip of Scotch Magic Tape at one end. 2. A mature leaf is attached, abaxial-side-up, to a piece of electrical tape. 3. The perforated tape is attached to the abaxial surface and pulled away to remove the epidermal layer. 4. The detached epidermal tissue is stained with FM 4-64. 5. The stained tissue is fixed to a microscope slide and imaged. Adapted from Ibata *et al.* (2013).

(ROI) using the Transmitted Light setting. An image of a group of well-stained mesophyll cells was taken in ZEN 2.6 Blue Edition (ZEISS) using the following settings: excitation at 488 nm, emission detection at 546-618 nm, 63x optical zoom, 0.5x digital zoom, 0.1% laser strength, 1 Airy unit pinhole size, 550 V of master gain, -2 digital offset, 1.0 digital gain, optimal frame size, and bidirectional scanning with 18.29 µs pixel time, no averaging, and 16 bits per pixel. After imaging, the stage was lowered and the dH_2O on the slide was drained by feeding a strip of filter paper into the chamber and holding it in place until all of the solution had been absorbed, ensuring not to move the peel or coverslip. For quenching, the dH_2O was replaced by an equivalent volume of 0.5 µM trypan blue solution (Sigma-Aldrich). After addition of the quencher to the chamber, the stage was raised once more and an image of the same ROI was taken using the same settings. Images were exported as 8-bit .tif files for analysis in ImageJ.

2.3.3.4 Image analysis

Images were imported to ImageJ (Fiji version; Abramoff *et al.* 2004, Schindelin *et al.* 2012). A box was drawn around the perimeter of the control image and an average intensity value was calculated for the whole image using the "Measure" function. An intensity value for the image taken after quenching was calculated in the same way. Intensity values were exported to Microsoft Excel for further analysis. Relative porosity was calculated for each sample by dividing control intensity by quenched intensity. Relative porosity values were averaged for each treatment or genotype.

2.3.4 Analysis of cell-wall mechanical properties

Cell-wall mechanical properties of leaf tissue were analysed by extensometry. An extensometer was built from scratch using a motorised actuator (X-LSM Miniature Motorised Linear Stage; Zaber; https://www.zaber.com/) and a load cell sensitive to 1 mN of force (ISA S-Beam Force Sensor (1-10 lb); Flintec; https://www.flintec.com/uk/). Further parts were 3D-printed with 2.85-mm Ultimaker Tough PLA Black technical filament (3DGBire; https://3dgbire.com/): a movement plate, a stationary plate, two identical sample holders, and a bridging plate. The layout of the extensometer is shown in **Figure 2.3A**.

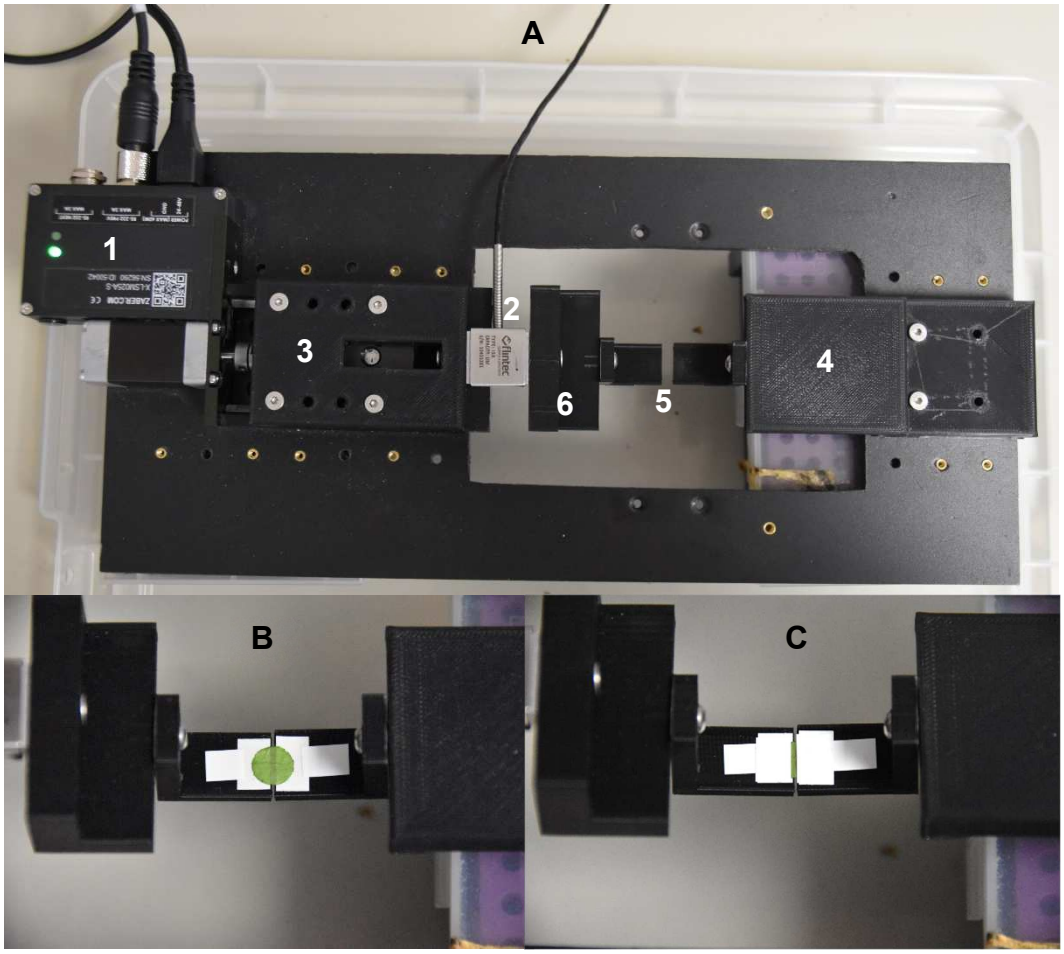

Figure 2.3: Layout of the extensometer used to measure cell-wall mechanical properties. A) Overview of the individual parts making up the extensometer. 1: motorised actuator. 2: load cell. 3: movement plate. 4: stationary plate. 5: sample holders. 6: bridging plate. A sample (8-mm leaf disc) is shown being loaded onto sample platforms that have been layered with sticky tags before (**B**) and after (**C**) securing from the top with additional sticky tags.

A video tutorial of the extensometer being set up can be viewed here: https://drive.google.com/file/d/1bjHoZQcrPA0rH7y4JRxUCtbxrYIag1CP/view?usp=share_link.

The movement plate was screwed into place at the motor-end of the actuator. The load cell was screwed into place between the movement plate and bridging plate. The sample holders were screwed into place, facing each other, between the bridging plate and the stationary plate. The actuator was powered by an X-Series 48 V/3.75 A power supply (Zaber) and connected to a laptop via an X-Series USB to Serial Converter Cable with M8 Female Plug (Zaber). The load cell was wired to an SG-Link-200 (Lord MicroStrain; https://www.microstrain.com/), a 3-channel wireless node which powered the load cell via a 1.5-V Type D battery. The node was connected wirelessly to a laptop via a WSDA-200-USB (Lord MicroStrain). Zaber Console version 2.7.4.5975 (Zaber) was used to control movement of the actuator. SensorConnect version 15.0.8 (Lord MicroStrain) was used to obtain force readings from the load cell.

Samples were individual 8-mm leaf discs prepared from mature leaf tissue. For sample loading, sample holders were positioned 0.5 mm away from each other to allow samples to be positioned evenly across sample holders. Samples were adhered to sample holders using Sidewall Tough-Tags (Diversified Biotech; https://www.divbio.com/default.aspx). Tags were used to secure samples from both above and below to ensure that they did not become unstuck while stretching. Samples were arranged so that the leaf midvein spanned across the sample holders, parallel with its edges (**Figure 2.3B**). Once secured, samples were stretched rapidly at 104 mm/s until breakage. Force data were exported from SensorConnect to Microsoft Excel for further analysis. As the load cell measures force 512 times per second by default, force data was condensed by taking an average of every ten values sequentially over each stretch. Force values were converted to percentages of the baseline measurement taken immediately before the stretch was initiated. Force curves were created for each sample by plotting percentage force values over time. Force curves were merged to create an average curve for each genotype or treatment by averaging the data points at each time point (approximately 20 ms apart). Curves were then overlaid on the same axes as their controls to allow for comparison of gradients (stiffness) and peaks (strength). The values from the peak of each graph (the point of tissue breakage) were included in separate analysis.

2.3.5 Analysis of cell adhesion

Four-day old dark-grown seedlings were immersed in 0.2 mg/ml propidium iodide (Sigma-Aldrich) in dH_2O for 10 mins and washed with dH_2O in a microcentrifuge tube prior to imaging. Samples were placed between a glass slide and coverslip separated by two additional coverslips which acted as spacers to prevent tissue crushing. Samples were imaged using a ZEISS LSM 800 confocal laser scanning microscope with a 20x objective lens. Propidium iodide excitation was performed using a 552-nm solid-state laser and fluorescence was detected at 600-650 nm. Images of stained hypocotyls were taken as z-stacks in ZEN 2.6 Blue Edition (ZEISS).

2.4 Stomatal Analysis

2.4.1 Leaf water-loss assay

Plants were grown to 5 weeks old as previously described. 24 hrs before experimentation, plants were sealed in a plastic bag still in their trays to subject them to a relative humidity of 100%. One leaf, matched closely for size, was excised from each of seven plants, blotted dry on paper towels, and weighed every hour for 8 hrs. Between measurements, leaves were placed into a weighing boat, abaxial side up, and kept at an ambient temperature of approximately 22°C and a relative humidity of approximately 50%. Leaves were weighed again after 24 hrs. Each measurement was expressed as a percentage of the original weight.

2.4.2 Morphological analysis

Plants were grown to 4 weeks old as previously described. Younger plants were used as epidermal peels can be obtained from their leaves more efficiently. One leaf was excised from each plant and placed abaxial side up onto a microscope slide with a few drops of dH_2O. The top edge and one side edge of the leaf were removed with a scalpel. An incision was made near the bottom of the leaf from the midvein to the cut edge. Curved tweezers were used to grip the top of the cut section and separate the epidermis from the rest of the leaf. The peel was then incubated in 10 mM 2-(N-morpholino)ethanesulfonic acid (MES)/50 mM KCl, pH 6.15 at 20°C for 2 hrs (Gonzales-Guzman *et al.* 2012). After incubation, peels were transferred to a

microscope slide containing a drop of MES solution and covered with a glass coverslip. Samples were imaged using a light microscope at 20x magnification. 15 stomata were imaged on each peel using a scanning method across the sample. Each experiment was repeated three times. For treatment with abscisic acid (ABA), experiments were carried out as above except, after the initial 2 h incubation, ABA was added to the incubation mixture at a final concentration of 5 µM, before incubating for a further 2 hrs. Microscopy was carried out by Dr. Paige Panter.

Images were imported into ImageJ for analysis. The scale was set according to the scale bar used when acquiring images on the microscope. Pore aperture was measured as the distance between the two inner edges of the guard cells at their widest point. Three measurements were made per stomata and an average was calculated. The elliptical tool, which can be adjusted for non-circular shapes, was used to measure the area of each stomatal pore, which was the total area inside of the inner edges of the guard cell, and total stomata area. **Figure 2.4** shows a diagrammatic representation of these measurements.

For stomatal density measurements, samples were prepared using the PED method and stained with FM4-64 as described above. They were imaged on a ZEISS LSM 800 confocal laser scanning microscope, as with the porosity assay, at 10x magnification.

2.5 Molecular Biology Methods

2.5.1 Mutant genotyping

2.5.1.1 Genomic DNA extraction

Genomic DNA (gDNA) was extracted using an adaptation of the method described by Edwards *et al.* (1991). Plant tissue was harvested and flash-frozen in liquid nitrogen in 1.5-ml microcentrifuge tubes. Samples were removed from liquid nitrogen and ground briefly using an electronic micropestle (Cole-Palmer). 400 µl of Edward's extraction buffer (200 mM Tris-HCl pH 7.5, 250 mM NaCl, 25 mM ethylenediaminetetraacetic acid (EDTA) pH 8.0, 0.5% sodium dodecyl sulphate

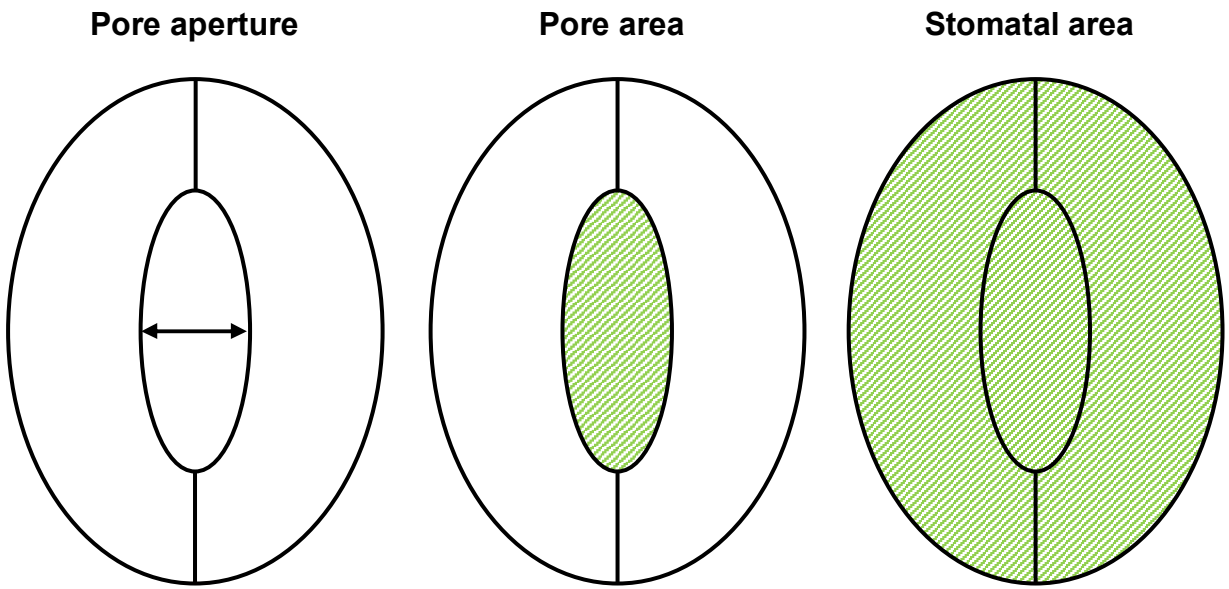

Figure 2.4: Diagrammatic representation of guard cell morphology measurements. Shown are three illustrations of stomata with open pores. Left: arrows show guard cell pore aperture. Middle: shaded area shows guard cell pore area. Right: shaded area shows total stomatal area.

(SDS)) was added to the microcentrifuge tube and the mixture was homogenised with the micropestle. Samples were vortexed briefly before centrifuging at 14,000 rpm for 1 min. 300 µl of supernatant were transferred to a new 1.5-ml microcentrifuge tube containing 300 µl of isopropanol. Samples were vortexed briefly and allowed to incubate at room temperature for 2 mins. Samples were then centrifuged at 14,000 rpm for 5 mins and the supernatant discarded. Pellets were dried for 10 mins in a Vacufuge Concentrator 5301 (Eppendorf; https://www.eppendorf.com). Pellets were then resuspended in 50 µl of TE buffer (10 mM Tris pH 8.0, 1 mM EDTA) and incubated at 5°C overnight to allow the DNA to dissolve. Samples were then stored long-term at -20°C.

2.5.1.2 Polymerase chain reaction

Amplification of DNA by polymerase chain reaction (PCR) was carried out using MyTaq™ Red Mix DNA polymerase (Bioline; https://www.bioline.com). A 50 µl reaction was prepared in a 0.5-ml microcentrifuge tube as follows: 25 µl of 2X MyTaq™ Red Mix, 1 µl each of 10 µM forward and reverse primers (final concentration 0.2 µM each), 22 µl of nuclease-free water (NFW), and 1 µl of gDNA template. Reagents were vortexed and centrifuged briefly before thermocycling in a PCR Express Thermal Cycler (Thermo Hybaid). The following programme was used: initial denaturation: 95°C for 60 secs; denaturation: 95°C for 15 secs; annealing: 15 secs at primer- and template-dependent temperatures; extension: 72°C for 15 secs. Denaturation, annealing and extension steps were repeated for 32-34 cycles.

2.5.1.3 Primers

Primer3Plus (Untergasser *et al.* 2007; https://primer3plus.com) was used to assist in primer design. Primers were designed to be a minimum of 20 bp and to have a GC content of 40-60% for optimal annealing. Primers were then synthesised by Integrated DNA Technologies (https://eu.idtdna.com/pages). Primer sequences can be found in **Appendices A & B**.

2.5.1.4 Agarose gel electrophoresis

Agarose gel electrophoresis was used to separate DNA fragments by size. 1% agarose gels were prepared by melting 0.5 g of molecular-grade agarose (Bioline) in 50 ml of 0.5X Tris-borate-EDTA (TBE) buffer (1.1 M Tris, 900 mM borate, 25 mM EDTA, pH 8.0).

Melted agarose was stained with 2 µl of Midori Green Advance DNA Stain (Nippon Genetics; https://www.nippongenetics.eu/en) before pouring into a gel tank set up with a plastic comb to create wells in the gel. The agarose was allowed to polymerise at room temperature for at least 30 mins. 0.5X TBE was used as a running buffer. 8 µl of HyperLadder™ 1kb (Bioline) was loaded into the first well and then 10 µl of PCR product was loaded into subsequent wells. Gels were electrophoresed for 60 mins at 35 mA before imaging under UV light using a Uvidoc Transilluminator (Uvitec; https://www.uvitec.co.uk).

2.5.1.5 PCR product extraction

A Monarch® DNA Gel Extraction Kit (New England Biolabs; https://www.neb.uk.com) was used to purify DNA from agarose gels for sequencing. Briefly, DNA bands were cut out and excess agarose trimmed from around the bands using a scalpel. Bands were weighed in a 1.5-ml microcentrifuge tube. Four volumes of Gel Dissolving Buffer were added to the microcentrifuge tube containing the gel slice. Samples were incubated at 50°C for 10 mins, vortexing periodically, until the gel slice was fully dissolved. Samples were loaded onto the supplied extraction column which was inserted into a 2-ml collection tube before centrifugation at 13,000 rpm for 1 min. Flow-through was discarded before addition of 200 µl of DNA Wash Buffer into the column inserted into the collection tube. Samples were centrifuged as above and the DNA wash step was repeated. Columns were transferred to a clean 1.5-ml microcentrifuge tube and DNA was eluted by addition of approximately 10 µl of DNA Elution Buffer directly to the centre of the column membrane. Samples were incubated for 1 min and then centrifuged as above. DNA concentration was measured using a NanoDrop 1000 Spectrophotometer (Thermo Fisher). Samples were stored at -20°C.

2.5.1.6 DNA sequencing

Sequencing of PCR products was carried out by Durham University DBS Genomics (https://www.durham.ac.uk/departments/academic/biosciences/research/services/dbsgenomics) using one of the primers used in PCR.

Sequence alignment was carried out using MultAlin (Corpet 1988; http://multalin.toulouse.inra.fr/multalin/).

2.5.2 Gene expression analysis

2.5.2.1 RNA extraction

For gene expression analysis, RNA was extracted from 10-14-day old seedlings, grown as described previously, using a ReliaPrep™ RNA Tissue Miniprep System (Promega; https://www.promega.co.uk). The manufacturer's protocol for non-fibrous tissue was followed. Seedlings were flash-frozen in 1.5-ml microcentrifuge tubes in liquid nitrogen and ground briefly with an electronic micropestle (Cole-Palmer). 0.5 ml of LBA Buffer supplemented with 1-thioglycerol was added to the ground plant tissue and further homogenised with the micropestle. Samples were vortexed briefly and centrifuged at 14,000 rpm for 3 mins. The supernatant was transferred to a new 1.5-ml microcentrifuge tube. 170 µl of isopropanol was added to each sample before briefly vortexing. The lysate was transferred to a Minicolumn mounted onto a collection tube and centrifuged at 14,000 rpm for 1 min. The flow-through was discarded and 500 µl of RNA Wash Solution was added to the Minicolumn before centrifuging as above for 30 secs. The flow-through was discarded and 30 µl of DNase incubation mixture (24 µl Yellow Core Buffer, 3 µl 90 mM $MnCl_2$, 3 µl DNase) was pipetted directly onto the Minicolumn membrane before incubation at room temperature for 15 mins. 200 µl of Column Wash Solution supplemented with ethanol was added to the Minicolumn before centrifugation as above for 30 secs. The Minicolumn was placed into a new collection tube and the RNA wash step was repeated. The Minicolumn was then placed into a 1.5-ml microcentrifuge tube and 30 µl of NFW was pipetted directly onto the membrane. Samples were centrifuged as above for 1 min to elute RNA. RNA was stored at -80°C.

2.5.2.2 Complementary DNA synthesis

Complementary DNA (cDNA) was synthesised from RNA using a High Capacity cDNA Reverse Transcription Kit (Applied Biosystems; https://www.thermofisher.com/uk/en/applied-biosystems.html). For each sample, solutions were prepared in a 0.5-ml microcentrifuge tube as follows: 2 µl of 10X RT Buffer, 0.8 µl of 100 mM 25X dNTP mix, 2 µl of 10X RT Random Primers, 1 µl MultiScribe™ Reverse Transcriptase, 4.2 µl NFW, and 2 µg RNA diluted up to 10 µl in NFW, giving a total reaction volume of 20 µl per sample. Two control reaction mixtures were also prepared: a no reverse transcriptase (NRT) control, containing 1 µl of NFW instead of MultiScribe™ Reverse Transcriptase, and a no template control (NTC), containing 10 µl of NFW instead of diluted RNA. Samples were vortexed and centrifuged briefly before being placed in a PCR Express Thermal Cycler (Thermo Hybaid). The following temperature profile was used to carry out cDNA synthesis: 25°C for 10 mins, 37°C for 2 hrs, 85°C for 5 secs. cDNA was diluted 1:50 in NFW and stored at -20°C.

2.5.2.3 Quantitative PCR

Quantitative PCR (qPCR) was used to carry out gene expression analysis. 96-well plates (Starlab) were prepared using triplicate wells for each sample and included NRT and NTC controls as described above. Each well contained 7.5 µl of 2X GoTaq® qPCR Master Mix (Promega), 0.9 µl of 5 µM forward and reverse primers, 0.7 µl NFW, and 5 µl of cDNA diluted 1:50 in NFW as described above. *PEX4* was used as an endogenous control gene (Moffat *et al.* 2012). Gene expression analysis was carried out using the ΔΔCt method as described by Applied Biosystems (https://assets.thermofisher.com/TFS-Assets/LSG/manuals/MAN0014820_RelativeQuant_UG.pdf). Error bars represent minimum and maximum relative quantification (RQ_{MIN} and RQ_{MAX}) and represent the acceptable error margin for a 95% confidence level according to the student's t-test.

Details of individual mutant genotyping can be found in **Appendices C-P**.

2.6 Statistical Analysis

All statistical analysis was carried out in Minitab Statistical Software (https://www.minitab.com/en-us/).

2.6.1 Freezing recovery assay

Percentage survival values from at least three biological replicate experiments were arcsine-transformed so that they followed a normal distribution. A linear mixed effects model, with genotype and/or treatment specified as fixed factors and experiment number specified as a random factor, was fitted to confirm that there was no significant variation in datasets between replicate experiments. Equal variance was also confirmed in the data between genotypes or treatments before analysis. For freezing recovery assays with two genotypes or treatments, 2-sample t tests were carried out on the datasets to identify significant differences in mean survival values between genotypes or treatments. For assays with three or more genotypes, one-way ANOVAs were carried out on datasets to determine the effect of genotype on survival. Post-hoc Tukey tests were carried out on datasets to identify significant differences in mean percentage survival between pairs of genotypes. For the freezing recovery assays of cold-acclimated or boron-supplemented plants, a general linear model was fitted with treatment/treatment length or genotype/treatment specified as interaction factors, respectively. Post-hoc Tukey tests were then carried out.

2.6.2 Electrolyte leakage assay

Percentage electrolyte leakage values from at least three biological replicate experiments were arcsine-transformed so that they followed a normal distribution. A linear mixed effects model, with genotype and/or treatment specified as fixed factors, and experiment number specified as a random factor, was fitted to the data at each temperature to confirm that there was no significant variation in datasets between replicate experiments. Equal variance was also confirmed in the data at each temperature between genotypes or treatments before analysis. For electrolyte leakage assays with two genotypes or treatments, 2-sample t tests were carried out on the datasets at each temperature to identify significant differences in mean

electrolyte leakage values between genotypes or treatments. For electrolyte leakage assays with three or more genotypes, one-way ANOVAs were carried out on datasets at each temperature to determine the effect of genotype on electrolyte leakage. Post-hoc Tukey tests were carried out on datasets at each temperature to identify significant differences in mean electrolyte leakage between pairs of genotypes. For the electrolyte leakage assays of cold-acclimated or boron-supplemented plants, a general linear model was fitted with treatment type/treatment length or genotype/treatment specified as interaction factors, respectively. Post-hoc Tukey tests were carried out at each temperature.

2.6.3 IRVT

Statistical analysis was performed on temperature and time values from the points of supercooling and freezing. Equal variance was confirmed in the data between treatments or genotypes. 2-sample t tests were carried out to identify significant differences in degrees and times of supercooling as well as points and times of freezing.

2.6.4 CoMPP

Percentage intensity values from three biological replicate experiments were arcsine-transformed so that they followed a normal distribution. A linear mixed effects model, with treatment type and treatment length specified as fixed factors and experiment number specified as a random factor, was fitted to the data from each probe to confirm that there was no significant variation in datasets between replicate experiments. Equal variance was also confirmed in the data from each probe between treatment types and lengths before analysis. One-way ANOVAs were carried out on datasets from each probe to determine the effect of treatment type and treatment length on probe binding efficacy. Post-hoc Tukey tests were carried out to identify significant differences in mean percentage intensity values between pairs of experimental groups.

2.6.5 Porosity assay

A linear mixed effects model, with genotype or treatment specified as a fixed factor and experiment number specified as a random factor, was fitted to the pooled

relative porosity data to confirm that there was no significant variation in datasets between replicate experiments. Equal variance was also confirmed in the data between genotypes or treatments before analysis. 2-sample t tests were carried out on datasets to identify significant differences in mean relative porosity values between genotypes or treatments

2.6.6 Extensometry assay

Percentage maximum relative tensile force values from three biological replicate experiments were arcsine-transformed so that they followed a normal distribution. A linear mixed effects model, with genotype or treatment specified as a fixed factor and experiment number specified as a random factor, was fitted to the data from the peak of each average force curve to confirm that there was no significant variation in datasets between replicate experiments. Equal variance was also confirmed in the data between genotypes or treatments before analysis. 2-sample t tests were carried out on arcsine-transformed datasets to identify significant differences in mean percentage maximum relative tensile force values between genotypes or treatments.

2.6.7 Leaf water-loss assay

Percentage mass values from at least three biological replicate experiments were arcsine-transformed so that they followed a normal distribution. A linear mixed effects model, with genotype and/or treatment specified as fixed factors and experiment number specified as a random factor, was fitted for the data at each time point to confirm that there was no significant variation in datasets between replicate experiments. Equal variance was also confirmed in the data at each time point between genotypes or treatments before analysis. For leaf water-loss assays including just two genotypes, 2-sample t tests were carried out on the datasets at each time point to identify significant differences in mean percentage mass values between genotypes. For the leaf water-loss assays of boron-supplemented plants, a general linear model was fitted with genotype/treatment specified as an interaction factor. Post-hoc-Tukey tests were carried out at each time point.

2.6.8 Stomatal density

A linear mixed effects model, with genotype specified as a fixed factor and experiment number specified as a random factor, was fitted to the pooled stomatal density data to confirm that there was no significant variation in datasets between replicate experiments. Equal variance was also confirmed in the data between genotypes before analysis. A 2-sample t test was carried out to identify significant differences in mean stomatal density values between genotypes.

2.6.9 Guard cell morphology

A linear mixed effects model, with genotype and treatment specified as fixed factors and experiment number specified as a random factor, was fitted to the pooled guard cell morphology data (separated by measurement type) to confirm that there was no significant variation in datasets between replicate experiments. Equal variance was also confirmed in the data between genotypes and treatments before analysis. A general linear model was fitted to the data for each measurement type with genotype/treatment specified as an interaction factor. Post-hoc Tukey tests were carried out to identify significant differences in measurements of guard cell morphology between genotypes/treatments.

Chapter 3

Cold acclimation induces cell-wall modifications that improve freezing tolerance

3.1 Introduction

As discussed in **Section 1.2,** most perennial plants cannot avoid ice nucleation at freezing temperatures and must tolerate ice formation in their tissues. This is facilitated by first undergoing cold acclimation: widespread transcriptional reprogramming brought about by extended exposure to low, non-freezing temperatures, leading to a range of biochemical, metabolic and physiological changes that enhance freezing tolerance. As established in **Section 1.3.3**, there is now a large body of evidence supporting a role for cell-wall modifications in the acquisition of freezing tolerance. This chapter aims to elucidate some of the changes that occur in the cell wall of the plant genetic model, *Arabidopsis*, during cold acclimation. Firstly, a cold acclimation protocol that clearly enhances plant freezing tolerance was established. Infrared video thermography (IRVT) was used to examine the freezing patterns of cold-acclimated leaves. The effects that the cold acclimation protocol has on the physical properties of the *Arabidopsis* cell wall were explored. Next, a range of cell-wall polysaccharides and proteins that change in abundance or structure during cold acclimation, and therefore potentially contribute to freezing tolerance, were identified. Finally, *Arabidopsis* mutants that are deficient in some of these identified cell-wall components were screened for freezing sensitivity and changes in the physical properties of their cell wall, providing additional evidence for their role in plant freezing tolerance.

3.2 Results

3.2.1 Freezing tolerance of cold-acclimated *Arabidopsis*

Freezing assays were used to verify that the cold acclimation treatments used throughout this study (continuous exposure to 5°C for 24 h or 2 weeks) induced an increase in freezing tolerance in wild-type *Arabidopsis* (Col-0).

3.2.1.1 Freezing recovery and electrolyte leakage

Mature, cold-acclimated wild-type *Arabidopsis*, along with non-acclimated controls, were subjected to freezing at -8°C for 24 h before being returned to ambient growth conditions. The capacity of the plants to recover and exhibit new growth was assessed after 1 week (**Figure 3.1A**). A linear mixed effects model confirmed that experiment number had no significant impact on data variation ($p>0.05$) so the data from three biological replicate experiments were pooled for analysis. Mean percentage survival of plants receiving each treatment was calculated from pooled data. Cold acclimation for both 24 h and 2 weeks significantly increased plant survival after freezing ($p<0.001$). After 24 h of acclimation, plant survival increased from 11% to 94%; after 2 weeks of acclimation, it increased from 6% to 100% (**Figure 3.1B**).

In order to quantify the freezing damage incurred by acclimated and non-acclimated plants, electrolyte leakage was measured in leaf tissue from plants from each group following exposure to three different sub-zero temperatures (-5, -7 and -9°C). A linear mixed effects model confirmed that experiment number had no significant impact on data variation ($p>0.2$) so the data from three biological replicate experiments were pooled for analysis. Mean percentage electrolyte leakage of plants receiving each treatment was calculated at each temperature from pooled data. At all three temperatures, cold-acclimated tissue had significantly less electrolyte leakage than non-acclimated tissue ($p<0.001$) and therefore incurred less severe freezing injury (**Figure 3.1C**). At each temperature, electrolyte leakage was significantly lower ($p<0.001$) in plants that had been acclimated for 2 weeks compared to those that had been acclimated for 24 h, suggesting that prolonged cold acclimation increases freezing tolerance.

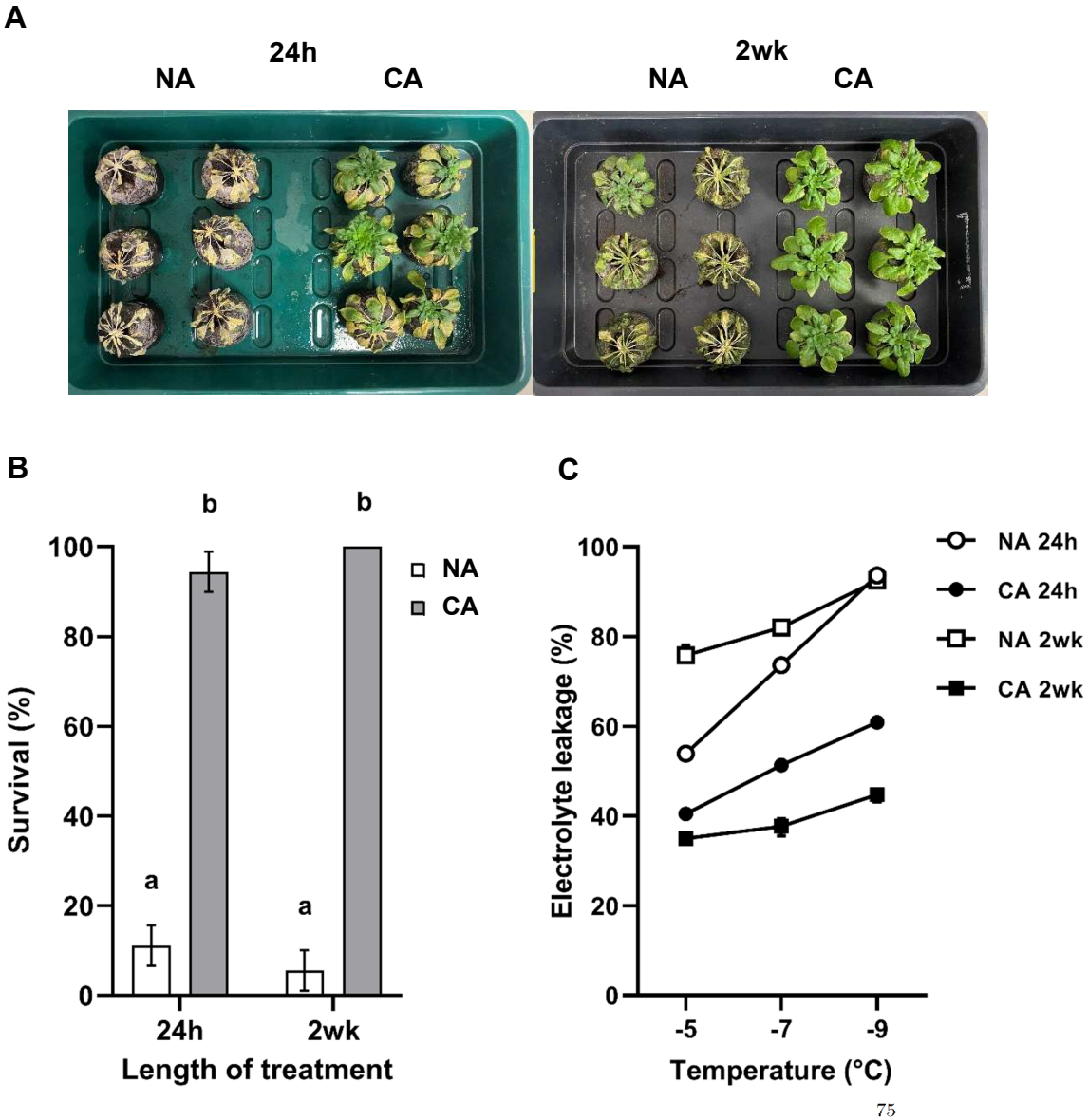

Figure 3.1: Effect of cold acclimation on freezing tolerance in *Arabidopsis*. **A)** Freezing recovery assay of mature, wild-type *Arabidopsis* cold-acclimated (CA) for either 24 h or 2 weeks (2wk) and their non-acclimated (NA) controls. Plants were subjected to freezing at -8°C for 24 h and allowed to recover under ambient conditions for one week. Photographed is one representative assay showing plants one week after freezing. **B)** Survival analysis of plants from freezing recovery assays. Plants were scored on survival based on whether regrowth of green tissue had occurred after one week. Bars represent mean percentage survival of plants from three biological replicate experiments; six plants per experimental group were used per experiment (n=18). Error bars represent one standard error of the mean of arcsine-transformed data, as is appropriate for proportional data. Means that do not share a letter are significantly different. **C)** Electrolyte leakage of mature leaf tissue from wild-type *Arabidopsis* cold-acclimated (CA) for either 24 h or 2 weeks (2wk) and their non-acclimated (NA) controls. Leaf tissue was subjected to freezing at -5, -7 or -9°C and loss of electrolytes was measured. Values represent mean percentage electrolyte leakage from three biological replicate experiments; each experiment used leaf tissue from six plants per treatment per temperature (n=18 at each point). Error bars represent one standard error of the mean of arcsine-transformed data.

3.2.1.2 Effect of leaf size and age on electrolyte leakage

Ideally, electrolyte leakage assays would involve matching leaves for both age and size between different treatments or genotypes. However, due to the effects that certain treatments and mutations can have on growth (see **Chapters 4 & 5**), this was not always possible. For example, cold-acclimated *Arabidopsis* plants tend to be substantially smaller than non-acclimated plants of the same age. Some mutants of *Arabidopsis* are so severely dwarfed that it is not possible to select leaves large enough from which to produce leaf discs, so whole leaves had to be used in electrolyte leakage assays instead (e.g. **Figure 5.10C**). Therefore, it was important to determine what effect, if any, leaf size and age has on electrolyte leakage. Electrolyte leakage assays were carried out using leaves from wild-type *Arabidopsis* divided into three groups: 1) small and young, 2) large and mid-aged, and 3) small and old (**Figure 3.2A**). **Figure 3.2B** shows a mature *Arabidopsis* rosette leaf series and how leaves were divided into groups for this experiment. A linear mixed effects model confirmed that experiment number had no significant impact on data variation ($p>0.1$) so the data from three biological replicate experiments were pooled for analysis. Mean percentage electrolyte leakage of leaves from each group was calculated at each temperature from pooled data. At -3°C, large leaves had significantly less electrolyte leakage than both groups of smaller leaves ($p<0.001$). For the smaller leaves, age had no significant impact on electrolyte leakage at this temperature ($p>0.05$). At -5°C, small/old leaves had significantly higher electrolyte leakage than both small/young and large/mid-aged leaves ($p<0.001$), which did not differ significantly from each other ($p>0.05$). At -7°C, neither leaf size nor age had a significant impact on electrolyte leakage ($p>0.1$). Due to these results, in future assays, leaves were matched as closely as possible for size in the first instance. If possible, they were also matched for age.

3.2.1.3 Infrared video thermography

In order to further explore the effect that cold acclimation has on freezing behaviour, IRVT was used to image cold-acclimated plants during freezing. Mature, two-week cold-acclimated wild-type *Arabidopsis*, along with non-acclimated controls, were subjected to freezing at -8°C and imaged with a FLIR A700-EST IR

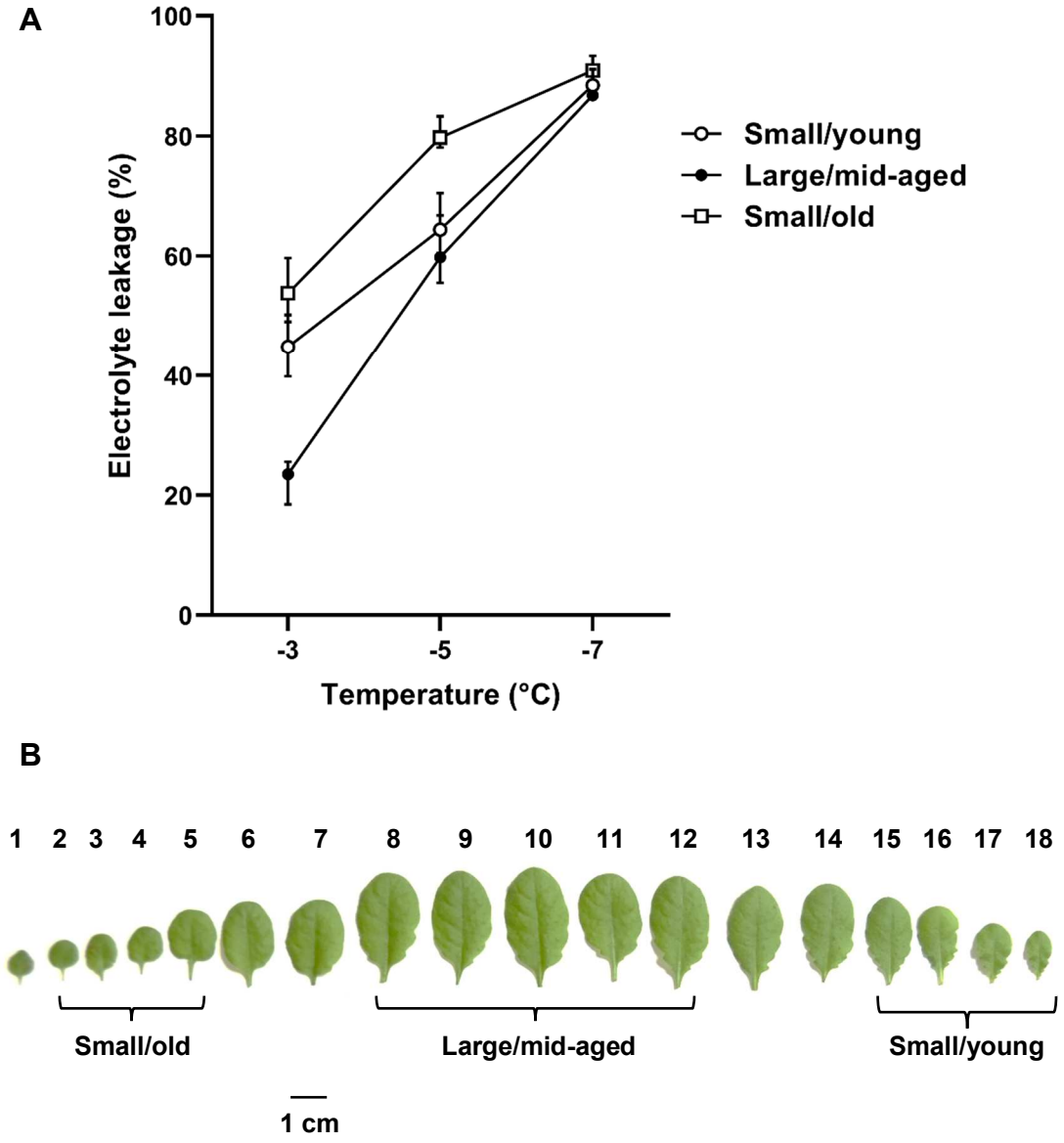

Figure 3.2: Effect of leaf size and age on electrolyte leakage after freezing. **A)** Electrolyte leakage of whole leaves of differing sizes and ages. Three sets of three leaves per mature, wild-type *Arabidopsis* plant were harvested for use in the assay, broadly divided into one of three groups: small/old, large/mid-aged, and small/young. Whole leaves were subjected to freezing at -3, -5 or -7°C and loss of electrolytes was measured. Values represent mean percentage electrolyte leakage from three biological replicate experiments; each experiment used leaves from six plants per temperature (n=18 at each point). Error bars represent one standard error of the mean of arcsine-transformed data, as is appropriate for proportional data. **B)** Rosette leaf series from a mature, wild-type *Arabidopsis* plant. Leaves are numbered based on order of emergence. For the small/old group, three of leaves 2-5 were used. For large/mid-aged, three of leaves 8-12 were used. For small/young, three of leaves 15-18 were used. Scale bar = 1 cm.

camera. The temperatures of leaves 8, 9 and 10, as well as the young inner leaves, were recorded continuously by creation of a 3-pixel by 3-pixel region of interest (ROI) in the centre of each leaf, as well as the centre of each plant to monitor the young inner leaves. Freezing patterns for each of the selected leaves were observed by 1) averaging the temperature within each ROI at each frame (plants were imaged at 1 frame per second), 2) averaging these values across leaves of the same number for different plants within the same group (for example, leaf 8 ROIs from each non-acclimated plant were included in the same average and leaf 8 ROIs from cold-acclimated plants were included in the same average), and 3) plotting these average values over time (**Figure 3.3A**). As freezing is an exothermic reaction, the point at which each leave froze was identified by a sharp increase in temperature (see **Section 1.2.5**). Interestingly, after each of the leaves had frozen, the average temperature of cold-acclimated leaves 8, 9 and 10 remained markedly higher than non-acclimated leaves for the duration of the experiment, up until they equilibrated with the temperature of the chamber at -8°C. The average temperature of the inner leaves remained largely the same for both groups of plants, except for the final 2 hours when non-acclimated leaves cooled to -8°C noticeably faster than cold-acclimated leaves. Both the average degree of supercooling and average point of freezing were also plotted for each leaf (**Figure 3.3B**). Non-acclimated leaves of each type supercooled both for longer and to a lower temperature, but the difference was not significant for any leaf ($p>0.05$). Non-acclimated leaves also froze later and at a lower temperature than cold-acclimated leaves but the difference was not significant for any leaf ($p>0.05$). The distribution of plants and the position of each ROI is shown in **Figure 3.3C**.

3.2.2 Cell-wall physical properties of cold-acclimated *Arabidopsis*

Clearly, cold acclimation induces a considerable increase in the freezing tolerance of *Arabidopsis*. Two key cell-wall physical properties, porosity and mechanics, were assessed in the leaves of cold-acclimated *Arabidopsis*. This was important in establishing a potential link between freezing tolerance and changes in these properties, as discussed in **Sections 1.3.3.1 & 1.3.3.2**.

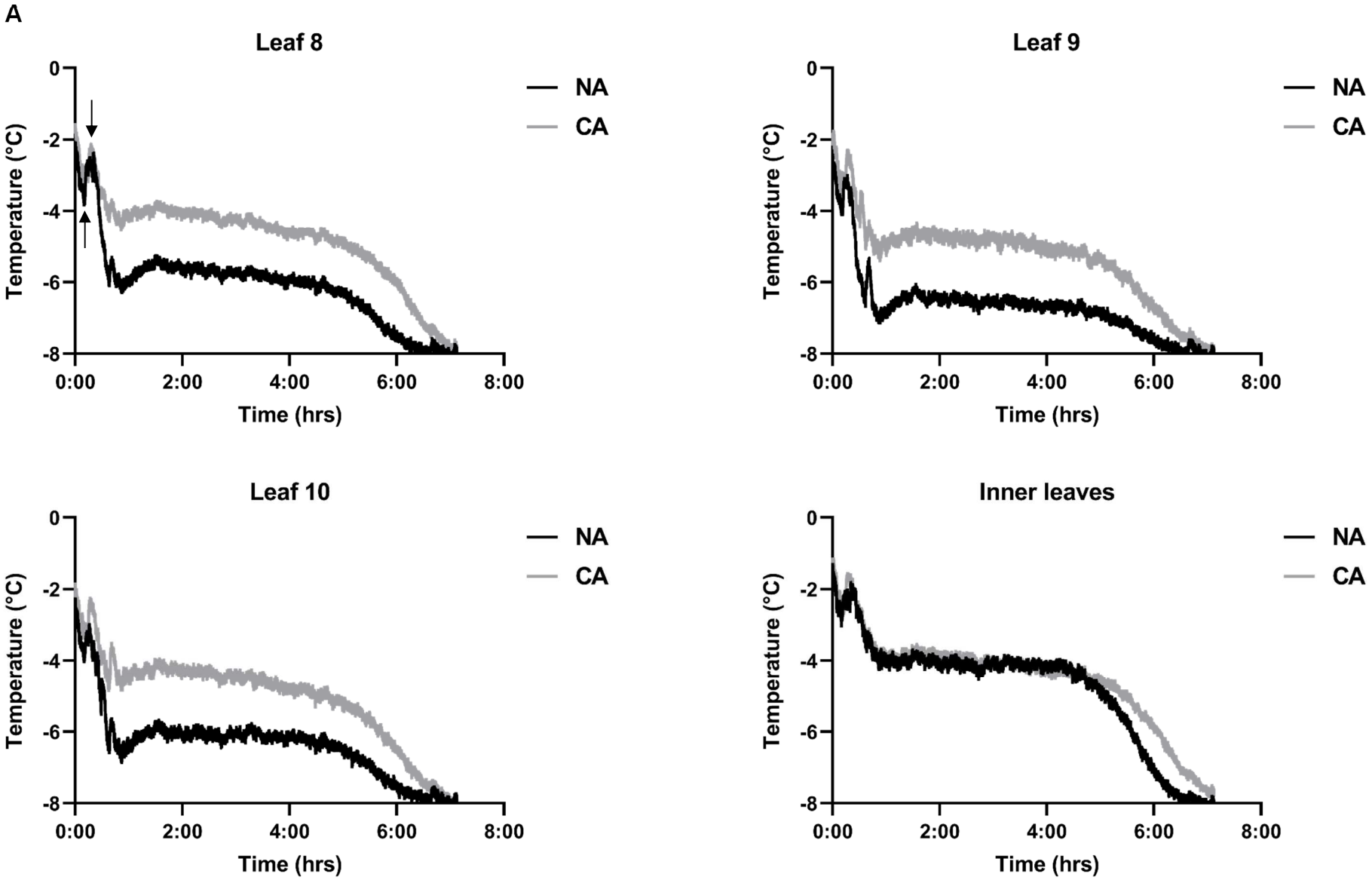
A
Leaf 8
Leaf 9
Leaf 10
Inner leaves
NA
CA
Temperature (°C)
0
-2
-4
-6
-8
0:00
2:00
4:00
6:00
8:00
Time (hrs)

B

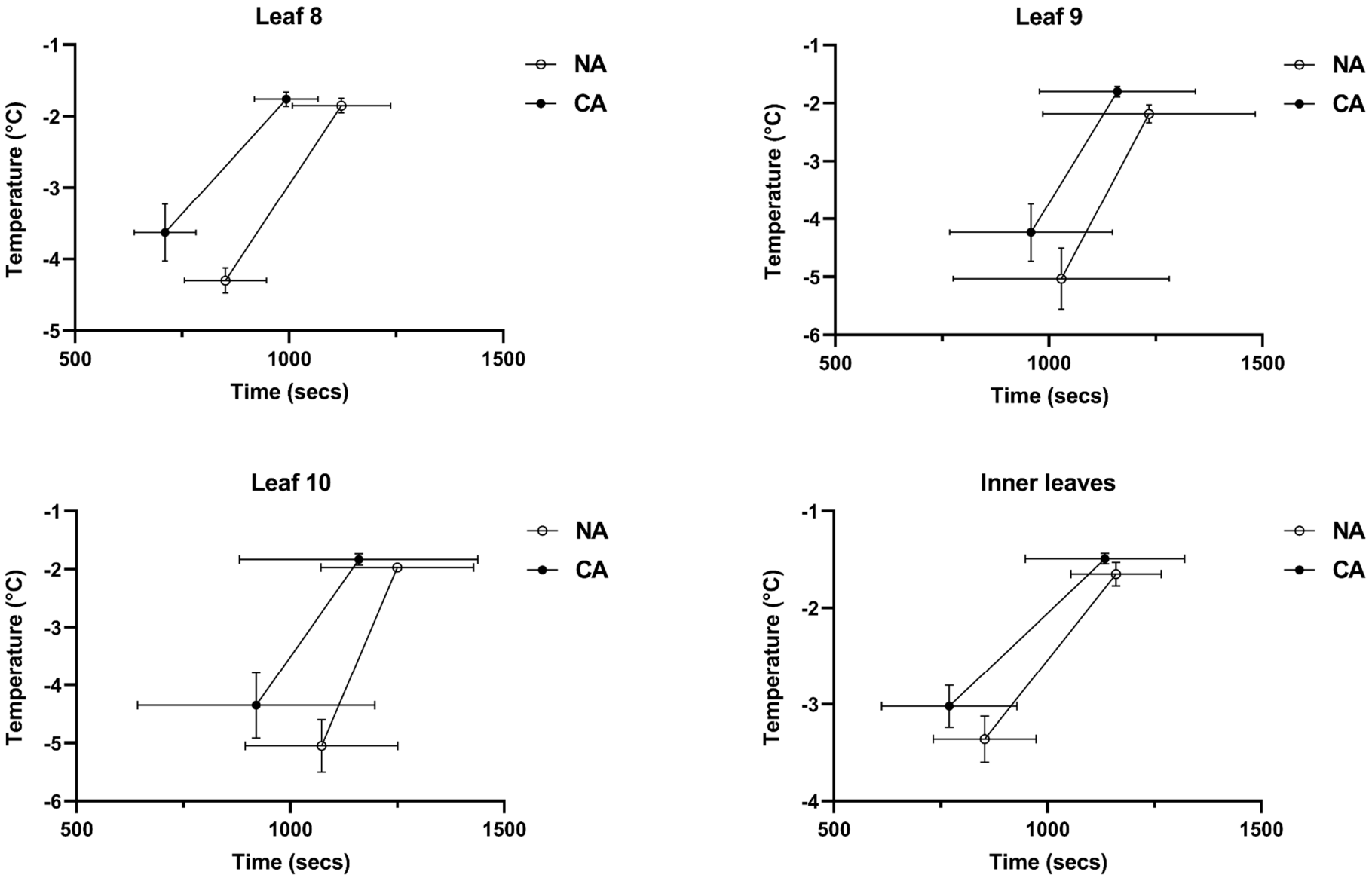
Leaf 8
Temperature (°C)
-1
-2
-3
-4
-5
500
1000
1500
Time (secs)
NA
CA
Leaf 9
Temperature (°C)
-1
-2
-3
-4
-5
-6
500
1000
1500
Time (secs)
NA
CA
Leaf 10
Temperature (°C)
-1
-2
-3
-4
-5
-6
500
1000
1500
Time (secs)
NA
CA
Inner leaves
Temperature (°C)
-1
-2
-3
-4
500
1000
1500
Time (secs)
NA
CA

C

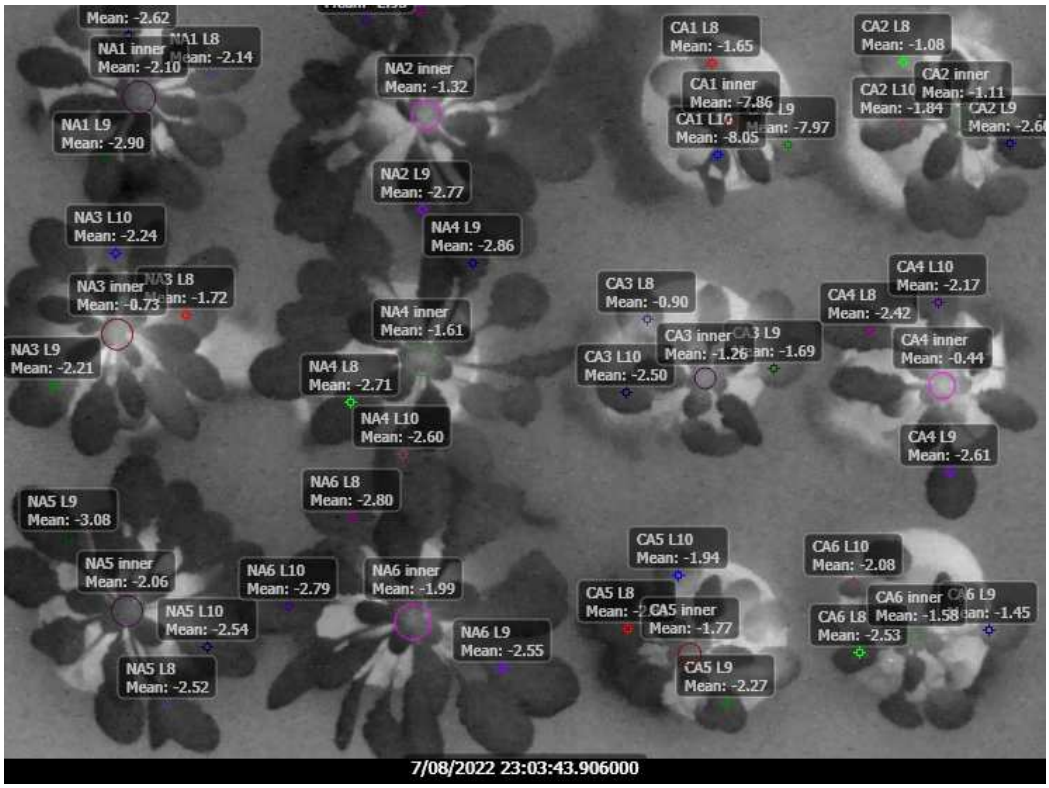

Figure 3.3: Infrared video thermography (IRVT) of cold-acclimated *Arabidopsis* during freezing. Mature, two-week cold-acclimated (CA) and non-acclimated (NA) wild-type *Arabidopsis* plants were subjected to freezing at -8°C and imaged with a FLIR A700-EST IR camera at 1 frame per second. The temperature of a 3-pixel by 3-pixel region of interest (ROI) was recorded continuously at the centre of leaves 8, 9 and 10, as well as at the young inner leaves, on each plant using FLIR Research Studio. **A)** The mean temperature of each ROI was averaged for each selected leaf at each frame between plants of the same group (NA or CA) and plotted over time. The plots, therefore, show the mean temperature of leaves of the same number over time. Although plants were placed in the chamber at an ambient temperature and gradually cooled to below freezing, only the data from shortly after the plants passed 0°C is shown. Arrows on the first graph indicate the supercooling and freezing points, which are plotted in more detail on the following page. **B)** The degree to which the leaves supercooled and the point at which they froze was averaged and plotted over time. The supercooling point was taken as the point at which plants stopped cooling and began freezing, i.e. the point immediately before the sharp increase in temperature which illustrates the exothermic process of ice nucleation. The freezing point was taken as the peak of this sharp temperature increase. Therefore, for each plot, the supercooling point is the lower, left-most point, and the freezing point is the upper, right-most point. Error bars represent one standard error of the mean. Six plants per treatment were used. **C)** Single frame from the IRVT experiment which shows the position of each ROI. L: leaf; Inner: young inner leaves.

3.2.2.1 Porosity

The cell-wall porosity of mature, cold-acclimated wild-type *Arabidopsis* was measured using a fluorescence quenching assay (**Figure 3.4A)**. The fluorescence of stained mesophyll cells was quantified (F_0;) and divided by the quantified fluorescence after quenching (F) to give a measure of relative porosity. In principle, more porous cell walls should give a higher F_0/F value as they are more permeable to the quenching agent, and thus subjected to more fluorescence quenching (Liu *et al.* 2019a). A linear mixed effects model confirmed that experiment number had no significant impact on data variation ($p>0.2$) so the data from three biological replicate experiments were pooled for analysis. Mean relative porosity of cold-acclimated and non-acclimated leaves was calculated from pooled data. Cold acclimation was found to significantly reduce cell-wall porosity ($p<0.05$). Cold-acclimated leaf tissue had a mean relative porosity of 2.92 compared to 4.76 for non-acclimated leaf tissue (**Figure 3.4B).**

3.2.2.2 Mechanical properties

The cell-wall mechanical properties of mature, cold-acclimated wild-type *Arabidopsis* were measured using extensometry. Eight-mm discs prepared from cold-acclimated and non-acclimated leaves were stretched until failure using an extensometer equipped with a load cell sensitive to 1 mN. A linear mixed effects model confirmed that experiment number had no significant impact on data variation ($p>0.5$) so the data from three biological replicate experiments were pooled for analysis. Mean percentage relative tensile force, normalised to the baseline reading taken before the stretch was initiated, was calculated from pooled data and plotted over time. Force curves for non-acclimated and cold-acclimated tissue were plotted on the same axes (**Figure 3.5A**). A steeper gradient is indicative of stiffer material, as more force is required to stretch the material an equivalent amount (Bidhendi & Geitmann 2019). The gradient of the curve for cold-acclimated tissue up to the point of failure was 0.441, compared to 0.393 for non-acclimated tissue, suggesting that cold acclimation produced higher cell-wall stiffness in leaf tissue.

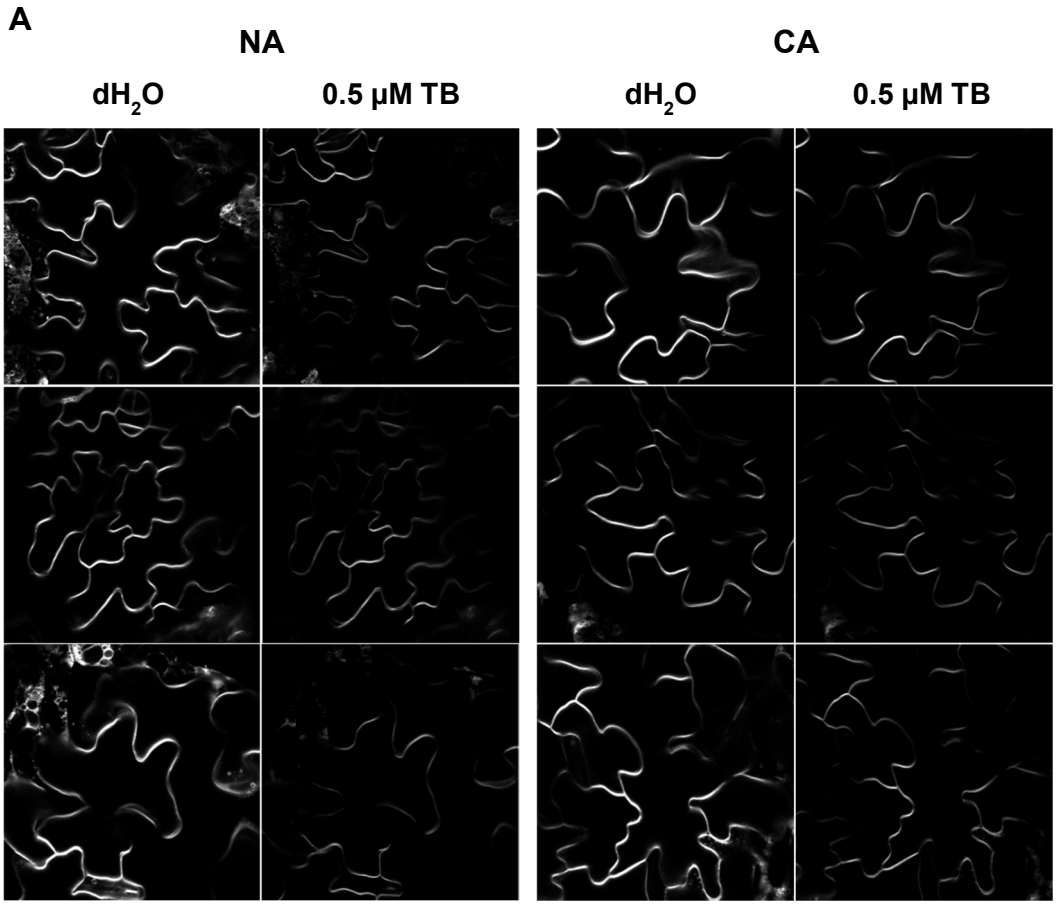

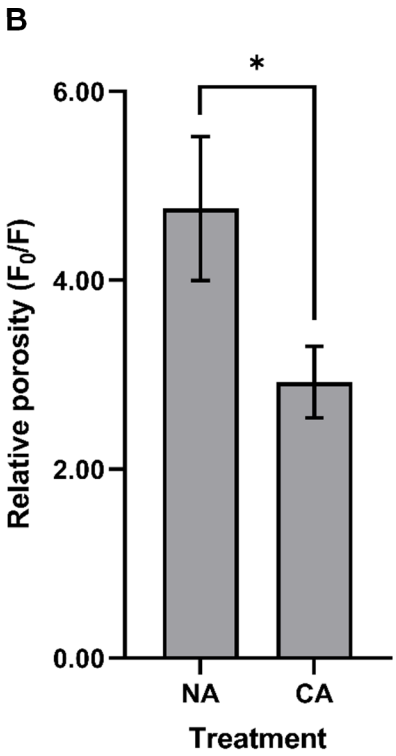

Figure 3.4: Effect of cold acclimation on cell-wall porosity. Relative porosity was calculated in non-acclimated (NA) and two-week cold-acclimated (CA) mature, wild-type *Arabidopsis* using fluorescence quenching. **A)** The plasma membranes of leaf epidermal cells were stained with a fluorescent dye and imaged before and after addition of 0.5 µM trypan blue (TB) quenching solution. Three example micrographs per treatment are shown. **B)** Fluorescence was quantified before (F_0) and after (F) addition of the quenching solution and a ratio of the two was calculated to give relative porosity (F_0/F). Bars represent mean relative porosity from three biological replicate experiments; each experiment measured porosity in three leaves from separate plants per group (n=9). Error bars represent one standard error of the mean. Asterisks indicate means that are significantly different (* $p<0.05$).

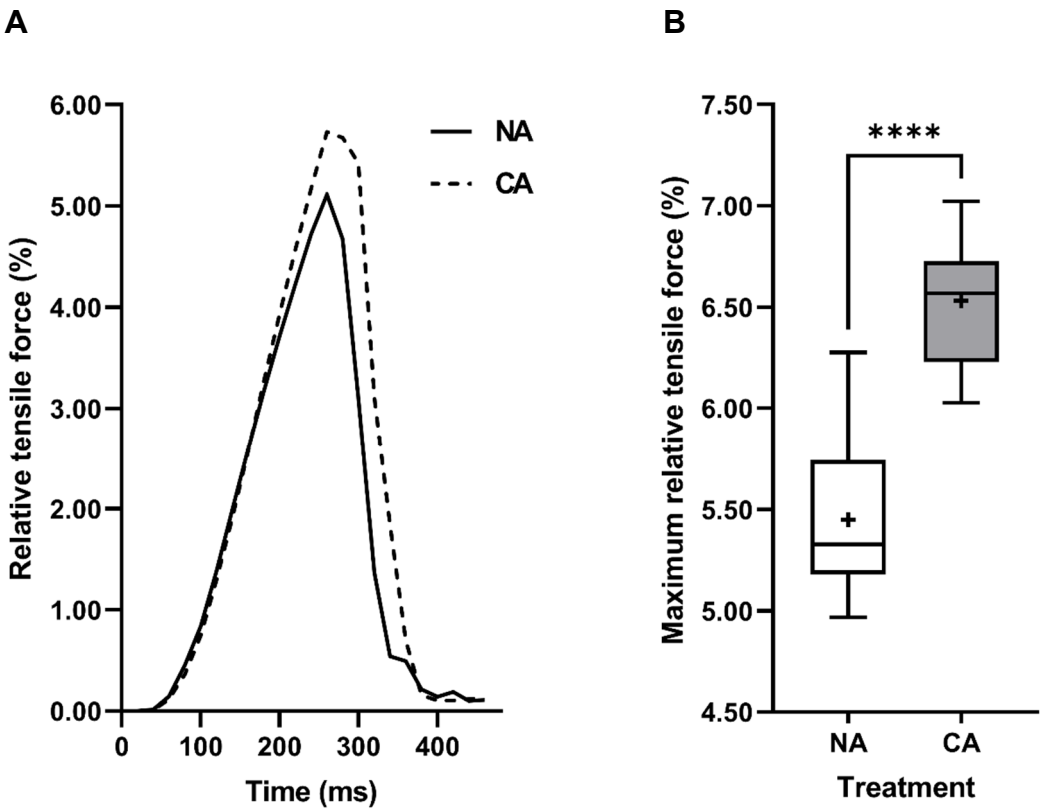

Figure 3.5: Effect of cold acclimation on cell-wall mechanical properties. Mechanical properties were assessed in non-acclimated (NA) and two-week cold-acclimated (CA) mature, wild-type *Arabidopsis* using extensometry. Leaf discs from each group were stretched until breakage and the force required to do so was recorded. Tensile force was normalised to the baseline force reading taken immediately before the stretch was initiated and converted to a percentage for each sample. Plots represent combined data for three biological replicate experiments; each experiment measured cell-wall mechanical properties in three leaf discs per group (n=9). **A)** Relative tensile force plotted over time for the duration of each stretch. A steeper gradient is indicative of stiffer material and a higher peak (more resistance to breaking pressure) is indicative of stronger material. Cold-acclimated tissue had both a steeper gradient and higher peak. **B)** Box-and-whisker plot showing the distribution of maximum tensile force values for each treatment. Values were taken from the absolute peak of each force curve, which represents the maximum tensile force that the tissue can withstand before breakage. Whiskers: maximum and minimum values; box edges: upper and lower quartiles; plus signs: mean values; horizontal lines: median values. Asterisks indicate means that are significantly different (**** $p<0.0001$).

The percentage relative tensile force values from the peak of force curves from individual samples were plotted to illustrate the mechanical strength of cold-acclimated and non-acclimated tissue (**Figure 3.5B**). Cold acclimation was found to significantly increase mechanical strength in mature leaf tissue ($p<0.0001$). The mean maximum relative tensile force for cold-acclimated tissue was 6.53% compared to 5.45% for non-acclimated tissue (means are the average absolute peaks of each individual curve, not the peak of the average curve).

3.2.3 Cell-wall profiling of cold-acclimated *Arabidopsis*

Comprehensive microarray polymer profiling (CoMPP) was carried out in order to elucidate specific components of the cell wall that change in abundance during cold acclimation. Numerous such changes have already been observed in various other species (see **Section 1.3.3.1**) so further investigation in *Arabidopsis* was warranted. The technique relies on the binding of monoclonal antibodies (mAbs) to specific epitopes present in cell-wall extractions printed as microarrays on nitrocellulose membranes. **Table 2.2** contains a list of the mAbs used in this study as well as their target epitopes. Signals from the microarrays were used to quantify the abundance of each component of interest. Cell-wall extractions from non-acclimated and cold-acclimated mature *Arabidopsis* leaf tissue were used so that cold-responsive changes in the cell wall could be observed, thereby highlighting components that may contribute to cold acclimation and, therefore, freezing tolerance. A linear mixed effects model confirmed that experiment number had no significant impact on data variation ($p>0.1$) so the data for each probe from three biological replicate experiments were pooled for analysis. Mean relative signal intensity was calculated for each probe and treatment from pooled data (**Figure 3.6**).

Three mAbs that detect extensin (EXT) were used: LM1, JIM12 and JIM20. The probes recognise and bind a short sugar residue specific to EXTs, but the structure of the epitope remains unknown (Castilleux *et al.* 2018). All three probes were used to provide some redundancy. LM1 detected significant accumulation of EXT after both 24 h and 2 weeks of cold acclimation ($p<0.001$). There was also a significant interaction effect ($p<0.05$) between treatment (NA or CA) and treatment length

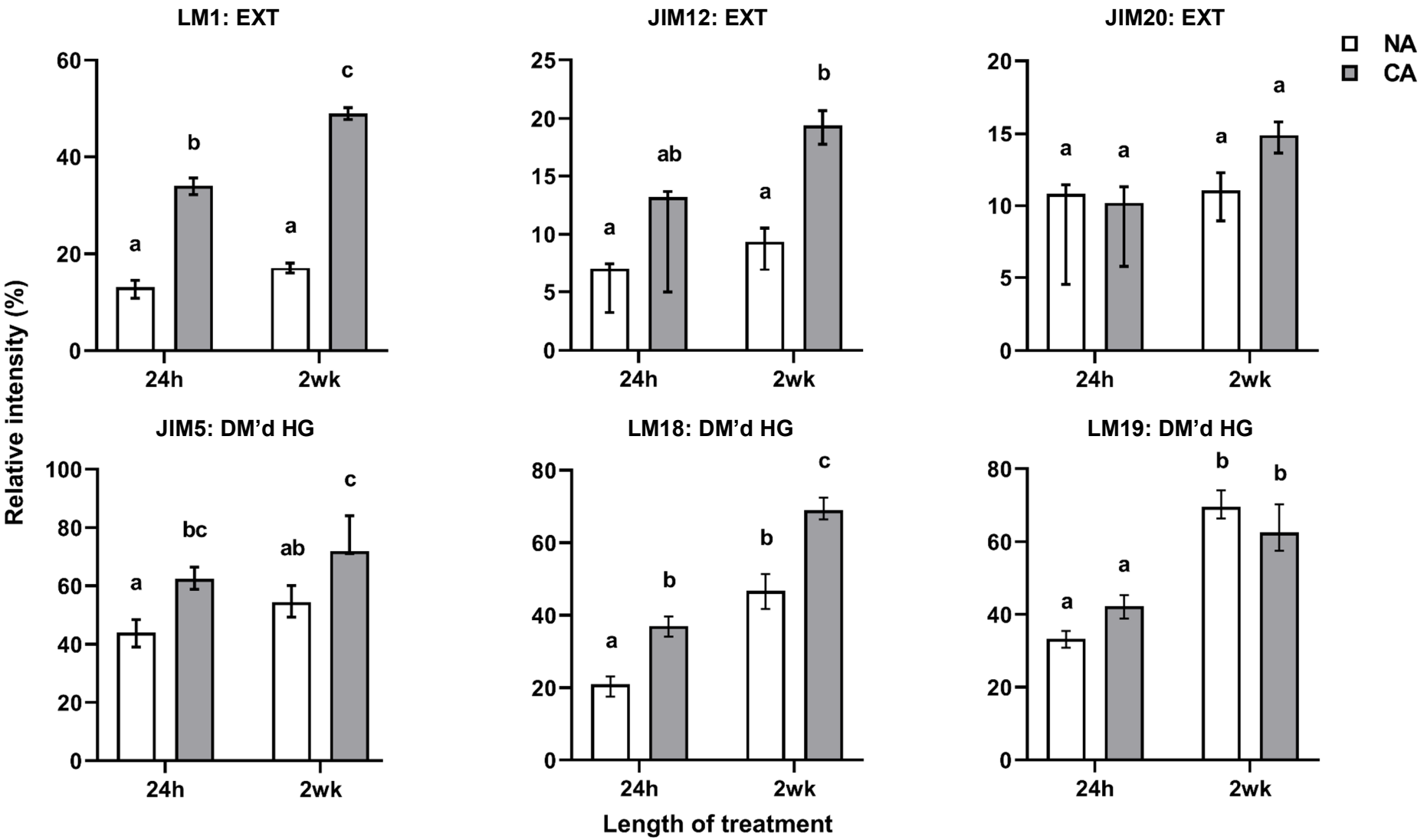
LM1: EXT
JIM12: EXT
JIM20: EXT
JIM5: DM'd HG
LM18: DM'd HG
LM19: DM'd HG
NA
CA
Relative intensity (%)
Length of treatment
24h
2wk
a
b
c
ab
bc

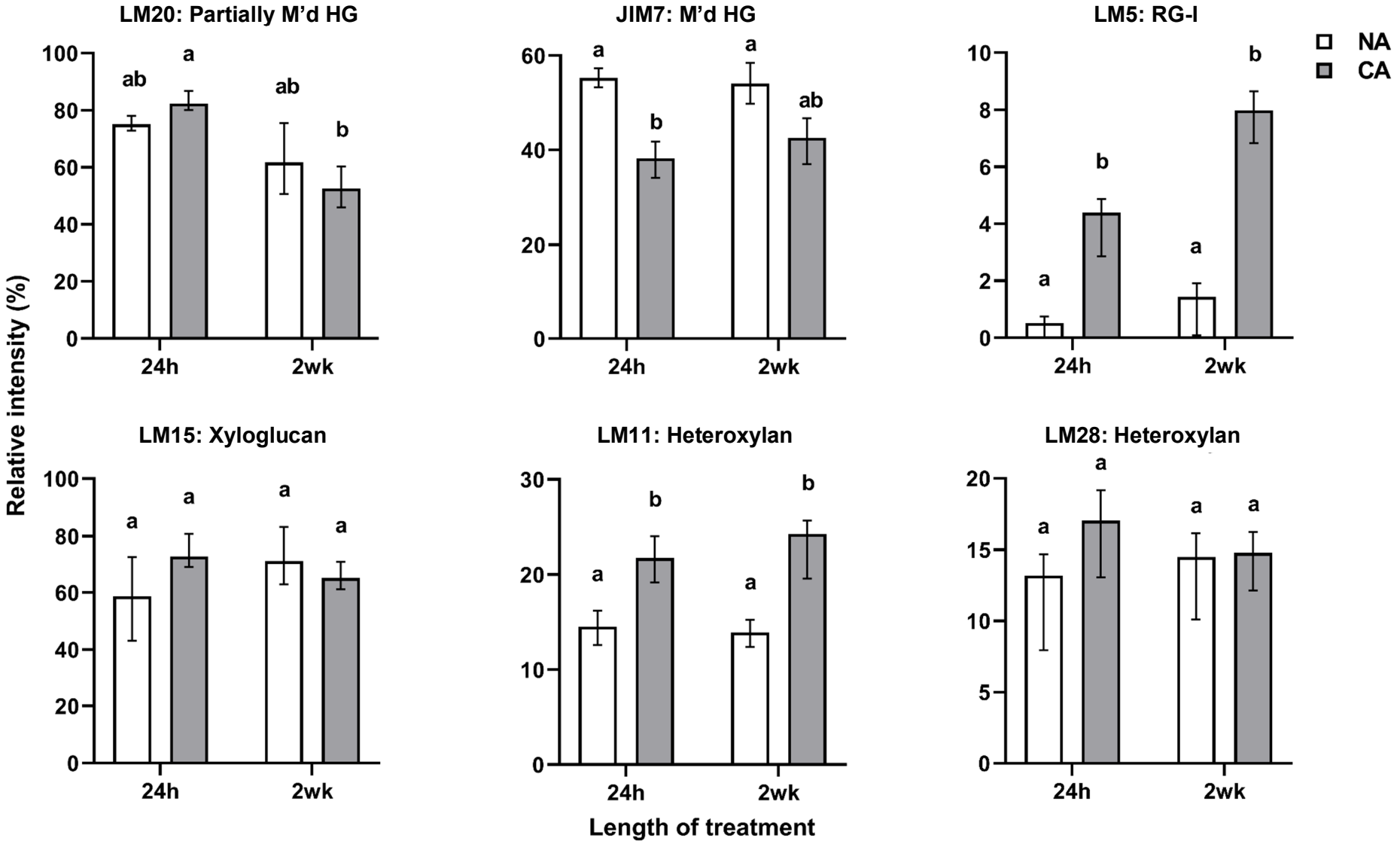
LM20: Partially M'd HG
JIM7: M'd HG
LM5: RG-I
LM15: Xyloglucan
LM11: Heteroxylan
LM28: Heteroxylan
NA
CA
Relative intensity (%)
24h
2wk
Length of treatment

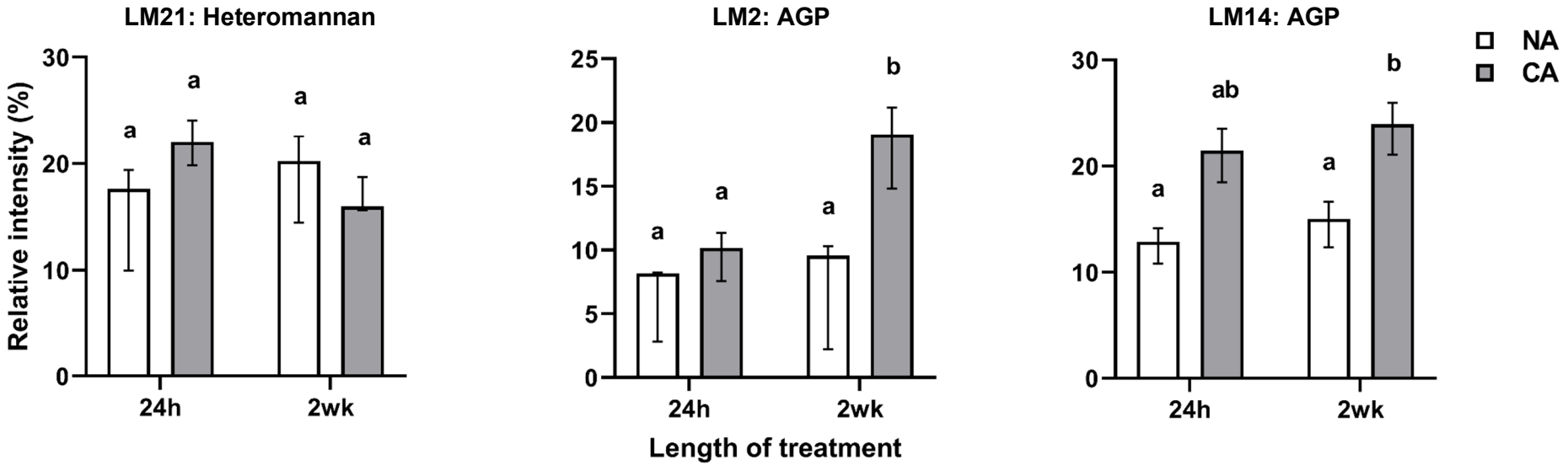

Figure 3.6: Comprehensive microarray polymer profiling (CoMPP) of cold-acclimated *Arabidopsis*. CoMPP was used to quantify the abundance of various cell-wall components in mature, wild-type *Arabidopsis* leaf tissue which had either been cold-acclimated (CA) or non-acclimated (NA) for either 24 h or 2 weeks (2wk). Cell-wall extractions from each of the four experimental groups were printed as microarrays and probed with a range of monoclonal antibodies (mAbs; shown in the title of each graph). Bars represent the mean percentage relative intensity of microarray signals from three biological replicate experiments; each experiment used cell-wall extractions from entire rosettes of six mature plants per experimental group (so n=18 for each bar). Raw intensity values were normalised to the highest value within each dataset before pooling the data across replicate experiments. Error bars represent one standard error of the mean of arcsine-transformed data, as is appropriate for proportional data. Means that do not share a letter are significantly different. EXT: extensin; DM'd HG: demethylesterified homogalacturonan; M'd HG: methylesterified homogalacturonan; RG-I: rhamnogalacturonan-I; AGP: arabinogalactan protein. NaOH extractions: LM1, LM15, LM11, LM28, LM21. CDTA extractions: JIM12, JIM20, JIM5, JIM7, LM18, LM19, LM20, LM5, LM2, LM14.

(24h or 2wk). JIM12 detected significant accumulation of EXT after 2 weeks of cold acclimation ($p< 0.001$) but not after 24 h ($p>0.4$), whereas JIM20 binding indicated that cold acclimation had no significant effect on EXT abundance at either treatment length ($p>0.05$).

Five mAbs that detect differing degrees of pectin methylesterification were used: JIM5, LM18, LM19 and LM20, which recognise partially demethylesterified homogalacturonan (HG), and JIM7, which recognises partially methylesterified HG. Both JIM5 and LM18 detected a significant increase in demethylesterified HG after both 24 h and 2 weeks of cold acclimation ($p<0.01$). Logically, JIM7 binding showed a significant decrease in methylesterified HG after 24 h of cold acclimation ($p<0.01$). There was also a decrease after 2 weeks of cold acclimation but the difference was not significant ($p>0.05$). Additionally, both LM19 and LM20 binding failed to show a significant increase in demethylesterified HG abundance after cold acclimation ($p>0.7$ and $p>0.9$, respectively).

Binding of LM5 showed a significant increase in RG-I abundance after both 24 h and 2 weeks of cold acclimation ($p<0.001$). Xyloglucan did not appear to change significantly in abundance at either treatment length ($p>0.6$), as per LM15 binding efficacy. Heteroxylan showed mixed results, with LM11 binding indicating that there was significant accumulation after cold acclimation at both 24 h and 2 weeks ($p<0.005$), but this was not reflected in LM28 binding, which showed non-significant changes in heteroxylan abundance for both treatment lengths ($p>0.3$). Cold acclimation did not appear to induce a significant change in heteromannan abundance for either treatment length ($p>0.3$). Binding of both LM2 and LM14 indicated that there was significant accumulation of AGPs after 2 weeks of cold acclimation ($p<0.05$ and $p<0.005$, respectively). Both probes also detected an increase in AGPs after 24 h of cold acclimation, but the difference was not significant ($p>0.5$ and $p>0.05$, respectively).

3.2.4 Analysis of mutants of cold-responsive cell-wall components

The cell-wall profiling experiments described above revealed several components of the cell wall that change in abundance during cold acclimation, and hence may be important contributors to freezing tolerance. *Arabidopsis* mutants of some of these

components were identified and their freezing tolerance and cell-wall physical properties were assessed.

3.2.4.1 Pectin methylesterase mutants

CoMPP data from the probes JIM5, LM18, and JIM7, which recognise HG with different degrees of methylesterification, suggested that cold acclimation may induce a decrease in methylesterified pectin (and a concomitant increase in demethylesterified pectin). Three pectin methylesterase (PME) mutants of *Arabidopsis*, *pme17, pme31* and *pme41*, which lack expression of specific PMEs and have reduced PME activity, and therefore increased pectin methylesterification (Qu *et al.* 2011, Sénéchal *et al.* 2014, Yan *et al.* 2018), were identified and screened for freezing sensitivity as well as changes in cell-wall porosity and mechanical properties. The purpose of these experiments was to determine if cold-induced changes in pectin methylesterification improve freezing tolerance by modifying the physical properties of the cell wall.

3.2.4.1.1 Freezing tolerance

Freezing assays were carried out on non-acclimated plants using each of the *pme* mutants as well as mature wild-type and *sfr8* (a known freezing-sensitive mutant; see **Chapter 4**) as negative and positive controls, respectively. Plants were subjected to freezing at -3°C for 24 h before being returned to ambient growth conditions. The capacity of the plants to recover and exhibit new growth was assessed after 1 week. In order to quantify the damage incurred by plants during freezing, electrolyte leakage was measured in leaf tissue from plants of each genotype following exposure to three different sub-zero temperatures (-3, -5 and -7°C) Results for each of the three mutants will be described separately.

For *pme17* recovery assays (**Figure 3.7A**), a linear mixed effects model confirmed that experiment number had no significant impact on data variation ($p>0.05$) so the data from three biological replicate experiments were pooled for analysis. Mean percentage survival of plants of each genotype was calculated from pooled data. Genotype had a significant effect on plant survival ($p<0.001$). However, *pme17* did not have a significantly different mean survival rate to that of wild-type (both were

100%), whereas the mean survival rate of *sfr8* was significantly lower than both, as expected (**Figure 3.7B**). For electrolyte leakage assays, a linear mixed effects model confirmed that experiment number had no significant impact on data variation ($p>0.2$) so the data from three biological replicate experiments were pooled for analysis. Mean percentage electrolyte leakage of plants from each genotype was calculated at each temperature from pooled data (**Figure 3.7C**). At -3 and -5°C, genotype had a significant impact on electrolyte leakage ($p<0.001$). However, electrolyte leakage of *pme17* was not significantly different to that of wild-type, whereas *sfr8* had significantly higher electrolyte leakage than both. At -7°C, electrolyte leakage did not differ significantly between all three genotypes ($p>0.1$).

For *pme31* recovery assays (**Figure 3.8A**), a linear mixed effects model confirmed that experiment number had no significant impact on data variation ($p>0.1$) so the data from three biological replicate experiments were pooled for analysis. Mean percentage survival of plants of each genotype was calculated from pooled data. Genotype had a significant effect on plant survival ($p<0.001$). Although *pme31* had a lower mean survival rate than that of wild-type, the difference was not significant. The mean survival rate of *sfr8* was significantly lower than both (**Figure 3.8B**). For *pme31* electrolyte leakage assays, a linear mixed effects model confirmed that experiment number had no significant impact on data variation ($p>0.1$) so the data from three biological replicate experiments were pooled for analysis. Mean percentage electrolyte leakage of plants from each genotype was calculated at each temperature from pooled data (**Figure 3.8C**). At -3°C, electrolyte leakage did not differ significantly between all three genotypes ($p>0.1$). At -5°C, genotype had a significant impact on electrolyte leakage ($p<0.005$); however, electrolyte leakage of *pme31* was not significantly higher than that of wild-type. Electrolyte leakage of *sfr8* was significantly higher than that of wild-type but not that of *pme31*. At -7°C, genotype had a significant impact on electrolyte leakage ($p<0.001$); however, electrolyte leakage of *pme31* was not significantly higher than that of wild-type, whereas *sfr8* had significantly higher electrolyte leakage than both.

For *pme41* recovery assays (**Figure 3.9A**), a linear mixed effects model confirmed that experiment number had no significant impact on data variation ($p>0.1$) so the data from three biological replicate experiments were pooled for analysis. Mean percentage survival of plants of each genotype was calculated from pooled data. Genotype had a significant impact on plant survival ($p<0.001$). Compared to wild-type, which had a mean survival rate of 100%, both *pme41* and *sfr8* had significantly lower mean survival rates of 33% and 7%, respectively (**Figure 3.9B**). For *pme41* electrolyte leakage assays, a linear mixed effects model confirmed that experiment number had no significant impact on data variation ($p>0.2$) so the data from three biological replicate experiments were pooled for analysis. Mean percentage electrolyte leakage of plants from each genotype was calculated at each temperature from pooled data (**Figure 3.9C**). At -3 and -5°C, genotype had a significant impact on electrolyte leakage ($p<0.05$); however, electrolyte leakage of *pme41* was not significantly higher than that of wild-type. Electrolyte leakage of *sfr8* was significantly higher than that of wild-type at -3°C and both genotypes at -5°C. Genotype also had a significant impact on electrolyte leakage at -7°C ($p<0.001$). Both *pme41* and *sfr8* had significantly higher electrolyte leakage than that of wild-type, though they did not differ significantly from each other.

3.2.4.1.2 Cell-wall physical properties

The fluorescence-quenching porosity assay was carried out on each of the three *pme* mutants. As above, the fluorescence of stained mesophyll cells was quantified (F_0;) and divided by the quantified fluorescence after quenching (F) to give a measure of relative porosity. Individual linear mixed effects models confirmed that experiment number had no significant impact on variation of the data from each of the three mutants (*pme17*: $p>0.2$; *pme31*: $p>0.05$; *pme41*: $p>0.1$), so the data for each mutant were pooled for analysis. Cell-wall porosity of both *pme17* (**Figure 3.10)** and *pme31* (**Figure 3.11)** did not differ significantly from that of wild-type ($p>0.1$). However, *pme41* was found to have significantly higher cell-wall porosity compared to wild-type ($p<0.05$; **Figure 3.12**).

Cell-wall mechanical properties were measured using extensometry. Eight-mm discs prepared from mature leaves of *pm17, pme31* and *pme41*, along with wild-type

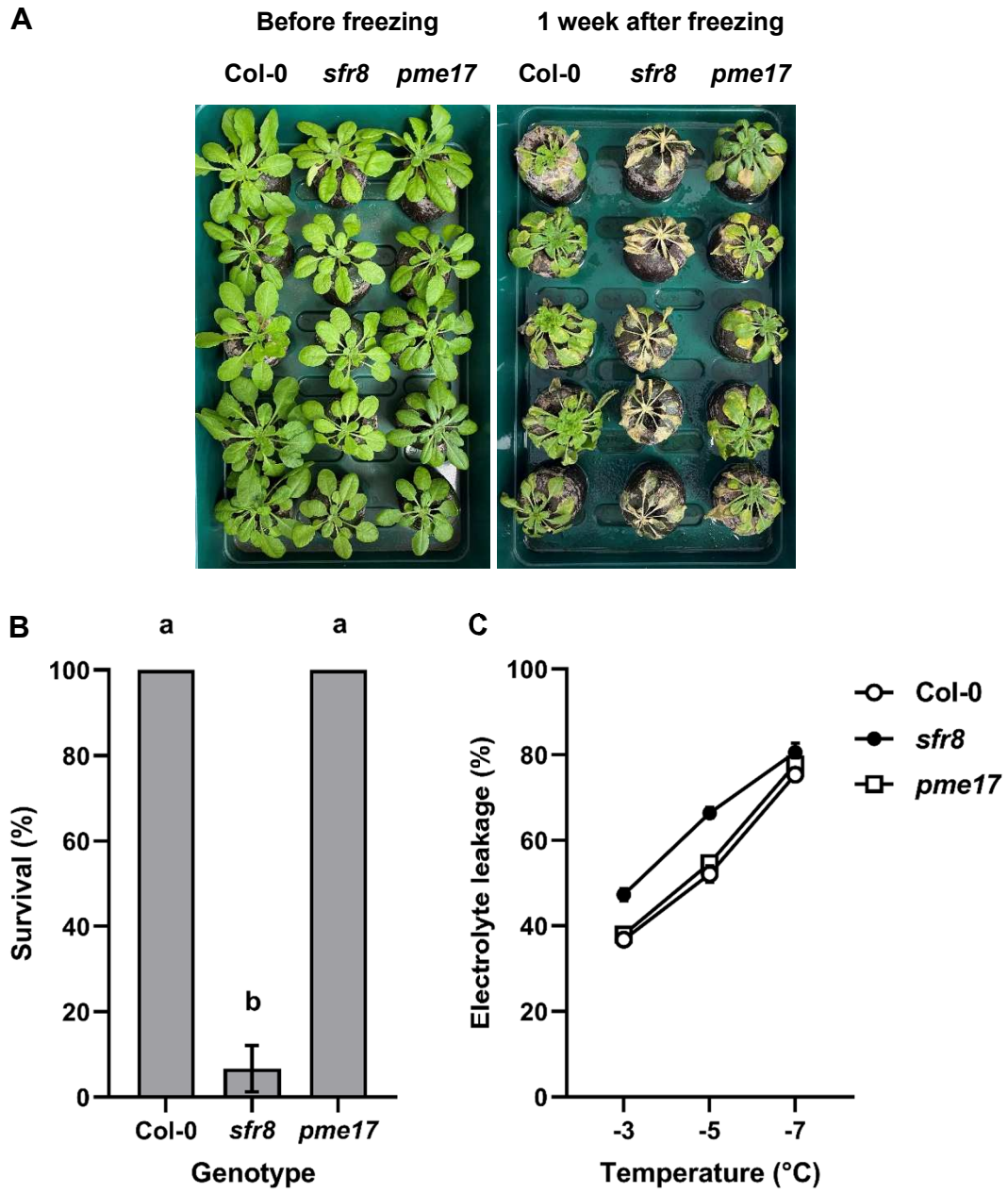

Figure 3.7: Freezing tolerance of the *pme17* mutant. **A)** Freezing recovery assay of mature wild-type (Col-0), *sfr8*, and *pme17* plants. Plants were subjected to freezing at -3°C for 24 h and recovered for one week. Photographed is one representative assay showing plants immediately before (left) and one week after (right) freezing. **B)** Survival analysis of plants from freezing recovery assays. Plants were scored on survival based on whether regrowth had occurred. Bars represent mean percentage survival of plants from three biological replicate experiments; five plants per genotype were used per experiment (n=15). Error bars represent one standard error of the mean of arcsine-transformed data. Means that do not share a letter are significantly different. **C)** Electrolyte leakage of mature leaf tissue from wild-type (Col-0), *sfr8,* and *pme17*. Tissue was subjected to freezing at -3, -5 or -7°C and electrolyte leakage measured. Points represent mean percentage electrolyte leakage from three biological replicate experiments; each experiment used tissue from six plants per genotype per temperature (n=18 at each point). Error bars represent one standard error of the mean of arcsine-transformed data.

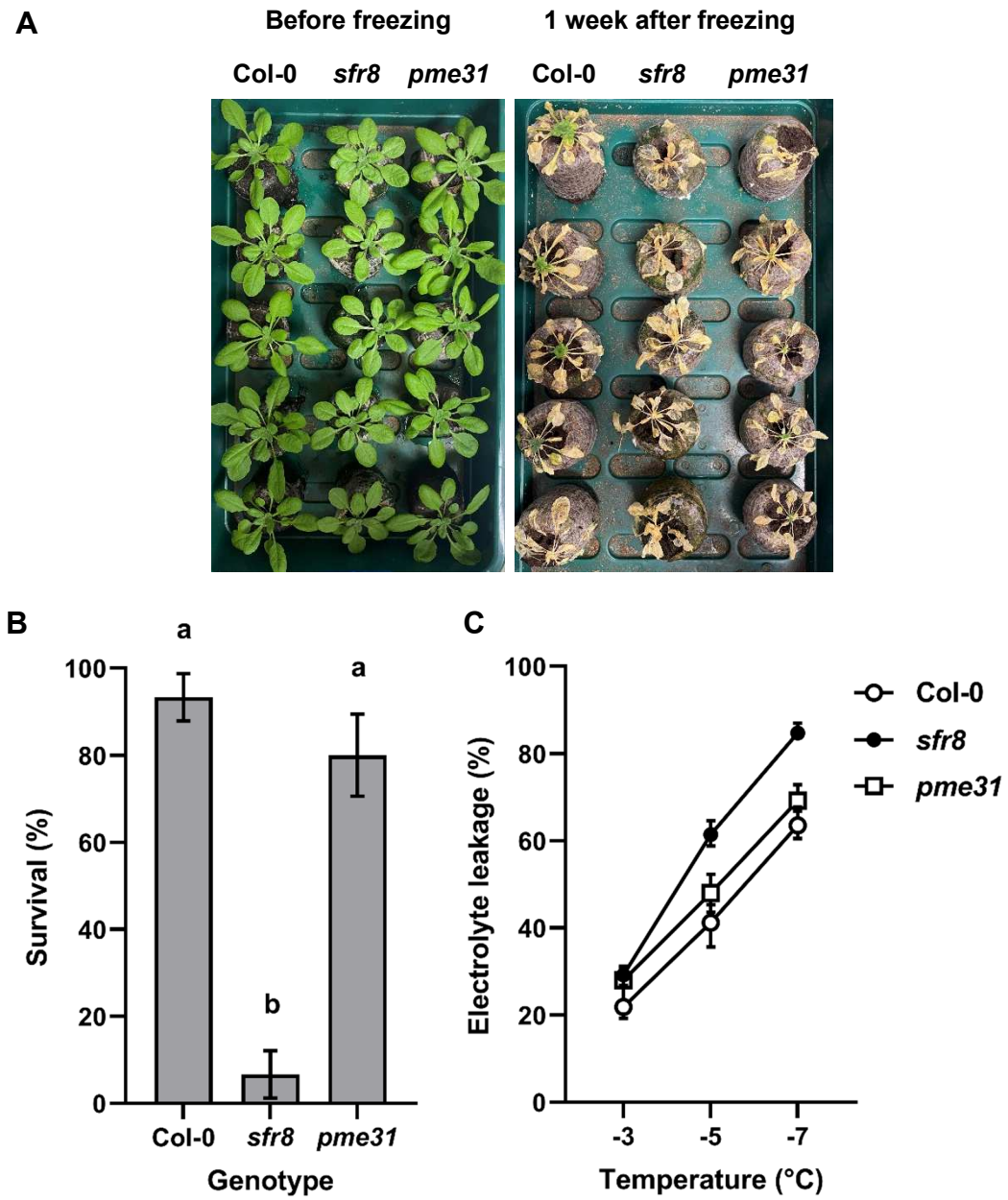

Figure 3.8: Freezing tolerance of the *pme31* mutant. A) Freezing recovery assay of mature wild-type (Col-0), *sfr8*, and *pme31* plants. Plants were subjected to freezing at -3°C for 24 h and recovered for one week. Photographed is one representative assay showing plants immediately before (left) and one week after (right) freezing. **B)** Survival analysis of plants from freezing recovery assays. Plants were scored on survival based on whether regrowth had occurred. Bars represent mean percentage survival of plants from three biological replicate experiments; five plants per genotype were used per experiment (n=15). Error bars represent one standard error of the mean of arcsine-transformed data. Means that do not share a letter are significantly different. **C)** Electrolyte leakage of mature leaf tissue from wild-type (Col-0), *sfr8,* and *pme31.* Tissue was subjected to freezing at -3, -5 or -7°C and electrolyte leakage measured. Points represent mean percentage electrolyte leakage from three biological replicate experiments; each experiment used tissue from six plants per genotype per temperature (n=18 at each point). Error bars represent one standard error of the mean of arcsine-transformed data.

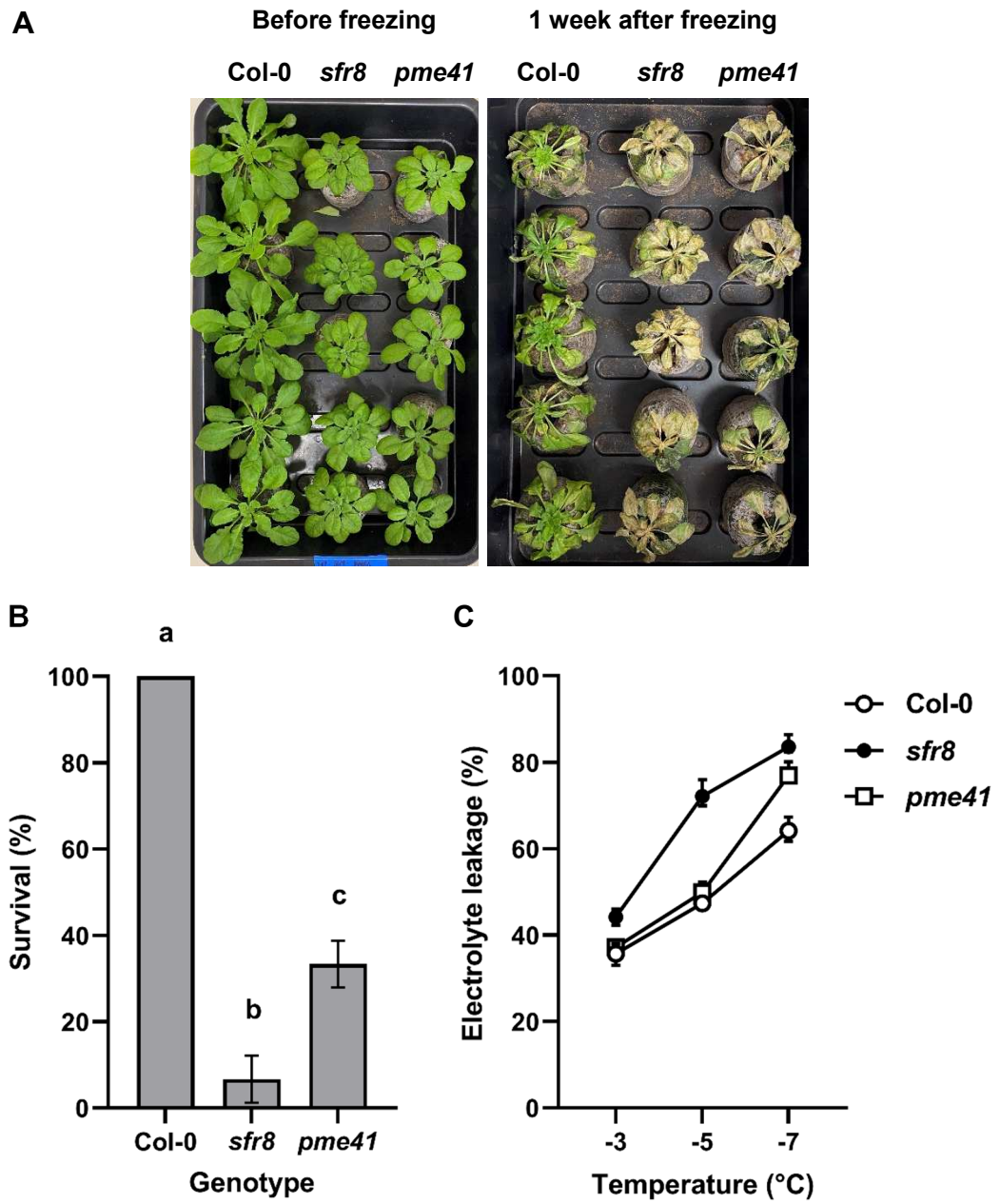

Figure 3.9: Freezing tolerance of the *pme41* mutant. A) Freezing recovery assay of mature wild-type (Col-0), *sfr8*, and *pme41* plants. Plants were subjected to freezing at -3°C for 24 h and recovered for one week. Photographed is one representative assay showing plants immediately before (left) and one week after (right) freezing. **B)** Survival analysis of plants from freezing recovery assays. Plants were scored on survival based on whether regrowth had occurred. Bars represent mean percentage survival of plants from three biological replicate experiments; five plants per genotype were used per experiment (n=15). Error bars represent one standard error of the mean of arcsine-transformed data. Means that do not share a letter are significantly different. **C)** Electrolyte leakage of mature leaf tissue from wild-type (Col-0), *sfr8,* and *pme41*. Tissue was subjected to freezing at -3, -5 or -7°C and electrolyte leakage measured. Points represent mean percentage electrolyte leakage from three biological replicate experiments; each experiment used tissue from six plants per genotype per temperature (n=18 at each point). Error bars represent one standard error of the mean of arcsine-transformed data.

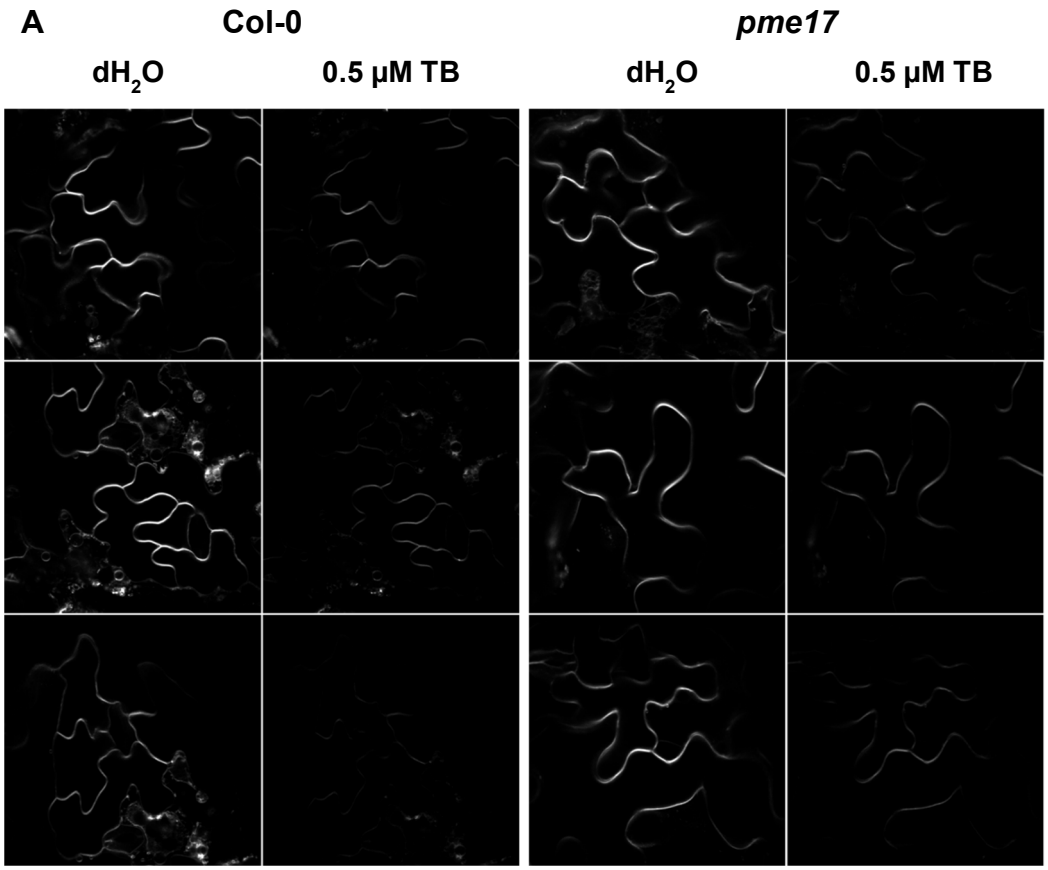

Figure 3.10: Cell-wall porosity of the *pme17* mutant. Relative porosity was calculated in mature wild-type (Col-0) and *pme17* plants using fluorescence quenching. **A)** The plasma membranes of leaf epidermal cells were stained with a fluorescent dye and imaged before and after addition of 0.5 µM trypan blue (TB) quenching solution. Three example micrographs per treatment are shown for each genotype. **B)** Fluorescence was quantified before (F_0) and after (F) addition of the quenching solution and a ratio of the two was calculated to give relative porosity (F_0/F). Bars represent mean relative porosity from three biological replicate experiments; each experiment measured porosity in three leaves from separate plants per genotype (n=9). Error bars represent one standard error of the mean. ns indicates means that are not significantly different ($p>0.2$).

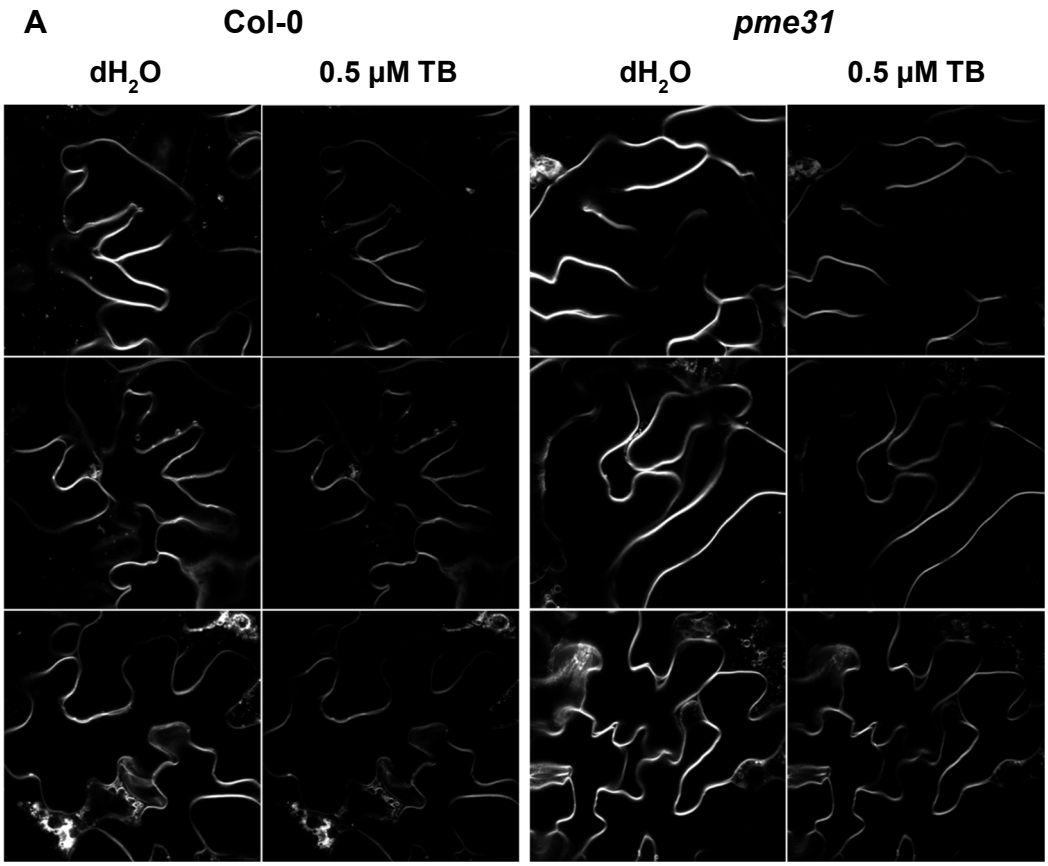

Figure 3.11: Cell-wall porosity of the *pme31* mutant. Relative porosity was calculated in mature wild-type (Col-0) and *pme31* plants using fluorescence quenching. **A)** The plasma membranes of leaf epidermal cells were stained with a fluorescent dye and imaged before and after addition of 0.5 µM trypan blue (TB) quenching solution. Three example micrographs per treatment are shown for each genotype. **B)** Fluorescence was quantified before (F_0) and after (F) addition of the quenching solution and a ratio of the two was calculated to give relative porosity (F_0/F). Bars represent mean relative porosity from three biological replicate experiments; each experiment measured porosity in three leaves from separate plants per genotype (n=9). Error bars represent one standard error of the mean. ns indicates means that are not significantly different ($p>0.2$).

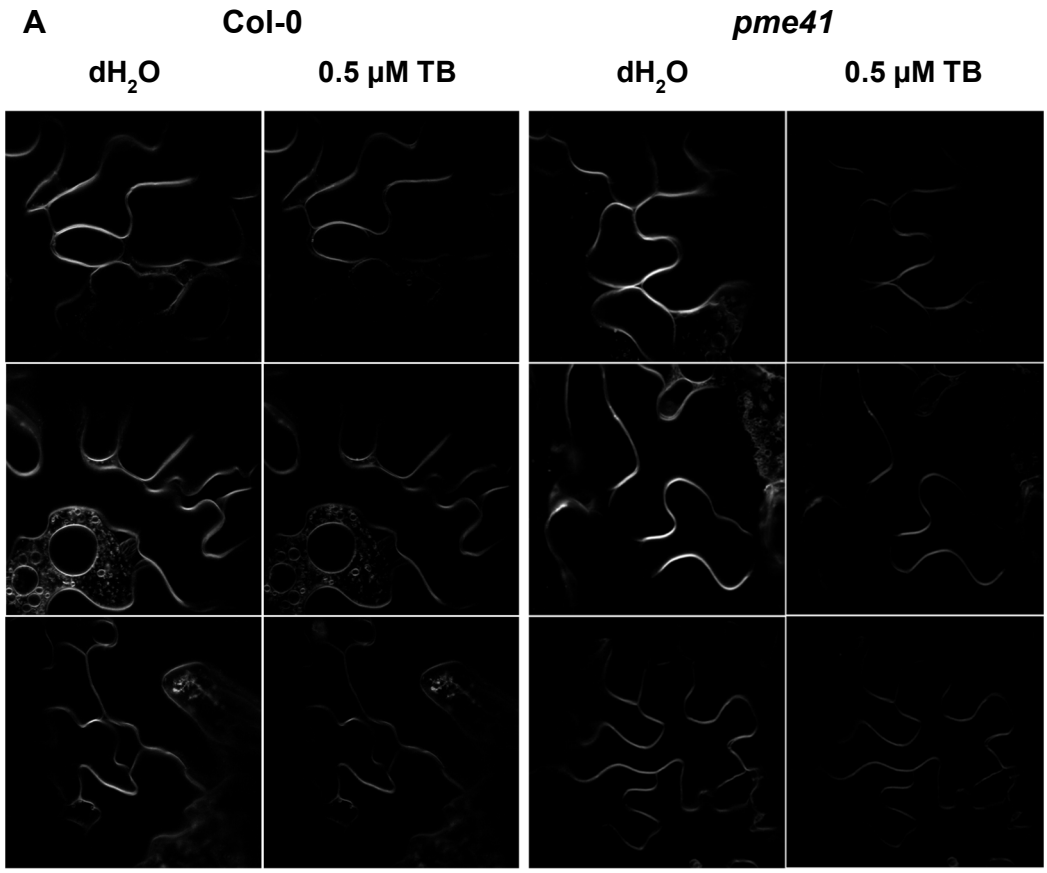

Figure 3.12: Cell-wall porosity of the *pme41* mutant. Relative porosity was calculated in mature wild-type (Col-0) and *pme41* plants using fluorescence quenching. **A)** The plasma membranes of leaf epidermal cells were stained with a fluorescent dye and imaged before and after addition of 0.5 µM trypan blue (TB) quenching solution. Three example micrographs per treatment are shown for each genotype. **B)** Fluorescence was quantified before (F_0) and after (F) addition of the quenching solution and a ratio of the two was calculated to give relative porosity (F_0/F). Bars represent mean relative porosity from three biological replicate experiments; each experiment measured porosity in three leaves from separate plants per genotype (n=9). Error bars represent one standard error of the mean. Asterisks indicate means that are significantly different (* $p<0.05$).

(Col-0) controls, were stretched until failure using an extensometer equipped with a load cell sensitive to 1 mN. Individual linear mixed effects models confirmed that experiment number had no significant impact on variation of the data from each of the three genotypes (*pme17*: $p>0.2$; *pme31*: $p>0.2$; *pme41*: $p>0.1$), so the data from three biological replicate experiments were pooled separately for each group for analysis. Mean percentage relative tensile force, normalised to the baseline force reading taken immediately before the stretch was initiated, was calculated from pooled data and plotted over time. Firstly, average force curves were plotted on the same axes for each group to allow for comparisons of cell-wall stiffness. Secondly, the percentage relative tensile force values from the peak of force curves from individual samples were plotted to illustrate the cell-wall mechanical strength of tissue of each genotype.

For *pme17*, the gradient of the curve up to the point of failure was 0.356, compared to 0.442 for wild-type, suggesting that the mutant has reduced cell-wall stiffness (**Figure 3.13A**). Furthermore, the mechanical strength of *pme17* was significantly lower than that of wild-type ($p<0.01$). The mean maximum relative tensile force for *pme17* was 4.80% compared to 6.31% for wild-type (**Figure 3.13B**).

For *pme31*, the gradient of the curve up to the point of failure was 0.437, compared to 0.426 for wild-type, suggesting that the mutant has comparable cell-wall stiffness to wild-type (**Figure 3.14A**). Similarly, the mechanical strength of *pme31* was not significantly different to that of wild-type ($p>0.6$). The mean maximum relative tensile force for *pme31* was 5.80% compared to 5.98% for wild-type (**Figure 3.14B**).

For *pme41*, the gradient of the curve up to the point of failure was 0.412, compared to 0.568 for wild-type, suggesting that the mutant has reduced cell-wall stiffness (**Figure 3.15A**). However, the mechanical strength of *pme41* was not significantly different to that of wild-type ($p>0.1$). The mean maximum relative tensile force for *pme41* was 6.64% compared to 7.37% for wild-type (**Figure 3.15B**).

These results indicate that knock-out of specific *PME* genes can have variable effects on the physical properties of the cell wall.

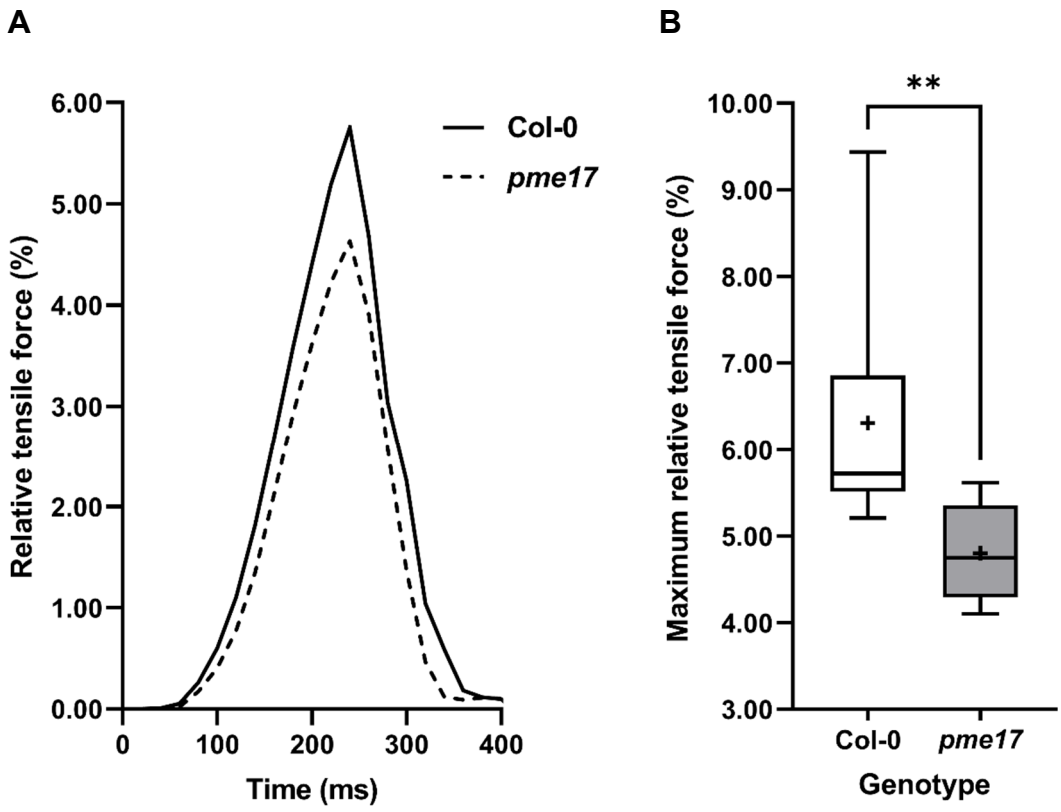

Figure 3.13: Cell-wall mechanical properties of the *pme17* mutant. Mechanical properties were assessed in mature wild-type (Col-0) and *pme17* plants using extensometry. Leaf discs from each genotype were stretched until breakage and the force required to do so was recorded. Tensile force was normalised to the baseline force reading taken immediately before the stretch was initiated and converted to a percentage for each sample. Plots represent combined data for three biological replicate experiments; each experiment measured cell-wall mechanical properties in three leaf discs per genotype (n=9). **A)** Relative tensile force plotted over time for the duration of each stretch. A steeper gradient is indicative of stiffer material and a higher peak (more resistance to breaking pressure) is indicative of stronger material. **B)** Box-and-whisker plot showing the distribution of maximum tensile force values for each genotype. Values were taken from the absolute peak of each force curve, which represents the maximum tensile force that the tissue can withstand before breakage. Whiskers: maximum and minimum values; box edges: upper and lower quartiles; plus signs: mean values; horizontal lines: median values. Asterisks indicate means that are significantly different (** $p<0.01$).

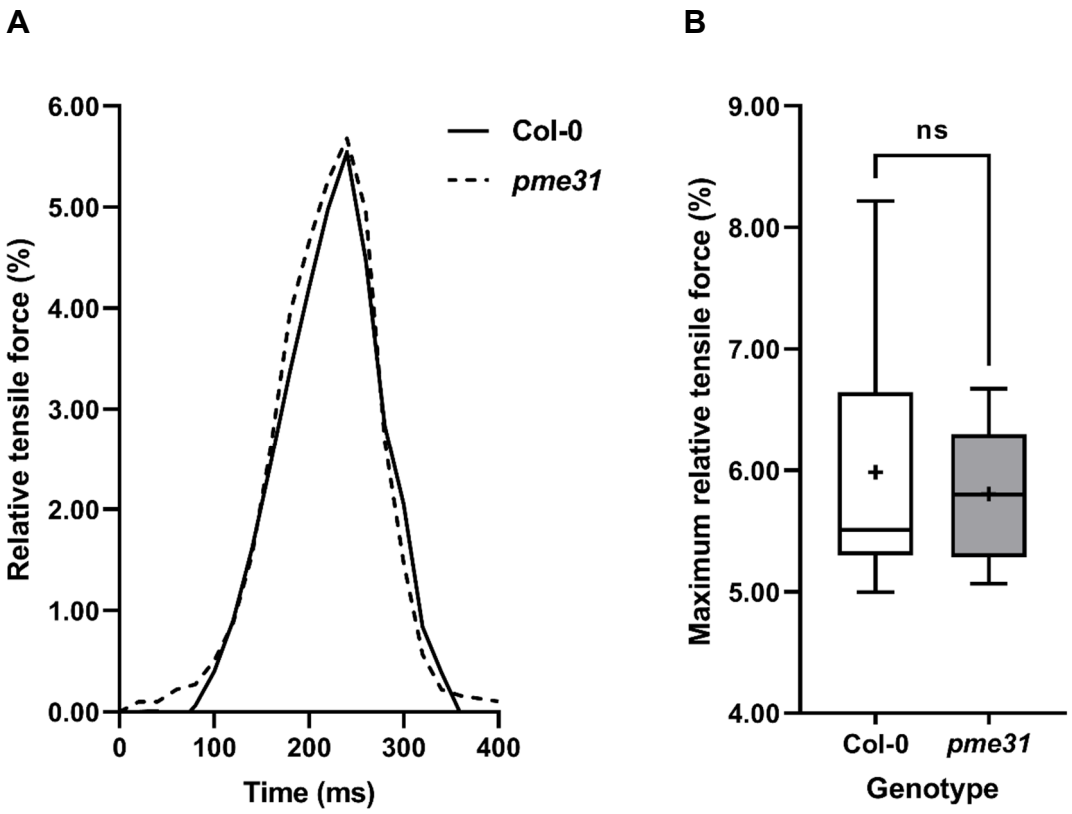

Figure 3.14: Cell-wall mechanical properties of the *pme31* mutant. Mechanical properties were assessed in mature wild-type (Col-0) and *pme31* plants using extensometry. Leaf discs from each genotype were stretched until breakage and the force required to do so was recorded. Tensile force was normalised to the baseline force reading taken immediately before the stretch was initiated and converted to a percentage for each sample. Plots represent combined data for three biological replicate experiments; each experiment measured cell-wall mechanical properties in three leaf discs per genotype (n=9). **A)** Relative tensile force plotted over time for the duration of each stretch. A steeper gradient is indicative of stiffer material and a higher peak (more resistance to breaking pressure) is indicative of stronger material. **B)** Box-and-whisker plot showing the distribution of maximum tensile force values for each genotype. Values were taken from the absolute peak of each force curve, which represents the maximum tensile force that the tissue can withstand before breakage. Whiskers: maximum and minimum values; box edges: upper and lower quartiles; plus signs: mean values; horizontal lines: median values. ns indicates means that are not significantly different (p>0.6).

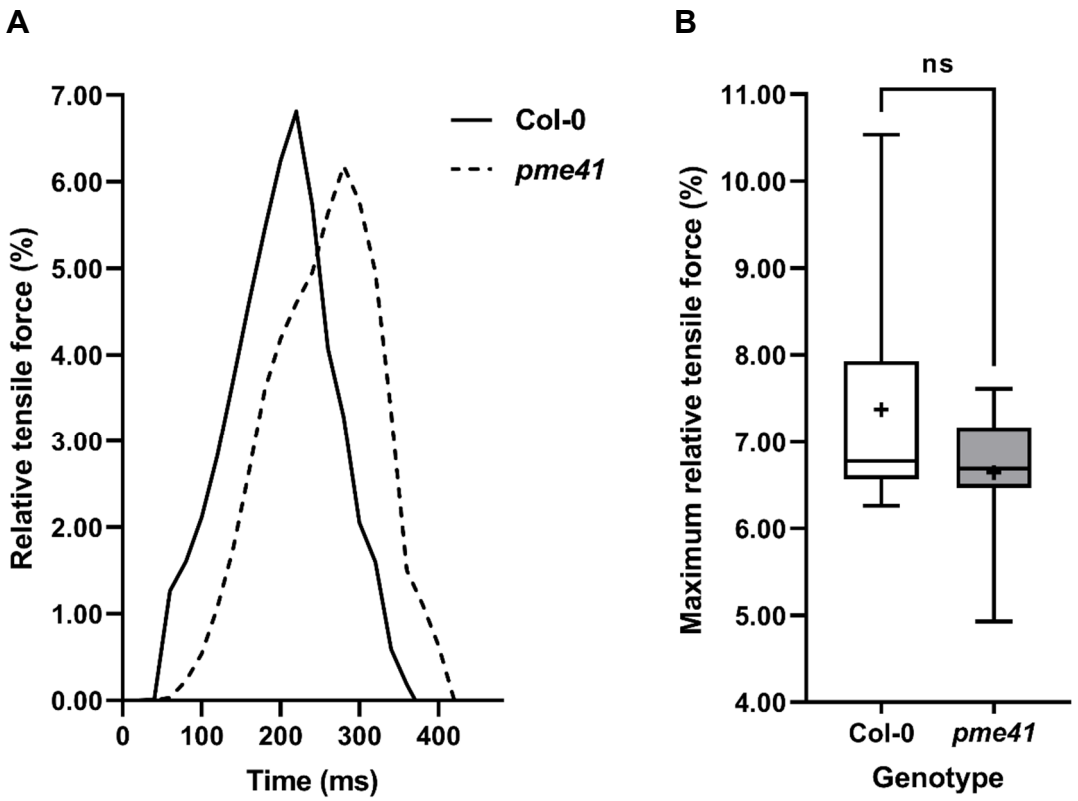

Figure 3.15: Cell-wall mechanical properties of the *pme41* mutant. Mechanical properties were assessed in mature wild-type (Col-0) and *pme41* plants using extensometry. Leaf discs from each genotype were stretched until breakage and the force required to do so was recorded. Tensile force was normalised to the baseline force reading taken immediately before the stretch was initiated and converted to a percentage for each sample. Plots represent combined data for three biological replicate experiments; each experiment measured cell-wall mechanical properties in three leaf discs per genotype (n=9). **A)** Relative tensile force plotted over time for the duration of each stretch. A steeper gradient is indicative of stiffer material and a higher peak (more resistance to breaking pressure) is indicative of stronger material. **B)** Box-and-whisker plot showing the distribution of maximum tensile force values for each genotype. Values were taken from the absolute peak of each force curve, which represents the maximum tensile force that the tissue can withstand before breakage. Whiskers: maximum and minimum values; box edges: upper and lower quartiles; plus signs: mean values; horizontal lines: median values. ns indicates means that are not significantly different (p>0.1).

3.2.4.2 Extensin mutants

3.2.4.2.1 Freezing tolerance

CoMPP data from the probes LM1 and JIM12, which recognise and bind epitopes of EXTs, suggested that cold acclimation may induce an accumulation of EXTs in the cell wall. A mutant that lacks expression of *EXT18*, an integral member of the *EXT* gene family required for normal vegetative growth (Choudhary *et al.* 2015), was screened for freezing sensitivity (both before and after cold acclimation) and changes in cell-wall physical properties.

Mature *ext18* plants, along with wild-type and *sfr8* controls, were subjected to freezing at either -3°C (non-acclimated plants) or -8°C (cold-acclimated plants) for 24 h before being returned to ambient growth conditions. The capacity of the plants to recover and exhibit new growth was assessed after 1 week (non-acclimated plants: **Figure 3.16A**; cold-acclimated plants: **Figure 3.17A**). Individual linear mixed effects models confirmed that experiment number had no significant impact on the variation of data from both datasets ($p>0.1$ for both) so the data from three biological replicate experiments were pooled separately for each treatment. Mean percentage survival of plants of each genotype was calculated from pooled data. In both non-acclimated and cold-acclimated states, genotype had a significant impact on plant survival ($p<0.01$ for both). In the non-acclimated state, compared to wild-type, which had a mean survival rate of 93%, both *ext18* and *sfr8* had significantly lower mean survival rates of 20% and 7%, respectively (**Figure 3.16B**). Similarly, cold-acclimated *ext18* and *sfr8* had mean survival rates of 27% and 13%, respectively, which were both significantly lower than that of cold-acclimated wild-type (99%; **Figure 3.17B**).

In order to quantify the damage incurred by plants during freezing, electrolyte leakage was measured in leaf tissue from plants of each genotype, in both non-acclimated and cold-acclimated states, following exposure to three different sub-zero temperatures (-3, -5 and -7°C for non-acclimated plants; -5, -7 and -9°C for cold-acclimated plants). Individual linear mixed effects models confirmed that experiment number had no significant impact on data variation ($p>0.1$ for both) so the data from three biological replicate experiments were pooled separately for

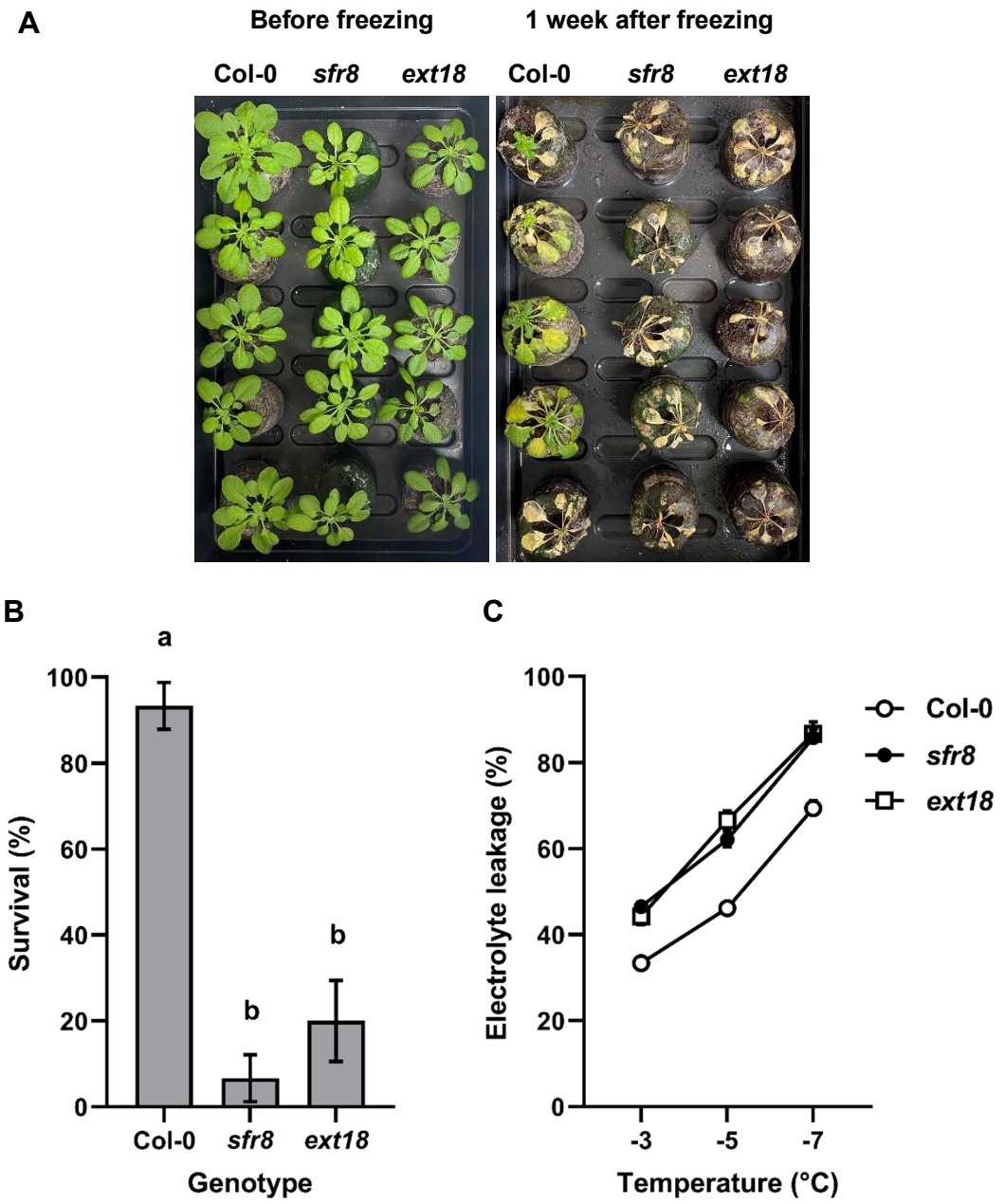

Figure 3.16: Freezing tolerance of the *ext18* mutant without cold acclimation. **A)** Freezing recovery assay of mature, non-acclimated wild-type (Col-0), *sfr8,* and *ext18* plants. Plants were subjected to freezing at -3°C for 24 h and recovered for one week. Photographed is one representative assay showing plants immediately before (left) and one week after (right) freezing. **B)** Survival analysis of plants from freezing recovery assays. Plants were scored on survival based on whether regrowth had occurred. Bars represent mean percentage survival of plants from three biological replicate experiments; five plants per genotype were used per experiment (n=15). Error bars represent one standard error of the mean of arcsine-transformed data. Means that do not share a letter are significantly different. **C)** Electrolyte leakage of mature leaf tissue from non-acclimated wild-type (Col-0), *sfr8,* and *ext18*. Tissue was subjected to freezing at -3, -5 or -7°C and electrolyte leakage measured. Points represent mean percentage electrolyte leakage from three biological replicate experiments; each experiment used tissue from six plants per genotype per temperature (n=18 at each point). Error bars represent one standard error of the mean of arcsine-transformed data.

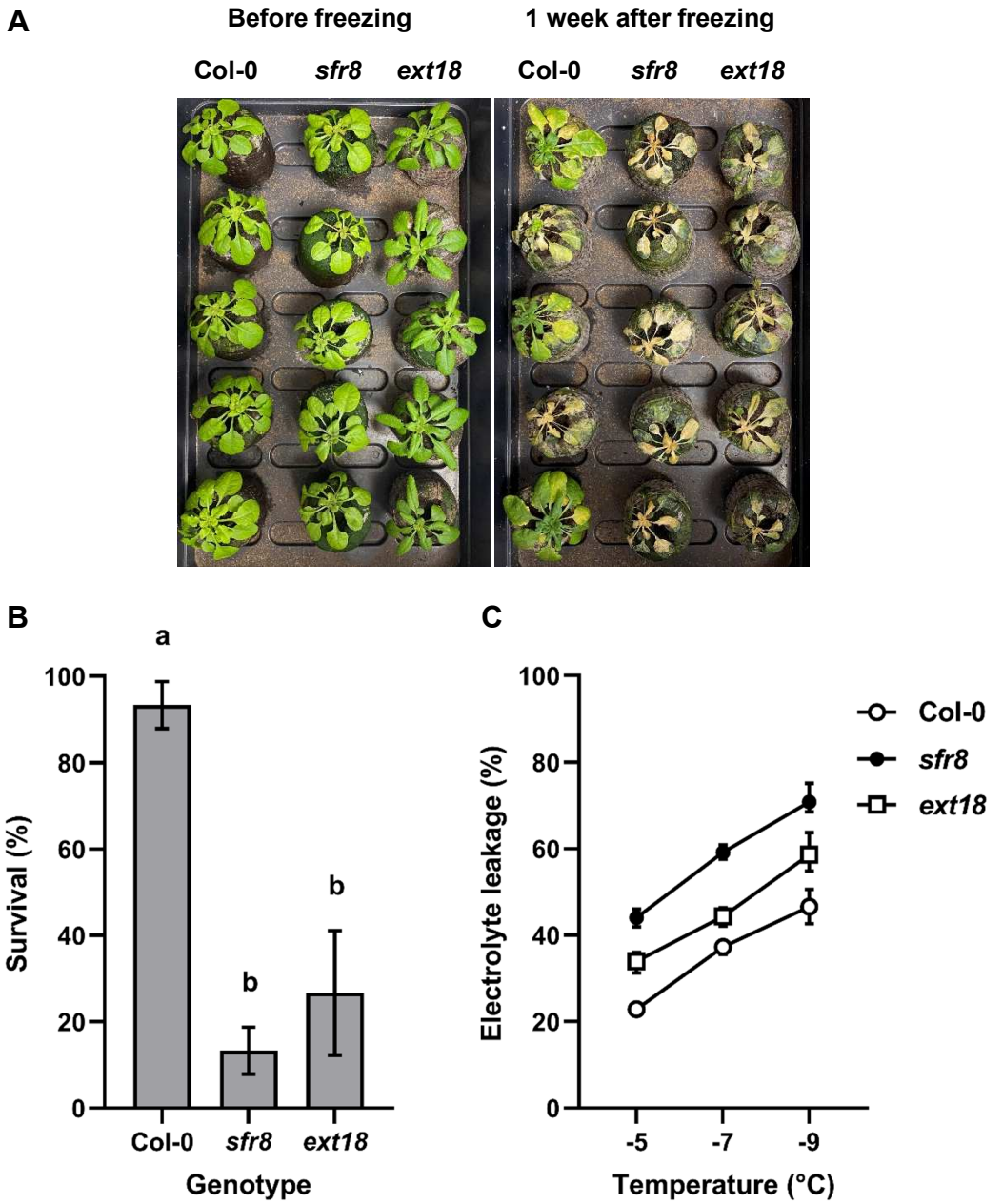

Figure 3.17: Freezing tolerance of the *ext18* mutant after cold acclimation. A) Freezing recovery assay of mature, cold-acclimated wild-type (Col-0), *sfr8,* and *ext18* plants. Plants were subjected to freezing at -8°C for 24 h and recovered for one week. Photographed is one representative assay showing plants immediately before (left) and one week after (right) freezing. **B)** Survival analysis of plants from freezing recovery assays. Plants were scored on survival based on whether regrowth had occurred. Bars represent mean percentage survival of plants from three biological replicate experiments; five plants per genotype were used per experiment (n=15). Error bars represent one standard error of the mean of arcsine-transformed data. Means that do not share a letter are significantly different. **C)** Electrolyte leakage of mature leaf tissue from cold-acclimated wild-type (Col-0), *sfr8,* and *ext18*. Tissue was subjected to freezing at -5, -7 or -9°C and electrolyte leakage measured. Points represent mean percentage electrolyte leakage from three biological replicate experiments; each experiment used tissue from six plants per genotype per temperature (n=18 at each point). Error bars represent one standard error of the mean of arcsine-transformed data.

each treatment. Mean percentage electrolyte leakage of plants of each genotype was calculated at each temperature from pooled data separated by treatment. In both non-acclimated and cold-acclimated states, genotype had a significant impact on electrolyte leakage ($p<0.001$ for both treatments at each temperature). In the non-acclimated state, both *ext18* and *sfr8* exhibited significantly higher electrolyte leakage than wild-type at each temperature (**Figure 3.16C**). In the cold-acclimated state, *ext18* and *sfr8* exhibited significantly higher electrolyte leakage than wild-type at -5 and -7°C. At -9°C, electrolyte leakage was higher in *ext18* and *sfr8* than in wild-type plants, but the difference was not significant for *ext18* (**Figure 3.17C**). Therefore, *ext18* is freezing-sensitive regardless of whether it has been cold-acclimated, and its freezing tolerance can still be improved through cold acclimation. An additional mutant allele of *EXT18* was later identified and also screened for freezing sensitivity (see **Appendix Q**).

3.2.4.2.2 Cell-wall physical properties

Cell-wall porosity was assessed in *ext18* plants using the fluorescence quenching assay (**Figure 3.18A**). A linear mixed effects model confirmed that experiment number had no significant impact on data variation ($p>0.05$) so the data from three biological replicate experiments were pooled for analysis. Mean relative porosity of wild-type and *ext18* plants was calculated from pooled data. The cell-wall porosity of *ext18* was found to be significantly higher than that of wild-type ($p<0.05$; **Figure 3.18B**).

The cell-wall mechanical properties of *ext18* were measured using extensometry. Eight-mm discs prepared from mature leaves of wild-type and *ext18* plants were stretched until failure using an extensometer equipped with a load cell sensitive to 1 mN. A linear mixed effects model confirmed that experiment number had no significant impact on data variation ($p>0.4$) so the data from three biological replicate experiments were pooled for analysis. Mean percentage relative tensile force, normalised to the baseline force reading taken immediately before the stretch was initiated, was calculated from pooled data and plotted over time. Average force curves for wild-type and *ext18* tissue were plotted on the same axes (**Figure 3.19A**). The gradient of the curve for *ext18* tissue up to the point of failure was

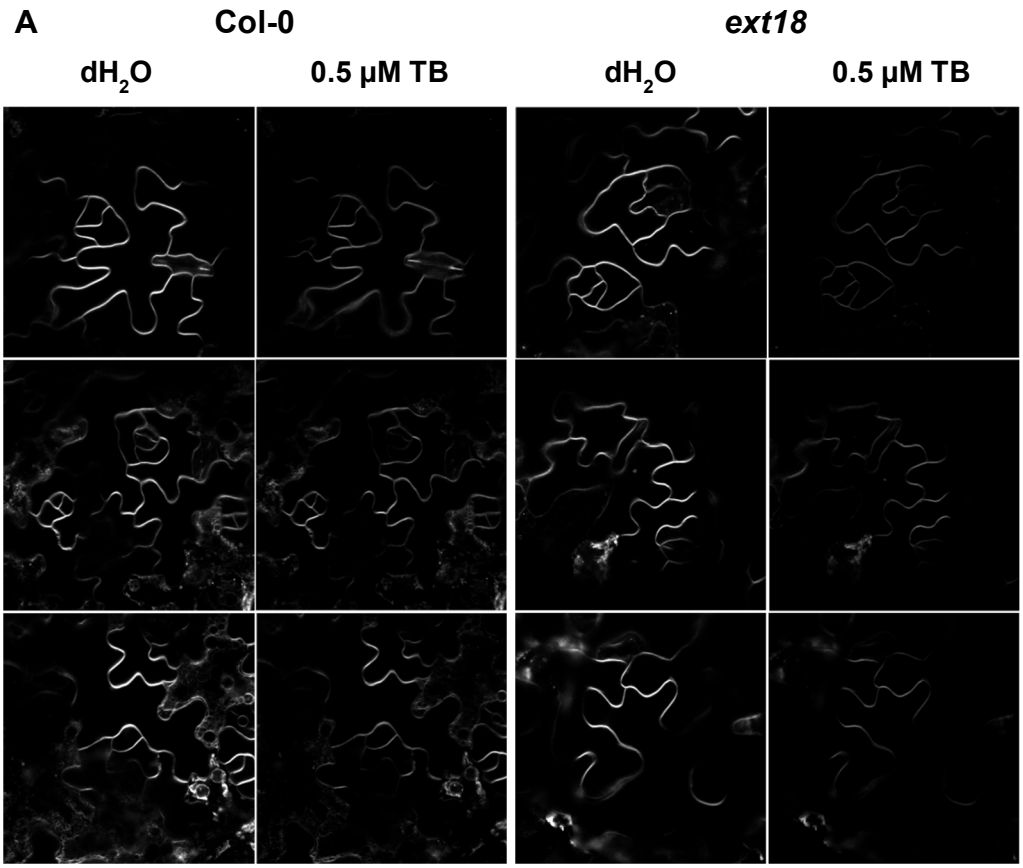

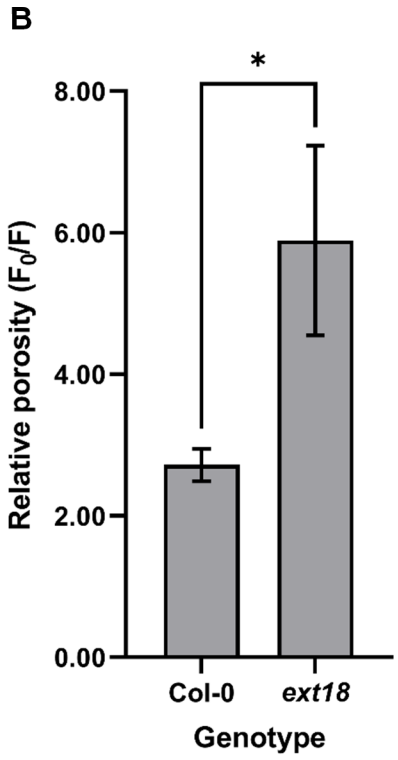

Figure 3.18: Cell-wall porosity of the *ext18* mutant. Relative porosity was calculated in mature wild-type (Col-0) and *ext18* plants using fluorescence quenching. **A)** The plasma membranes of leaf epidermal cells were stained with a fluorescent dye and imaged before and after addition of 0.5 µM trypan blue (TB) quenching solution. Three example micrographs per treatment are shown for each genotype. **B)** Fluorescence was quantified before (F_0) and after (F) addition of the quenching solution and a ratio of the two was calculated to give relative porosity (F_0/F). Bars represent mean relative porosity from three biological replicate experiments; each experiment measured porosity in three leaves from separate plants per genotype (n=9). Error bars represent one standard error of the mean. Asterisks indicate means that are significantly different (* $p<0.05$).

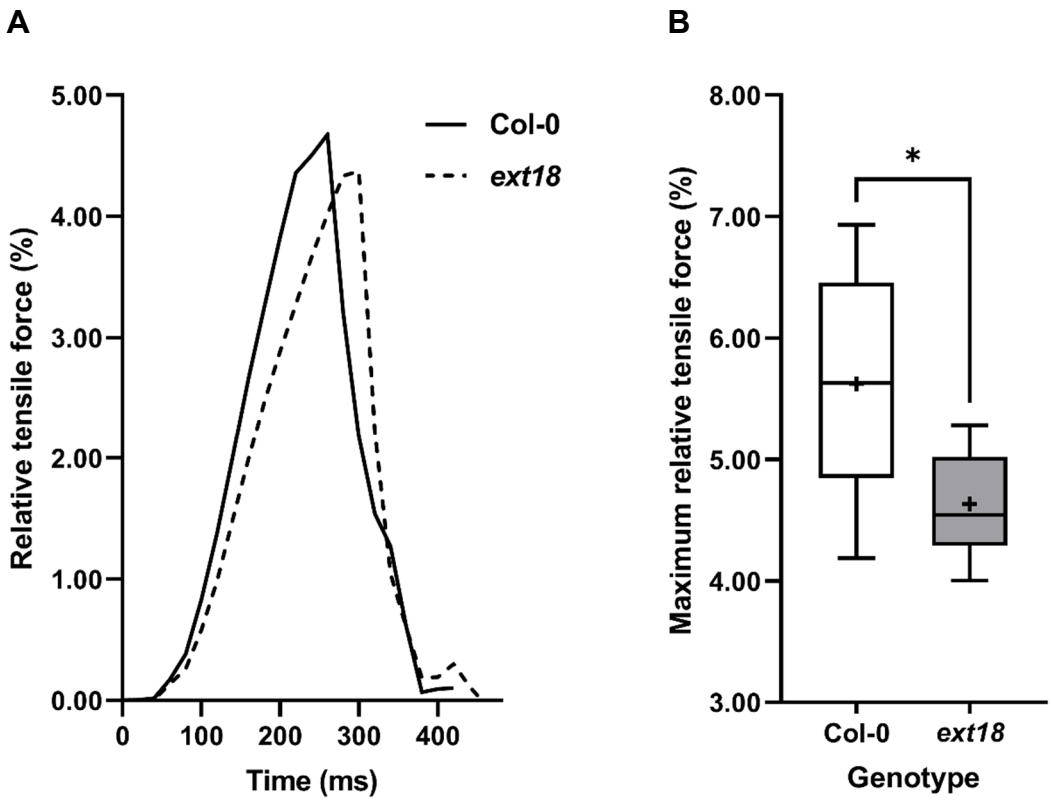

Figure 3.19: Cell-wall mechanical properties of the *ext18* mutant. Mechanical properties were assessed in mature wild-type (Col-0) and *ext18* plants using extensometry. Leaf discs from each genotype were stretched until breakage and the force required to do so was recorded. Tensile force was normalised to the baseline force reading taken immediately before the stretch was initiated and converted to a percentage for each sample. Plots represent combined data for three biological replicate experiments; each experiment measured cell-wall mechanical properties in three leaf discs per genotype (n=9). **A)** Relative tensile force plotted over time for the duration of each stretch. A steeper gradient is indicative of stiffer material and a higher peak (more resistance to breaking pressure) is indicative of stronger material. **B)** Box-and-whisker plot showing the distribution of maximum tensile force values for each genotype. Values were taken from the absolute peak of each force curve, which represents the maximum tensile force that the tissue can withstand before breakage. Whiskers: maximum and minimum values; box edges: upper and lower quartiles; plus signs: mean values; horizontal lines: median values. Asterisks indicate means that are significantly different (* $p<0.05$).

0.273, compared to 0.334 for wild-type, suggesting that *ext18* has reduced cell-wall stiffness. The percentage relative tensile force values from the peak of force curves from individual samples were plotted to illustrate the cell-wall mechanical strength of tissue from each genotype. The mechanical strength of *ext18* was found to be significantly lower than that of wild-type ($p<0.05$). The mean maximum relative tensile force for *ext18* was 4.63% compared to 5.62% for wild-type (**Figure 3.19B**).

3.3 Discussion

Cold acclimation for both 24 hours and 2 weeks resulted in clear improvements in freezing tolerance in wild-type *Arabidopsis*. This is not surprising nor is it a novel finding: it has long been established that cold acclimation, even for just 24 hours, induces marked improvements in freezing tolerance in *Arabidopsis* (Gilmour *et al.* 1988). The purpose of these experiments was to establish cold acclimation protocols that result in measurable increases in plant freezing tolerance for application in later experiments. Both treatments significantly increased plant survival and significantly decreased the degree of electrolyte leakage after freezing, indicating that the leaf tissue had incurred less severe freezing injury. The duration of cold acclimation made no significant difference to overall plant survival, but plants that were acclimated for 2 weeks exhibited significantly less electrolyte leakage than those that were acclimated for 24 hours, suggesting that cold acclimation is incomplete after 24 hours, and further freezing tolerance can be acquired with prolonged cold exposure (Gilmour *et al.* 1988). Due to this difference, subsequent experiments involving cold-acclimated plants used either the two-week protocol or both protocols, but not the 24-hour protocol alone.

Five-week non-acclimated plants fared better than 7-week non-acclimated plants in electrolyte leakage assays, suggesting that there was a reduction in freezing tolerance either as plants got older or as leaves got bigger. To investigate this, electrolyte leakage assays were set up to assess the freezing tolerance of leaves of differing ages and sizes. The results were not straightforward, with large/mid-aged leaves having the lowest electrolyte leakage at each temperature, though the difference was only significant at the highest temperature. There was also no significant difference in electrolyte leakage between young and old leaves of the

same size, at the highest and lowest temperatures, but older leaves had significantly higher leakage at the middle temperature. This was consistent with the results in **Figure 3.1C** that showed older leaves incurring more freezing damage. The brief investigation into the effect of leaf size and age pointed towards leaf size having more of an impact on electrolyte leakage. Because of this, in subsequent assays, leaves were matched as closely as possible for size and then age.

As freezing is an exothermic process, IRVT is a useful tool for studying freezing events that has been utilised extensively to observe ice nucleation and propagation in plants (Wisniewski *et al.* 1997, Fuller & Wisniewski 1998, Wisniewski & Fuller 1999, Pearce & Fuller 2001, Livingston *et al.* 2018, Villouta *et al.* 2022). IRVT was used in the present study to detect potential differences in the freezing patterns of cold-acclimated and non-acclimated plants; specifically, the rates and degrees of supercooling and freezing. The leaves of non-acclimated plants appeared to supercool for slightly longer and to a lower temperature than those of cold-acclimated plants, but the difference was not significant. They also froze slightly later and at a lower temperature but, again, the difference was not statistically significant. One consistent aspect of freezing behaviour was exhibited after the initial freezing event: leaves of cold-acclimated plants remained at a higher temperature after freezing than those of non-acclimated plants. This persisted for several hours until both sets of plants equilibrated with the chamber at -8°C. This could be evidence of cold-acclimated leaves reducing the spread of ice through their tissues but further investigation is required. Differences in freezing behaviour between leaves of the same plant were negligible but there was substantial variation between plants of the same group, particularly temporal variation in supercooling and freezing. It would have been more useful, therefore, to reduce the number of leaves studied per plant, and instead increase the number of plants and repetitions of the experiment. The number of plants studied here, as well as the lack of replication, meant that it was difficult to draw final conclusions. Instead, this experiment represents a promising pilot study into using IRVT to investigate freezing behaviour in cold-acclimated plants.

As discussed in **Section 1.3.3.1**, cold acclimation has been shown to have profound effects on the mass, thickness, strength, stiffness and porosity of the cell wall in a range of species. The evidence for changes in these properties being linked to freezing tolerance is discussed at length in **Section 1.3.3.2**. However, changes in these properties are rarely linked directly to increased freezing tolerance in the same species, and measurements in *Arabidopsis* are lacking. The experiments carried out in the present study aimed to determine whether the cold acclimation protocol that leads to substantially increased freezing tolerance in *Arabidopsis* also induces measurable changes in the cell-wall physical properties of the same species.

The fluorescence quenching assay used to quantify cell-wall porosity, adapted from the method described by Liu *et al.* (2019a), has the advantage of measuring porosity in leaf tissue samples within minutes of sample preparation, thus providing an accurate reflection of cell-wall porosity *in vivo*. Seedling roots were used when initially developing the assay as they allowed for more straightforward sample preparation and imaging. Although they gave some promising results, the assay was ultimately adapted to use leaf tissue to allow for more direct correlations to be made with freezing tolerance, as the electrolyte leakage assay uses the same tissue. The finding that cold acclimation significantly reduced cell-wall porosity in *Arabidopsis* is consistent with the results of studies in other species, including peach (Wisniewski *et al.* 1987), apple and grape (Rajashekar & Lafta 1996), and Japanese bunching onion (Liu *et al.* 2022). These investigations used varying methods to measure porosity but all found the same association between cold acclimation and a reduction in porosity, further validating the results of the present study. Reducing cell-wall pore size is conducive to supercooling, as the freezing point of minute volumes of water present in a porous structure is lower than that of free, bulk water (Mazur 1963, Homshaw 1980, Ashworth & Abeles 1984). Increased pore size has also been linked to a reduced capacity to supercool *in vivo* (Wisniewski *et al.* 1991, Wisniewski & Davis 1995). Despite this, an increased propensity to supercool was not detected with IRVT in the present study. In fact, non-acclimated plants appeared to supercool to a lower temperature than cold-acclimated plants, though the difference was not significant. There could be different pools of water present in the tissue of cold-acclimated leaves compared to non-acclimated leaves, some of

which freeze earlier to give the initial freezing event, and some which freeze more gradually, hence the persistent elevated temperature. As discussed, this particular experiment used a small number of plants and more replicates would be needed to support these findings. IRVT data could also be supplemented with direct measurements of the presence of ice in cells: Rajashekar & Lafta (1996), who reported reduced cell-wall porosity in cold-acclimated apple and grape cells, also detected significantly less intracellular ice in cold-acclimated cells.

Cold-acclimated leaf tissue was also found to have increased mechanical stiffness and strength, evidenced by a steeper gradient and a higher peak compared to non-acclimated leaf tissue, respectively, during application of the tensile force and production of the resultant force curves. A force curve with a steeper gradient indicates that more force was required per unit time to displace or "stretch" the tissue sample, hence it is a stiffer material. The peak of a force curve is the point of mechanical failure and therefore represents the maximum force that the material can withstand before breakage. A force curve with a higher peak, therefore, indicates that the material has greater resistance to breaking pressure, and is a stronger material (Ryden *et al.* 2003, Bidhendi & Geitmann 2016, 2019, Robinson *et al.* 2017, Zhang *et al.* 2019). The data presented here for the mechanical properties of *Arabidopsis* leaves are consistent with data for numerous other species that points towards cold acclimation serving to enhance the mechanical properties of the cell wall (Rajashekar & Lafta 1996, Solecka *et al.* 2008, Scholz *et al.* 2012, Arias *et al.* 2015). It is likely, therefore, that cold acclimation has the potential to do the same in *Arabidopsis*. A stiffer or stronger cell wall has a greater capacity to resist freezing-induced cellular dehydration and is therefore less susceptible to deformation or cytorrhysis (Pearce 1988, Fujikawa *et al.* 1999, Yamada *et al.* 2002). This likely accounts, in part, for the decrease in electrolyte leakage observed in cold-acclimated tissue compared to non-acclimated tissue after freezing.

Accumulation and organisation of specific cell-wall components during cold acclimation may be responsible for the observed changes in cell-wall physical properties. It is also likely that the changes in porosity and mechanical properties observed during cold acclimation are linked, with cold-acclimation mediated cell-

wall remodelling leading to a thicker, denser cell wall that is both stronger and less porous. For instance, cold acclimation has been linked to accumulation of pectin and its side-chains (Kubacka-Zębalska & Kacperska 1999, Solecka *et al.* 2008, Carvalho *et al.* 2013, Baldwin *et al.* 2014, Takahashi *et al.* 2019) as well as decreased methylesterification or increased cross-linking of pectin (Wisniewski & Davis 1995, Solecka *et al.* 2008, Qu *et al.* 2011, Lee *et al.* 2017, Liu *et al.* 2022). Pectin abundance and structure has repeatedly been shown to underpin cell-wall porosity, with the consensus being that more pectin that is heavily cross-linked is associated with a less porous cell wall (Baron-Epel *et al.* 1988, Ehwald *et al.* 1991, 1992, Fleischer *et al.* 1999, Liu *et al.* 2022). Pectin cross-linking may also contribute to cell-wall stiffness (Reiter *et al.* 1993, Ryden *et al.* 2003, Zerzour *et al.* 2009, Chebli *et al.* 2012, Hongo *et al.* 2012, Vogler *et al.* 2013). Furthermore, cold acclimation may induce an increase in EXTs in the cell wall (Weiser *et al.* 1990, Kozbial *et al.* 2002), proteins that potentially contribute to decreased porosity (Wei & Shirsat 2006, Castilleux *et al.* 2021) and increased stiffness (Iraki *et al.* 1989), perhaps even through the formation of a pectin-EXT network (Nuñez *et al.* 2009). It is of considerable interest, therefore, that the present study found that cold acclimation resulted in an increase in both the abundance of EXTs and the proportion of demethylesterified pectin, a form more conducive to cross-linking (Willats *et al.* 2001a,b). Moreover, mutants lacking expression of an *EXT* gene, *EXT18*, were found to have significantly reduced freezing tolerance (both before and after cold acclimation), increased cell-wall porosity, and decreased mechanical strength and stiffness, supporting the above hypotheses. Furthermore, an additional mutant allele of *EXT18* was later identified and found to have significantly increased electrolyte leakage after freezing, confirming beyond doubt that *ext18* mutants are sensitive to freezing (**Appendix Q**). Although EXT18 is considered an integral member of the EXT protein family (Choudhary *et al.* 2015), it was initially surprising to find that knock-out of this gene could have such profound effects on freezing tolerance and cell-wall properties, given that there are at least 58 other EXT-coding genes with some redundancy in *Arabidopsis* (Showalter *et al.* 2010). However, knock-out of *EXT18* was found to reduce the expression of ten other *EXT* genes (Choudhary *et al.* 2015), thus the *ext18* phenotype observed in the present

study may be a result of the compounding effect of a broad reduction in *EXT* gene expression. Alternatively, the *ex18* phenotype may be explained by a compromised pectin structure, as the existence of a rigid EXT-pectin network has been hypothesised (Nuñez *et al.* 2009).

The same logic may also explain why knock-out of individual *PME* genes generally had little impact on freezing tolerance or cell-wall physical properties, with the exception of *PME41*. Although *PME17* and *PME31* are highly induced in response to pathogen invasion (Bethke *et al.* 2014, Del Corpo *et al.* 2020), suggesting they may play a role in pectin remodelling during stress responses, mutants of either gene did not have altered freezing tolerance or cell-wall porosity. It is likely that knock-out of single *PME* genes does not sufficiently reduce overall PME activity or subsequent pectin cross-linking to the extent that it produces measurable differences in these properties. This highlights the complexity and redundancy of the *PME* gene family and suggests that knock-out of multiple PMEs may be required to produce differences measurable by the methods employed in the present study. On the other hand, *pme41* mutants appeared to have a slight freezing-sensitive phenotype; compared to wild-type, *pme41* had decreased plant survival after freezing and increased electrolyte leakage at the lowest temperature, though not at the two higher temperatures. *PME41* is induced by chilling stress at 0°C and *pme41* mutants have been shown to be chilling-sensitive, as well as exhibiting a 71% reduction in total PME activity (Qu *et al.* 2011). Clearly, PME41 is more central to cold and freezing stress responses than the other PMEs that were investigated, and knock-out of *PME41* may have knock-on effects on the expression of other *PME* genes, much like in the case of *ext18*. The large reduction in total PME activity in *pme41* mutants supports this idea. Total PME activity is not significantly reduced in *pme31* mutants (Bethke *et al.* 2014) and is reduced by just 20% in *pme17* (Sénéchal *et al.* 2014). This may explain why cell-wall porosity was increased in *pme41* but not the other *pme* mutants: there may be a threshold of PME activity reduction that must be surpassed before measurable differences in porosity can be observed, and this could also have implications on freezing tolerance. It may also explain why both *pme41* and *pme17* appear to have impaired cell-wall mechanical properties but *pme31* does not.

The cell-wall profiling experiments revealed other components of the cell wall of interest, such as RG-I, which were found to accumulate during cold acclimation. The extent to which RG-I contributes to the mechanical properties of the cell wall remains unclear (McCartney *et al.* 2000, Ulvskov *et al.* 2005), but it is almost certainly associated with HG, either as a spacer along HG backbones (Albersheim *et al.* 1996) or as the main backbone itself with HG acting as a side-chain (Vincken *et al.* 2003, Coenen *et al.* 2007). The increased RG-I content detected in cold-acclimated leaves may be reflective of a broader accumulation of pectin content in preparation for sub-zero temperatures. Alternatively, in a study of RG-I in potato, Larsen *et al.* (2011) showed that arabinan side-chains are more readily hydrated than other side-chains after drought, thus the high arabinan content of RG-I may help to rehydrate cell walls after freezing-induced dehydration. Furthermore, Stranne *et al.* (2018) suggested that RG-I may have a role in water uptake and transport, and Moore *et al.* (2008a) suggested that pectin-associated arabinans may be necessary to maintain cell-wall flexibility during severe dehydration stress.

It has been hypothesised that AGPs contribute to rigidification of the cell wall through oxidative cross-linking (Bradley *et al.* 1992), potentially helping to protect cells from freezing-induced collapse, which may be one reason for their accumulation during cold acclimation. However, if the overarching interpretation of the cell-wall profiling results is that accumulation of the various cell-wall components is, in part, a mechanism through which to increase cell-wall mass or stiffness, then it is surprising that there was no detectable change in xyloglucan content. Xyloglucan has been established as a major load-bearing element of the cell wall along with cellulose (Peña *et al.* 2004, Cavalier *et al.* 2008), thus it could be beneficial to increase its synthesis during cold acclimation. However, it may be modification of existing xyloglucan, rather than synthesis of new xyloglucan, that is important for cell-wall stiffening (Cosgrove 2022). This is supported by several studies that highlighted the importance of xyloglucan modification, rather than abundance, in cold acclimation and freezing tolerance (Shi *et al.* 2014, Takahashi *et al.* 2021a).

As CoMPP is a relatively low-resolution screening assay, it would be beneficial to confirm the above results with alternative methods of mapping the quantities of cell-wall polymers. As was first noted by Moller *et al.* (2007), CoMPP provides quantification data about polymer epitopes but is not appropriate for absolute quantification and comparison of different cell-wall polymers. Different mAbs bind with varying affinities for their epitopes, therefore differences in signal intensities between different probes cannot be used to make comparisons of the abundances of different polymers. Additionally, mAbs may exhibit non-target binding, such as LM5 binding to galactan residues present in cell-wall components other than RG-I (Jones *et al.* 1997). However, it is still a useful tool for mapping the relative levels of a particular polymer across a range of treatments or samples, as was done in the present investigation.

3.4 Summary

In this chapter, a cold acclimation protocol was established that substantially enhances the freezing tolerance of *Arabidopsis*. According to IRVT data, cold acclimation did not appear to increase a plant's propensity to supercool, but it did induce significant decreases in cell-wall porosity and increases in cell-wall mechanical stiffness and strength. Numerous components of the cell wall were found to accumulate during cold acclimation, including EXTs and demethylesterified pectins. Investigation of EXT and PME mutants revealed their contributions to freezing tolerance and cell-wall physical properties.

Chapter 4

Dimerisation of rhamnogalacturonan-II can alter both freezing tolerance and guard cell dynamics

4.1 Introduction

Rhamnogalacturonan-II (RG-II) is one of the three major pectic polysaccharides present in the plant cell wall, with its most significant feature being its ability to dimerise by means of borate-ester cross-linking (**Figure 1.5**). For most of the 20th century, the primary role of boron in plants was unknown, until it was found to bind apiose residues in side-chain A of RG-II, catalysing its dimerisation (O'Neill *et al.* 1996). Over 95% of the RG-II residues present in the plant cell wall exist as covalently linked dimers centred on a borate-ester bond (Matoh *et al.* 1996). *Arabidopsis* mutants deficient in RG-II dimerisation can have drastically altered phenotypes: *mur1*, which has RG-II dimerisation reduced to 50%, is dwarfed and has reduced cell-wall mechanical strength, which can be reversed when plants are supplemented with additional boron (Reiter *et al.* 1993, O'Neill *et al.* 2001, Ryden *et al.* 2003). As discussed in **Section 1.3.3.2**, *sfr8*, which also has a mutation in *MUR1* and reduced RG-II dimerisation, has reduced freezing tolerance (Panter 2018, Panter *et al.* 2019). Another interesting facet of *sfr8* is its severe water-loss phenotype, indicating that it has altered guard-cell dynamics (Panter 2018).

In the first part of this chapter, *sfr8* was used to explore the role of RG-II dimerisation in freezing tolerance. The freezing-sensitive phenotype of *sfr8* was confirmed and studied further with infrared video thermography (IRVT). As RG-II cross-linking has been proposed to affect cell-wall porosity and mechanical properties (Reiter *et al.* 1993, Fleischer *et al.* 1999), these were measured in *sfr8*.

A boron-supplementation protocol that likely restores RG-II dimerisation was established. The freezing tolerance and cell-wall physical properties of boron-supplemented *sfr8* were investigated. To further explore the role of RG-II dimerisation in freezing tolerance, freezing assays were carried out on plants with reduced expression of a GDP-sugar transporter (GGLT1). *GGLT1*-silenced plants (hereafter referred to as hp*GGLT1*, where hp is hairpin) have a 50% reduction in the amount of L-galactose present in side-chain A of RG-II, decreasing the degree of RG-II dimer formation by approximately 25% (Sechet *et al.* 2018). The cell-wall physical properties of hp*GGLT1* were also analysed.

In the second part of this chapter, *sfr8* was used to explore the role of RG-II dimerisation in guard cell dynamics. The water-loss phenotype (decreased leaf water retention) of *sfr8*, identified by Panter (2018), was first confirmed, and studied further through analysis of stomatal density and guard cell morphology. The water-loss phenotype of *sfr8* was then analysed in boron-supplemented plants. The presence of a water-loss phenotype was determined in hp*GGLT1* plants. Finally, cell adhesion was investigated in *sfr8*. Verger *et al.* (2016) demonstrated that cell adhesion in plants may be under the control of fucosyltransferases, and defects in cell adhesion are easily detectable by microscopy in affected hypocotyls. As *sfr8* is deficient in cell-wall fucose (Panter *et al.* 2019), it was hypothesised that defective cell adhesion may be contributing to its water-loss phenotype.

4.2 Results

4.2.1 Freezing tolerance of *sfr8*

The freezing-sensitive phenotype of *sfr8*, and therefore its suitability to act as a positive control in screening other cell-wall mutants for freezing sensitivity, was confirmed with freezing recovery and electrolyte leakage assays. The freezing behaviour of *sfr8* was then explored further using IRVT.

4.2.1.1 Freezing recovery and electrolyte leakage

Mature s*fr8* plants, along with wild-type controls, were subjected to freezing at either -3°C (non-acclimated plants) or -8°C (cold-acclimated plants) for 24 h before being returned to ambient growth conditions. The capacity of the plants to recover

and exhibit new growth was assessed after 1 week (non-acclimated plants: **Figure 4.1A**; cold-acclimated plants: **Figure 4.2A**). Individual linear mixed effects models confirmed that experiment number had no significant impact on the variation of data from both datasets ($p>0.05$ for both) so the data from multiple biological replicate experiments were pooled separately for each treatment (non-acclimated: 24 replicate experiments; cold-acclimated: 9 replicate experiments). Mean percentage survival of plants of each genotype was calculated from pooled data. In both the non-acclimated and cold-acclimated state, *sfr8* had significantly reduced survival after freezing compared to wild-type ($p<0.001$). Non-acclimated *sfr8* had a mean survival rate of 7%, compared to 98% for wild-type (**Figure 4.1B**), and cold-acclimated *sfr8* had a mean survival rate of 10%, compared to 98% for wild-type (**Figure 4.2B**).

In order to quantify the damage incurred by plants during freezing, electrolyte leakage was measured in leaf tissue from plants of both genotypes in both non-acclimated and cold-acclimated states, following exposure to three different sub-zero temperatures (-3, -5 and -7°C for non-acclimated plants; -5, -7 and -9°C for cold-acclimated plants). Individual linear mixed effects models confirmed that experiment number had no significant impact on data variation ($p>0.05$ for both) so the data from multiple biological replicate experiments were pooled separately for each treatment (non-acclimated: 24 replicate experiments; cold-acclimated; 9 replicate experiments). Mean percentage electrolyte leakage of plants of either genotype was calculated at each temperature from pooled data separated by treatment (non-acclimated: **Figure 4.1C**; cold-acclimated: **Figure 4.2C**). In both non-acclimated and cold-acclimated states, *sfr8* had significantly higher electrolyte leakage than wild-type ($p<0.001$ at each temperature). Taken together, these experiments provide overwhelming evidence that *sfr8* has reduced freezing tolerance regardless of acclimation state.

4.2.1.2 Infrared video thermography

Mature wild-type and *sfr8* were subjected to freezing at -3°C and imaged with a FLIR A700-EST IR camera. The temperatures of leaves 8, 9 and 10, as well as the young inner leaves, were recorded continuously by creation of a 3-pixel by 3-pixel

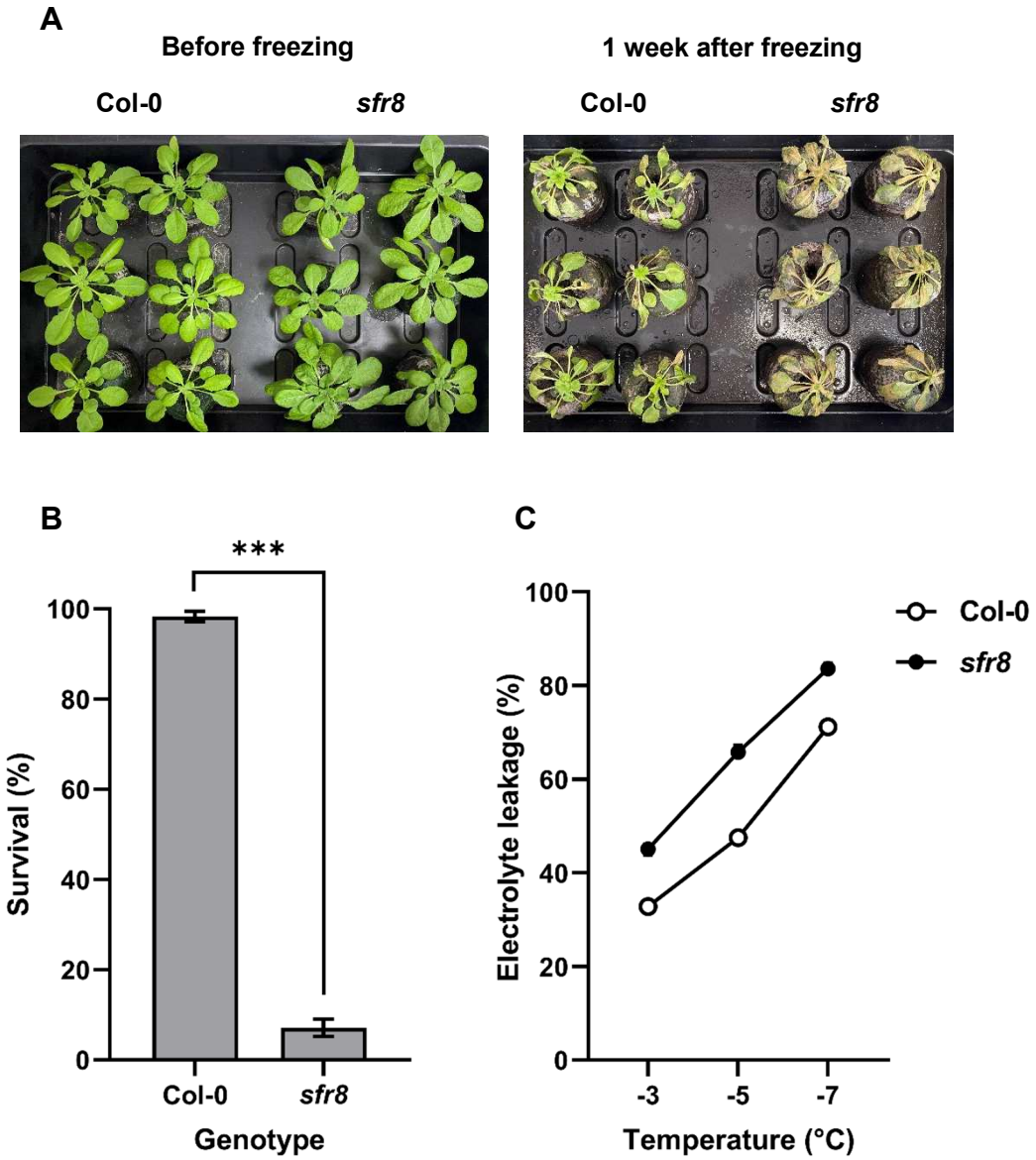

Figure 4.1: Freezing tolerance of *sfr8* without cold acclimation. A) Freezing recovery assay of mature, non-acclimated wild-type (Col-0) and *sfr8* plants. Plants were subjected to freezing at -3°C for 24 h and allowed to recover under ambient conditions for one week. Photographed is representative assay showing plants immediately before (left) one week after (right) freezing. **B)** Survival analysis of plants from freezing recovery assays. Plants were scored on survival based on whether regrowth of green tissue had occurred after one week. Bars represent mean percentage survival of plants from 24 replicate experiments; each experiment used six plants per genotype (n=144). Error bars represent one standard error of the mean of arcsine-transformed data, as is appropriate for proportional data. Asterisks indicate means that are significantly different (*** $p<0.001$). **C)** Electrolyte leakage of mature leaf tissue from non-acclimated wild-type (Col-0) and *sfr8*. Leaf tissue was subjected to freezing at -3, -5 or -7°C and loss of electrolytes was measured. Values represent mean percentage electrolyte leakage from 24 replicate experiments; each experiment used leaf tissue from six plants per genotype per temperature (n=144 at each point). Error bars represent one standard error of the mean of arcsine-transformed data.

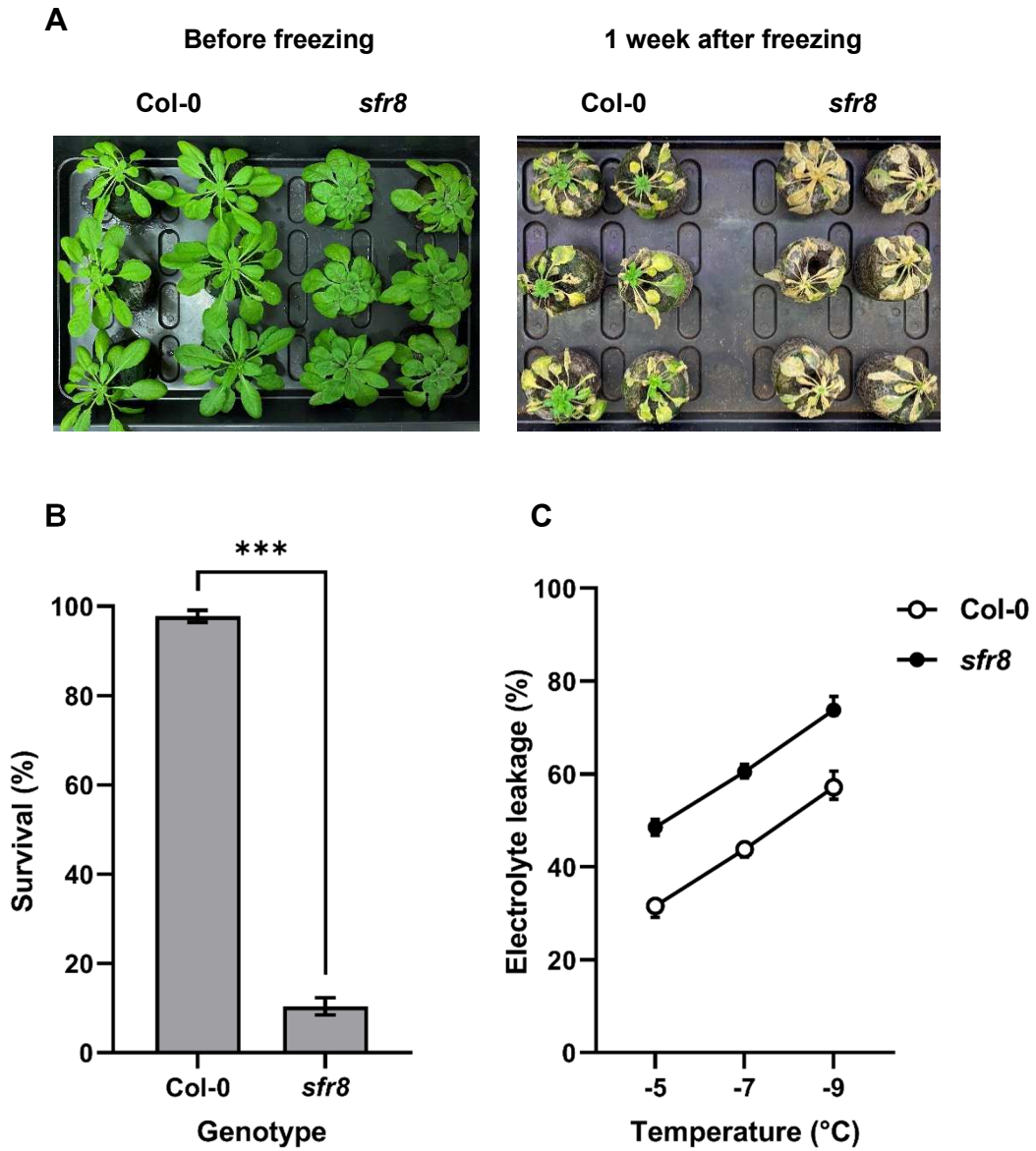

Figure 4.2: Freezing tolerance of *sfr8* after cold acclimation. A) Freezing recovery assay of mature, cold-acclimated wild-type (Col-0) and *sfr8* plants. Plants were subjected to freezing at -8°C for 24 h and allowed to recover under ambient conditions for one week. Photographed is one representative assay showing plants immediately before (left) and one week after (right) freezing. **B)** Survival analysis of plants from freezing recovery assays. Plants were scored on survival based on whether regrowth of green tissue had occurred after one week. Bars represent mean percentage survival of plants from 9 replicate experiments; each experiment used six plants per genotype (n=54). Error bars represent one standard error of the mean of arcsine-transformed data, as is appropriate for proportional data. Asterisks indicate means that are significantly different (*** $p<0.001$). **C)** Electrolyte leakage of mature leaf tissue from cold-acclimated wild-type (Col-0) and *sfr8*. Leaf tissue was subjected to freezing at -5, -7 or -9°C and loss of electrolytes was measured. Values represent mean percentage electrolyte leakage from 9 replicate experiments; each experiment used leaf tissue from six plants per genotype per temperature (n=54 at each point). Error bars represent one standard error of the mean of arcsine-transformed data.

ROI in the centre of each leaf, as well as in the centre of each plant to monitor the inner leaves, in the same manner described in **Figure 3.3C**. Freezing patterns for each of the selected leaves were observed in the same manner described in **Section 3.2.1.3**: combining the data for leaves of the same number, separated by genotype, and plotting the average temperature over time (**Figure 4.3A**). As freezing is an exothermic reaction, the point at which ice nucleation began was identified by a sharp increase in temperature. Interestingly, after freezing, the average temperature of leaves 9 and 10, as well as the inner leaves, remained slightly higher in *sfr8* compared to wild-type plants. The average temperature of leaf 8 after freezing remained broadly the same between the two genotypes. Based on these plots, wild-type leaves appeared to both supercool to and freeze at a lower temperature than *sfr8*. In order to explore this further, the average degree of supercooling and average point of freezing were plotted for each leaf (**Figure 4.3B**). In each case, wild-type leaves supercooled to a lower temperature than *sfr8* but the difference was only significant in the case of leaf 9 ($p<0.05$). Leaves of *sfr8* supercooled for longer than those of wild-type but the difference was only significant in the case of the inner leaves ($p<0.01$). The temperature at which leaves froze was not significantly different between genotypes for any leaves ($p>0.6$). However, in the case of leaves 8 and 9, and the inner leaves, *sfr8* leaves froze significantly later than those of wild-type ($p<0.05$).

4.2.2 Cell-wall physical properties of *sfr8*

Cell-wall porosity and mechanical properties were assessed in *sfr8* to determine if there was a correlation between the freezing sensitivity of *sfr8* and the physical properties of its cell wall.

4.2.2.1 Porosity

The cell-wall porosity of *sfr8* was measured using a fluorescence quenching assay (**Figure 4.4A**). The fluorescence of stained mesophyll cell plasma membranes was quantified (F_0;) and divided by the quantified fluorescence after quenching (F) to give a measure of relative porosity. A linear mixed effects model confirmed that experiment number had no significant impact on data variation ($p>0.1$) so the data from three biological replicate experiments were pooled for analysis.

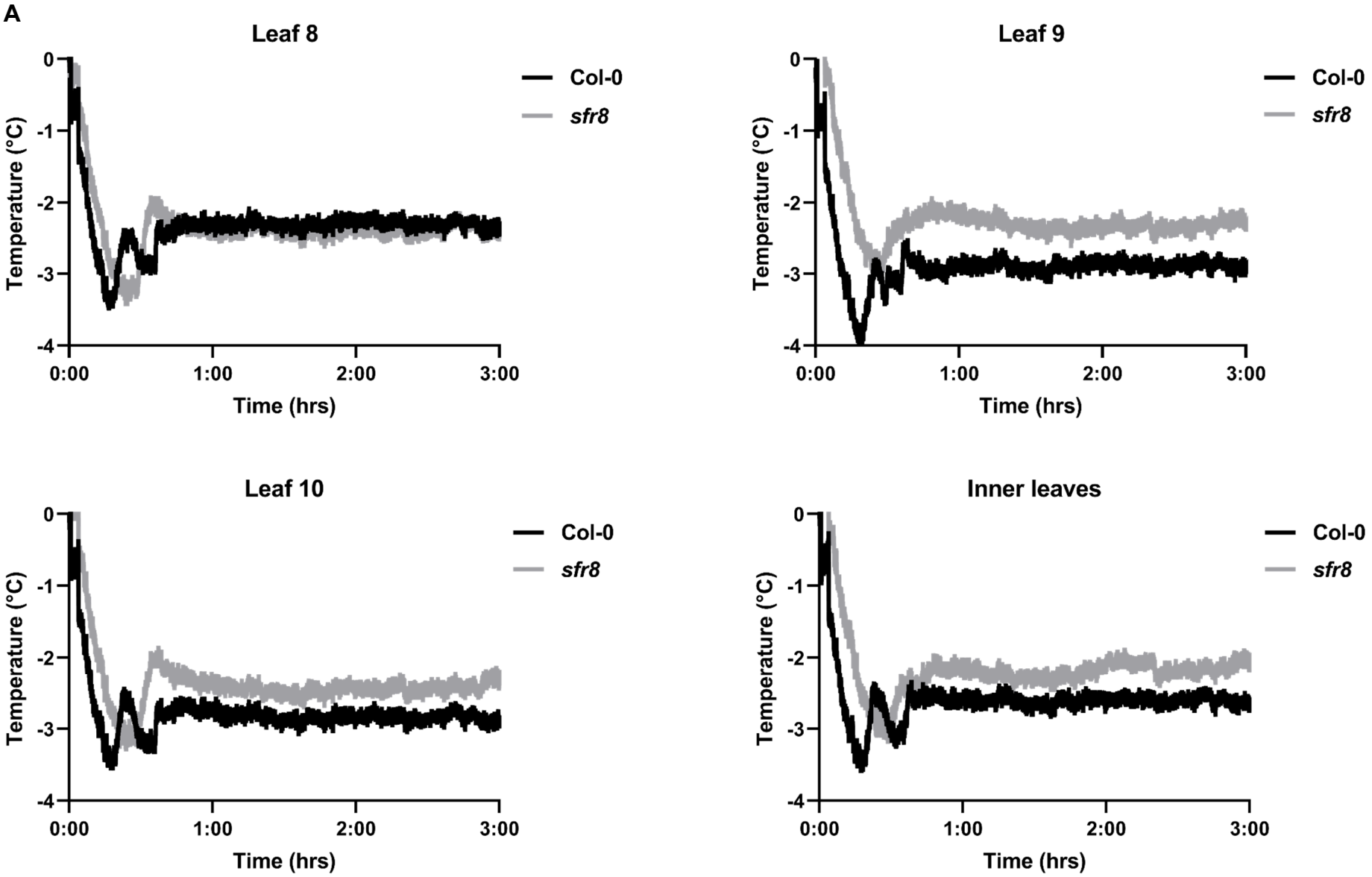
A
Leaf 8
Leaf 9
Leaf 10
Inner leaves
Col-0
sfr8
Temperature (°C)
0
-1
-2
-3
-4
0:00
1:00
2:00
3:00
Time (hrs)

B

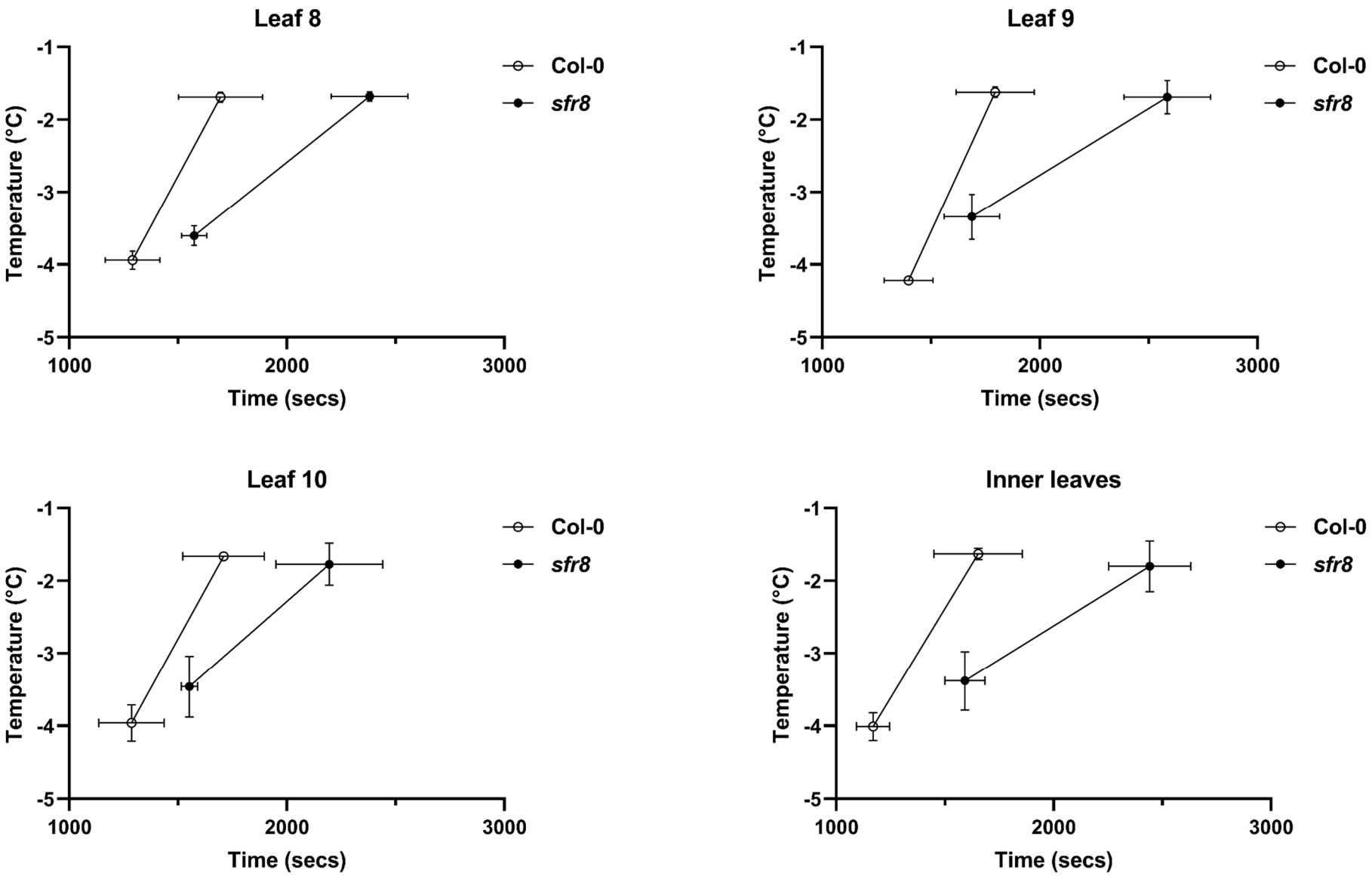
Leaf 8
Leaf 9
Leaf 10
Inner leaves
Col-0
sfr8
Temperature (°C)
Time (secs)
-1
-2
-3
-4
-5
1000
2000
3000

Figure 4.3 Infrared video thermography (IRVT) of *sfr8* during freezing. Mature wild-type (Col-0) and *sfr8* plants were subjected to freezing at -3°C and imaged with a FLIR A700-EST IR camera at 1 frame per second. The temperature of a 3-pixel by 3-pixel region of interest (ROI) was recorded continuously at the centre of leaves 8, 9 and 10, as well as at the young inner leaves, on each plant using FLIR Research Studio. **A)** The mean temperature of each ROI was averaged for each selected leaf at each frame between genotypes and plotted over time. The plots, therefore, show the mean temperature of leaves of the same number over time. Although plants were placed into the chamber at an ambient temperature and gradually cooled to below freezing, only the data from shortly after the plants passed 0°C is shown. **B)** The degree to which the leaves supercooled and the point at which they froze was averaged and plotted over time. The supercooling point was taken as the point at which plants stopped cooling and begun freezing, i.e. the point immediately before the sharp increase in temperature which illustrates the exothermic process of ice nucleation. The freezing point was taken as the peak of this sharp temperature increase. Therefore, for each plot, the supercooling point is the lower, left-most point, and the freezing point is the upper, right-most point. Error bars represent one standard error of the mean. Six plants per genotype were used.

Mean relative porosities of *sfr8* and wild-type leaves were calculated from pooled data. *sfr8* was found to have significantly increased cell-wall porosity relative to wild-type ($p<0.01$). The mean relative porosity of *sfr8* was 7.13 compared to 3.15 for wild-type (**Figure 4.4B**).

4.2.2.2 Mechanical properties

The cell-wall mechanical properties of *sfr8* were measured using extensometry. Eight-mm discs prepared from mature leaves of wild-type and *sfr8* plants were stretched until failure using an extensometer equipped with a load cell sensitive to 1 mN. A linear mixed effects model confirmed that experiment number had no significant impact on data variation ($p>0.2$) so the data from three biological replicate experiments were pooled for analysis. Mean percentage relative tensile force, normalised to the baseline force reading taken immediately before the stretch was initiated, was calculated from pooled data and plotted over time. Average force curves for wild-type and *sfr8* were plotted on the same axes (**Figure 4.5A**). The gradient of the curve for *sfr8* tissue up to the point of failure was 0.302, compared to 0.363 for wild-type, suggesting that *sfr8* has reduced cell-wall stiffness. The percentage relative tensile force values from the peak of force curves from individual samples were plotted to illustrate the cell-wall mechanical strength of tissue from each genotype. The mechanical strength of *sfr8* was found to be significantly lower than that of wild-type ($p<0.001$). The mean maximum relative tensile force for *sfr8* was 5.02%, compared to 6.33% for wild-type (**Figure 4.5B**).

4.2.3 RG-II dimerisation and boron supplementation in *sfr8*

Previous work has established that *mur1* and *sfr8* mutants have reduced RG-II dimerisation, a defect that can be reversed through boron supplementation (O'Neill *et al.* 2001, Panter *et al.* 2019). The purpose of these experiments was to establish a method of supplementing plants with boron that does not rely on boric acid, which may alter the pH of the cell wall and cause undesired effects. Instead, plants were treated with potassium borate (KBO). Control plants were treated with an equivalent amount of potassium chloride (KCl).

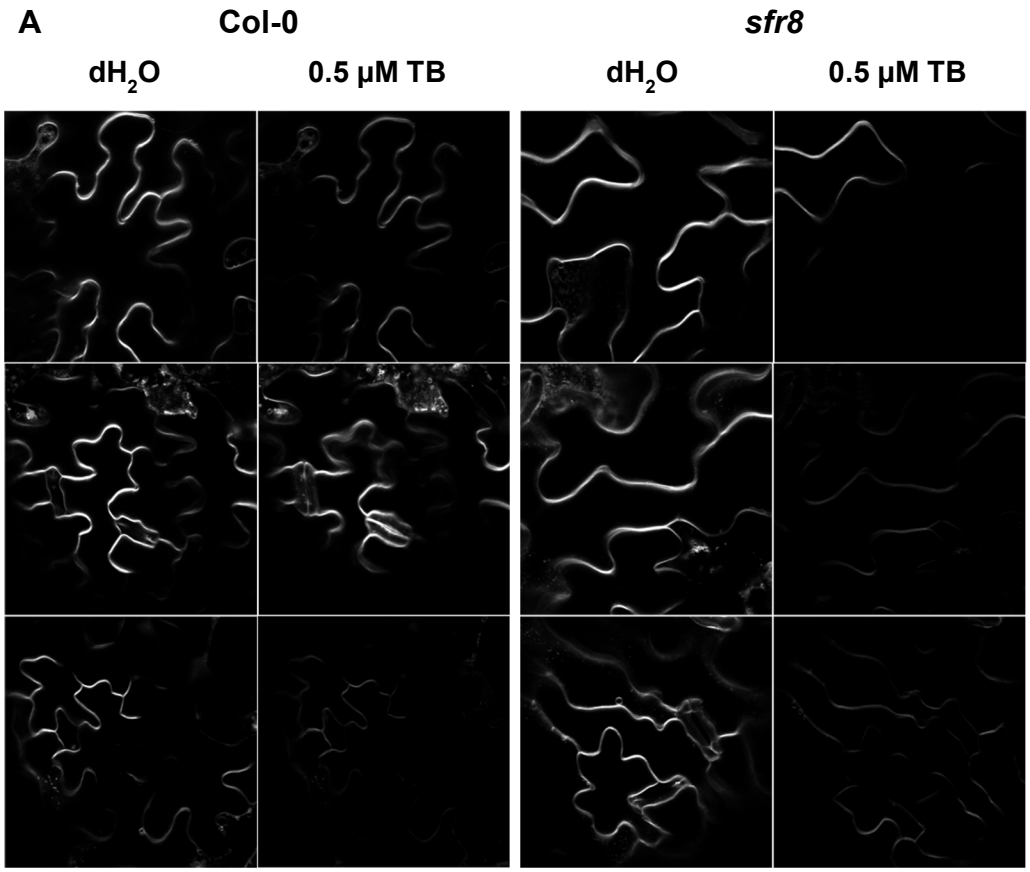

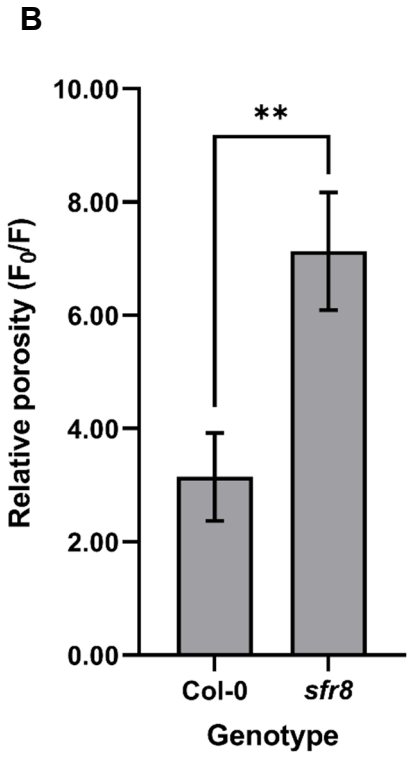

Figure 4.4: Cell-wall porosity of *sfr8*. Relative porosity was calculated in mature wild-type (Col-0) and *sfr8* plants using fluorescence quenching. **A)** The plasma membranes of leaf epidermal cells were stained with a fluorescent dye and imaged before and after addition of 0.5 µM trypan blue (TB) quenching solution. Three example micrographs per treatment are shown for each genotype. **B)** Fluorescence was quantified before (F_0) and after (F) addition of the quenching solution and a ratio of the two was calculated to give relative porosity (F_0/F). Bars represent mean relative porosity from three biological replicate experiments; each experiment measured porosity in three leaves from separate plants per genotype (n=9). Error bars represent one standard error of the mean. Asterisks indicate means that are significantly different (** $p<0.01$).

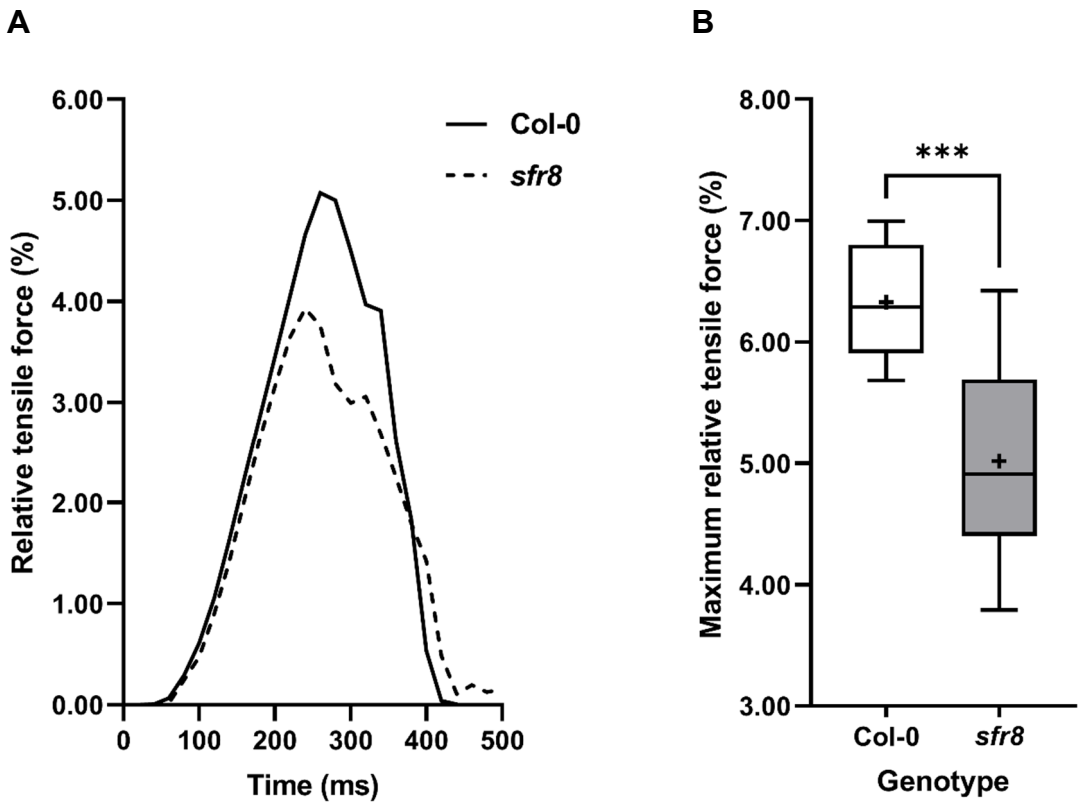

Figure 4.5: Cell-wall mechanical properties of *sfr8*. Mechanical properties were assessed in mature wild-type (Col-0) and *sfr8* plants using extensometry. Leaf discs from each genotype were stretched until breakage and the force required to do so was recorded. Tensile force was normalised to the baseline force reading taken immediately before the stretch was initiated and converted to a percentage for each sample. Plots represent combined data for three biological replicate experiments; each experiment measured cell-wall mechanical properties in three leaf discs per genotype (n=9). **A)** Relative tensile force plotted over time for the duration of each stretch. A steeper gradient is indicative of stiffer material and a higher peak (more resistance to breaking pressure) is indicative of stronger material. **B)** Box-and-whisker plot showing the distribution of maximum tensile force values for each genotype. Values were taken from the absolute peak of each force curve, which represents the maximum tensile force that the tissue can withstand before breakage. Whiskers: maximum and minimum values; box edges: upper and lower quartiles; plus signs: mean values; horizontal lines: median values. Asterisks indicate means that are significantly different (*** $p<0.001$).

A phenotypic assessment was carried out on mature boron-supplemented (B+) and non-supplemented (B-) wild-type and *sfr8* plants to determine the effects of supplementation (**Figure 4.6A**). The morphology of B- *sfr8* plants was typical of *sfr8* and *mur1*: shorter petioles and smaller, rounder leaves. These characteristics were largely reversed in B+ *sfr8*, and they actually resembled wild-type plants. On the other hand, boron supplementation appeared to have little effect on wild-type plants, with both B+ and B- plants exhibiting similar morphologies. This was a strong indication that the supplementation protocol served the desired purpose of providing plants with supplementary boron and increasing RG-II dimerisation in *sfr8*.

To test this further, RG-II dimerisation was measured in both B+ and B- wild-type and *sfr8* using polyacrylamide gel electrophoresis (PAGE). Briefly, cell-wall extracts were prepared from mature leaves from plants of each group and digested with a polygalacturonase (PG) enzyme. PAGE was used to separate RG-II monomer and dimer from each digested extract so that their relative proportions could be determined. The results of the PAGE analysis were inconclusive (**Figure 4.6B**). Firstly, boron supplementation appeared to have no effect on RG-II dimerisation in wild-type plants, as the monomer and dimer bands for B- and B+ plants were of comparable sizes and intensities. As expected, the RG-II monomer band for B- *sfr8* appeared more intense than that of wild-type, indicating that there was a larger proportion of RG-II monomer present in the cell-wall extract. Similarly, the corresponding dimer band for *sfr8* appeared smaller and less intense than that of wild-type, indicative of a smaller proportion of dimerised RG-II. The monomer band for B+ *sfr8* was arguably smaller and less intense than that of B- *sfr8*, but any differences were slight. The same was true of the *sfr8* dimer bands. These results provide weak evidence, if any, of the supplementation protocol reversing the reduction in RG-II dimerisation in *sfr8* mutants. However, it may be the case that the PAGE method used here is not appropriate for measuring RG-II dimerisation in boron-supplemented plants due to the instability of mutant dimers. This is discussed in more detail in **Section 4.3**.

A

Col-0

B-

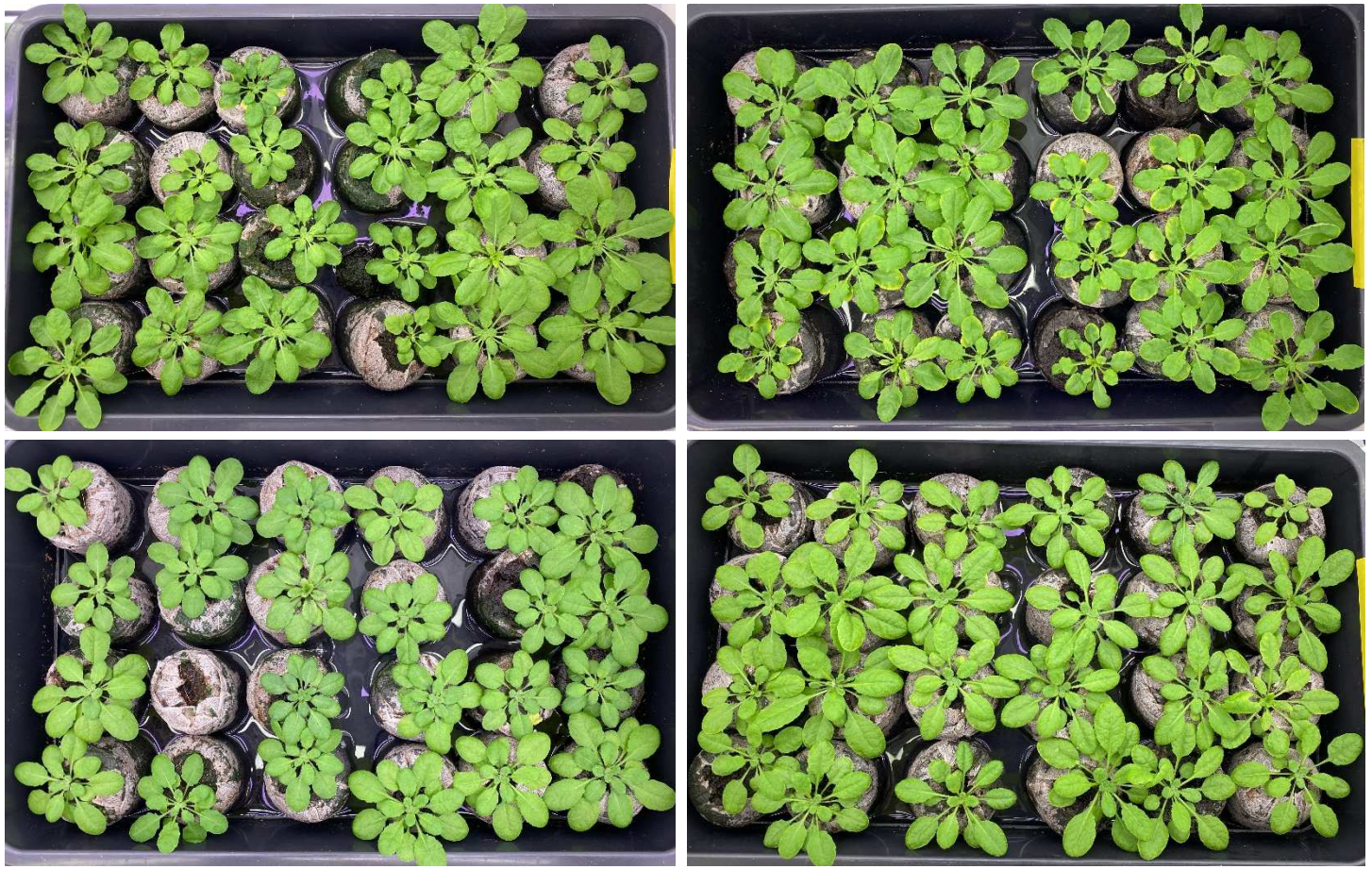

B+

sfr8

B

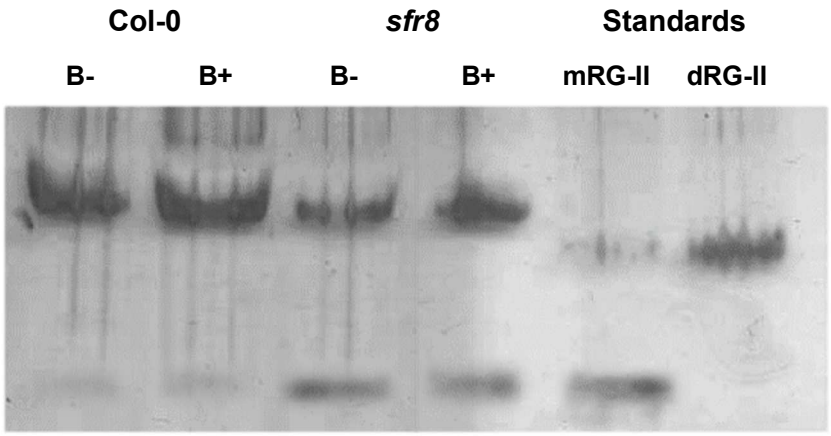

Figure 4.6: Effect of boron supplementation on RG-II dimerisation in *sfr8*. Wild-type (Col-0) and *sfr8* plants were grown to maturity and either deprived of (B-) or supplemented with (B+) boron throughout their lifetimes. **A)** Phenotypic assessment of mature plants. Top: wild-type; bottom: *sfr8*; left: non-supplemented plants; right: boron-supplemented plants. **B)** Polyacrylamide gel electrophoresis (PAGE) analysis of RG-II compositions from mature leaves. Cell-wall extractions from each group were prepared and digested with a polygalacturonase (PG) enzyme. PAGE was then used to separate RG-II monomer from RG-II dimer in each cell-wall digest. Two left-most lanes: RG-II from non-supplemented (left) and boron-supplemented (right) wild-type leaves. Middle lanes: RG-II from non-supplemented (left) and boron-supplemented (right) *sfr8* leaves. Two right-most lanes: purified monomerised (mRG-II; left) and dimerised (dRG-II; right) RG-II standards from sugar beet. The smaller mRG-II molecules run further down the gel compared to the larger dRG-II molecules so the positions of the standards can be used to identify mRG-II and dRG-II in test samples.

4.2.4 Freezing tolerance of boron-supplemented *sfr8*

To assess the effect that increased boron-mediated RG-II dimerisation has on freezing tolerance, freezing assays were carried out on B+ and B- *sfr8* plants. Plants were subjected to freezing at -3°C for 24 h before being returned to ambient growth conditions. The capacity of the plants to recover and exhibit new growth was assessed after 1 week (**Figure 4.7A**). A linear mixed effects model confirmed that experiment number had no significant impact on data variation ($p>0.1$) so the data from three biological replicate experiments were pooled for analysis. Mean percentage survival of plants of each genotype and treatment was calculated from pooled data (**Figure 4.7B**). Both genotype ($p<0.001$) and treatment ($p<0.005$) had a significant impact on plant survival. There was also a significant interaction effect between genotype and treatment ($p<0.005$). Boron supplementation had no effect on wild-type survival, with both B+ and B- plants exhibiting a mean survival rate of 94%. B- *sfr8* plants had a mean survival rate of 11%, which was significantly lower than that of both wild-type groups. Boron supplementation increased mean *sfr8* survival to 67%, which was significantly higher than that of B- *sfr8*, but still significantly lower than that of both wild-type groups.

In order to quantify the damage incurred by plants during freezing, electrolyte leakage was measured in leaf tissue from plants of both genotypes and treatment groups following exposure to three different sub-zero temperatures (-3, -5 and -7°C). A linear mixed effects model confirmed that experiment number had no significant impact on data variation ($p>0.1$) so the data from three biological replicate experiments were pooled for analysis. Mean percentage electrolyte leakage of plants from each group was calculated at each temperature from pooled data (**Figure 4.7C**). At -3°C and -5°C, both genotype (-3°C: $p<0.001$; -5°C: $p<0.05$) and treatment (-3°C: $p<0.005$; -5°C: $p<0.05$) had a significant impact on electrolyte leakage, and there was also a significant interaction effect between the two (-3°C: $p<0.01$; -5°C: $p<0.05$). At both temperatures, B+ *sfr8* plants had significantly lower electrolyte leakage than B- *sfr8* plants. In fact, B- *sfr8* had significantly higher electrolyte leakage than every other group, which were not significantly different from each other. At -7°C, genotype had a significant impact on electrolyte leakage

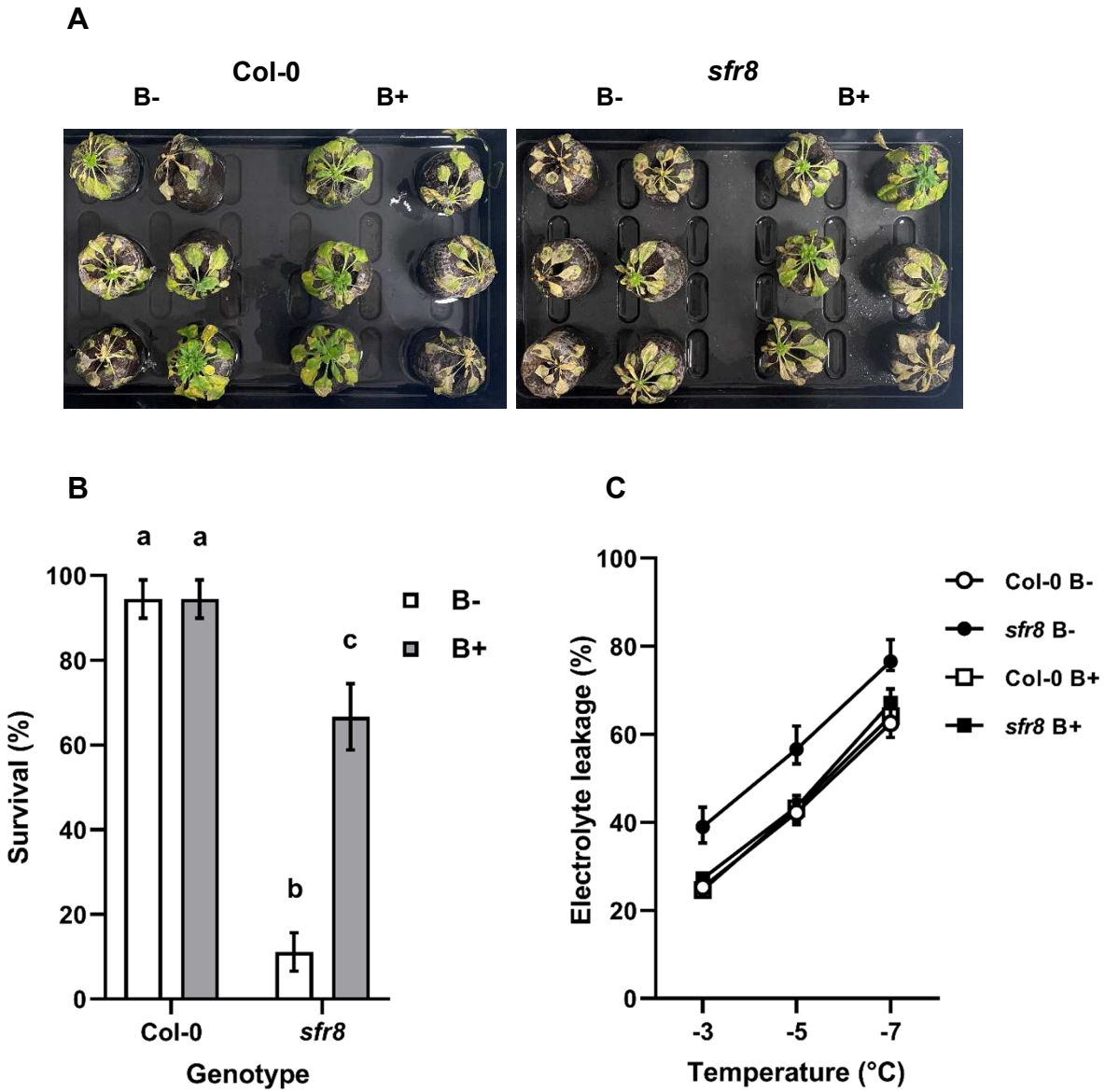

Figure 4.7: Freezing tolerance of boron-supplemented *sfr8*. A) Freezing recovery assay of mature wild-type (Col-0) and *sfr8* either deprived of (B-) or supplemented with (B+) boron. Plants were subjected to freezing at -3°C for 24 h and allowed to recover under ambient conditions for one week. Photographed is one representative assay showing plants one week after freezing. **B)** Survival analysis of plants from freezing recovery assays. Plants were scored on survival based on whether regrowth of green tissue had occurred after one week. Bars represent mean percentage survival of plants from 3 replicate experiments; each experiment used six plants per genotype/treatment (n=18). Error bars represent one standard error of the mean of arcsine-transformed data, as is appropriate for proportional data. Means that do not share a letter are significantly different. **C)** Electrolyte leakage of leaf tissue from mature wild-type (Col-0) and *sfr8* either deprived of (B-) or supplemented with (B+) boron. Leaf tissue was subjected to freezing at -3, -5 or -7°C and loss of electrolytes was measured. Values represent mean percentage electrolyte leakage from 3 replicate experiments; each experiment used leaf tissue from six plants per genotype/treatment per temperature (n=18 at each point). Error bars represent one standard error of the mean of arcsine-transformed data.

($p<0.005$) but treatment did not ($p>0.1$), and there was no significant interaction effect between the two ($p>0.05$). B+ *sfr8* exhibited lower electrolyte leakage than B- *sfr8* but the difference was not significant. B- *sfr8* had significantly higher electrolyte leakage than both B+ and B- wild-type plants. Electrolyte leakage of B+ *sfr8* was not significantly different to that of both wild-type groups. Taken together, these freezing assays show that boron supplementation partially rescues the freezing sensitivity of *sfr8*.

4.2.5 Cell-wall physical properties of boron-supplemented *sfr8*

The same physical properties were measured in boron-supplemented *sfr8* plants in order to assess that increased RG-II dimerisation has on them.

4.2.5.1 Porosity

The cell-wall porosities B+ and B- wild-type (**Figure 4.8A**) and *sfr8* (**Figure 4.9A**) plants were measured using fluorescence quenching. The porosities of wild-type and *sfr8* plants had to be measured in separate assays due to facility limitations*. The fluorescence of stained mesophyll cells was quantified (F_0;) and divided by the quantified fluorescence after quenching (F) to give a measure of relative porosity. Individual linear mixed effects models confirmed that experiment number had no significant impact on data variation ($p>0.05$ for both) so the data from three biological replicate experiments per genotype were pooled for analysis. Mean relative porosities were calculated from pooled data. Boron supplementation was found to have no significant effect on the cell-wall porosity of wild-type plants ($p>0.7$; **Figure 4.8B**), but B+ *sfr8* had significantly lower porosity than B- *sfr8* ($p<0.05$; **Figure 4.9B**). This suggests that boron supplementation can reverse the decrease in cell-wall porosity in *sfr8*.

4.2.5.2 Mechanical properties

The cell-wall mechanical properties of B+ and B- wild-type (Col-0) and *sfr8* plants were measured using extensometry. Eight-mm discs prepared from mature leaves

*Microscopy facilities are a communal resource bookable for a maximum of three hours per session. This was insufficient time to carry out all necessary measurements of both genotypes and treatments, so genotypes were divided into separate experiments.

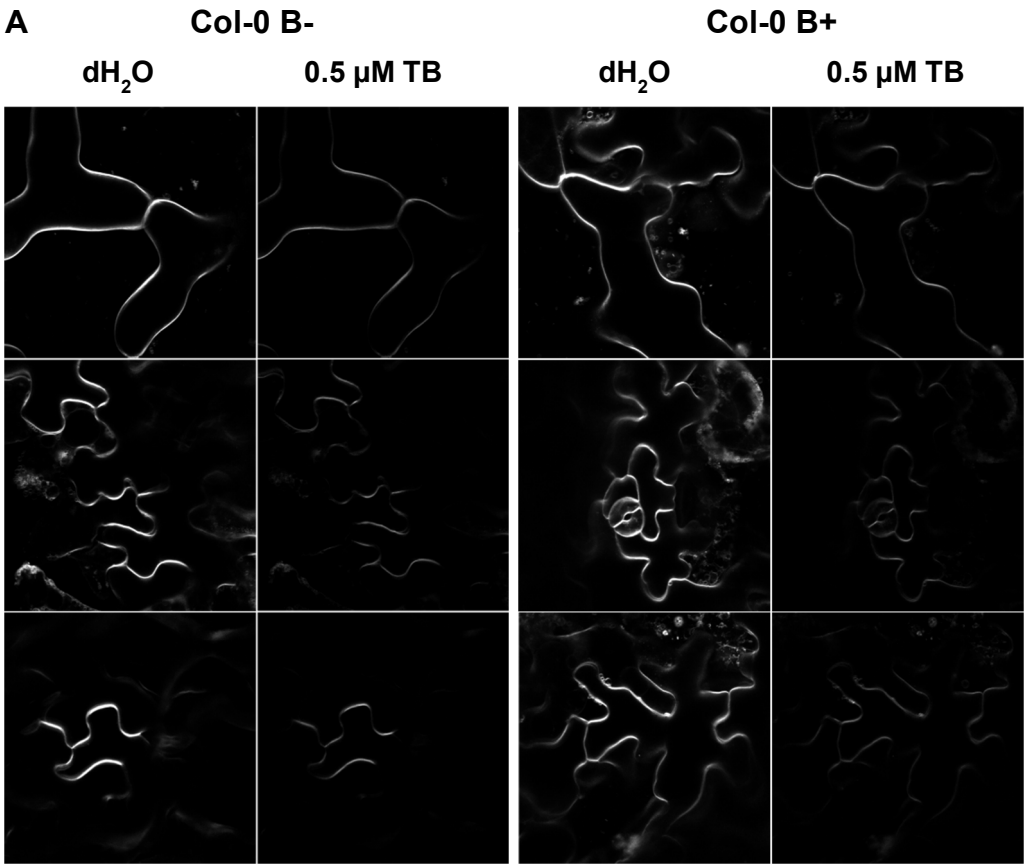

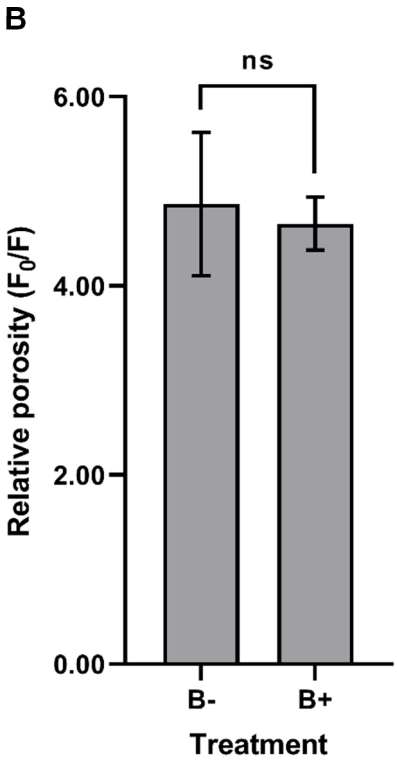

Figure 4.8: Cell-wall porosity of boron-supplemented wild-type *Arabidopsis*. Relative porosity was calculated in mature non-supplemented (B-) and boron-supplemented (B+) wild-type (Col-0) plants using fluorescence quenching. **A)** The plasma membranes of leaf epidermal cells were stained with a fluorescent dye and imaged before and after addition of 0.5 µM trypan blue (TB) quenching solution. Three example micrographs per treatment are shown. **B)** Fluorescence was quantified before (F_0) and after (F) addition of the quenching solution and a ratio of the two was calculated to give relative porosity (F_0/F). Bars represent mean relative porosity from three biological replicate experiments; each experiment measured porosity in three leaves from separate plants per treatment (n=9). Error bars represent one standard error of the mean. ns indicates means that are not significantly different ($p>0.7$).

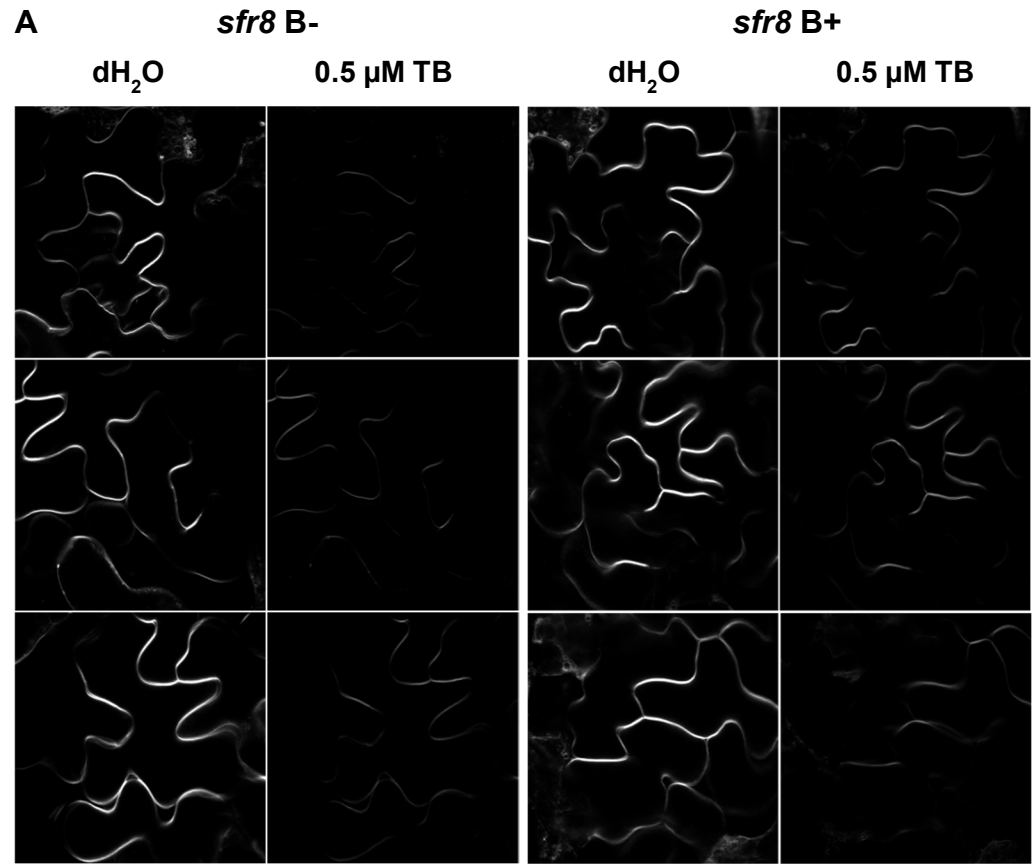

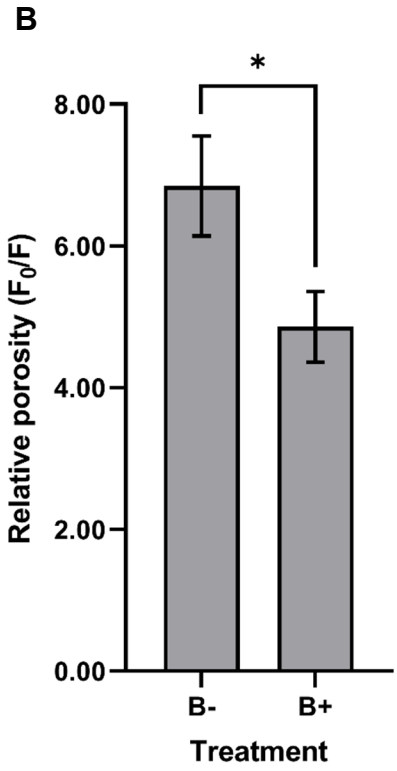

Figure 4.9: Cell-wall porosity of boron-supplemented *sfr8*. Relative porosity was calculated in mature non-supplemented (B-) and boron-supplemented (B+) *sfr8* mutants using fluorescence quenching. **A)** The plasma membranes of leaf epidermal cells were stained with a fluorescent dye and imaged before and after addition of 0.5 µM trypan blue (TB) quenching solution. Three example micrographs per treatment are shown. **B)** Fluorescence was quantified before (F_0) and after (F) addition of the quenching solution and a ratio of the two was calculated to give relative porosity (F_0/F). Bars represent mean relative porosity from three biological replicate experiments; each experiment measured porosity in three leaves from separate plants per treatment (n=9). Error bars represent one standard error of the mean. Asterisks indicate means that are significantly different (* $p<0.05$).

of plants from each group were stretched until failure using an extensometer equipped with a load cell sensitive to 1 mN. A linear mixed effects model confirmed that experiment number had no significant impact on data variation ($p>0.1$) so the data from three biological replicate experiments were pooled for analysis. Mean percentage relative tensile force, normalised to the baseline force reading taken immediately before the stretch was initiated, was calculated from pooled data and plotted over time. Average force curves for each group were plotted on the same axes (**Figure 4.10A**). The gradient of the curve up to the point of failure for B- wild-type tissue was 0.359, compared to 0.344 for B+ tissue, suggesting that boron supplementation had very little effect on the cell-wall stiffness of wild-type tissue. Stiffness was actually marginally lower in B+ samples. For *sfr8*, the gradient of the curve up to the point of failure for B- tissue was 0.283, compared to 0.324 for B+ tissue, suggesting that boron supplementation had a much larger impact on *sfr8* tissue and increased stiffness markedly.

The percentage relative tensile force values from the peak of force curves from individual samples were plotted to illustrate the cell-wall mechanical strength of tissue from each group (**Figure 4.10B**). Genotype ($p<0.001$), but not treatment ($p>0.3$), had a significant impact on cell-wall mechanical strength. There was no significant interaction effect between genotype and treatment ($p>0.3$). Pairwise comparisons found that boron supplementation had no significant effect on the cell-wall mechanical strength of wild-type plants. The mean maximum relative tensile force for both B+ and B- wild-type tissue was 6.03%. Despite the general linear model not detecting a significant effect of treatment, pairwise comparisons revealed that boron supplementation had a significant effect on the mechanical strength of *sfr8*. The mean maximum relative tensile force for B- *sfr8* was 4.13%, compared to 4.92% for B+ plants, and the difference was statistically significant.

4.2.6 Freezing tolerance of *GGLT1* knock-down plants

To further explore the role of RG-II dimerisation in freezing tolerance, freezing assays were carried out on hp*GGLT1* plants along with their empty-vector (EV) controls. Wild-type (Col-0) and *sfr8* plants were also included as additional controls. Plants were subjected to freezing at -3°C for 24 h before being returned

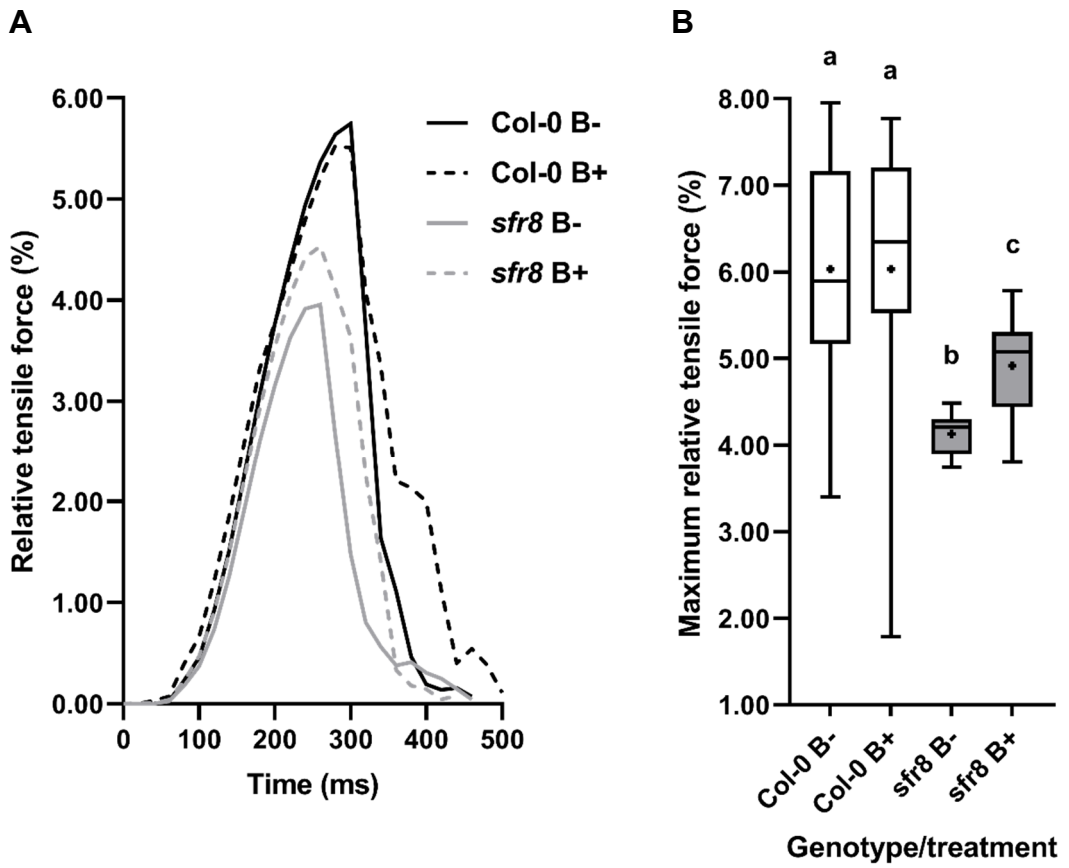

Figure 4.10: Cell-wall mechanical properties of boron-supplemented *sfr8*. Mechanical properties were assessed in mature wild-type (Col-0) and *sfr8* plants that had either been supplemented with (B+) or deprived of (B-) boron using extensometry. Leaf discs from plants of each group were stretched until breakage and the force required to do so was recorded. Tensile force was normalised to the baseline force reading taken immediately before the stretch was initiated and converted to a percentage for each sample. Plots represent combined data for three biological replicate experiments; each experiment measured cell-wall mechanical properties in three leaf discs per group (n=9). **A)** Relative tensile force plotted over time for the duration of each stretch. A steeper gradient is indicative of stiffer material and a higher peak (more resistance to breaking pressure) is indicative of stronger material. **B)** Box-and-whisker plot showing the distribution of maximum tensile force values for each group. Values were taken from the absolute peak of each force curve, which represents the maximum tensile force that the tissue can withstand before breakage. Whiskers: maximum and minimum values; box edges: upper and lower quartiles; plus signs: mean values; horizontal lines: median values. Means that do not share a letter are significantly different.

to ambient growth conditions. The capacity of the plants to recover and exhibit new growth was assessed after 1 week (**Figure 4.11A**). A linear mixed effects model confirmed that experiment number had no significant impact on the variation of data from both datasets ($p>0.2$) so the data from three biological replicate experiments were pooled for analysis. Mean percentage survival of plants of each genotype was calculated from pooled data. Genotype had a significant impact on plant survival ($p<0.001$). However, only *sfr8* had significantly decreased survival; there was no significant difference in the mean survival rates of wild-type, EV or hp*GGLT1* plants (**Figure 4.11B**).

In order to quantify the damage incurred by plants during freezing, electrolyte leakage was measured in leaf tissue from plants of each genotype following exposure to three different sub-zero temperatures (-3, -5 and -7°C). A linear mixed effects model confirmed that experiment number had no significant impact on data variation ($p>0.1$) so the data from three biological replicate experiments were pooled separately for analysis. Mean percentage electrolyte leakage of plants of each genotype was calculated at each temperature from pooled data (**Figure 4.11C**). At -3 and -5°C, genotype had a significant impact on electrolyte leakage ($p<0.001$). However, at both temperatures, only *sfr8* had significantly increased electrolyte leakage; there was no significant difference in mean electrolyte leakage between wild-type, EV or hp*GGLT1* plants. Genotype also had a significant impact on electrolyte leakage at -7°C ($p<0.05$). However, again, the electrolyte leakage of hp*GGLT1* did not differ significantly from that of Col-0 or EV controls.

4.2.7 Cell-wall physical properties of *GGLT1* knock-down plants

Cell-wall porosity and mechanical properties were assessed in hp*GGLT1* to further investigate the potential link between RG-II dimerisation and cell-wall physical properties.

4.2.7.1 Porosity

The cell-wall porosities of hp*GGLT1* and EV controls were measured using fluorescence quenching (**Figure 4.12A**). The fluorescence of stained mesophyll cells was quantified (F_0;) and divided by the quantified fluorescence after quenching

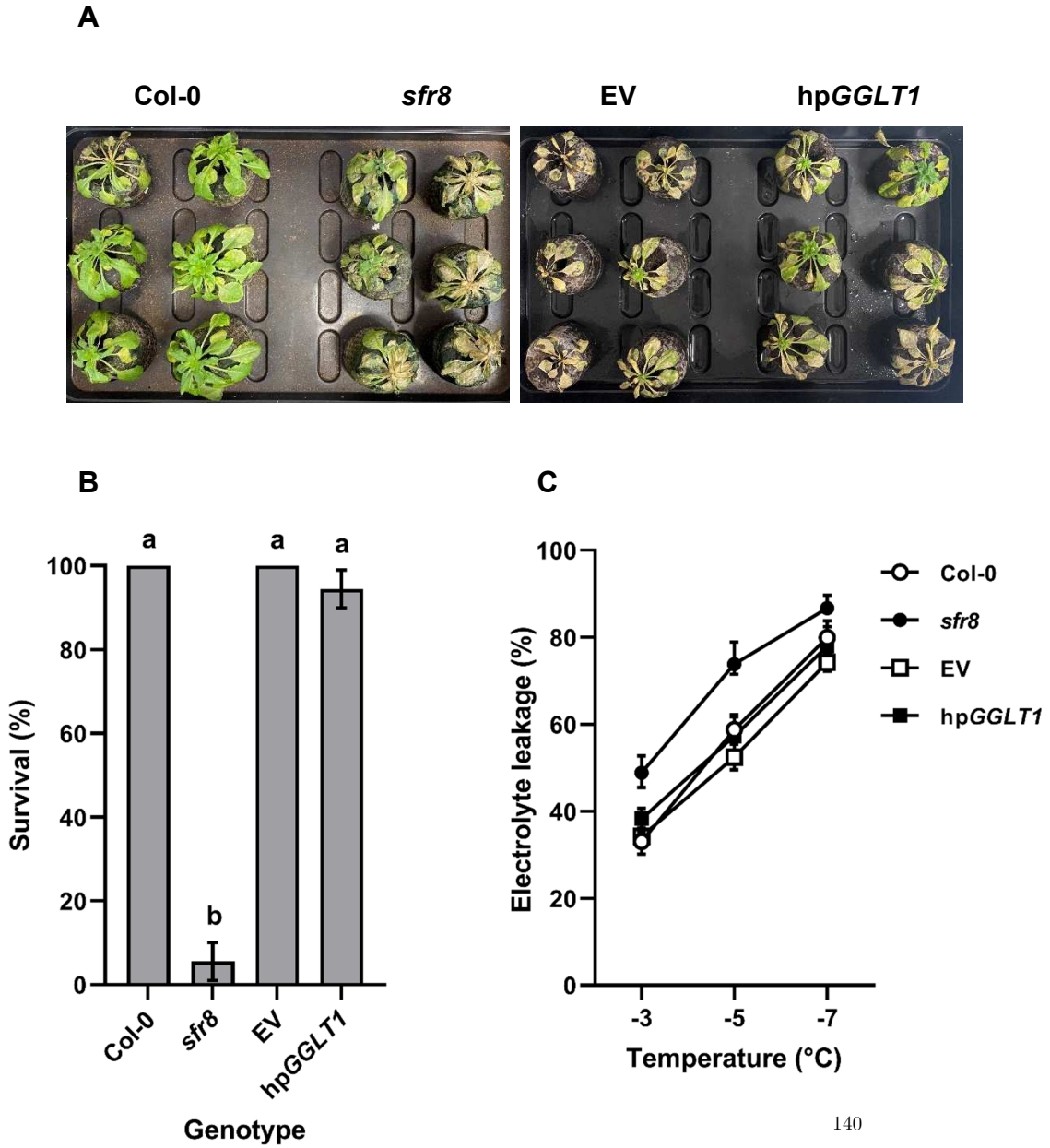

Figure 4.11: Freezing tolerance of *GGLT1* knock-down plants. A) Freezing recovery assay of mature wild-type (Col-0), *sfr8*, *GGLT1* empty-vector (EV) control and *GGLT1* knock-down (hp*GGLT1*) plants. Plants were subjected to freezing at -3°C for 24 h and allowed to recover under ambient conditions for one week. Photographed is one representative assay showing plants one week after freezing. **B)** Survival analysis of plants from freezing recovery assays. Plants were scored on survival based on whether regrowth of green tissue had occurred after one week. Bars represent mean percentage survival of plants from 3 replicate experiments; each experiment used six plants per genotype (n=18). Error bars represent one standard error of the mean of arcsine-transformed data, as is appropriate for proportional data. Means that do not share a letter are significantly different. **C)** Electrolyte leakage of mature leaf tissue from wild-type (Col-0), *sfr8*, *GGLT1* EV control and hp*GGLT1* plants. Leaf tissue was subjected to freezing at -3, -5 or -7°C and loss of electrolytes was measured. Values represent mean percentage electrolyte leakage from 3 replicate experiments; each experiment used leaf tissue from six plants per genotype per temperature (n=18 at each point). Error bars represent one standard error of the mean of arcsine-transformed data.

(F) to give a measure of relative porosity. A linear mixed effects model confirmed that experiment number had no significant impact on data variation ($p>0.05$) so the data from three biological replicate experiments were pooled for analysis. Mean relative porosities of hp*GGLT1* and EV leaves were calculated from pooled data. hp*GGLT1* plants were found to have significantly increased cell-wall porosity relative to EV controls ($p<0.01$). The mean relative porosity of hp*GGLT1* was 5.79 compared to 4.41 for EV plants (**Figure 4.12B**).

4.2.7.2 Mechanical properties

The cell-wall mechanical properties of hp*GGLT1* were measured using extensometry. Eight-mm discs prepared from mature leaves were stretched until failure using an extensometer equipped with a load cell sensitive to 1 mN. A linear mixed effects model confirmed that experiment number had no significant impact on data variation ($p>0.3$) so the data from three biological replicate experiments were pooled for analysis. Mean percentage relative tensile force, normalised to the baseline force reading taken immediately before the stretch was initiated, was calculated from pooled data and plotted over time. Average force curves for hp*GGLT1* and EV control tissue were plotted on the same axes (**Figure 4.13A**). The gradient of the curve for hp*GGLT1* tissue up to the point of failure was 0.446, compared to 0.498 for controls, suggesting that hp*GGLT1* has reduced cell-wall stiffness. The percentage relative tensile force values from the peak of force curves from individual samples were plotted to illustrate the cell-wall mechanical strength of tissue from each genotype. The mechanical strength of hp*GGLT1* was found to be not significantly different to that of EV controls ($p>0.6$). The mean maximum relative tensile force for hp*GGLT1* was 6.48% compared to 6.69% for EV plants (**Figure 4.13B**).

4.2.8 Guard cell dynamics of *sfr8*

The guard cell dynamics of *sfr8* mutants were investigated with a simple leaf water-loss assay. Stomatal density and morphology were also assessed.

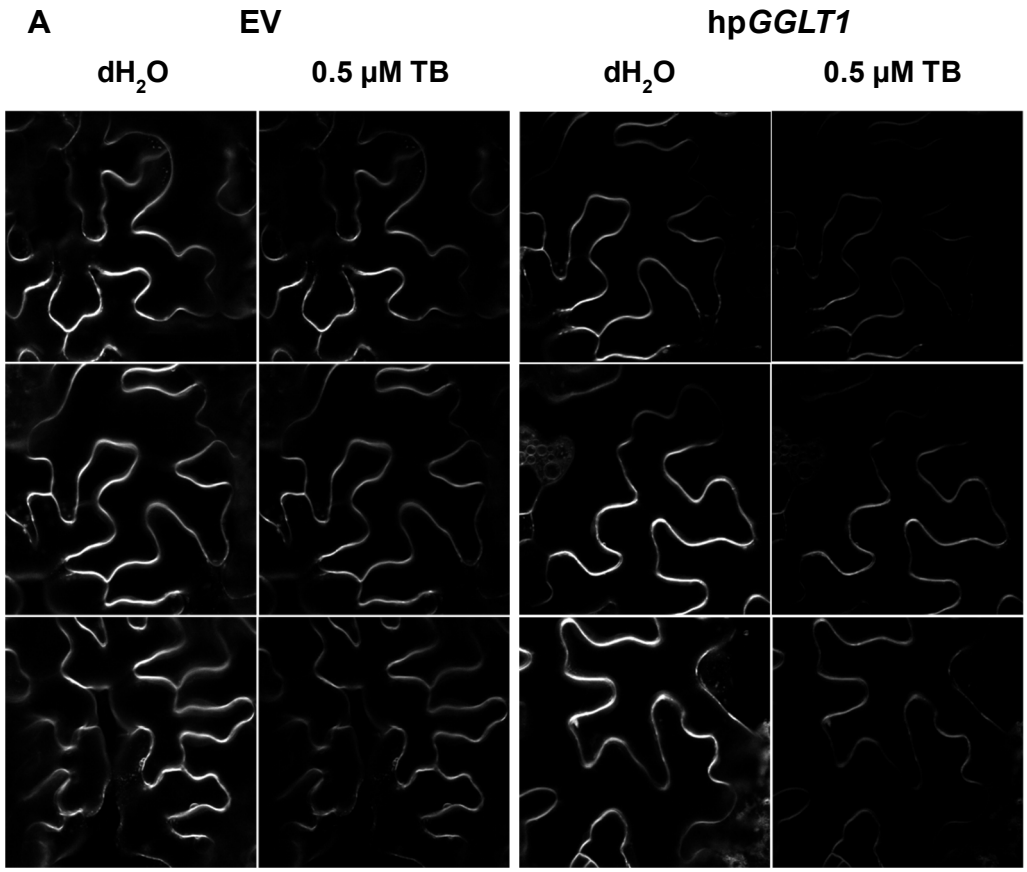

Figure 4.12: Cell-wall porosity of *GGLT1* knock-down plants. Relative porosity was calculated in mature empty-vector (EV) control and *GGLT1* knock-down (hp*GGLT1*) plants using fluorescence quenching. **A)** The plasma membranes of leaf epidermal cells were stained with a fluorescent dye and imaged before and after addition of 0.5 µM trypan blue (TB) quenching solution. Three example micrographs per treatment are shown for each genotype. **B)** Fluorescence was quantified before (F_0) and after (F) addition of the quenching solution and a ratio of the two was calculated to give relative porosity (F_0/F). Bars represent mean relative porosity from three biological replicate experiments; each experiment measured porosity in three leaves from separate plants per genotype (n=9). Error bars represent one standard error of the mean. Asterisks indicate means that are significantly different (** $p<0.01$).

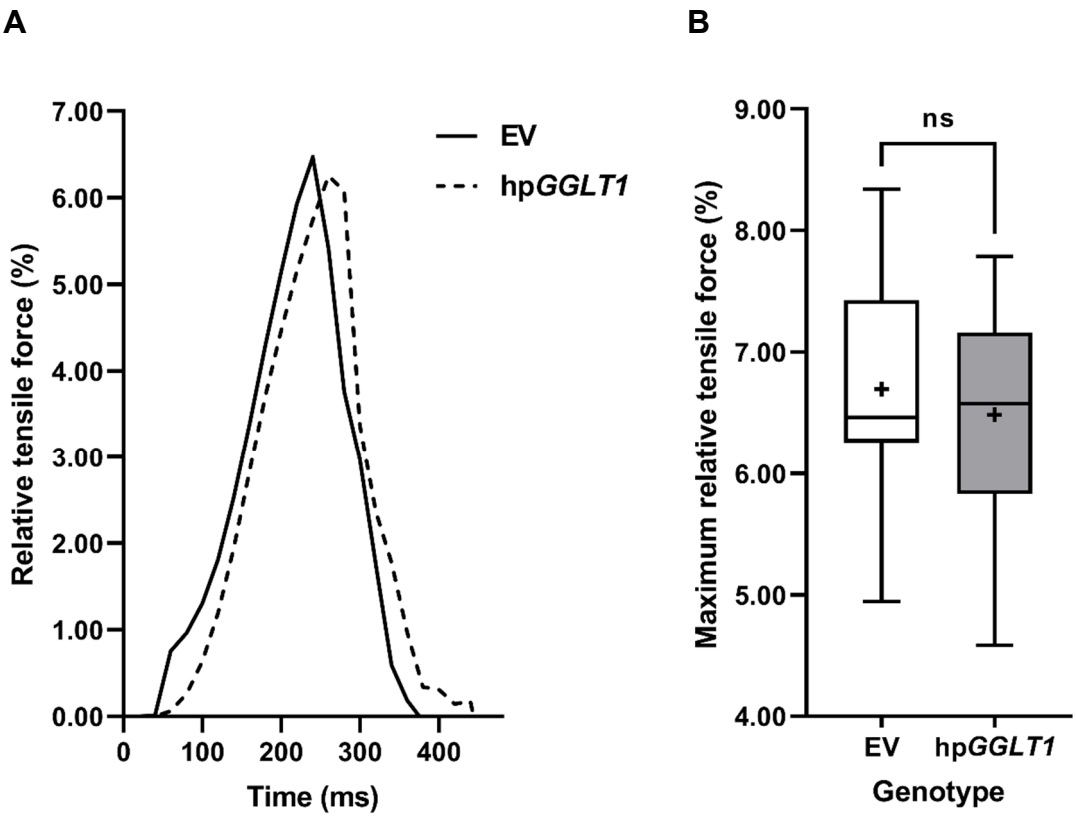

Figure 4.13: Cell-wall mechanical properties of *GGLT1* knock-down plants. Mechanical properties were assessed in mature empty-vector (EV) controls and *GGLT1* knock-down plants (hp*GGLT1*) using extensometry. Leaf discs from each genotype were stretched until breakage and the force required to do so was recorded. Tensile force was normalised to the baseline force reading taken immediately before the stretch was initiated and converted to a percentage for each sample. Plots represent combined data for three biological replicate experiments; each experiment measured cell-wall mechanical properties in three leaf discs per genotype (n=9). **A)** Relative tensile force plotted over time for the duration of each stretch. A steeper gradient is indicative of stiffer material and a higher peak (more resistance to breaking pressure) is indicative of stronger material. **B)** Box-and-whisker plot showing the distribution of maximum tensile force values for each genotype. Values were taken from the absolute peak of each force curve, which represents the maximum tensile force that the tissue can withstand before breakage. Whiskers: maximum and minimum values; box edges: upper and lower quartiles; plus signs: mean values; horizontal lines: median values. ns indicates means that are not significantly different (p>0.6).

4.2.8.1 Leaf water-loss

Leaf water-loss was measured in *sfr8* and wild-type plants. A linear mixed effects model confirmed that experiment number had no significant impact on data variation ($p>0.05$) so the data from three biological replicate experiments were pooled for analysis. Each measurement of mass was expressed as a percentage of the initial leaf mass. Mean percentage mass of leaves of each genotype was calculated from pooled data at each time point. Leaves from *sfr8* plants decreased in mass substantially faster than wild-type controls, indicating that they lost water at a higher rate (**Figure 4.14**). Pairwise comparisons of mean percentage mass showed that, at every time point (after 0), *sfr8* leaves had a significantly lower relative mass than wild-type ($p<0.001$).

4.2.8.2 Stomatal density

It was hypothesised that increased stomatal density could be one reason for the water-loss phenotype of *sfr8*. Stomatal density was measured in epidermal peels of *sfr8* and wild-type leaves. A linear mixed effects model confirmed that experiment number had no significant impact on data variation ($p>0.6$) so the data from three biological replicate experiments were pooled for analysis. Mean stomatal densities of *sfr8* and wild-type leaves were calculated from pooled data. There was no significant difference in stomatal density between *sfr8* and wild-type plants ($p>0.2$). In fact, leaves of *sfr8* had a lower mean stomatal density than those of wild-type but the difference was not significant (**Figure 4.15**).

4.2.8.3 Guard cell morphology

An alternative explanation for the water-loss phenotype of *sfr8* is the presence of larger stomata or the inability of stomata to respond to closure stimuli. Stomatal pore aperture and area, as well as total stomatal area (**Figure 2.4**), were measured in stomata from epidermal peels of *sfr8* and wild-type leaves that had either been treated with ABA (a closure stimulus) or MES (control)*.

*Sample preparation and imaging were carried out by Dr. Paige Panter, who kindly provided images for analysis.

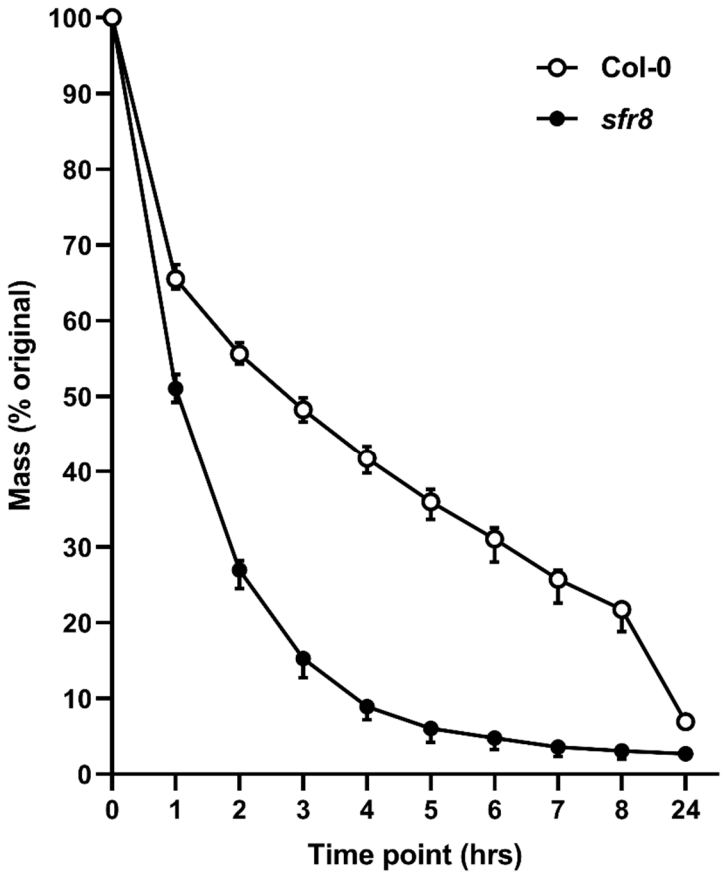

Figure 4.14: Rate of leaf water-loss in *sfr8*. The rate of water loss was measured in mature wild-type (Col-0) and *sfr8* leaves. Leaves were excised and weighed every hour for 8 hours, then once more after 24 hours. Each measurement is expressed as a percentage of the original leaf mass. Values represent mean percentage mass values from three biological replicate experiments; each experiment used seven leaves per genotype, each from a separate plant (n=21 at each point). Error bars represent one standard error of the mean of arcsine-transformed data, as is appropriate for proportional data.

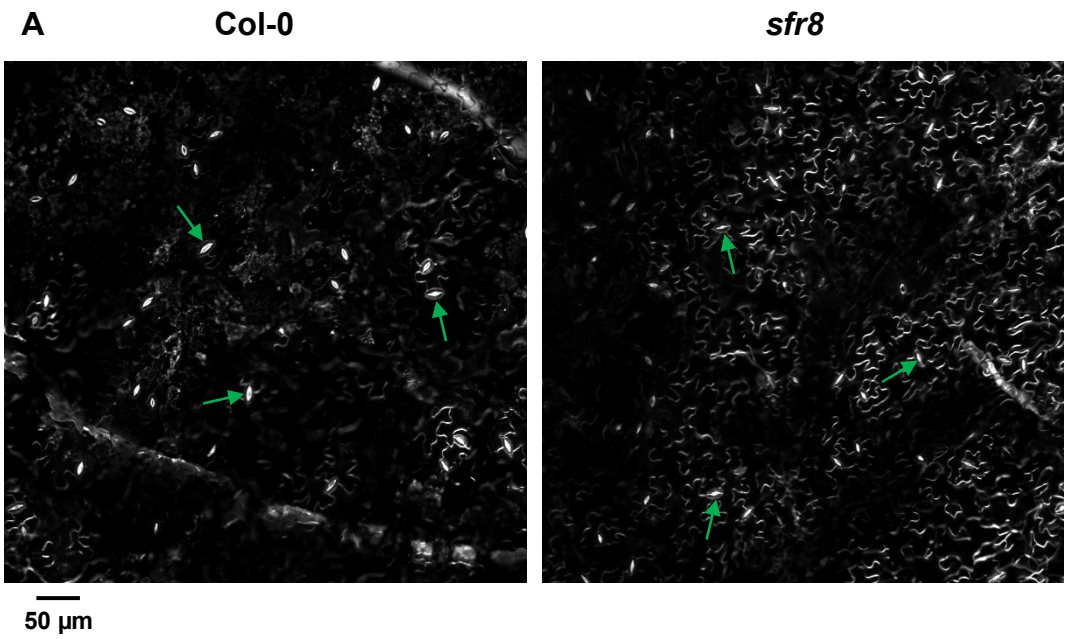

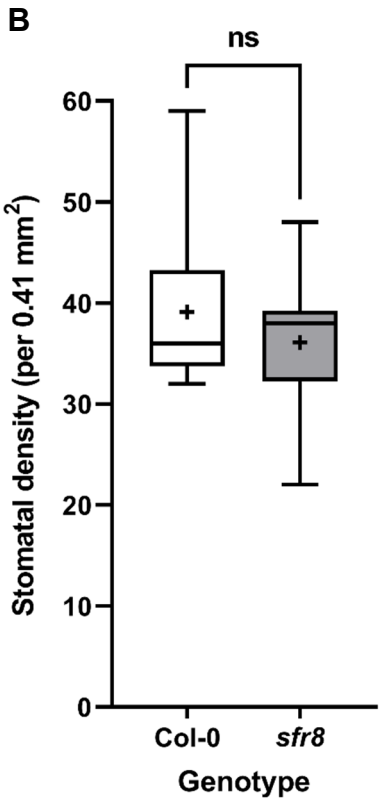

Figure 4.15: Stomatal density of *sfr8*. The total number of stomata were counted in 0.41 mm^2 sections of epidermal peels from mature wild-type (Col-0) and *sfr8* leaves. **A)** Example micrographs from wild-type (left) and *sfr8* (right) epidermal peels. Green arrows indicate examples of stomata that were counted. **B)** Box-and-whisker plots show the distribution of stomatal densities from three biological replicate experiments; each experiment measured stomatal density in six leaves per genotype, each from a separate plant (n=18). Whiskers: maximum and minimum values; box edges: upper and lower quartiles; plus signs: mean values; horizontal lines: median values. ns indicates means that are not significantly different (p>0.7).

A linear mixed effects model confirmed that experiment number had no significant impact on data variation ($p>0.05$ for each measurement type) so the data from three biological replicate experiments were pooled for analysis. Each experiment imaged epidermal peels from at least 30 different plants per genotype per treatment, and each image contained multiple stomata that were included in the analysis, giving a very large sample size (**Figure 4.16A**). Mean measurements of stomatal area, pore area and pore aperture were calculated from pooled data. Both genotype ($p<0.001$) and treatment ($p<0.001$) had a significant impact on stomatal pore aperture, and there was also a significant interaction effect between the two ($p<0.001$). Treatment with ABA caused a significant reduction in stomatal pore aperture in wild-type leaves, whereas it made no significant difference in *sfr8* (**Figure 4.16B**). Both genotype ($p<0.001$) and treatment ($p<0.01$) had a significant impact on stomatal pore area, and there was also a significant interaction effect between the two ($p<0.05$). Treatment with ABA caused a significant reduction in stomatal pore area in wild-type leaves, whereas it made no significant difference in *sfr8*. Both treated and untreated *sfr8* leaves had significantly larger stomatal pore areas than those of wild-type leaves (**Figure 4.16C**). Both genotype ($p<0.001$) and treatment ($p<0.001$) had a significant impact on total stomatal area, and there was a significant interaction effect between the two ($p<0.001$). Treatment with ABA had no significant effect on total stomatal area in wild-type leaves, whereas ABA caused a significant increase in total stomatal area in *sfr8*. Both treated and untreated *sfr8* leaves also had significantly larger stomata than those of wild-type leaves (**Figure 4.16D**).

4.2.9 Leaf water-loss of boron-supplemented *sfr8*

To assess the effect that increased boron-mediated RG-II dimerisation has on guard cell dynamics, leaf water-loss assays were carried out on *sfr8* and wild-type plants either supplemented with (B+) or deprived of (B-) boron. A linear mixed effects model confirmed that experiment number had no significant impact on data variation ($p>0.05$) so the data from three biological replicate experiments were pooled for analysis. Each measurement was expressed as a percentage of the initial leaf mass. Mean percentage mass of leaves of each genotype and treatment

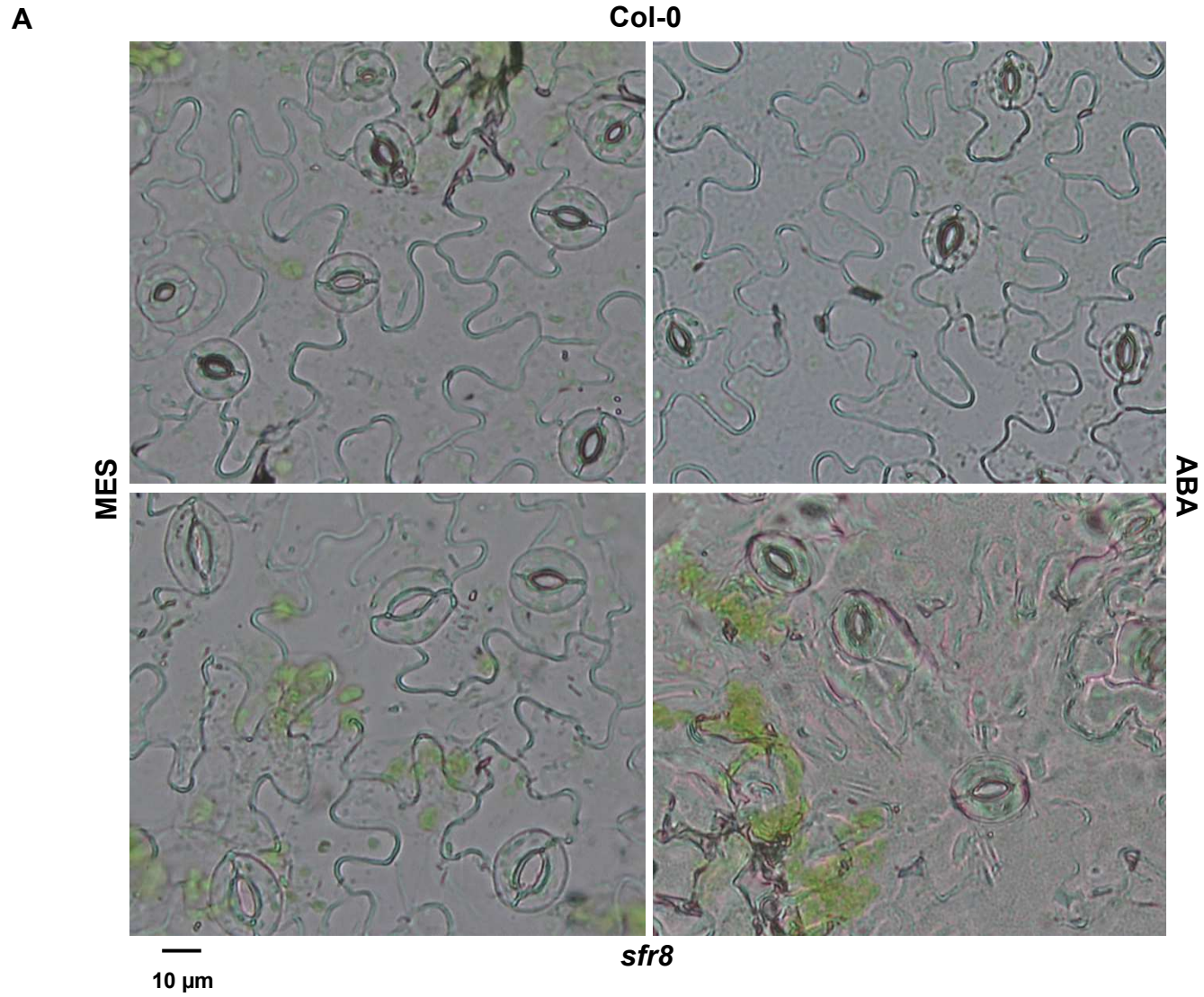
A
Col-0
MES
ABA
sfr8
10 µm

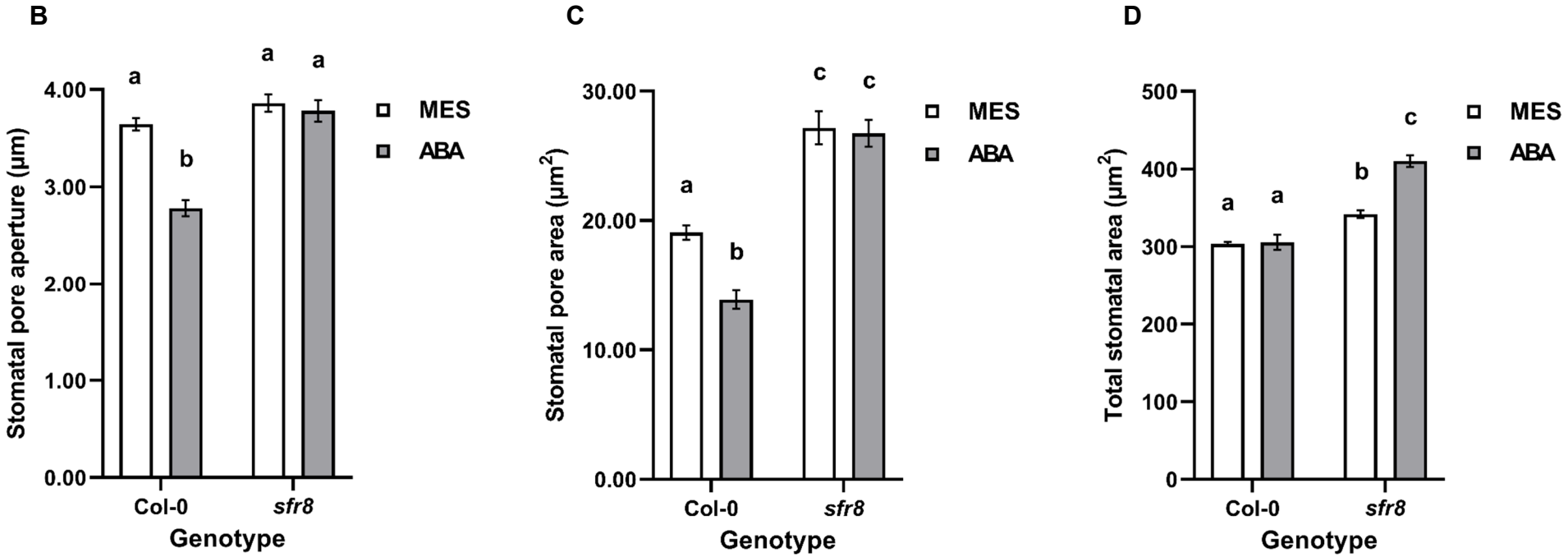

Figure 4.16: Morphology and ABA-responsiveness of *sfr8* guard cells. Epidermal peels from mature wild-type (Col-0) and *sfr8* leaves were prepared and either treated with MES (control) or ABA (closure stimulus) prior to imaging. Representative micrographs showing stomata of wild-type (top) and *sfr8* (bottom) epidermal peels treated with either MES (left) or ABA (right) are shown **(A)**. Measurements of stomatal pore aperture **(B)**, pore area **(C)**, and total stomatal area **(D)** were made in individual stomata from each of the four experimental groups. Bars represent mean measurements from three biological replicate experiments; each experiment measured at least 30 stomata per genotype per treatment (Col-0/MES n=179; Col-0/ABA n=111; *sfr8*/MES n=119; *sfr8*/ABA n=137). Error bars represent one standard error of the mean. Means that do not share a letter within each plot are significantly different.

was calculated from pooled data at each time point. Boron supplementation appeared to make little difference to the rate of water loss in wild-type leaves, but there was a dramatic decrease in the rate of water loss in B+ *sfr8* (**Figure 4.17**). Indeed, at every time point (after 0), both genotype ($p<0.001$) and treatment ($p<0.001$) had a significant impact on mean percentage mass, and there was also a significant interaction effect between the two ($p<0.05$). Pairwise comparisons showed that B- *sfr8* leaves had a significantly lower relative mass than B+ *sfr8* leaves and both B+ and B- wild-type leaves at every time point (after 0). At time points 3-7, B+ *sfr8* leaves had a significantly lower relative mass than both wild-type groups. At every time point, there was no significant difference in relative mass between B+ and B- wild-type leaves.

4.2.10 Leaf water-loss of *GGLT1* knock-down plants

Leaf water-loss was measured in hp*GGLT1* and EV plants. A linear mixed effects model confirmed that experiment number had no significant impact on data variation ($p>0.2$) so the data from three biological replicate experiments were pooled for analysis. Each measurement of mass was expressed as a percentage of the initial leaf mass. Mean percentage mass of leaves of each genotype was calculated from pooled data at each time point. Leaves from hp*GGLT1* plants did not appear to decrease in mass at a rate different from those of EV plants, indicating that there was little difference in the rate of water loss (**Figure 4.18**). Pairwise comparisons of mean percentage mass showed that there was no significant difference in mean relative mass between hp*GGLT1* and EV leaves at every time point ($p>0.1$).

4.2.11 Cell adhesion of *sfr8*

It has been suggested that cell adhesion in *Arabidopsis* may be partly under the control of fucosyltransferases (Verger *et al.* 2016). As *sfr8* is deficient in cell-wall fucose (Panter 2018), the possibility of a cell-adhesion defect was explored in seedling hypocotyls. Four-day old dark-grown seedlings were stained with propidium iodide and their hypocotyls were imaged to examine their cell adhesion.

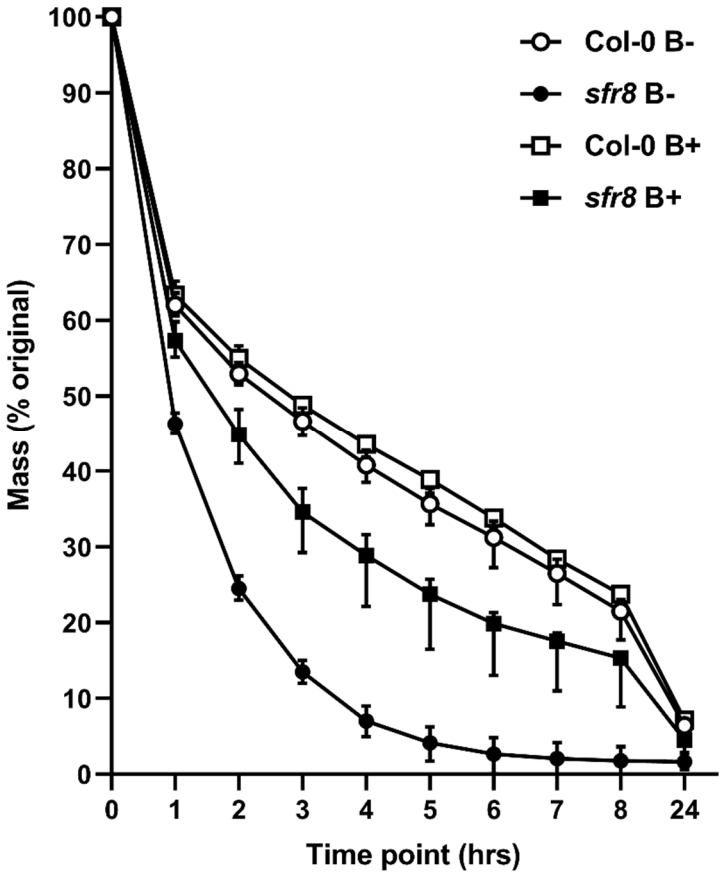

Figure 4.17: Rate of leaf water-loss in boron-supplemented *sfr8*. The rate of water loss was measured in mature wild-type (Col-0) and *sfr8* leaves that had either been supplemented with (B+) or deprived of (B-) boron. Leaves were excised and weighed every hour for 8 hours, then once more after 24 hours. Each measurement is expressed as a percentage of the original leaf mass. Values represent mean percentage mass values from three biological replicate experiments; each experiment used six leaves per genotype, each from a separate plant (n=18 at each point). Error bars represent one standard error of the mean of arcsine-transformed data, as is appropriate for proportional data.

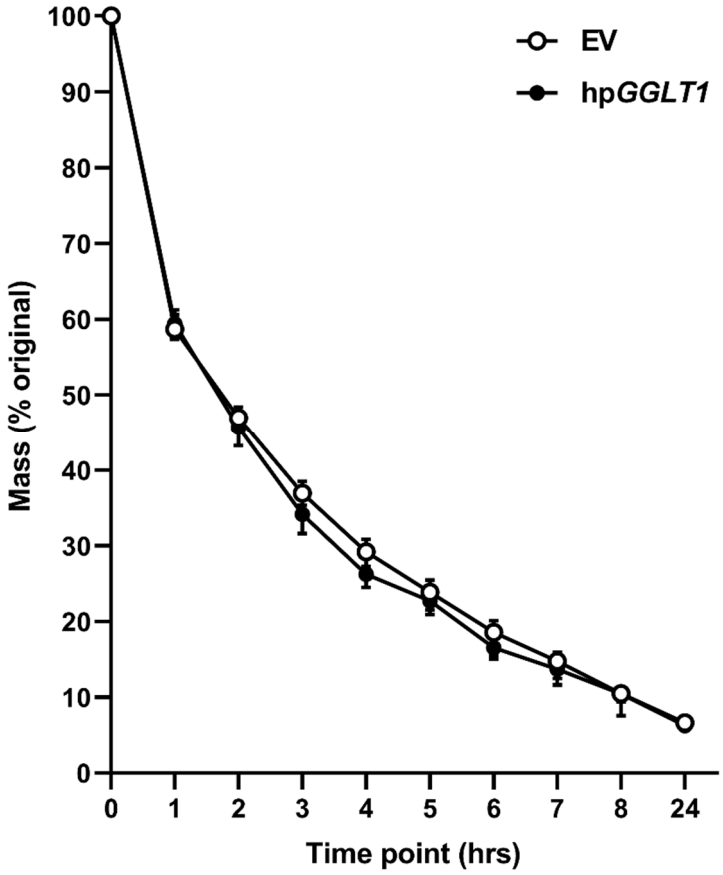

Figure 4.18: Rate of leaf water-loss in *GGLT1* knock-down plants. The rate of water loss was measured in mature empty-vector (EV) control and *GGLT1* knock-down (hp*GGLT1*) leaves. Leaves were excised and weighed every hour for 8 hours, then once more after 24 hours. Each measurement is expressed as a percentage of the original leaf mass. Values represent mean percentage mass values from three biological replicate experiments; each experiment used seven leaves per genotype, each from a separate plant (n=21 at each point). Error bars represent one standard error of the mean of arcsine-transformed data, as is appropriate for proportional data.

Nine *sfr8* seedlings were imaged, along with wild-type controls, but none appeared to exhibit a defective cell-adhesion phenotype (**Figure 4.19**). Seedlings with impaired cell adhesion are easily identifiable when imaged using the above method, as seen in *qau2* and *frb1* mutants by Verger *et al.* (2016). *sfr8* did not share any of the morphological characteristics exhibited by these mutants and essentially resembled wild-type seedlings during imaging, suggesting that cell adhesion in *sfr8* is unaffected. The water-loss phenotype of *sfr8*, therefore, cannot be explained by impaired cell adhesion.

4.3 Discussion

Freezing recovery and electrolyte leakage assays confirmed that *sfr8* has reduced freezing tolerance. This is not a novel finding: the freezing-sensitive phenotype of *sfr8* is well-documented (Warren *et al.* 1996, Thorlby *et al.* 1999, Panter 2018, Panter *et al.* 2019). The purpose of these experiments, beyond confirming the established phenotype of *sfr8*, was to establish a set of freezing protocols that can successfully screen for freezing sensitivity in other cell-wall mutants by using *sfr8* as a positive control. As expected, *sfr8* exhibited significantly reduced plant survival and increased electrolyte leakage after freezing, indicating that the leaf tissue had incurred more severe freezing injury. These results held even after cold acclimation, suggesting that *sfr8* has a reduced level of basal freezing tolerance that cannot be overcome through cold acclimation, though cold acclimation does improve its freezing tolerance somewhat. This was also expected, as *sfr8* is only deficient in cell-wall fucose and RG-II dimerisation (Panter *et al.* 2019), whereas full cold acclimation involves a suite of changes in the cell wall that go far beyond these two components (see **Section 1.3.3.1** and **Chapter 3**). Furthermore, cold-responsive gene expression is not impaired in *sfr8* (see Panter *et al.* 2019 supplementary material), so it still has the many other facets of cold acclimation at its disposal.

Phenotypic assessment of boron-supplemented *sfr8* suggested that treating plants with KBO reversed the reduction in RG-II dimerisation. Both *mur1* and *sfr8* mutants have characteristic morphological traits that distinguish them from wild-type plants: shortened petioles and smaller, rounder leaves (O'Neill *et al.* 2001,

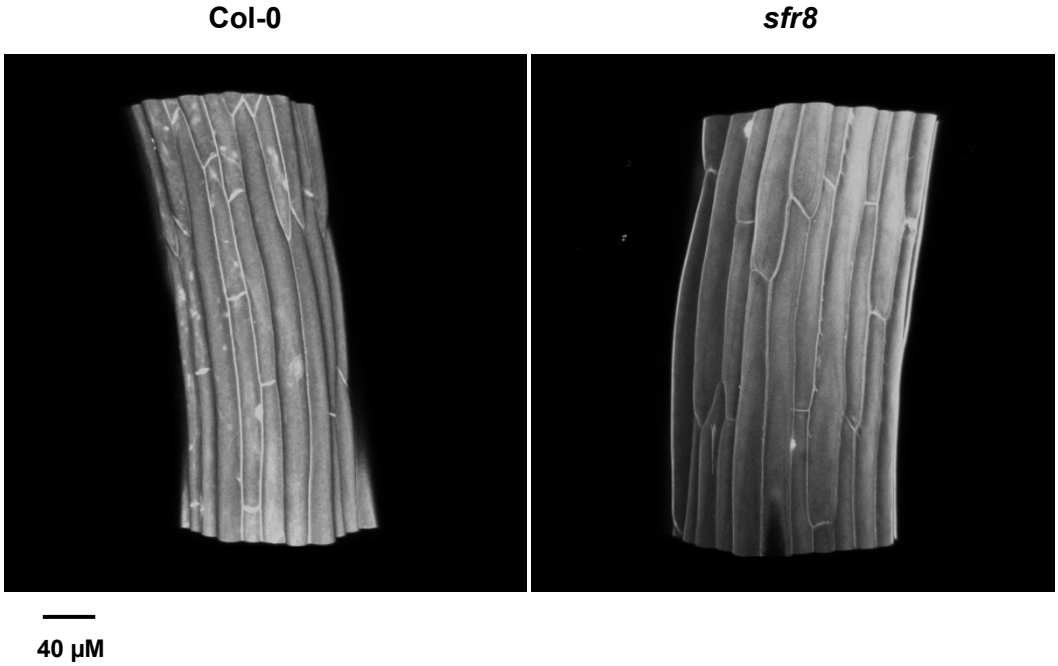

Figure 4.19: Cell adhesion of *sfr8*. Four-day old dark-grown wild-type (Col-0) and *sfr8* seedlings were immersed in 0.2 mg/ml propidium iodide in dH_2O for 10 mins before imaging stained hypocotyls at 20x magnification. Images were taken as z-stacks to allow for hypocotyl cell morphology to be examined in 3D. Nine seedlings per genotype were imaged in total across three replicate experiments; shown is one example micrograph per genotype. Note: the slightly wider appearance of the *sfr8* sample shown here is unremarkable and is not a pattern that persisted among other samples.

Panter *et al.* 2019) These characteristics were visible whenever *sfr8* was grown for use in experiments throughout this study. In *mur1*, it is believed that the difference in leaf shape is a consequence of reduced RG-II dimerisation rather than impaired fucosylation of xyloglucans (Gonçalves *et al.* 2017). In the present study, boron supplementation via KBO appeared to reverse the dwarfed petiole and leaf morphology phenotypes to the extent that supplemented *sfr8* resembled wild-type plants, while apparently having little or no effect on wild-type morphology. Paired with the finding that the same boron-supplementation protocol also reversed the freezing sensitivity and impairments to cell-wall physical properties in *sfr8* (discussed in more detail below), all of which have been linked to pectin composition, this is strong evidence for boron supplementation via KBO reversing the reduction in RG-II dimerisation in *sfr8*.

On the other hand, the PAGE analysis was less clear. Banding for non-supplemented and boron-supplemented *sfr8* cell-wall samples were similar, though the gel arguably showed marginally less RG-II monomer, and more dimer, present in the boron-supplemented *sfr8* sample. Boron supplementation has already been shown to be an effective means of increasing the extent of RG-II dimerisation in *Chenopodium album* and *Arabidopsis* (Fleischer *et al.* 1999, O'Neill *et al.* 2001, Panter 2018, Sechet *et al.* 2018). The lack of a clear result with PAGE analysis could be due to the nature of the RG-II extracted from the mutant. In *mur1*, it has been reported that the dimeric form of RG-II is less stable than that of wild-type (O'Neill *et al.* 2001, Sechet *et al.* 2018). Borate-ester cross-links formed between side-chain A of two fucosylated RG-II monomers in wild-type plants are thought to be relatively stable; however, in *mur1* and *sfr8*, side-chain A lacks fucose and is truncated. Even when dimerisation is forced through supplementary boron, the resultant dimers are less stable and readily dissociate after extraction (O'Neill *et al.* 2001). Given the multiple rescuing effects that boron supplementation had on *sfr8 in vivo*, it is likely that the restored RG-II dimers could not survive the extraction process for the result to be reflected *in vitro*. These rescuing effects, paired with independent data from boron transporter mutants showing reduced RG-II dimerisation and freezing tolerance (Panter *et al.* 2019), mean that it probably is not necessary to demonstrate that the boron-supplementation protocol

brings about a restoration of RG-II dimerisation *in vitro*: the multiple lines of evidence from experimentation *in vivo* are compelling enough. Alternatively, the watering regime employed to provide plants with supplementary boron may have resulted in non-uniform uptake and distribution of boron across cell types and tissues, causing inconsistent results between extractions.

The fluorescence-quenching assay showed that *sfr8* has significantly increased cell-wall porosity. This is consistent with existing literature suggesting that cell-wall porosity is, in part, determined by pectin composition (Baron-Epel *et al.* 1988, Ehwald *et al.* 1991, 1992, Liu *et al.* 2022). The finding that boron supplementation reverses the decrease in porosity in *sfr8* suggests that it is a lack of RG-II dimerisation causing its porous phenotype: the primary role of boron in the plant cell wall is binding apiose residues in side-chain A of RG-II, catalysing its dimerisation (cross-linking) through formation of a borate-ester bond between two monomers (O'Neill *et al.* 1996). Supplementary boron has been shown to restore RG-II cross-linking in mutants of *Arabidopsis* that have a truncated form of MUR1, the fucose biosynthesis enzyme that is also mutated in *sfr8* (O'Neill *et al.* 2001). Moreover, boron supplementation has also been shown to both restore RG-II dimerisation and reduce cell-wall porosity in suspension-cultured *C. album* (Fleischer *et al.* 1999). It is also possible that reduced RG-II dimerisation may impede HG dimerisation, as it has been suggested that both molecules may be covalently linked on the same pectic backbone (Darvill *et al.* 1978). It is highly likely, therefore, that reduced RG-II dimerisation in *sfr8* accounts for its increased porosity, with the less-thoroughly cross-linked pectin matrix creating a more porous cell wall. As discussed in **Section 3.3**, the quenching assay was first applied to seedling roots before it was adapted for application on leaf tissue. The increased porosity of *sfr8* was first detected in seedling roots (data not shown), thus the phenotype appears to be independent of tissue type.

Extensometry was used to show that the cell wall of *sfr8* is both mechanically weaker and softer (less stiff) that of wild-type plants, a defect that was also reversible through boron supplementation. Although the cellulose microfibrils primarily define the mechanical properties of the plant cell wall (Probine & Preston

1961, Whitney *et al.* 1999), other components of the cell wall are also important contributors, including pectins (Willats *et al.* 2001a, Wakabayashi *et al.* 2003, Brummell 2006, Zerzour *et al.* 2009, Peaucelle *et al.* 2011, Chebli *et al.* 2012, Hongo *et al.* 2012, Kierzkowski *et al.* 2012, Li *et al.* 2012, Wolf & Greiner 2012, Braybrook & Peaucelle 2013, Vogler *et al.* 2013, Xi *et al.* 2015, Phyo *et al.* 2017). It has already been demonstrated that *mur1* mutants have compromised mechanical strength, a phenotype that can be rescued with boron (Ryden *et al.* 2003) or fucose (Reiter *et al.* 1993) supplementation. This indicates that borate-complexed RG-II dimers can influence cell-wall mechanical properties, much as they do with cell-wall porosity. The two properties are undoubtedly correlated, as a strong, extensively cross-linked polymeric network will inevitably have smaller intermolecular spaces.

Given that boron supplementation also restored the compromised freezing tolerance of *sfr8* closer to the level of wild-type plants, taken together, the data suggests the following: *sfr8* has increased cell-wall porosity and impaired mechanical properties because it is deficient in borate-complexed RG-II dimerisation, and these both may contribute to its reduced freezing tolerance. Mutants of boron transporters, which are deficient in cell-wall boron and RG-II dimerisation, have also been shown to be freezing-sensitive (Panter *et al.* 2019). The fact that boron supplementation had no impact on the freezing tolerance or cell-wall physical properties of wild-type plants is yet more evidence that it is solely down to the degree of RG-II dimerisation in *sfr8,* and not some other effect of boron deficiency, especially as the majority of cell-wall boron is associated with RG-II complexes (Matoh *et al.* 1996).

It has been suggested that the cell wall is an intrinsic barrier to ice formation and propagation, and a more porous cell wall would be less able to serve this purpose (Olien 1974, Wisniewski 1995, Yamada *et al.* 2002, McCully *et al.* 2004). A more porous cell wall would also likely be less conducive to supercooling as the freezing point of free, bulk water is higher than that of minute volumes of water in a confined, porous material (Mazur 1963, Homshaw 1980, Ashworth & Abeles 1984, Wisniewski *et al.* 1991, Wisniewski & Davis 1995). Indeed, the IRVT data presented here, though produced from a small number of samples, suggests that leaves of *sfr8* were unable to supercool to the same extent as wild-type leaves.

Additionally, it was reported that, in suspension-cultured apple and grape cells, reduced cell-wall porosity was associated with a large reduction in the presence of lethal intracellular ice, and it was concluded that smaller cell-wall pores help to exclude ice from the cell (Rajashekar & Lafta 1996). In Japanese bunching onion, reduced cell-wall porosity was associated with a sharp increase in freezing tolerance (Liu *et al.* 2022). It has been proposed that a mechanically stiff cell wall is also important in freezing tolerance, as it will be better able to resist freezing-induced cellular dehydration and subsequent cell collapse (Pearce 1988, Fujikawa *et al.* 1999, Yamada *et al.* 2002). This idea is discussed in great detail in **Section 1.3.3.2**. The results of the present study, in the context of the literature described above, provide compelling support for the hypothesis that impaired cell-wall porosity and mechanical properties of *sfr8*, brought about by reduced dimerisation of RG-II, are responsible for its sensitivity to freezing.

Despite also being deficient in RG-II dimerisation, hp*GGLT1* plants do not share the same freezing-sensitive phenotype as *sfr8*: their survival and electrolyte leakage values after freezing were largely comparable to controls. It was interesting, therefore, to find that hp*GGLT1* has increased cell-wall porosity, and marginally reduced cell-wall stiffness, but no accompanying freezing sensitivity. Although RG-II dimerisation is reduced in hp*GGLT1*, it is not reduced to the same extent as it is in *mur1* (Sechet *et al.* 2018). It may be the case that cell-wall porosity and stiffness are highly sensitive to the degree of RG-II monomerisation, whereas a certain threshold of RG-II monomerisation must be surpassed before it begins to have any effect on freezing tolerance. Sechet *et al.* (2018) demonstrated that boron supplementation is able to restore dimerisation of RG-II in hp*GGLT1*, so it would be useful to determine if it also restores cell-wall porosity and mechanical properties in hp*GGLT1* to levels seen in controls.

The water-loss phenotype exhibited by *sfr8* was first identified by Panter (2018), who found that leaves of both *sfr8* and *mur1* mutants decreased in mass far more rapidly after excision than wild-type leaves, indicative of an impaired ability to retain water. The leaf water-loss assays carried out in the present study reflect those results and confirmed the water-loss phenotype of *sfr8*. As with freezing

sensitivity, this phenotype was partially reversible through boron-mediated restoration of RG-II dimerisation: boron-supplemented *sfr8* exhibited a lower rate of water loss than non-supplemented *sfr8*. As boron supplementation had a negligible effect on the rate of water loss in wild-type plants, this suggested that the phenotype is indeed due to a lack of RG-II dimerisation. Water is transported in plant tissues primarily through the apoplastic (through the cell wall) and symplastic (through cytoplasm) pathways (Kaufmann 1976). It is possible that a defective cell-wall structure could impact on water movement through the apoplastic pathway, with the increased porosity of *sfr8* facilitating more rapid movement of water through the cell wall. Alternatively, monomeric RG-II, which is abundant in *sfr8*, may have a reduced water-binding capacity compared to the dimeric form. Pectins have considerable water-binding properties and may be involved in protection against drought and desiccation in both plants and algae (Piro *et al.* 2003, Konno *et al.* 2008, Leucci *et al.* 2008, Einhorn-Stoll *et al.* 2012, Karim *et al.* 2012, Abdel-Motagally & El-Zohri 2018, Herburger *et al.* 2019). Furthermore, reduced methylesterification (and subsequent increased cross-linking) has been linked to an improved ability to bind water molecules in HG (Willats *et al.* 2001b), and increased calcium- or boron-mediated pectin cross-linking has been correlated with reduced water loss *in vitro* (Forand *et al.* 2022). Mutants of *Arabidopsis* lacking a boron transporter, *bor1*, also have an impaired water retention phenotype (Forand *et al.* 2022). Therefore, a reduction in RG-II cross-linking could hinder a plant's ability to retain water by facilitating the movement of water through the cell wall and into the environment.

Still, the main source of water loss in plants is transpiration through open stomata (Maercker 1965), so it is more likely that any enhanced rate of water loss would be due to defects in the stomata themselves. To address this hypothesis, two avenues of investigation were pursued. Firstly, it was determined whether *sfr8* simply has more stomata than wild-type plants and hence more routes through which water can be lost through transpiration. However, analysis of stomatal density showed that *sfr8* and wild-type leaves have a comparable number of stomata, with *sfr8* actually having a lower stomatal density, though the difference was not significant. This finding is in agreement with Panter (2018). Next, the guard cell morphology

of *sfr8* was analysed, including measurements of stomatal pore aperture, pore area, and total stomatal area, both with and without ABA treatment. ABA is a major signalling component in the guard cells, induced by stimuli such as drought, causing stomatal closure (Schroeder *et al.* 2001). Even without ABA treatment, it was found that the stomata of *sfr8* have significantly larger pore areas and total areas compared to wild-type, though there was no significant difference in stomatal aperture. This shows that leaves of *sfr8* intrinsically have more surface area in contact with the environment through which to lose water. Perhaps more importantly, the stomata of *sfr8* appeared completely unable to respond to an ABA closure stimulus: there was no significant difference in stomatal pore aperture or stomatal pore area between control and ABA-treated *sfr8*, and total stomatal area was actually significantly larger in ABA-treated *sfr8*. Wild-type plants, on the other hand, showed a significant reduction in both stomatal pore aperture and stomatal pore area after treatment with ABA, suggesting that the closure stimulus was working normally in control plants. These results are in partial agreement with Panter (2018), who also found that *sfr8* stomata were unable to respond to a closure stimulus, but also found that the stomata of untreated *sfr8* were not significantly different in size to those of wild-type. This could explain the increased rate of water loss observed in *sfr8*: after excision, leaves are either unable to close their stomata, or there is a delay in doing so. Either way, the result is a dramatic increase in the rate of water loss. The resultant desiccation phenotype may also be explained by a lower degree of RG-II dimerisation in *sfr8* guard cell walls. Studies have shown that guard cells rely on a specific composition of polysaccharides in their cell walls to function normally, and this composition can impact on their mechanical properties which are also likely involved in proper functioning (Majewska-Sawka *et al.* 2002, Verhertbruggen *et al.* 2009, Rui & Anderson 2016, Rui *et al.* 2016). Furthermore, enzymes involved in pectin modification have been specifically linked to normal stomatal functioning (Huang *et al.* 2017, Rui *et al.* 2017). Amsbury *et al.* (2016) demonstrated that mutants lacking expression of a pectin methylesterase (PME) gene normally expressed in guard cells, *PME6*, have defective, unresponsive stomata. It was found that the mutant guard cell walls had a higher degree of pectin methylesterification, preventing efficient cross-linking. Pectin cross-linking,

and the knock-on effects this has on cell-wall mechanics, may be required for normal stomatal opening and closure. This would certainly explain the unresponsiveness of *sfr8* guard cells which lack RG-II cross-linking. Although no water-loss phenotype was observed in hp*GGLT1* plants, which also have reduced RG-II dimerisation, this could also be explained by the fact that RG-II dimerisation is not reduced to the same extent in these plants, and does not necessarily mean that the water-loss phenotype of *sfr8* is not linked to its RG-II structure. As with freezing tolerance, it could be that the threshold of RG-II monomerization to produce an observable phenotype was not met in these plants. Measurements of guard cell morphology in these plants would also be of interest.

An obvious next step in this investigation would be to repeat the guard cell morphology experiments on boron-supplemented plants to see if the larger, unresponsive guard cell phenotype can be reversed, thus indicating that it is caused by reduced RG-II dimerisation in guard cell walls. Given that boron supplementation brought about a reduction in the rate of leaf water-loss, this is a plausible outcome. IRVT could also be a useful, less-invasive tool for investigating the guard cell dynamics of *sfr8*. IRVT has previously been used to identify mutants of *Arabidopsis* with defective guard cell regulation by measuring leaf temperature and hence the rate of evaporative cooling via transpiration (Merlot *et al.* 2002, Wang *et al.* 2004, Amsbury *et al.* 2016). Panter (2018) successfully used IRVT to show that *sfr8* had an increased rate of evaporative cooling and hence lost water at a faster rate. Repeating this experiment with boron-supplemented plants would provide yet more evidence supporting the role of RG-II dimerisation in guard cell mechanics and responsiveness.

4.4 Summary

In this chapter, *sfr8* was used to explore the role of RG-II cross-linking in freezing tolerance. Cell-wall assays suggested that *sfr8* is compromised in cell-wall porosity and mechanical integrity and it was hypothesised that these defects contribute to its reduced freezing tolerance. Boron supplementation reversed these defects, as well as its freezing sensitivity, indicating that they were probably caused by a lack of RG-II dimerisation. hp*GGLT1* plants, which also have reduced RG-II

dimerisation (though not to the same extent as *sfr8*), also had impaired cell-wall porosity and marginally reduced mechanical stiffness, but no concomitant reduction in freezing tolerance.

Guard cell dynamics were explored in *sfr8*. It was concluded that the water-loss phenotype of *sfr8* is caused by larger stomata that are unable to adequately respond to closure stimuli, rather than more stomata or impaired cell adhesion which has suggested previously. This phenotype was also partially reversible with boron supplementation, again indicating that it is likely a result of reduced RG-II dimerisation.

Chapter 5

Plant freezing tolerance is linked to the physical properties of the cell wall

5.1 Introduction

The previous two chapters have highlighted a clear role of the cell wall in freezing tolerance. In this chapter, cell-wall polysaccharides other than rhamnogalacturonan-II (RG-II) were investigated for a potential role in contributing to freezing tolerance. **Section 1.3.3** summarises the existing evidence for the involvement of some of these.

To assess the importance of cellulose in plant freezing tolerance, two mutants of cellulose synthesis were studied. One of these, *cesa3*^{S211A}, expresses a truncated cellulose synthase 3 (CESA3), due to a single amino acid substitution at position 211 (Chen *et al.* 2016). The resultant mutant has a slight, but significant, reduction in cell-wall cellulose content, reduced root and hypocotyl growth, and altered cell-wall porosity (Chen *et al.* 2016, Liu *et al.* 2019b). The other has a mutation in *PROCUSTE1* (*PRC1*), which was found to encode CESA6 (Fagard *et al.* 2000). *prc1* mutants also have reduced root and hypocotyl growth, as well as a "gapped" cell wall that is deficient in cellulose (Desnos *et al.* 1996, Fagard *et al.* 2000). CESA6 and CESA3 are two of the three CESAs required to form a functional cellulose synthase complex (CSC) capable of synthesising primary cell-wall cellulose, the other being CESA1 (Arioli *et al.* 1998, Fagard *et al.* 2000). To complement the study of plants that have genetically-altered cellulose compositions, plants treated with a chemical inhibitor of cellulose biosynthesis, isoxaben (ISX; Huggenberger *et al.* 1982), were also included in the study.

Mutants in the synthesis of two major hemicelluloses, xyloglucan and mannan, were investigated to elucidate a potential contribution of hemicelluloses to freezing tolerance. Xyloglucans are a major group of hemicelluloses whose backbones resemble cellulose, but they are interspaced with xylose residues which can be galactosylated and fucosylated (Hayashi 1989). To investigate the importance of xyloglucan in plant freezing tolerance, three mutants with aberrant xyloglucan phenotypes were studied. The first, *xxt1 xxt2*, is a double knock-out of two xylosyltransferase genes involved in xyloglucan biosynthesis, *XXT1* and *XXT2* (Cavalier *et al.* 2008). *xxt1 xxt2* mutants lack detectable xyloglucan in their cell wall. The other two mutants, *mur2* and *mur3*, have mutations in xyloglucan-specific fucosyl- and galactosyl-transferases, respectively. As a result, *mur2* completely lacks xyloglucan fucosylation (Vanzin *et al.* 2002), whereas *mur3* lacks the entire disaccharide extension from the first xylosyl residue; consequently, there is increased galactosylation in the middle xylosyl residue (Madson *et al.* 2003). It has already been demonstrated that all three mutants are compromised in their cell-wall mechanical properties (Peña *et al.* 2004, Cavalier *et al.* 2008). Mannans are widespread in plants and are comprised of a linear β(1,4)-linked backbone of mannosyl residues (Reid 1985). The freezing tolerance of an *Arabidopsis* mutant deficient in mannan synthesis, *msr1-2*, was investigated. The mutant has reduced expression of *MSR1* (*MANNAN SYNTHESIS-RELATED 1*) and, as a result, has a 40% reduction in cell-wall mannosyl content (Wang *et al.* 2013).

Several other plants with interesting, complex cell-wall phenotypes were also screened for freezing sensitivity. The aim was to add further links between freezing tolerance and specific components or compositions of the cell wall. An *Arabidopsis* line that overexpresses a polygalacturonase (PG) gene, *PGX2* (*POLYGALACTURONASE INVOLVED IN EXPANSION 2*), was studied. The transgenic line has higher total PG activity, smaller pectin molecular masses, longer hypocotyls, larger leaves, early flowering, earlier stem lignification and, interestingly, lodging stems with increased mechanical stiffness (Xiao *et al.* 2016). The authors concluded that PGX2 is involved in pectin degradation and so the plant, $PGX2^{AT}$, was a useful tool for studying the effect of pectin structure on freezing tolerance. The *pmr5* mutant, also included in the study, has altered pectin

structure, reduced cellulose content and increased susceptibility to *Botrytis*, due to a mutation in *PMR5* (*POWDERY MILDEW RESISTANT 5;* Chiniquy *et al.* 2019). Finally, a mutant of *REDUCED WALL ACETYLATION 2* (*RWA2*) has reduced *O*-acetylation of both pectins and hemicelluloses, as well as increased leaf surface permeability (Nafisi *et al.* 2015). Acetylation of pectins, like methylation, prevents the formation of cross-links between pectic backbones (Harholt *et al.* 2010), and so this mutant provided another opportunity to investigate the relationship between pectin cross-linking and freezing tolerance.

5.2 Results

5.2.1 Cellulose

To further understand the role of cellulose in plant freezing tolerance and cell-wall physical properties, three groups of plants with modified cellulose compositions were studied: the *cesa3*^{S211A} (Chen *et al.* 2016) and *prc1* (Fargard *et al.* 2000) mutants, which express truncated forms of CESA3 and CESA6 complexes, respectively, and are deficient in cellulose, as well as wild-type plants treated with ISX, a chemical inhibitor of cellulose synthesis (Huggenberger *et al.* 1982).

5.2.1.1 Freezing tolerance

Freezing assays were carried out using both of the mutants as well as mature wild-type (Col-0) and *sfr8* (a confirmed freezing-sensitive mutant; see **Chapter 4**) as negative and positive controls, respectively. Plants were subjected to freezing at -3°C for 24 h before being returned to ambient growth conditions. The capacity of the plants to recover and exhibit new growth was assessed after 1 week. In order to quantify the damage incurred by plants during freezing, electrolyte leakage was measured in leaf tissue from plants of each genotype following exposure to three sub-zero temperatures (-3, -5 and -7°C) Results for each of the two mutants will be described separately.

For *cesa3*^{S211A} recovery assays (**Figure 5.1A**), a linear mixed effects model confirmed that experiment number had no significant impact on data variation (p>0.1) so the data from three biological replicate experiments were pooled for analysis. Mean percentage survival of plants of each genotype was calculated from

pooled data. Genotype had a significant effect on plant survival ($p<0.001$). Compared to wild-type, which had a mean survival rate of 100%, both *cesa3*^{S211A} and *sfr8* had significantly lower mean survival rates of 17% and 0%, respectively (**Figure 5.1B**). For electrolyte leakage assays, a linear mixed effects model confirmed that experiment number had no significant impact on data variation ($p>0.1$) so the data from three biological replicate experiments were pooled for analysis. Mean percentage electrolyte leakage of plants of each genotype was calculated at each temperature from pooled data (**Figure 5.1C**). At all three temperatures, genotype had a significant impact on electrolyte leakage (-3°C: $p<0.05$; -5°C and -7°C: $p<0.001$). At -3°C, *cesa3*^{S211A} had higher electrolyte leakage than wild-type and lower electrolyte leakage than *sfr8* but neither difference was significant. At -5 and -7°C, the electrolyte leakage of both *cesa3*^{S211A} and *sfr8* was significantly higher than that of wild-type.

For *prc1* recovery assays (**Figure 5.2A**), a linear mixed effects model confirmed that experiment number had no significant impact on data variation ($p>0.2$) so the data from three biological replicate experiments were pooled for analysis. Mean percentage survival of plants of each genotype was calculated from pooled data. Genotype had a significant effect on plant survival ($p<0.001$). Compared to wild-type, which had a mean survival rate of 100%, both *prc1* and *sfr8* had significantly lower mean survival rates of 47% and 7%, respectively (**Figure 5.2B**). For electrolyte leakage assays, a linear mixed effects model confirmed that experiment number had no significant impact on data variation ($p>0.1$) so the data from three biological replicate experiments were pooled for analysis. Mean percentage electrolyte leakage of plants of each genotype was calculated at each temperature from pooled data (**Figure 5.2C**). At -3 and -5°C, genotype had a significant impact on electrolyte leakage ($p<0.001$). At both temperatures, the electrolyte leakage of both *prc1* and *sfr8* was significantly higher than that of wild-type. At -7°C, genotype did not have a significant effect on electrolyte leakage ($p>0.1$). Although *prc1* and *sfr8* exhibited higher electrolyte leakage than that of wild-type, the difference was not significant.

For assays involving ISX-treated plants, wild-type plants were sprayed with 5 nM ISX twice per week beginning two weeks prior to experimentation. Control plants were sprayed with 5 nM DMSO. For recovery assays (**Figure 5.3A**), a linear mixed effects model confirmed that experiment number had no significant impact on data variation ($p>0.3$) so the data from three biological replicate experiments were pooled for analysis. Mean percentage survival of plants receiving each treatment was calculated from pooled data. Compared to control plants, which had a mean survival rate of 100%, ISX-treated plants had a significantly lower ($p<0.001$) mean survival rate of 6% (**Figure 5.3B**). In order to quantify the damage incurred by plants during freezing, electrolyte leakage was measured in leaf tissue from plants receiving each treatment following exposure to three temperatures (0, -3 and -6°C). As ISX is used commercially as a herbicide, 0°C was used to determine whether treatment would cause altered electrolyte leakage under non-freezing conditions. A linear mixed effects model confirmed that experiment number had no significant impact on data variation ($p>0.1$), so the data from three biological replicate experiments were pooled for analysis. Mean percentage electrolyte leakage of plants receiving each treatment was calculated at each temperature from pooled data (**Figure 5.3C**). At 0°C, there was no significant difference in electrolyte leakage between ISX-treated and control plants ($p>0.2$), confirming that treatment with ISX did not cause altered electrolyte leakage under non-freezing conditions. At both -3 and -6°C, ISX-treated plants had significantly higher electrolyte leakage than control plants ($p<0.001$).

Taken together, these results show that freezing tolerance can be reduced in plants deficient in cellulose, or with aberrant cellulose synthesis phenotypes.

5.2.1.2 Cell-wall physical properties

As *cesa3*^{S211A} and *prc1* mutants, as well as ISX-treated plants, appeared to have compromised freezing tolerance, their cell-wall porosity and mechanical properties were analysed to determine if these could be contributing factors. For the mutants, mature wild-type (Col-0) leaves were used as controls; for ISX-treated plants, DMSO-treated plants were used as controls.

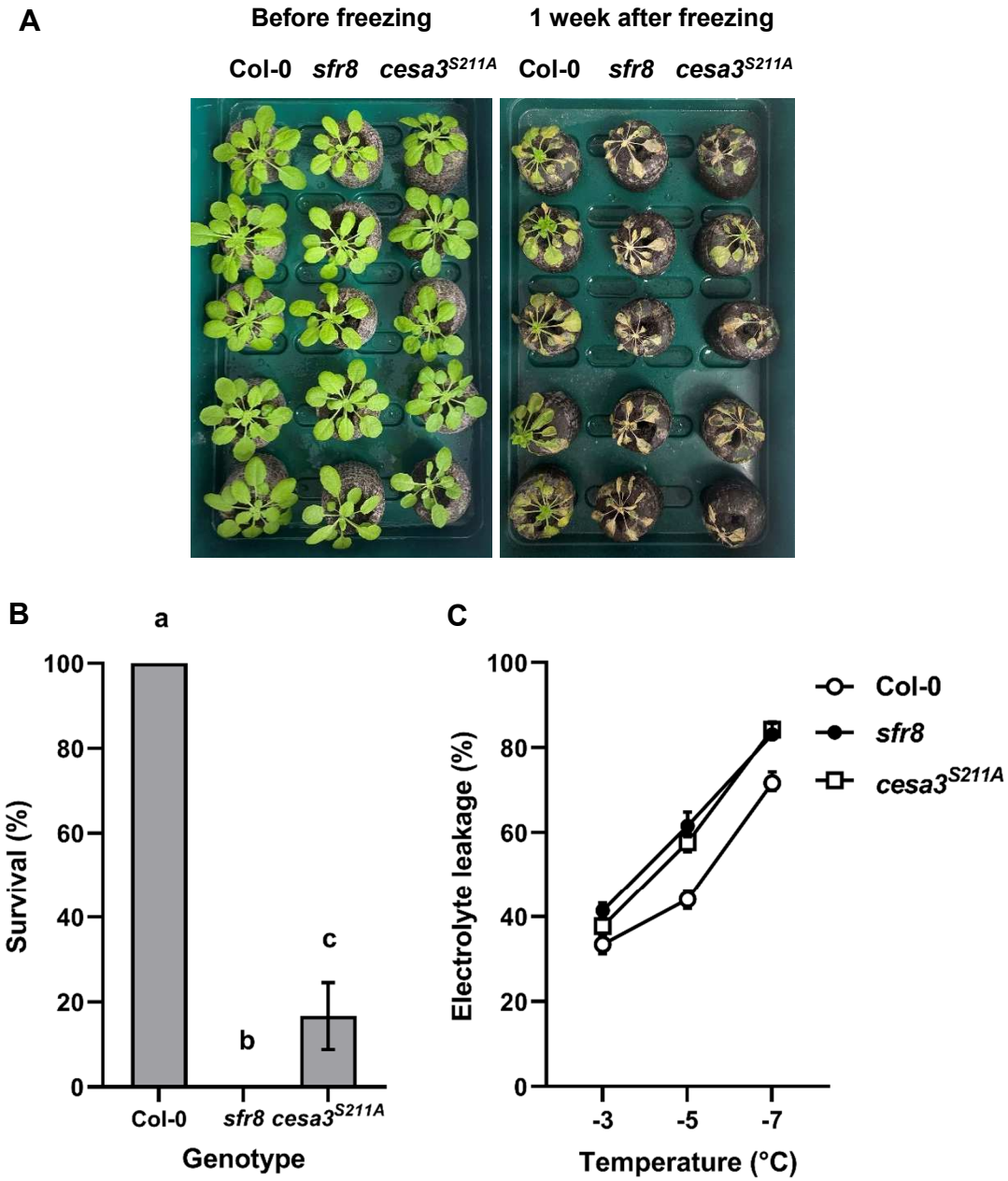

Figure 5.1: Freezing tolerance of the *cesa3^{S211A}* mutant. A) Freezing recovery assay of mature wild-type (Col-0), *sfr8*, and *cesa3^{S211A}* plants. Plants were subjected to freezing at -3°C for 24 h and recovered for one week. Photographed is one representative assay showing plants immediately before (left) and one week after (right) freezing. **B)** Survival analysis of plants from freezing recovery assays. Plants were scored on survival based on whether regrowth had occurred. Bars represent mean percentage survival of plants from three biological replicate experiments; five plants per genotype were used per experiment (n=15). Error bars represent one standard error of the mean of arcsine-transformed data. Means that do not share a letter are significantly different. **C)** Electrolyte leakage of mature leaf tissue from wild-type (Col-0), *sfr8,* and *cesa3^{S211A}*. Tissue was subjected to freezing at -3, -5 or -7°C and electrolyte leakage measured. Points represent mean percentage electrolyte leakage from three biological replicate experiments; each experiment used tissue from six plants per genotype per temperature (n=18 at each point). Error bars represent one standard error of the mean of arcsine-transformed data.

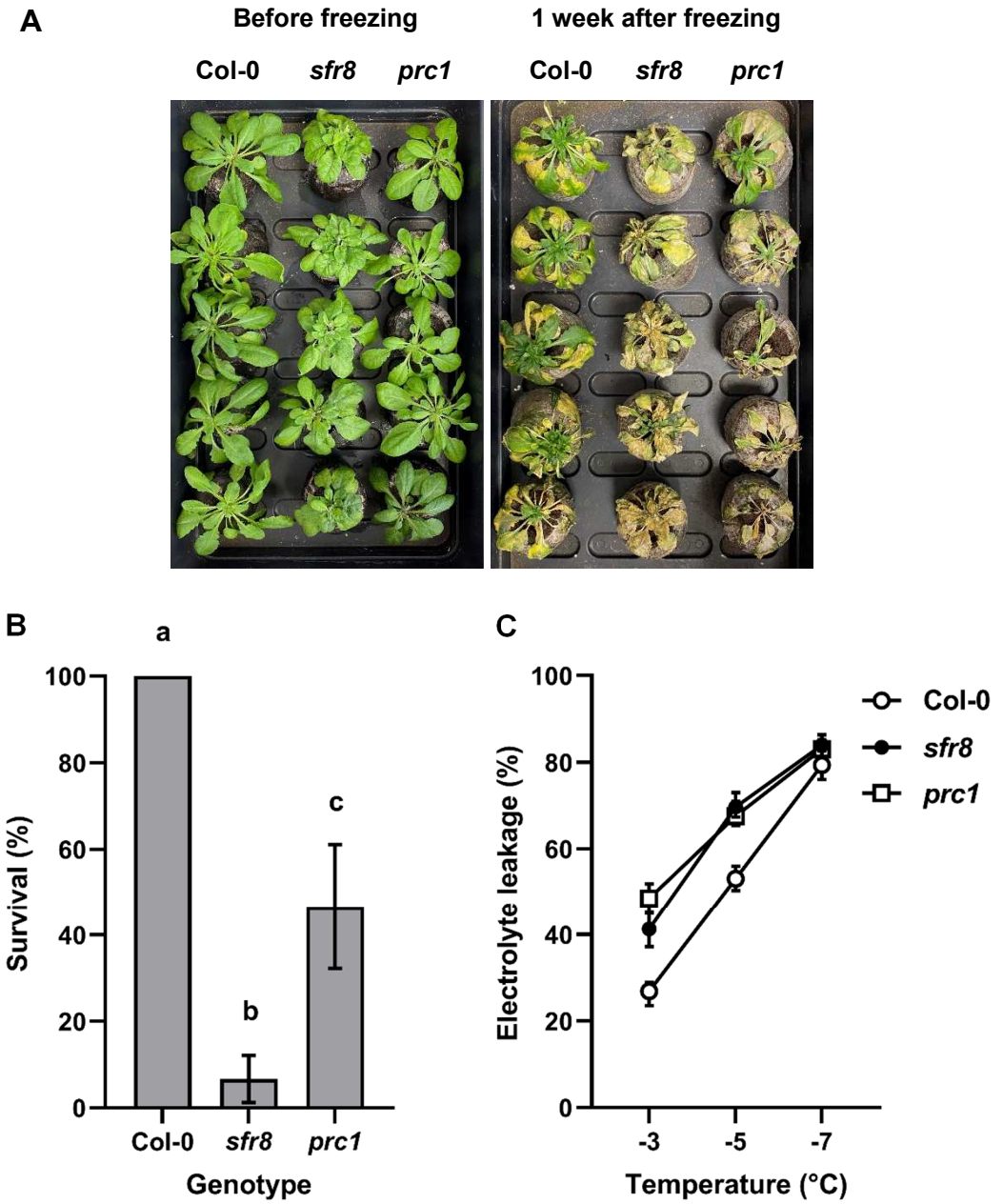

Figure 5.2: Freezing tolerance of the *prc1* mutant. **A)** Freezing recovery assay of mature wild-type (Col-0), *sfr8*, and *prc1* plants. Plants were subjected to freezing at -3°C for 24 h and recovered for one week. Photographed is one representative assay showing plants immediately before (left) and one week after (right) freezing. **B)** Survival analysis of plants from freezing recovery assays. Plants were scored on survival based on whether regrowth had occurred. Bars represent mean percentage survival of plants from three biological replicate experiments; five plants per genotype were used per experiment (n=15). Error bars represent one standard error of the mean of arcsine-transformed data. Means that do not share a letter are significantly different. **C)** Electrolyte leakage of mature leaf tissue from wild-type (Col-0), *sfr8*, and *prc1*. Tissue was subjected to freezing at -3, -5 or -7°C and electrolyte leakage measured. Points represent mean percentage electrolyte leakage from three biological replicate experiments; each experiment used tissue from six plants per genotype per temperature (n=18 at each point). Error bars represent one standard error of the mean of arcsine-transformed data.

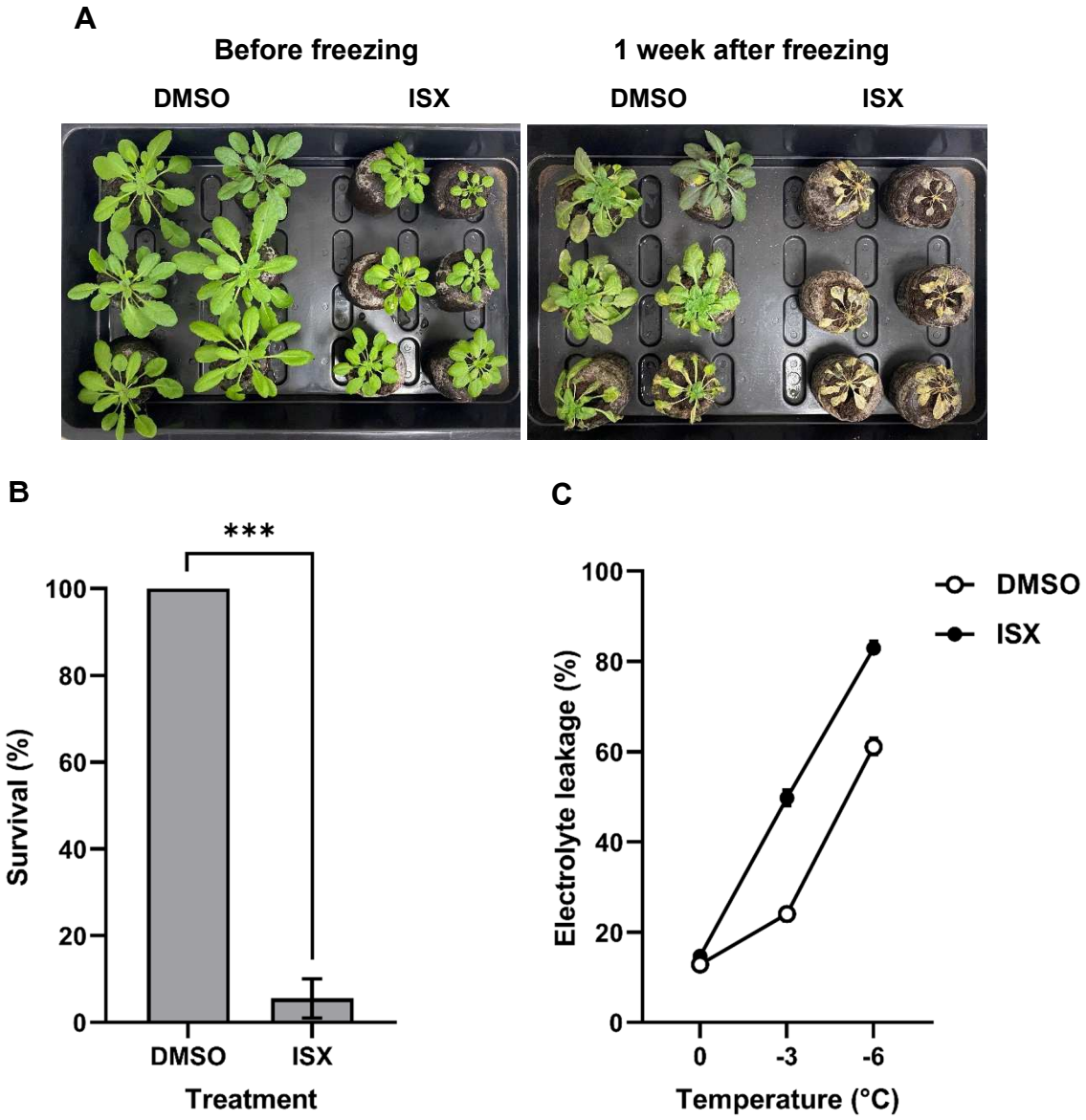

Figure 5.3: Effect of isoxaben treatment on freezing tolerance in *Arabidopsis*. A) Freezing recovery assay of mature, wild-type *Arabidopsis* treated with isoxaben (ISX). Control plants were treated with an equivalent amount of DMSO. Plants were subjected to freezing at -3°C for 24 h and allowed to recover under ambient conditions for one week. Photographed is one representative assay showing plants one week after freezing. **B)** Survival analysis of plants from freezing recovery assays. Plants were scored on survival based on whether regrowth of green tissue had occurred after one week. Bars represent mean percentage survival of plants from three biological replicate experiments; six plants per treatment were used per experiment (n=18). Error bars represent one standard error of the mean of arcsine-transformed data. Asterisks indicate means that are significantly different (*** $p<0.001$). **C)** Electrolyte leakage of leaf tissue from mature, wild-type *Arabidopsis* treated with ISX. Control plants were treated with an equivalent amount of DMSO. Leaf tissue was subjected to freezing at 0, -3 or -6°C and loss of electrolytes was measured. Values represent mean percentage electrolyte leakage from three biological replicate experiments; each experiment used leaf tissue from six plants per treatment per temperature (n=18 at each point). Error bars represent one standard error of the mean of arcsine-transformed data.

Cell-wall porosity was measured using the fluorescence-quenching assay. The fluorescence of stained mesophyll cells was quantified (F_0) and divided by the quantified fluorescence after quenching (F) to give a measure of relative porosity. Individual linear mixed effects models confirmed that experiment number had no significant impact on variation of the data from each of the three plant groups (*cesa3*^{S211A}: $p>0.1$; *prc1*: $p>0.05$; ISX: $p>0.1$), so the data from three biological replicate experiments were pooled separately for each group for analysis. Cell-wall porosity of the *cesa3*^{S211A} mutant (**Figure 5.4**) was significantly lower than that of wild-type plants ($p<0.01$). Conversely, cell-wall porosity of both the *prc1* mutant (**Figure 5.5**) and ISX-treated plants (**Figure 5.6**) was significantly higher than their respective controls ($p<0.05$ and $p<0.001$, respectively). Clearly, the effect of aberrant cellulose phenotypes on cell-wall porosity is not straightforward.

Cell-wall mechanical properties were measured using extensometry. Eight-mm discs prepared from mature leaves of *cesa3*^{S211A}, *prc1*, and ISX-treated plants, along with their controls, were stretched until failure using an extensometer equipped with a load cell sensitive to 1 mN. Individual linear mixed effects models confirmed that experiment number had no significant impact on variation of the data from each of the three plant groups (*cesa3*^{S211A}: $p>0.3$; *prc1*: $p>0.2$; ISX: $p>0.2$), so the data from three biological replicate experiments were pooled separately for each group for analysis. Mean percentage relative tensile force, normalised to the baseline force reading taken immediately before the stretch was initiated, was calculated from pooled data and plotted over time. Firstly, average force curves were plotted on the same axes for each group to allow for comparisons of cell-wall stiffness. Secondly, the percentage relative tensile force values from the peak of force curves from individual samples were plotted to illustrate the cell-wall mechanical strength of tissue from each plant group. For *cesa3*^{S211A}, the gradient of the curve up to the point of failure was 0.299, compared to 0.317 for wild-type, suggesting that the mutant has marginally reduced cell-wall stiffness (**Figure 5.7A**). However, the mechanical strength of *cesa3*^{S211A} was not significantly different to that of wild-type ($p>0.8$). The mean maximum relative tensile force for *cesa3*^{S211A} was 5.01% compared to 5.06% for wild-type (**Figure 5.7B**). For *prc1*, the gradient of the curve up to the point of failure was 0.374, compared to 0.397 for wild-type,

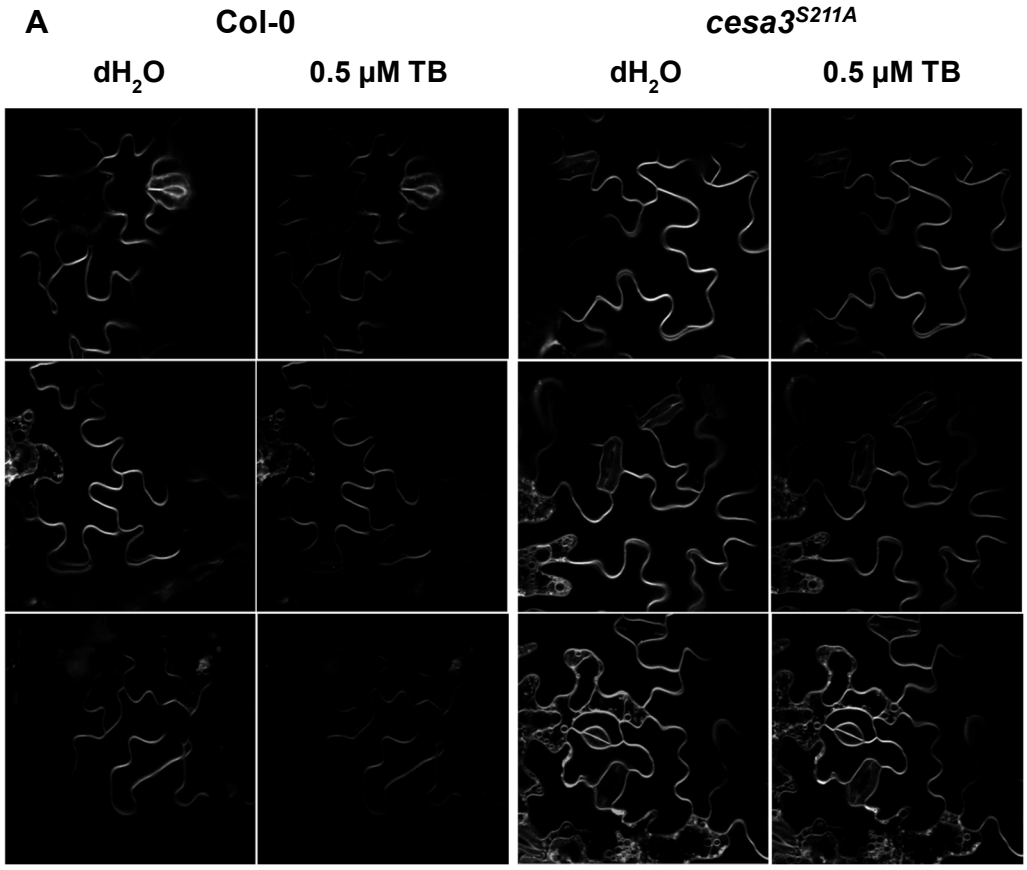

Figure 5.4: Cell-wall porosity of the *cesa3*^{S211A} mutant. Relative porosity was calculated in mature wild-type (Col-0) and *cesa3*^{S211A} plants using fluorescence quenching. **A)** The plasma membranes of leaf epidermal cells were stained with a fluorescent dye and imaged before and after addition of 0.5 µM trypan blue (TB) quenching solution. Three example micrographs per treatment are shown for each genotype. **B)** Fluorescence was quantified before (F_0) and after (F) addition of the quenching solution and a ratio of the two was calculated to give relative porosity (F_0/F). Bars represent mean relative porosity from three biological replicate experiments; each experiment measured porosity in three leaves from separate plants per genotype (n=9). Error bars represent one standard error of the mean. Asterisks indicate means that are significantly different (** $p<0.01$).

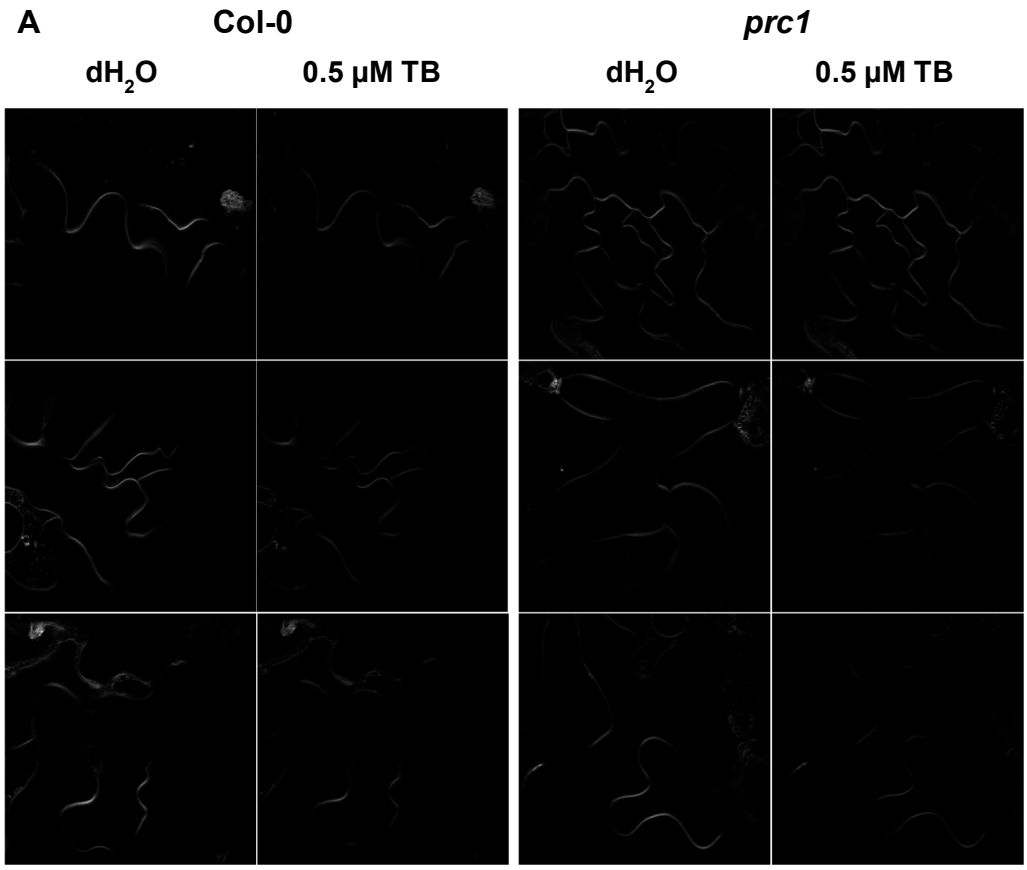

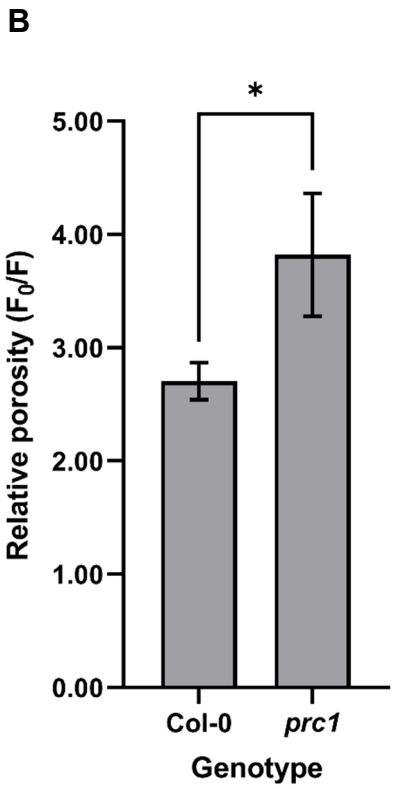

Figure 5.5: Cell-wall porosity of the *prc1* mutant. Relative porosity was calculated in mature wild-type (Col-0) and *prc1* plants using fluorescence quenching. **A)** The plasma membranes of leaf epidermal cells were stained with a fluorescent dye and imaged before and after addition of 0.5 µM trypan blue (TB) quenching solution. Three example micrographs per treatment are shown for each genotype. **B)** Fluorescence was quantified before (F_0) and after (F) addition of the quenching solution and a ratio of the two was calculated to give relative porosity (F_0/F). Bars represent mean relative porosity from three biological replicate experiments; each experiment measured porosity in three leaves from separate plants per genotype (n=9). Error bars represent one standard error of the mean. Asterisks indicate means that are significantly different (* $p<0.05$).

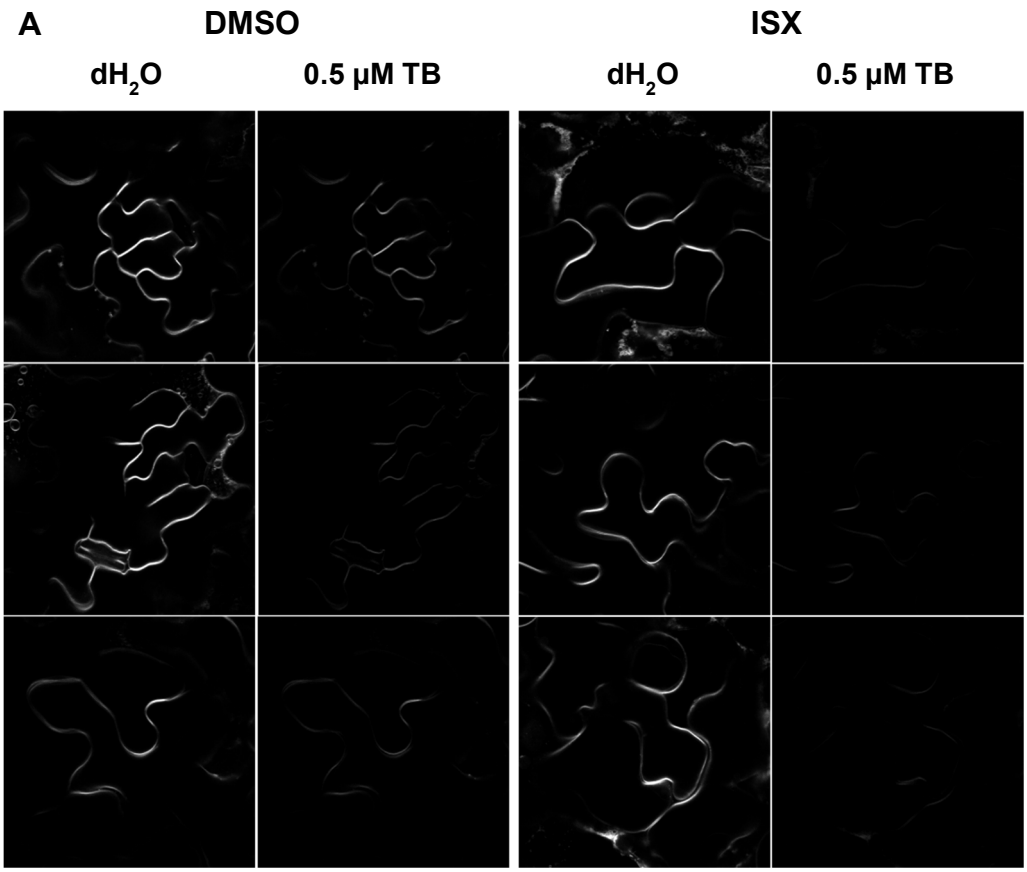

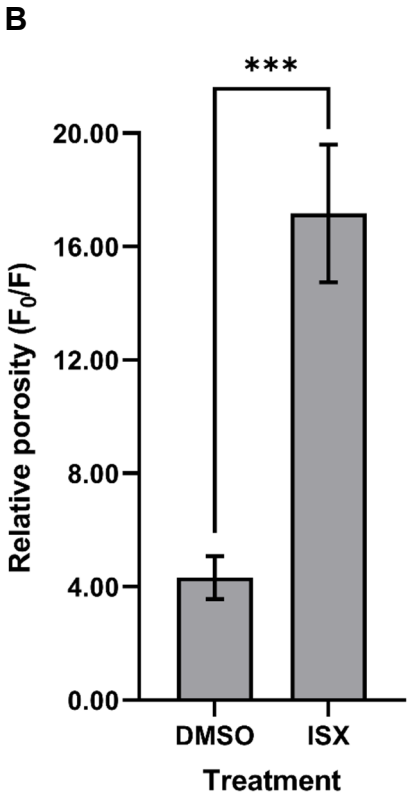

Figure 5.6: Effect of isoxaben treatment on cell-wall porosity in *Arabidopsis*. Relative porosity was calculated in mature, wild-type *Arabidopsis* treated with isoxaben (ISX) using fluorescence quenching. Control plants were treated with an equivalent amount of DMSO. **A)** The plasma membranes of leaf epidermal cells were stained with a fluorescent dye and imaged before and after addition of 0.5 µM trypan blue (TB) quenching solution. Three example micrographs per treatment are shown for each genotype. **B)** Fluorescence was quantified before (F_0) and after (F) addition of the quenching solution and a ratio of the two was calculated to give relative porosity (F_0/F). Bars represent mean relative porosity from three biological replicate experiments; each experiment measured porosity in three leaves from separate plants per treatment (n=9). Error bars represent one standard error of the mean. Asterisks indicate means that are significantly different (*** $p<0.001$).

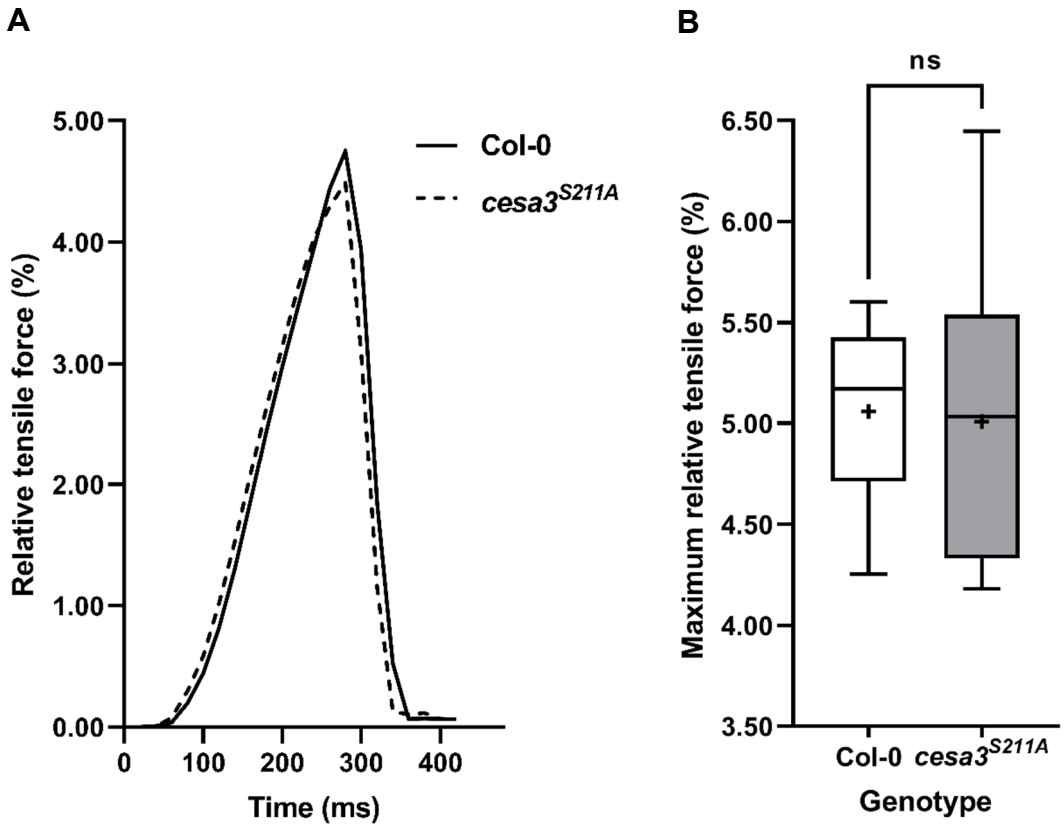

Figure 5.7: Cell-wall mechanical properties of the *cesa3*^{S211A} mutant. Mechanical properties were assessed in mature wild-type (Col-0) and *cesa3*^{S211A} plants using extensometry. Leaf discs from each genotype were stretched until breakage and the force required to do so was recorded. Tensile force was normalised to the baseline force reading taken immediately before the stretch was initiated and converted to a percentage for each sample. Plots represent combined data for three biological replicate experiments; each experiment measured cell-wall mechanical properties in three leaf discs per genotype (n=9). **A)** Relative tensile force plotted over time for the duration of each stretch. A steeper gradient is indicative of stiffer material and a higher peak (more resistance to breaking pressure) is indicative of stronger material. **B)** Box-and-whisker plot showing the distribution of maximum tensile force values for each genotype. Values were taken from the absolute peak of each force curve, which represents the maximum tensile force that the tissue can withstand before breakage. Whiskers: maximum and minimum values; box edges: upper and lower quartiles; plus signs: mean values; horizontal lines: median values. ns indicates means that are not significantly different (p>0.8).

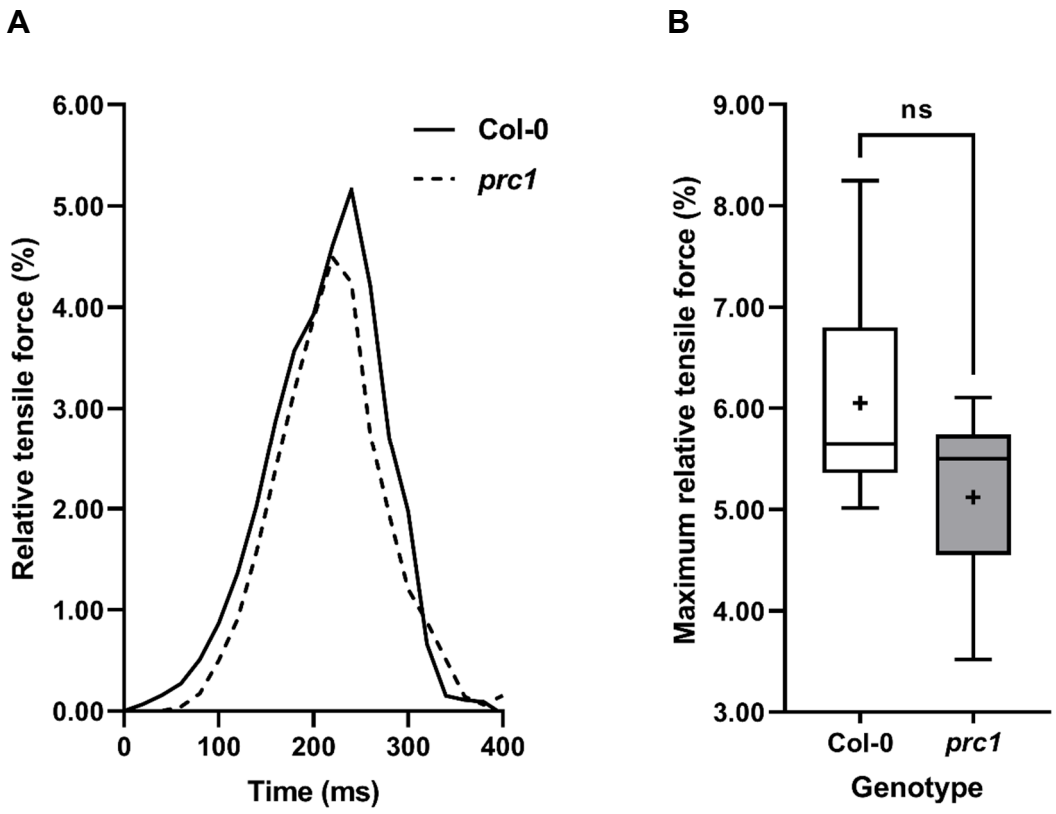

Figure 5.8: Cell-wall mechanical properties of the *prc1* mutant. Mechanical properties were assessed in mature wild-type (Col-0) and *prc1* plants using extensometry. Leaf discs from each genotype were stretched until breakage and the force required to do so was recorded. Tensile force was normalised to the baseline force reading taken immediately before the stretch was initiated and converted to a percentage for each sample. Plots represent combined data for three biological replicate experiments; each experiment measured cell-wall mechanical properties in three leaf discs per genotype (n=9). **A)** Relative tensile force plotted over time for the duration of each stretch. A steeper gradient is indicative of stiffer material and a higher peak (more resistance to breaking pressure) is indicative of stronger material. **B)** Box-and-whisker plot showing the distribution of maximum tensile force values for each genotype. Values were taken from the absolute peak of each force curve, which represents the maximum tensile force that the tissue can withstand before breakage. Whiskers: maximum and minimum values; box edges: upper and lower quartiles; plus signs: mean values; horizontal lines: median values. ns indicates means that are not significantly different (p>0.05).

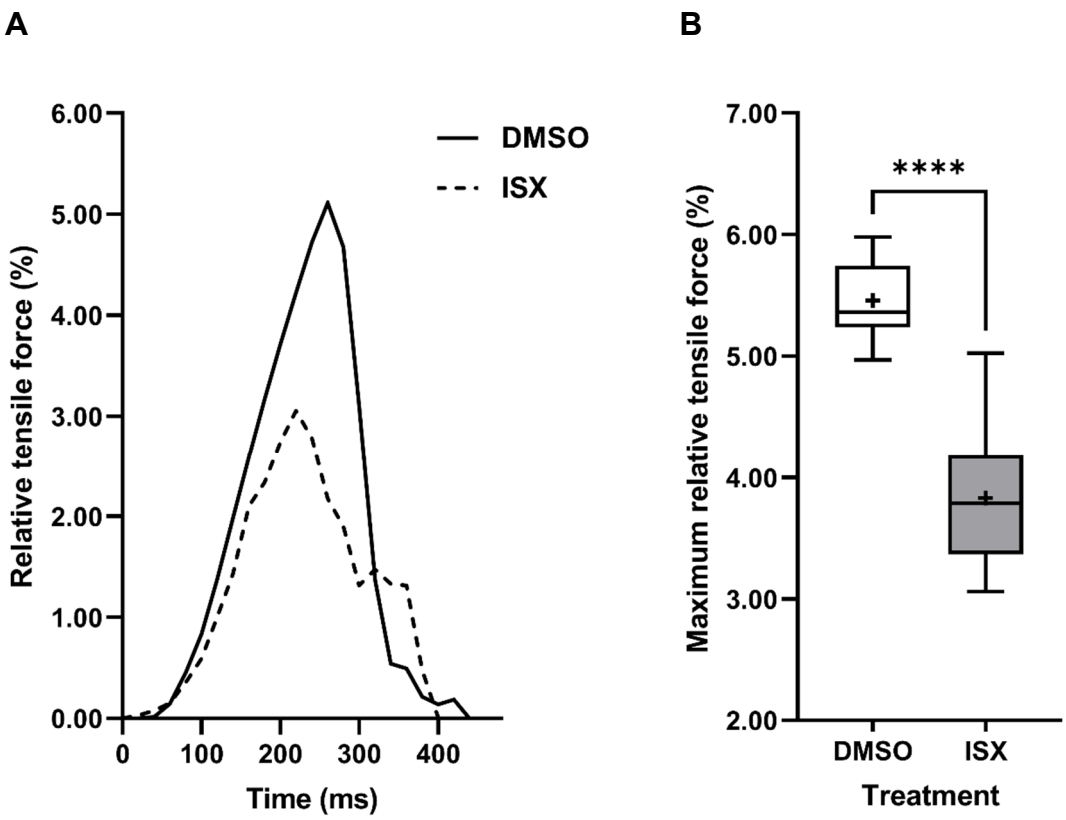

Figure 5.9: Effect of isoxaben treatment on cell-wall mechanical properties in *Arabidopsis*. Mechanical properties were assessed in mature, wild-type *Arabidopsis* treated with isoxaben (ISX) using extensometry. Control plants were treated with an equivalent amount of DMSO. Leaf discs from each group were stretched until breakage and the force required to do so was recorded. Tensile force was normalised to the baseline force reading taken immediately before the stretch was initiated and converted to a percentage for each sample. Plots represent combined data for three biological replicate experiments; each experiment measured cell-wall mechanical properties in three leaf discs per group (n=9). **A)** Relative tensile force plotted over time for the duration of each stretch. A steeper gradient is indicative of stiffer material and a higher peak (more resistance to breaking pressure) is indicative of stronger material. **B)** Box-and-whisker plot showing the distribution of maximum tensile force values for each treatment. Values were taken from the absolute peak of each force curve, which represents the maximum tensile force that the tissue can withstand before breakage. Whiskers: maximum and minimum values; box edges: upper and lower quartiles; plus signs: mean values; horizontal lines: median values. Asterisks indicate means that are significantly different (**** $p<0.0001$).

suggesting that the mutant has marginally reduced cell-wall stiffness (**Figure 5.8A**). Although the mechanical strength of *prc1* was lower than that of wild-type, the difference was not significant ($p>0.05$). The mean maximum relative tensile force for *prc1* was 5.12% compared to 6.18% for wild-type (**Figure 5.8B**). For ISX-treated plants, the gradient of the curve up to the point of failure was 0.255, compared to 0.363 for controls, suggesting that they had reduced cell-wall stiffness (**Figure 5.9A**). The mechanical strength of ISX-treated plants was also significantly lower than that of controls ($p<0.0001$). The mean maximum relative tensile force for ISX-treated plants was 3.83% compared to 5.46% for controls (**Figure 5.9B**).

5.2.2 Hemicellulose

To further understand the role of hemicelluloses in plant freezing tolerance and cell-wall physical properties, the *xxt1 xxt2*, *mur2*, *mur3* and *msr1-2* mutants were studied. *xxt1 xxt2* lacks detectable cell-wall xyloglucan (Cavalier *et al.* 2008), whereas *mur2* and *mur3* have mutations in xyloglucan-specific fucosyltransferases and galactosyltransferases, respectively (Vanzin *et al.* 2002, Madson *et al.* 2003). *msr1-2* has a 40% reduction in cell-wall mannosyl residues which make up the backbone of hemicellulosic mannan polysaccharides (Wang *et al.* 2013).

5.2.2.1 Freezing tolerance

Freezing assays were carried out using each of the mutants as well as mature wild-type (Col-0) and *sfr8* as negative and positive controls, respectively. Plants were subjected to freezing at -3°C for 24 h before being returned to ambient growth conditions. The capacity of the plants to recover and exhibit new growth was assessed after 1 week. In order to quantify the damage incurred by plants during freezing, electrolyte leakage was measured in leaf tissue from plants of each genotype following exposure to three sub-zero temperatures (-3, -5 and -7°C) Results for each of the mutants will be described separately.

For *xxt1 xxt2* recovery assays (**Figure 5.10A**), a linear mixed effects model confirmed that experiment number had no significant impact on data variation ($p>0.1$) so the data from three biological replicate experiments were pooled for

analysis. Mean percentage survival of plants of each genotype was calculated from pooled data. Genotype had a significant effect on plant survival ($p<0.001$). Compared to wild-type, which had a mean survival rate of 93%, both *xxt1 xxt2* and *sfr8* had significantly lower mean survival rates of 33% and 7%, respectively (**Figure 5.10B**). For electrolyte leakage assays, whole leaves were used due to the small size of *xxt1 xxt2*. A linear mixed effects model confirmed that experiment number had no significant impact on data variation ($p>0.1$) so the data from three biological replicate experiments were pooled for analysis. Mean percentage electrolyte leakage of plants of each genotype was calculated at each temperature from pooled data (**Figure 5.10C**). At -3 and -5°C, genotype had a significant impact on electrolyte leakage ($p<0.001$). Both *xxt1 xxt2* and *sfr8* had significantly higher electrolyte leakage than wild-type plants at both temperatures. At -7°C, genotype did not have a significant impact on electrolyte leakage ($p>0.8$). The electrolyte leakage of *xxt1 xxt2* did not differ significantly from either wild-type or *sfr8*. The results of these assays suggest that tissue that lacks cell-wall xyloglucan has increased freezing sensitivity, so some amount of xyloglucan is required for full freezing tolerance.

The *mur2* and *mur3* mutants were included together in the same freezing assays. For recovery assays (**Figure 5.11A**), a linear mixed effects model confirmed that experiment number had no significant impact on data variation ($p>0.2$) so the data from three biological replicate experiments were pooled for analysis. Mean percentage survival of plants of each genotype was calculated from pooled data. Genotype had a significant effect on plant survival ($p<0.01$). Compared to wild-type, which had a mean survival rate of 100%, both *mur3* and *sfr8* had significantly lower mean survival rates of 11% and 6%, respectively; *mur2*, on the other hand, had a mean survival rate of 94%, which was not significantly different to that of wild-type (**Figure 5.11B**). For electrolyte leakage assays, a linear mixed effects model confirmed that experiment number had no significant impact on data variation ($p>0.3$) so the data from three biological replicate experiments were pooled for analysis. Mean percentage electrolyte leakage of plants of each genotype was calculated at each temperature from pooled data (**Figure 5.11C**). At all three temperatures, genotype had a significant impact on electrolyte leakage ($p<0.001$

for each temperature). At all three temperatures, *mur3* and *sfr8* had significantly higher electrolyte leakage than that of wild-type and *mur2*. The electrolyte leakage of *mur2* did not differ significantly from that of wild-type at any temperature. The results of these assays support the idea of xyloglucan galactosylation, but not fucosylation, contributing to plant freezing tolerance.

Data from a preliminary cell-wall profiling experiment suggested that mannan may accumulate during cold acclimation (see **Appendix R**), so *msr1-2* freezing assays were carried out on both cold-acclimated and non-acclimated plants. For recovery assays, plants were subjected to freezing at either -3°C (non-acclimated plants) or -8°C (cold-acclimated plants) before being returned to ambient growth conditions. The capacity of the plants to recover and exhibit new growth was assessed after 1 week (non-acclimated plants: **Figure 5.12A**; cold-acclimated plants: **Figure 5.13A**). Individual linear mixed effects models confirmed that experiment number had no significant impact on the variation of data from both datasets ($p>0.05$ for both) so the data from three biological replicate experiments were pooled separately for each treatment. Mean percentage survival of plants of each genotype was calculated from pooled data. Genotype had a significant effect on plant survival ($p<0.05$ for both). In both non-acclimated (**Figure 5.12B**) and cold-acclimated (**Figure 5.13B**) states, *msr1-2* had a mean survival rate of 93%, which was not significantly different to that of wild-type (100%). For electrolyte leakage assays, leaf tissue was subjected to freezing at three different sub-zero temperatures (-3, -5 and -7°C for non-acclimated plants; -5, -7 and -9°C for cold-acclimated plants). Individual linear mixed effects models confirmed that experiment number had no significant impact on data variation ($p>0.2$ for both) so the data from three biological replicate experiments were pooled separately for each treatment. Mean percentage electrolyte leakage of plants of each genotype was calculated at each temperature from pooled data. For both non-acclimated and cold-acclimated plants, genotype had a significant impact on electrolyte leakage (non-acclimated: -3 and -5°C, $p<0.001$; -7°C, $p<0.05$; cold-acclimated: -5 and -7°C, $p<0.001$; -9°C, $p<0.05$). However, the electrolyte leakage of *msr1-2* did not differ significantly from that of wild-type at any temperature, regardless of acclimation state (non-acclimated: **Figure 5.12C**; cold-acclimated: **Figure 5.13C**).

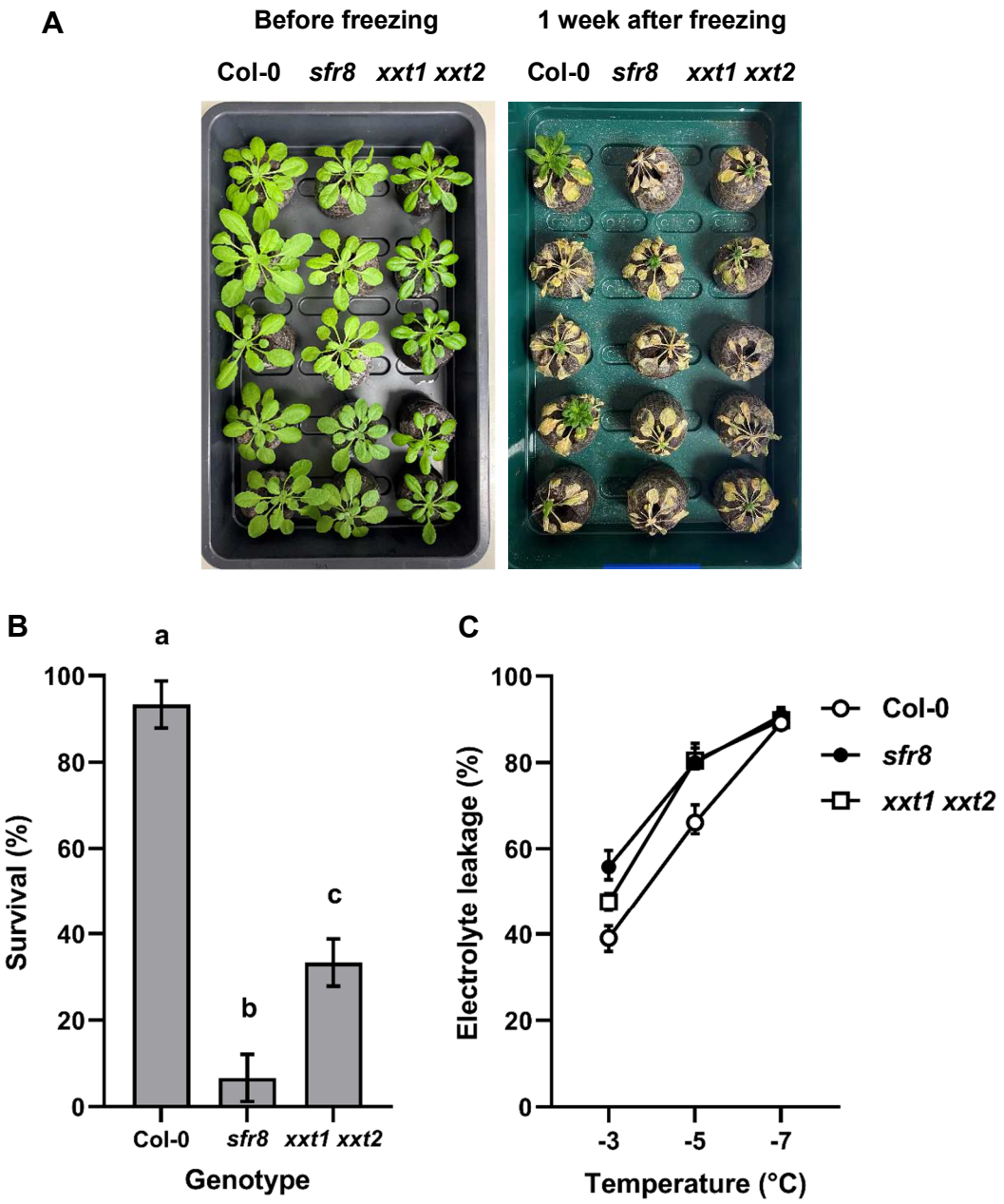

Figure 5.10: Freezing tolerance of the *xxt1 xxt2* mutant. A) Freezing recovery assay of mature wild-type (Col-0), *sfr8*, and *xxt1 xxt2* plants. Plants were subjected to freezing at -3°C for 24 h and recovered for one week. Photographed is one representative assay showing plants immediately before (left) and one week after (right) freezing. **B)** Survival analysis of plants from freezing recovery assays. Plants were scored on survival based on whether regrowth had occurred. Bars represent mean percentage survival of plants from three biological replicate experiments; five plants per genotype were used per experiment (n=15). Error bars represent one standard error of the mean of arcsine-transformed data. Means that do not share a letter are significantly different. **C)** Electrolyte leakage of whole leaves from wild-type (Col-0), *sfr8,* and *xxt1 xxt2*. Tissue was subjected to freezing at -3, -5 or -7°C and electrolyte leakage measured. Points represent mean percentage electrolyte leakage from three biological replicate experiments; each experiment used tissue from six plants per genotype per temperature (n=18 at each point). Error bars represent one standard error of the mean of arcsine-transformed data.

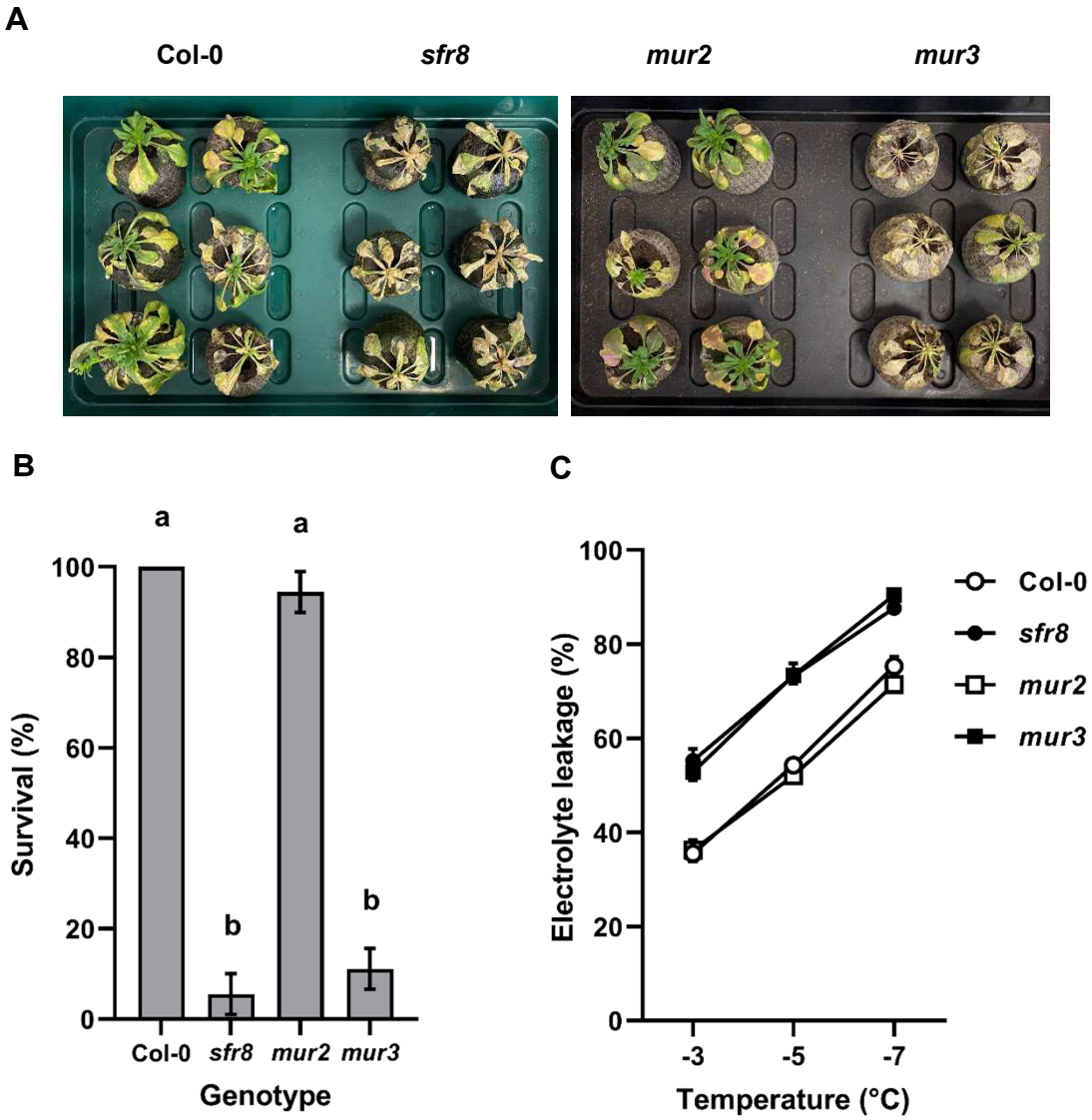

Figure 5.11: Freezing tolerance of the *mur2* and *mur3* mutants. A) Freezing recovery assay of mature wild-type (Col-0), *sfr8*, *mur2* and *mur3* plants. Plants were subjected to freezing at -3°C for 24 h and recovered for one week. Photographed is one representative assay showing plants one week after freezing. **B)** Survival analysis of plants from freezing recovery assays. Plants were scored on survival based on whether regrowth had occurred. Bars represent mean percentage survival of plants from three biological replicate experiments; six plants per genotype were used per experiment (n=18). Error bars represent one standard error of the mean of arcsine-transformed data. Means that do not share a letter are significantly different. **C)** Electrolyte leakage of mature leaf tissue from wild-type (Col-0), *sfr8*, *mur2* and *mur3*. Tissue was subjected to freezing at -3, -5 or -7°C and electrolyte leakage measured. Points represent mean percentage electrolyte leakage from three biological replicate experiments; each experiment used tissue from six plants per genotype per temperature (n=18 at each point). Error bars represent one standard error of the mean of arcsine-transformed data.

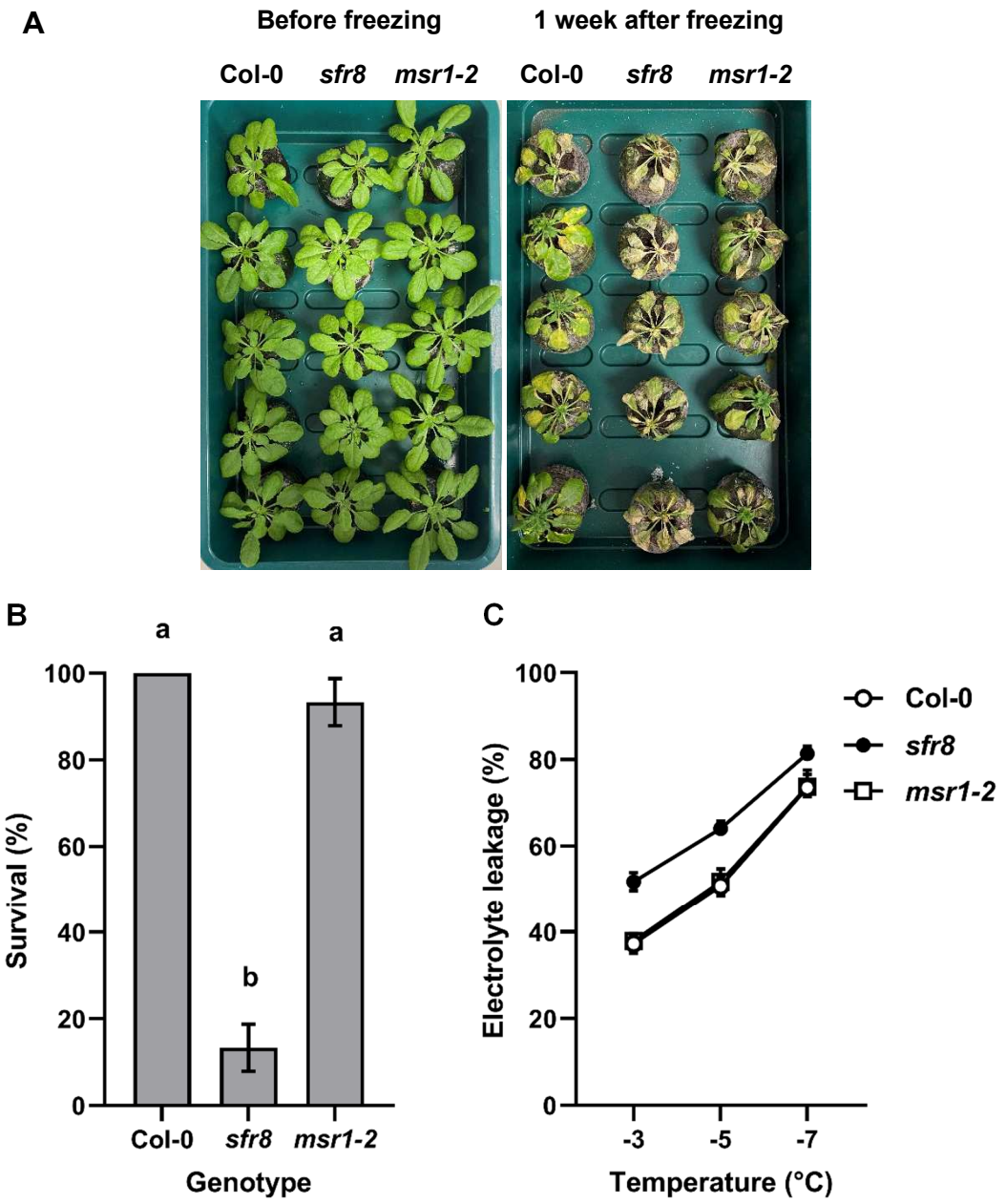

Figure 5.12: Freezing tolerance of the *msr1-2* mutant without cold acclimation. **A)** Freezing recovery assay of mature, non-acclimated wild-type (Col-0), *sfr8*, and *msr1-2* plants. Plants were subjected to freezing at -3°C for 24 h and recovered for one week. Photographed is one representative assay showing plants immediately before (left) and one week after (right) freezing. **B)** Survival analysis of plants from freezing recovery assays. Plants were scored on survival based on whether regrowth had occurred. Bars represent mean percentage survival of plants from three biological replicate experiments; five plants per genotype were used per experiment (n=15). Error bars represent one standard error of the mean of arcsine-transformed data. Means that do not share a letter are significantly different. **C)** Electrolyte leakage of mature leaf tissue from non-acclimated wild-type (Col-0), *sfr8* and *msr1-2*. Tissue was subjected to freezing at -3, -5 or -7°C and electrolyte leakage measured. Points represent mean percentage electrolyte leakage from three biological replicate experiments; each experiment used tissue from six plants per genotype per temperature (n=18 at each point). Error bars represent one standard error of the mean of arcsine-transformed data.

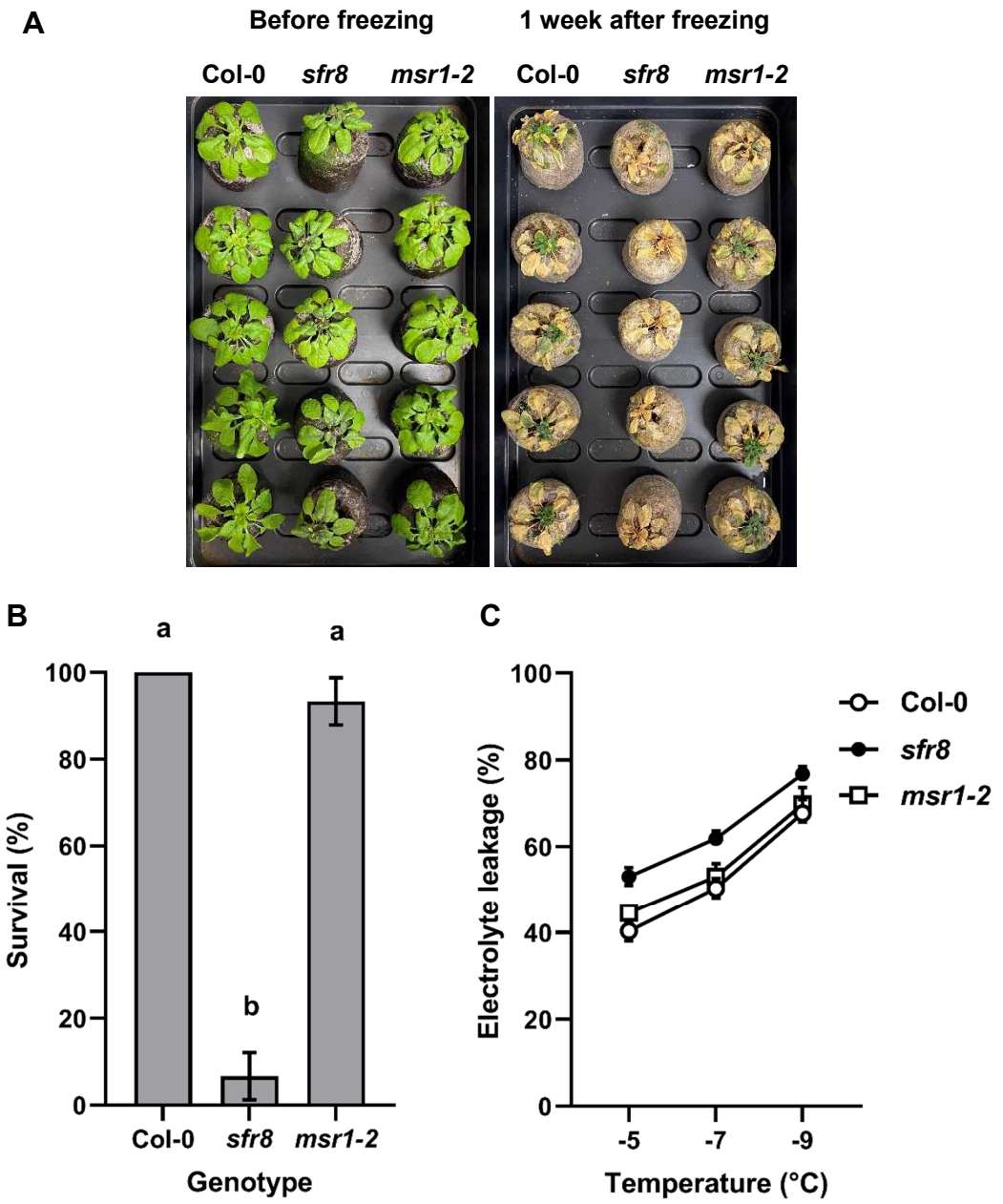

Figure 5.13: Freezing tolerance of the *msr1-2* mutant after cold acclimation. **A)** Freezing recovery assay of mature, cold-acclimated wild-type (Col-0), *sfr8*, and *msr1-2* plants. Plants were subjected to freezing at -8°C for 24 h and recovered for one week. Photographed is one representative assay showing plants immediately before (left) and one week after (right) freezing. **B)** Survival analysis of plants from freezing recovery assays. Plants were scored on survival based on whether regrowth had occurred. Bars represent mean percentage survival of plants from three biological replicate experiments; five plants per genotype were used per experiment (n=15). Error bars represent one standard error of the mean of arcsine-transformed data. Means that do not share a letter are significantly different. **C)** Electrolyte leakage of mature leaf tissue from cold-acclimated wild-type (Col-0), *sfr8*, and *msr1-2*. Tissue was subjected to freezing at -5, -7 or -9°C and electrolyte leakage measured. Points represent mean percentage electrolyte leakage from three biological replicate experiments; each experiment used tissue from six plants per genotype per temperature (n=18 at each point). Error bars represent one standard error of the mean of arcsine-transformed data.

The results of these assays suggest that a large reduction in cell-wall mannan levels has no measurable impact on plant freezing tolerance.

5.2.2.2 Cell-wall physical properties

As *xxt1 xxt2* and *mur3* mutants appeared to have compromised freezing tolerance, their cell-wall porosity and mechanical properties were analysed to determine if these were contributing factors. These properties were also measured in *mur2* and *msr1-2* to see if their respective cell-wall defects resulted in changes to their physical properties without impacting freezing tolerance.

Cell-wall porosity was measured using the fluorescence-quenching assay. The fluorescence of stained mesophyll cells was quantified (F_0) and divided by the quantified fluorescence after quenching (F) to give a measure of relative porosity. Individual linear mixed effects models confirmed that experiment number had no significant impact on variation of the data for each of the four genotypes (*xxt1 xxt2*: $p>0.1$; *mur2*: $p>0.1$; *mur3*: $p>0.05$; *msr1-2*: $p>0.2$), so the data from three biological replicate experiments were pooled separately for each genotype for analysis. Interestingly, the cell-wall porosities of *xxt1 xxt2* ($p<0.05$; **Figure 5.14**), *mur2* ($p<0.01$; **Figure 5.15**) and *mur3* ($p<0.05$; **Figure 5.16**) were all significantly lower than their wild-type controls. The cell-wall porosity of *msr1-2* was also lower than its wild-type control but the difference was not significant ($p>0.2$; **Figure 5.17**). The results of these assays show a clear pattern of aberrant hemicellulose phenotypes resulting in a reduction in cell-wall porosity.

Cell-wall mechanical properties were measured using extensometry. Eight-mm discs prepared from mature leaves of *xxt1 xxt2, mur2, mur3* and *msr1-2*, along with their wild-type controls, were stretched until failure using an extensometer equipped with a load cell sensitive to 1 mN. Individual linear mixed effects models confirmed that experiment number had no significant impact on variation of the data for each of the four genotypes (*xxt1 xxt2*: $p>0.2$; *mur2*: $p>0.05$; *mur3*: $p>0.2$; *msr1-2*: $p>0.1$), so the data from three biological replicate experiments were pooled separately for each genotype for analysis. Mean percentage relative tensile force, normalised to the baseline force reading taken immediately before the stretch was initiated, was calculated from pooled data and plotted over time.

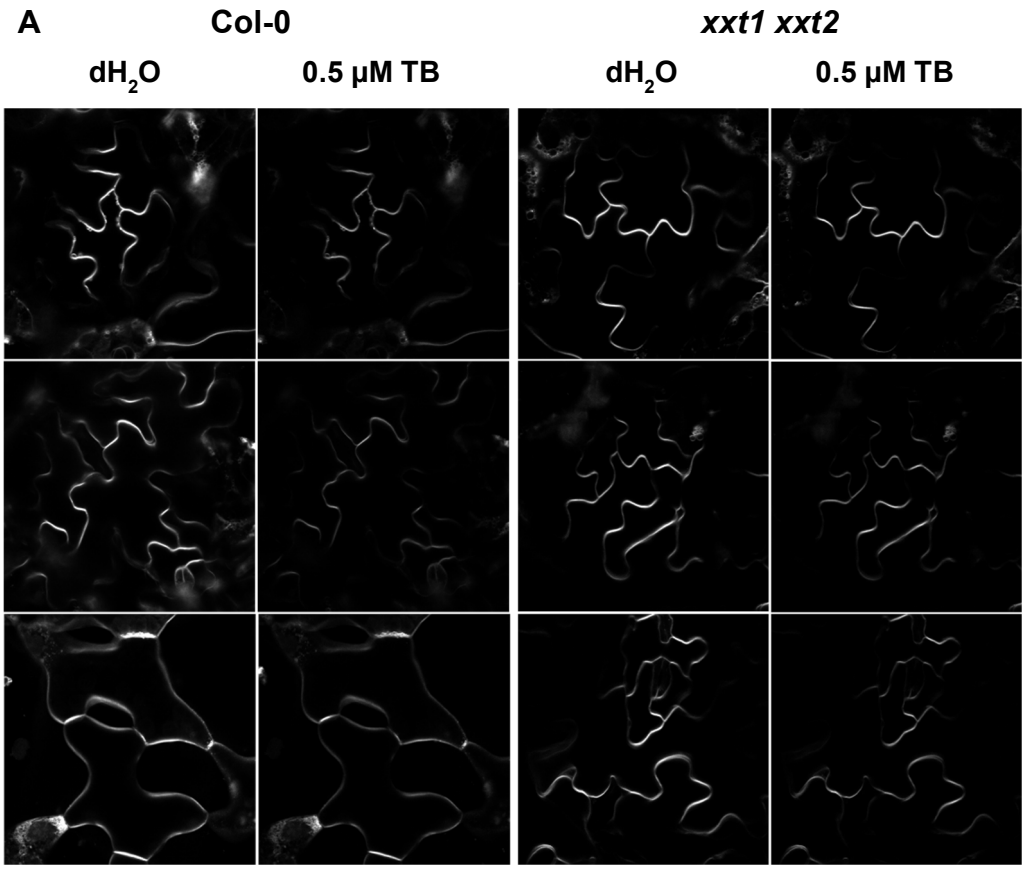

Figure 5.14: Cell-wall porosity of the *xxt1 xxt2* mutant. Relative porosity was calculated in mature wild-type (Col-0) and *xxt1 xxt2* plants using fluorescence quenching. **A)** The plasma membranes of leaf epidermal cells were stained with a fluorescent dye and imaged before and after addition of 0.5 µM trypan blue (TB) quenching solution. Three example micrographs per treatment are shown for each genotype. **B)** Fluorescence was quantified before (F_0) and after (F) addition of the quenching solution and a ratio of the two was calculated to give relative porosity (F_0/F). Bars represent mean relative porosity from three biological replicate experiments; each experiment measured porosity in three leaves from separate plants per genotype (n=9). Error bars represent one standard error of the mean. Asterisks indicate means that are significantly different (* $p<0.05$).

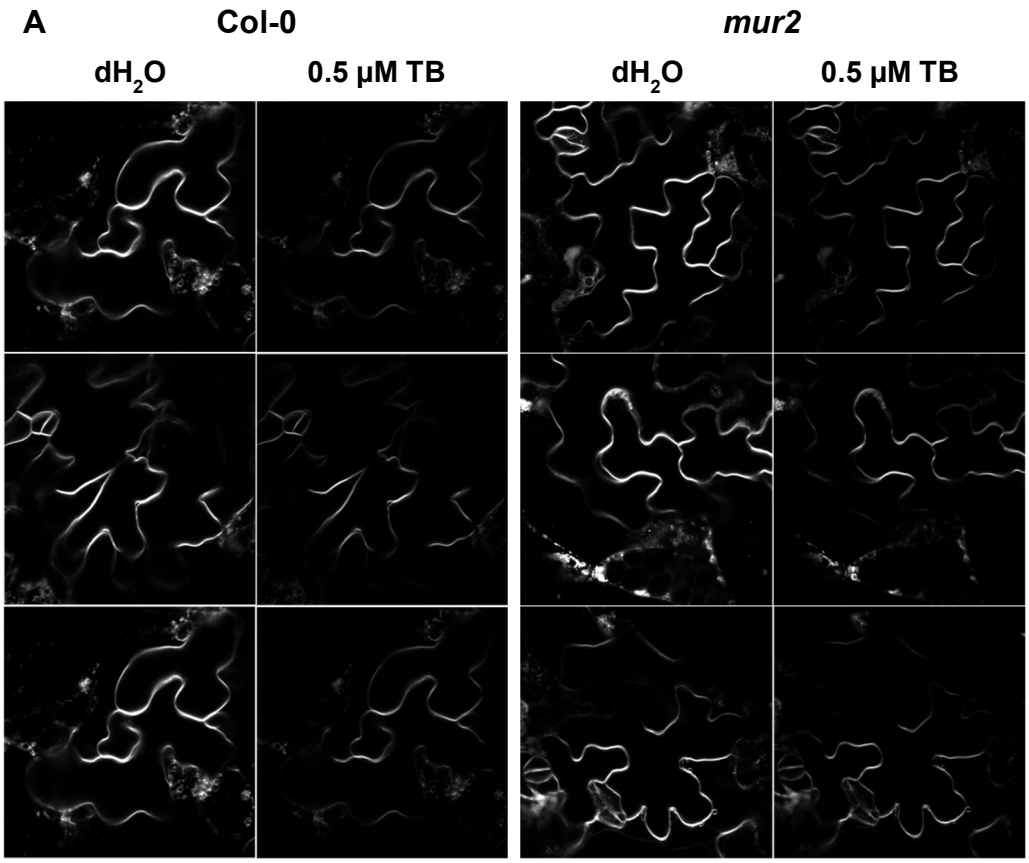

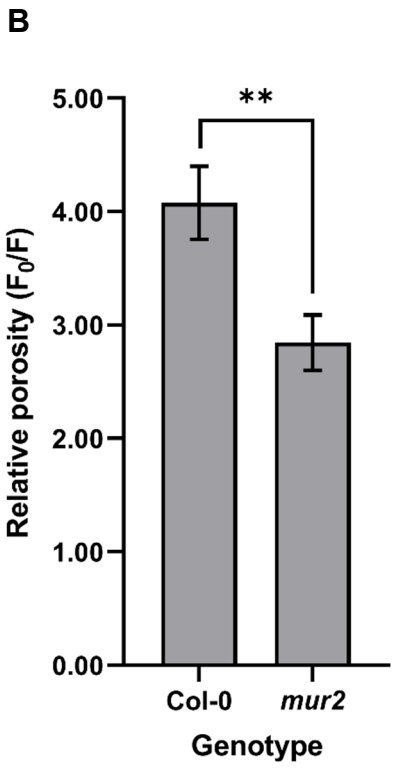

Figure 5.15: Cell-wall porosity of the *mur2* mutant. Relative porosity was calculated in mature wild-type (Col-0) and *mur2* plants using fluorescence quenching. **A)** The plasma membranes of leaf epidermal cells were stained with a fluorescent dye and imaged before and after addition of 0.5 µM trypan blue (TB) quenching solution. Three example micrographs per treatment are shown for each genotype. **B)** Fluorescence was quantified before (F_0) and after (F) addition of the quenching solution and a ratio of the two was calculated to give relative porosity (F_0/F). Bars represent mean relative porosity from three biological replicate experiments; each experiment measured porosity in three leaves from separate plants per genotype (n=9). Error bars represent one standard error of the mean. Asterisks indicate means that are significantly different (** $p<0.01$).

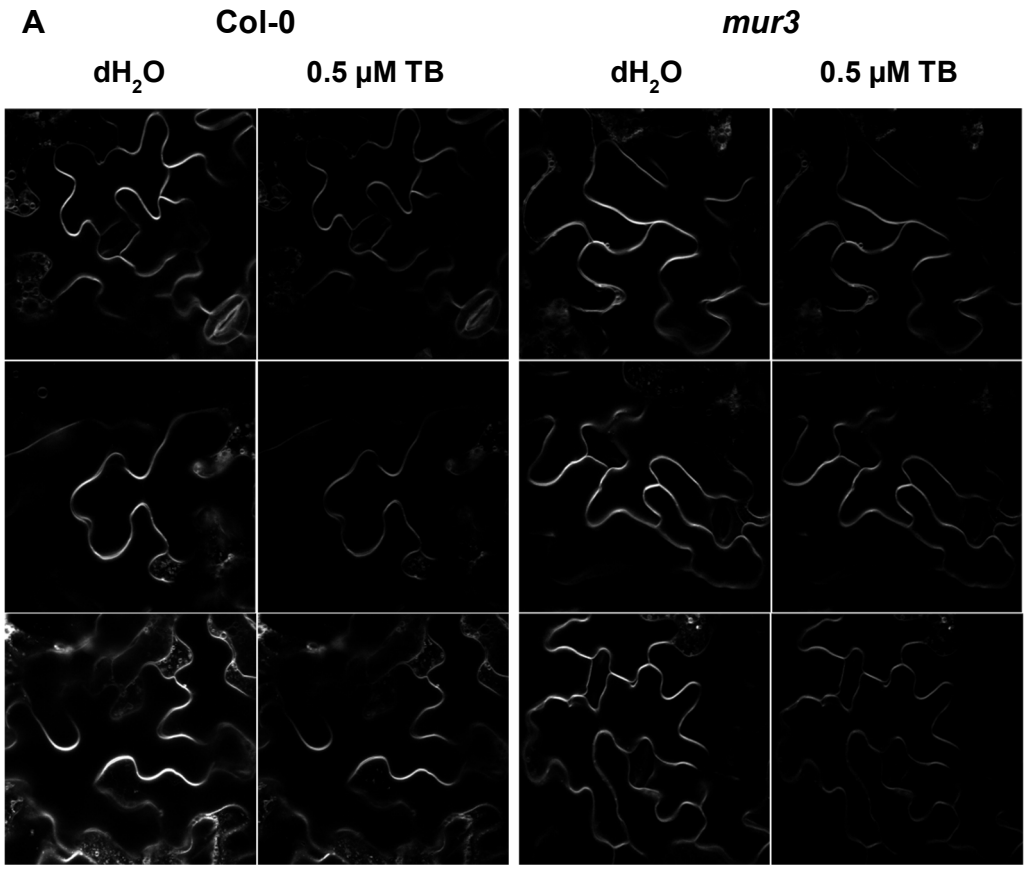

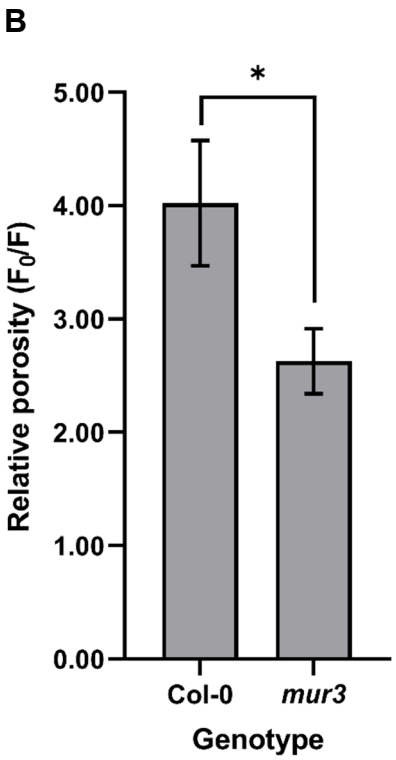

Figure 5.16: Cell-wall porosity of the *mur3* mutant. Relative porosity was calculated in wild-type (Col-0) and *mur3* plants using fluorescence quenching. **A)** The plasma membranes of leaf epidermal cells were stained with a fluorescent dye and imaged before and after addition of 0.5 µM trypan blue (TB) quenching solution. Three example micrographs per treatment are shown for each genotype. **B)** Fluorescence was quantified before (F_0) and after (F) addition of the quenching solution and a ratio of the two was calculated to give relative porosity (F_0/F). Bars represent mean relative porosity from three biological replicate experiments; each experiment measured porosity in three leaves from separate plants per genotype (n=9). Error bars represent one standard error of the mean. Asterisks indicate means that are significantly different (* $p<0.05$).

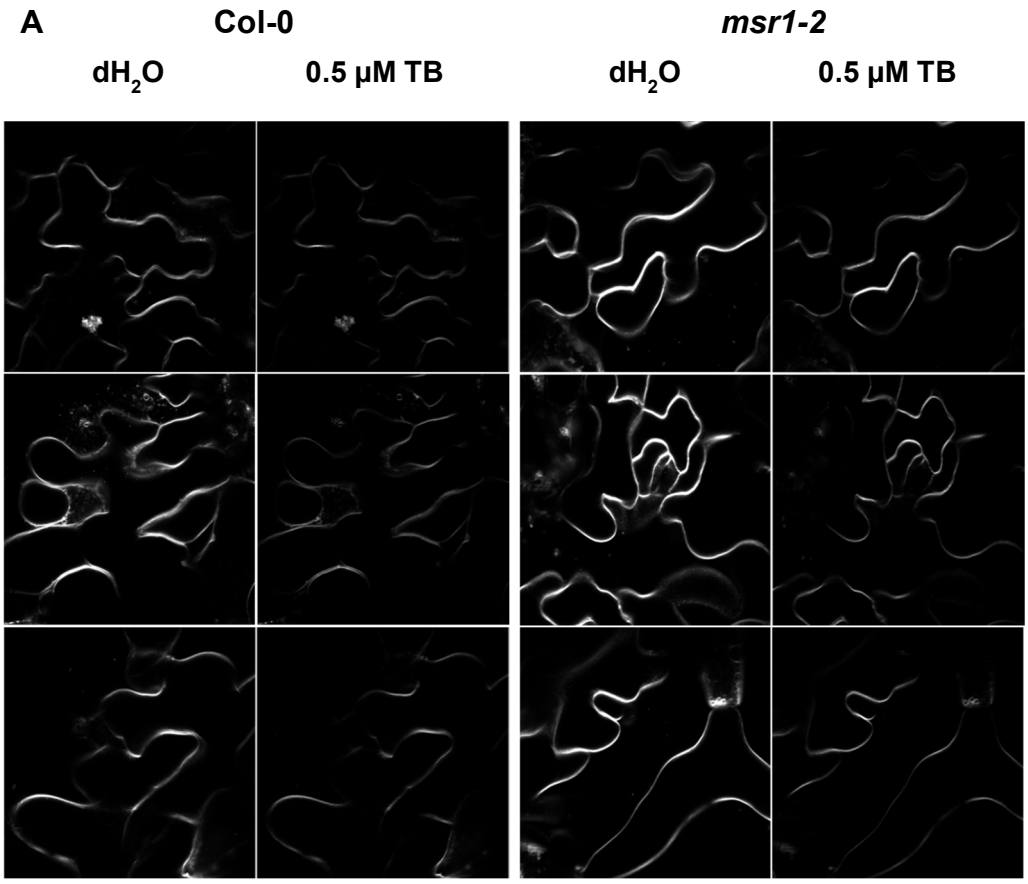

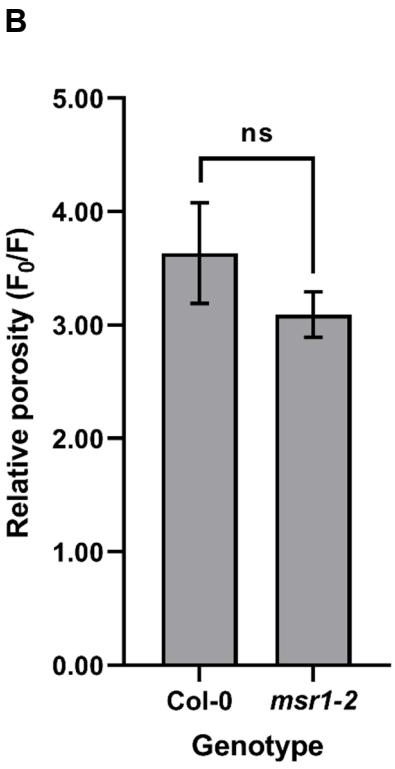

Figure 5.17: Cell-wall porosity of the *msr1-2* mutant. Relative porosity was calculated in wild-type (Col-0) and *msr1-2* plants using fluorescence quenching. **A)** The plasma membranes of leaf epidermal cells were stained with a fluorescent dye and imaged before and after addition of 0.5 µM trypan blue (TB) quenching solution. Three example micrographs per treatment are shown for each genotype. **B)** Fluorescence was quantified before (F_0) and after (F) addition of the quenching solution and a ratio of the two was calculated to give relative porosity (F_0/F). Bars represent mean relative porosity from three biological replicate experiments; each experiment measured porosity in three leaves from separate plants per genotype (n=9). Error bars represent one standard error of the mean. ns indicates means that are not significantly different ($p>0.2$).

Firstly, average force curves were plotted on the same axes for each genotype to allow for comparisons of cell-wall stiffness. Secondly, the percentage relative tensile force values from the peak of force curves from individual samples were plotted to illustrate the cell-wall mechanical strength of tissue from each plant group.

For *xxt1 xxt2*, the gradient of the curve up to the point of failure was 0.270, compared to 0.365 for wild-type, suggesting that the mutant has reduced cell-wall stiffness (**Figure 5.18A**). The cell-wall mechanical strength of *xxt1 xxt2* was also found to be significantly lower than that of wild-type ($p<0.001$). The mean maximum relative tensile force for *xxt1 xxt2* was 4.34% compared to 5.45% for wild-type (**Figure 5.18B**).

For *mur2*, the gradient of the curve up to the point of failure was 0.310, compared to 0.367 for wild-type, suggesting that the mutant has reduced cell-wall stiffness (**Figure 5.19A**). The cell-wall mechanical strength of *mur2* was also found to be significantly lower than that of wild-type ($p<0.0001$). The mean maximum relative tensile force for *mur2* was 4.76% compared to 6.35% for wild-type (**Figure 5.19B**).

For *mur3*, the gradient of the curve up to the point of failure was 0.333, compared to 0.372 for wild-type, suggesting that this mutant also has reduced cell-wall stiffness (**Figure 5.20A**). The cell-wall mechanical strength of *mur3* was also found to be significantly lower than that of wild-type ($p<0.0001$). The mean maximum relative tensile force for *mur3* was 4.72% compared to 6.32% for wild-type (**Figure 5.20B**).

For *msr1-2*, the gradient of the curve up to the point of failure was 0.316, compared to 0.333 for wild-type, suggesting that the mutant may have marginally reduced cell-wall stiffness (**Figure 5.21A**). The cell-wall mechanical strength of *msr1-2* was also found to be significantly lower than that of wild-type ($p<0.01$). The mean maximum relative tensile force for *msr1-2* was 4.51% compared to 5.62% for wild-type (**Figure 5.21B**). These results support the idea of hemicellulose abundance and structure contributing to cell-wall load-bearing capacity.

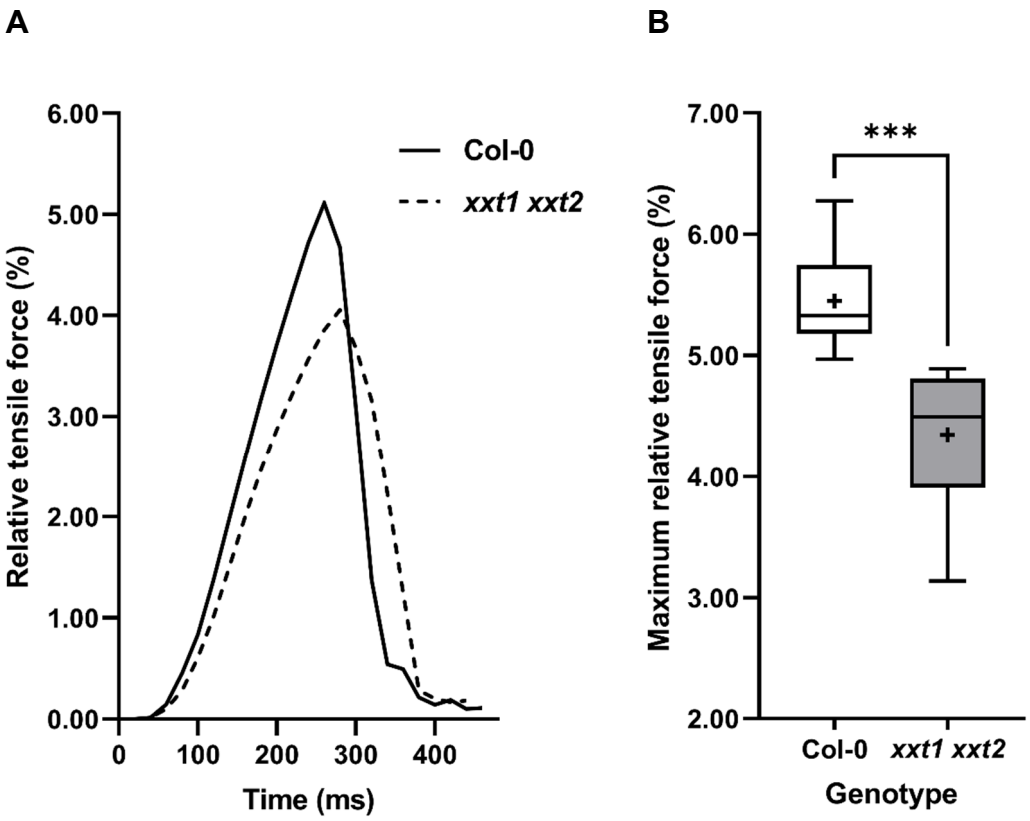

Figure 5.18: Cell-wall mechanical properties of the *xxt1 xxt2* mutant. Mechanical properties were assessed in mature wild-type (Col-0) and *xxt1 xxt2* plants using extensometry. Leaf discs from each genotype were stretched until breakage and the force required to do so was recorded. Tensile force was normalised to the baseline force reading taken immediately before the stretch was initiated and converted to a percentage for each sample. Plots represent combined data for three biological replicate experiments; each experiment measured cell-wall mechanical properties in three leaf discs per genotype (n=9). **A)** Relative tensile force plotted over time for the duration of each stretch. A steeper gradient is indicative of stiffer material and a higher peak (more resistance to breaking pressure) is indicative of stronger material. **B)** Box-and-whisker plot showing the distribution of maximum tensile force values for each genotype. Values were taken from the absolute peak of each force curve, which represents the maximum tensile force that the tissue can withstand before breakage. Whiskers: maximum and minimum values; box edges: upper and lower quartiles; plus signs: mean values; horizontal lines: median values. Asterisks indicate means that are significantly different (*** $p<0.001$).

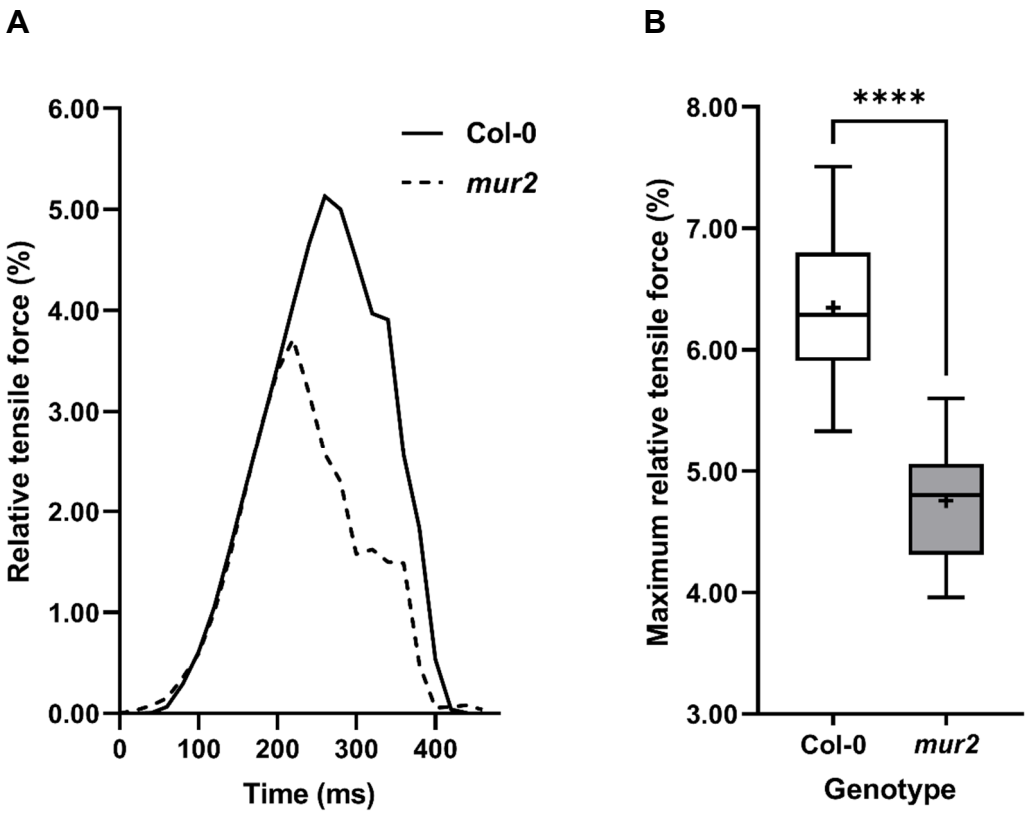

Figure 5.19: Cell-wall mechanical properties of the *mur2* mutant. Mechanical properties were assessed in mature wild-type (Col-0) and *mur2* plants using extensometry. Leaf discs from each genotype were stretched until breakage and the force required to do so was recorded. Tensile force was normalised to the baseline force reading taken immediately before the stretch was initiated and converted to a percentage for each sample. Plots represent combined data for three biological replicate experiments; each experiment measured cell-wall mechanical properties in three leaf discs per genotype (n=9). **A)** Relative tensile force plotted over time for the duration of each stretch. A steeper gradient is indicative of stiffer material and a higher peak (more resistance to breaking pressure) is indicative of stronger material. **B)** Box-and-whisker plot showing the distribution of maximum tensile force values for each genotype. Values were taken from the absolute peak of each force curve, which represents the maximum tensile force that the tissue can withstand before breakage. Whiskers: maximum and minimum values; box edges: upper and lower quartiles; plus signs: mean values; horizontal lines: median values. Asterisks indicate means that are significantly different (**** $p<0.0001$).

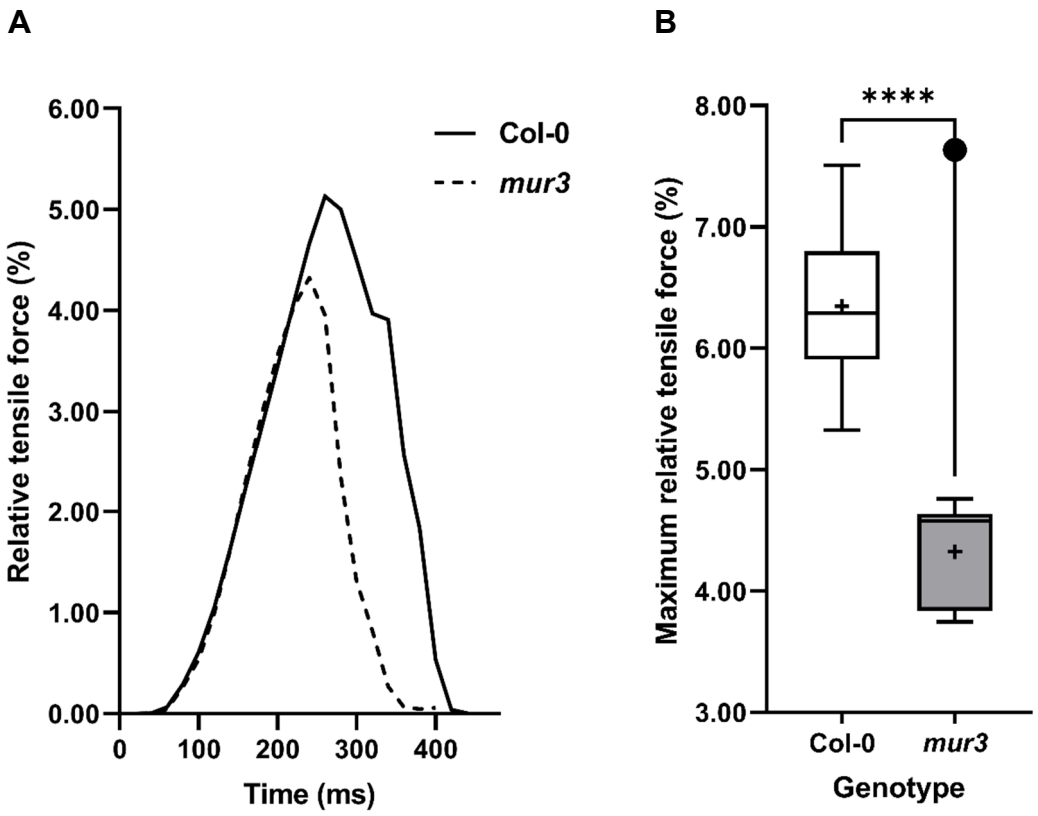

Figure 5.20: Cell-wall mechanical properties of the *mur3* mutant. Mechanical properties were assessed in mature wild-type (Col-0) and *mur3* plants using extensometry. Leaf discs from each genotype were stretched until breakage and the force required to do so was recorded. Tensile force was normalised to the baseline force reading taken immediately before the stretch was initiated and converted to a percentage for each sample. Plots represent combined data for three biological replicate experiments; each experiment measured cell-wall mechanical properties in three leaf discs per genotype (n=9). **A)** Relative tensile force plotted over time for the duration of each stretch. A steeper gradient is indicative of stiffer material and a higher peak (more resistance to breaking pressure) is indicative of stronger material. **B)** Box-and-whisker plot showing the distribution of maximum tensile force values for each genotype. Values were taken from the absolute peak of each force curve, which represents the maximum tensile force that the tissue can withstand before breakage. Whiskers: maximum and minimum values; box edges: upper and lower quartiles; plus signs: mean values; horizontal lines: median values; solid circle: single outlying value identified by ROUT analysis. Asterisks indicate means that are significantly different (**** $p<0.0001$).

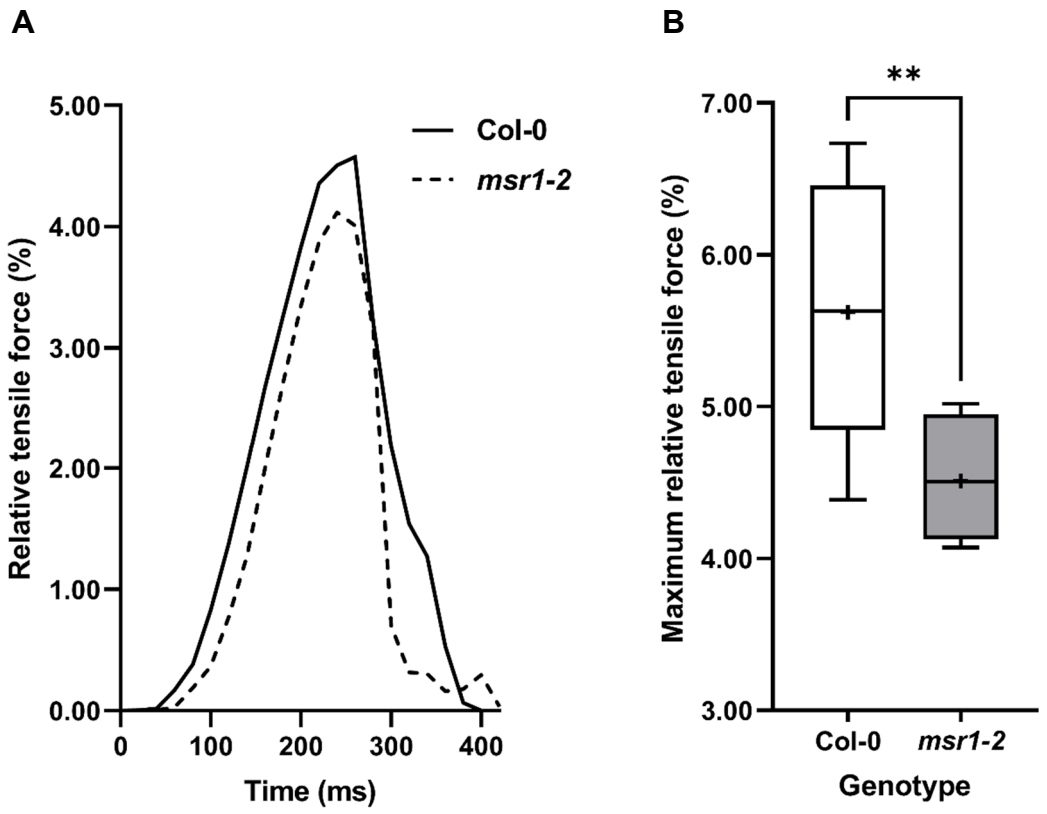

Figure 5.21: Cell-wall mechanical properties of the *msr1-2* mutant. Mechanical properties were assessed in mature wild-type (Col-0) and *msr1-2* plants using extensometry. Leaf discs from each genotype were stretched until breakage and the force required to do so was recorded. Tensile force was normalised to the baseline force reading taken immediately before the stretch was initiated and converted to a percentage for each sample. Plots represent combined data for three biological replicate experiments; each experiment measured cell-wall mechanical properties in three leaf discs per genotype (n=9). **A)** Relative tensile force plotted over time for the duration of each stretch. A steeper gradient is indicative of stiffer material and a higher peak (more resistance to breaking pressure) is indicative of stronger material. **B)** Box-and-whisker plot showing the distribution of maximum tensile force values for each genotype. Values were taken from the absolute peak of each force curve, which represents the maximum tensile force that the tissue can withstand before breakage. Whiskers: maximum and minimum values; box edges: upper and lower quartiles; plus signs: mean values; horizontal lines: median values. Asterisks indicate means that are significantly different (** $p<0.01$).

5.2.3 Other cell-wall components

A transgenic *Arabidopsis* line and two T-DNA mutants, all with defective cell-wall phenotypes, were screened for freezing sensitivity to reveal other aspects of the cell wall that may contribute to freezing tolerance. The transgenic line, $PGX2^{AT}$, overexpresses a PG enzyme that degrades cell-wall pectin. As a result, the plants have drastically reduced pectin molecular masses, as well as other interesting morphological characteristics. The first mutant, *pmr5*, has altered cell-wall pectin and reduced cellulose content, as well as an enhanced susceptibility to a fungal pathogen. The second mutant, *rwa2*, has reduced *O*-acetylation of its cell-wall pectins and hemicelluloses, as well as increased surface permeability of its leaves. Freezing assays were carried out on each of these, with wild-type and *sfr8* plants acting as negative and positive controls, respectively. Unfortunately, their cell-wall physical properties could not be analysed due to germination issues; this would have doubtless been a fruitful line of enquiry given the interesting cell-wall phenotypes involved. Plants were subjected to freezing at -3°C for 24 h before being returned to ambient growth conditions. The capacity of the plants to recover and exhibit new growth was assessed after 1 week. In order to quantify the damage incurred by plants during freezing, electrolyte leakage was measured in leaf tissue from plants of each genotype following exposure to three sub-zero temperatures (-3, -5 and -7°C). Results for each of the groups will be described separately.

For $PGX2^{AT}$ recovery assays (**Figure 5.22A**), a linear mixed effects model confirmed that experiment number had no significant impact on data variation ($p>0.05$) so the data from three biological replicate experiments were pooled for analysis. Mean percentage survival of plants of each genotype was calculated from pooled data. Genotype had a significant effect on plant survival ($p<0.001$). Compared to wild-type, which had a mean survival rate of 100%, both $PGX2^{AT}$ and *sfr8* had significantly lower mean survival rates of 33% and 13%, respectively (**Figure 5.22B**). For electrolyte leakage assays, a linear mixed effects model confirmed that experiment number had no significant impact on data variation ($p>0.2$) so the data from three biological replicate experiments were pooled for analysis. Mean percentage electrolyte leakage of plants of each genotype was

calculated at each temperature from pooled data (**Figure 5.22C**). At all three temperatures, genotype had a significant impact on electrolyte leakage (-3°C: $p<0.005$; -5°C: $p<0.05$; -7°C: $p<0.001$). At -3 and -7°C, both *PGX2*^{AT} and *sfr8* had significantly higher electrolyte leakage than that of wild-type plants. At -5°C, *PGX2*^{AT} had higher electrolyte leakage than wild-type controls but the difference was not significant. These results suggest that the presence of partially degraded pectin in the cell wall hinders a plant's freezing tolerance.

For *pmr5* recovery assays (**Figure 5.23A**), a linear mixed effects model confirmed that experiment number had no significant impact on data variation ($p>0.1$) so the data from three biological replicate experiments were pooled for analysis. Mean percentage survival of plants of each genotype was calculated from pooled data. Genotype had a significant effect on plant survival ($p<0.001$). Compared to wild-type, which had a mean survival rate of 100%, both *pmr5* and *sfr8* had significantly lower mean survival rates of 67% and 20%, respectively (**Figure 5.23B**). For electrolyte leakage assays, a linear mixed effects model confirmed that experiment number had no significant impact on data variation ($p>0.3$) so the data from three biological replicate experiments were pooled for analysis. Mean percentage electrolyte leakage of plants of each genotype was calculated at each temperature from pooled data (**Figure 5.23C**). At all three temperatures, genotype had a significant impact on electrolyte leakage ($p<0.001$ for each temperature). However, *pmr5* only had significantly higher electrolyte leakage than wild-type at -3°C; at the other two temperatures, there was no significant difference between the two, whereas *sfr8* had significantly higher electrolyte leakage than both. These results suggest that a reduction in cell-wall cellulose, paired with changes to pectin structure, can result in a slight decrease in plant freezing tolerance.

For *rwa2* recovery assays (**Figure 5.24A**), a linear mixed effects model confirmed that experiment number had no significant impact on data variation ($p>0.1$) so the data from three biological replicate experiments were pooled for analysis. Mean percentage survival of plants of each genotype was calculated from pooled data. Genotype had a significant effect on plant survival ($p<0.001$). Compared to wild-type, which had a mean survival rate of 100%, both *rwa2* and *sfr8* had significantly

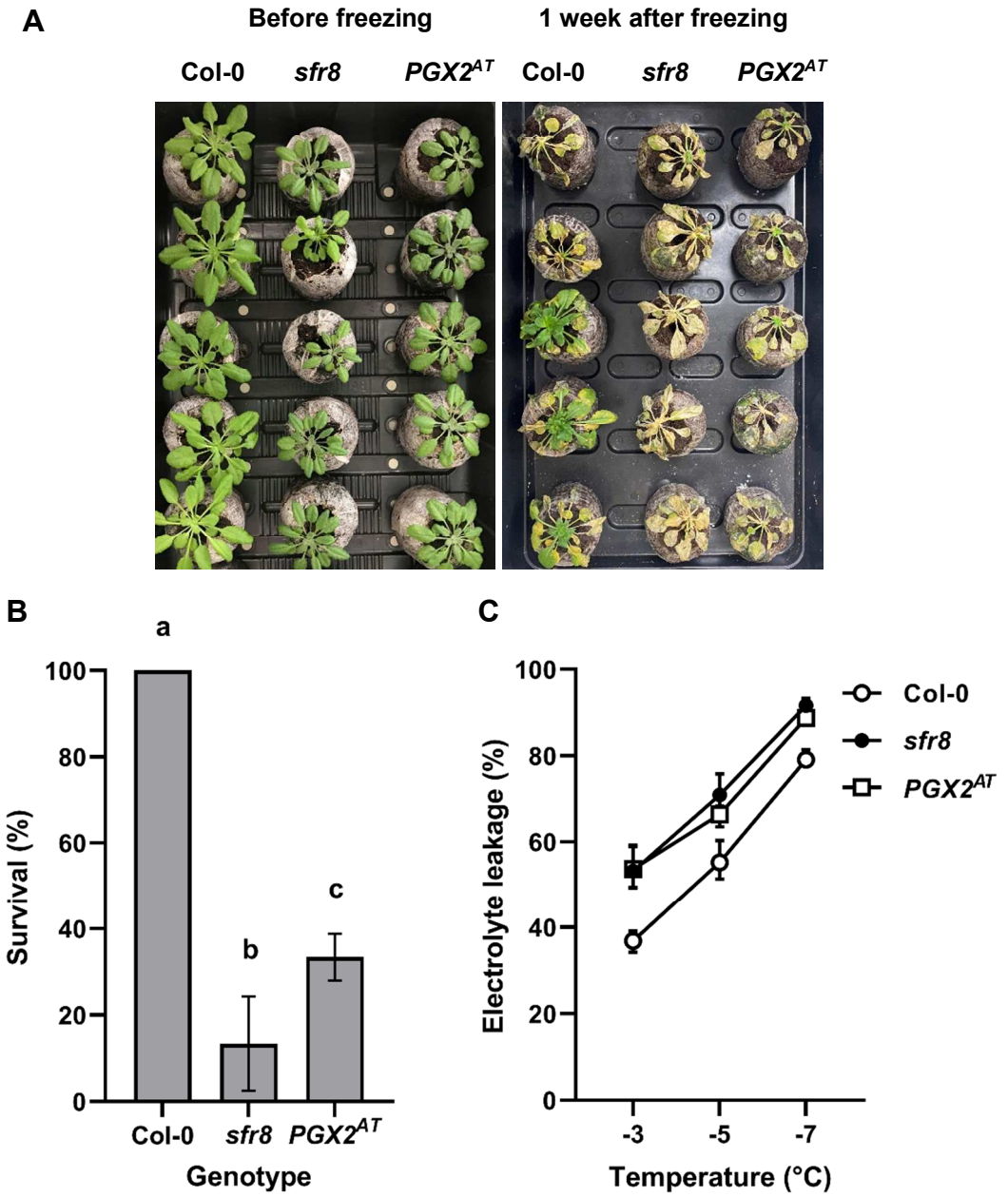

Figure 5.22: Freezing tolerance of *PGX2*-overexpressing plants. A) Freezing recovery assay of mature wild-type (Col-0), *sfr8* and *PGX2*-overexpressing ($PGX2^{AT}$) plants. Plants were subjected to freezing at -3°C for 24 h and recovered for one week. Photographed is one representative assay showing plants immediately before (left) and one week after (right) freezing. **B)** Survival analysis of plants from freezing recovery assays. Plants were scored on survival based on whether regrowth had occurred. Bars represent mean percentage survival of plants from three biological replicate experiments; five plants per genotype were used per experiment (n=15). Error bars represent one standard error of the mean of arcsine-transformed data. Means that do not share a letter are significantly different. **C)** Electrolyte leakage of mature leaf tissue from wild-type (Col-0), *sfr8* and $PGX2^{AT}$. Tissue was subjected to freezing at -3, -5 or -7°C and electrolyte leakage measured. Points represent mean percentage electrolyte leakage from three biological replicate experiments; each experiment used tissue from six plants per genotype per temperature (n=18 at each point). Error bars represent one standard error of the mean of arcsine-transformed data.

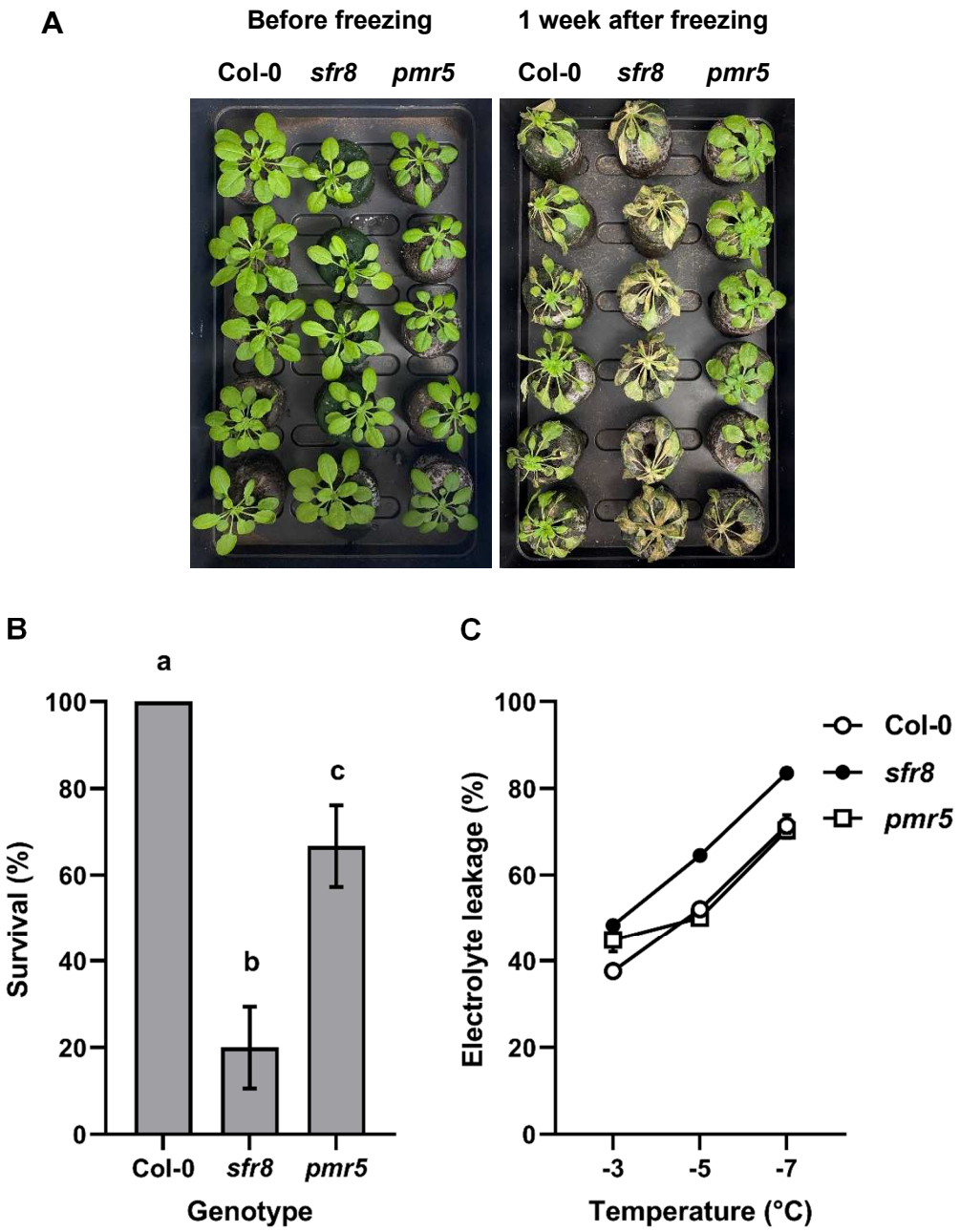

Figure 5.23: Freezing tolerance of the *pmr5* mutant. A) Freezing recovery assay of mature wild-type (Col-0), *sfr8*, and *pmr5* plants. Plants were subjected to freezing at -3°C for 24 h and recovered for one week. Photographed is one representative assay showing plants immediately before (left) and one week after (right) freezing. **B)** Survival analysis of plants from freezing recovery assays. Plants were scored on survival based on whether regrowth had occurred. Bars represent mean percentage survival of plants from three biological replicate experiments; five plants per genotype were used per experiment (n=15). Error bars represent one standard error of the mean of arcsine-transformed data. Means that do not share a letter are significantly different. **C)** Electrolyte leakage of mature leaf tissue from wild-type (Col-0), *sfr8,* and *pmr5.* Tissue was subjected to freezing at -3, -5 or -7°C and electrolyte leakage measured. Points represent mean percentage electrolyte leakage from three biological replicate experiments; each experiment used tissue from six plants per genotype per temperature (n=18 at each point). Error bars represent one standard error of the mean of arcsine-transformed data.

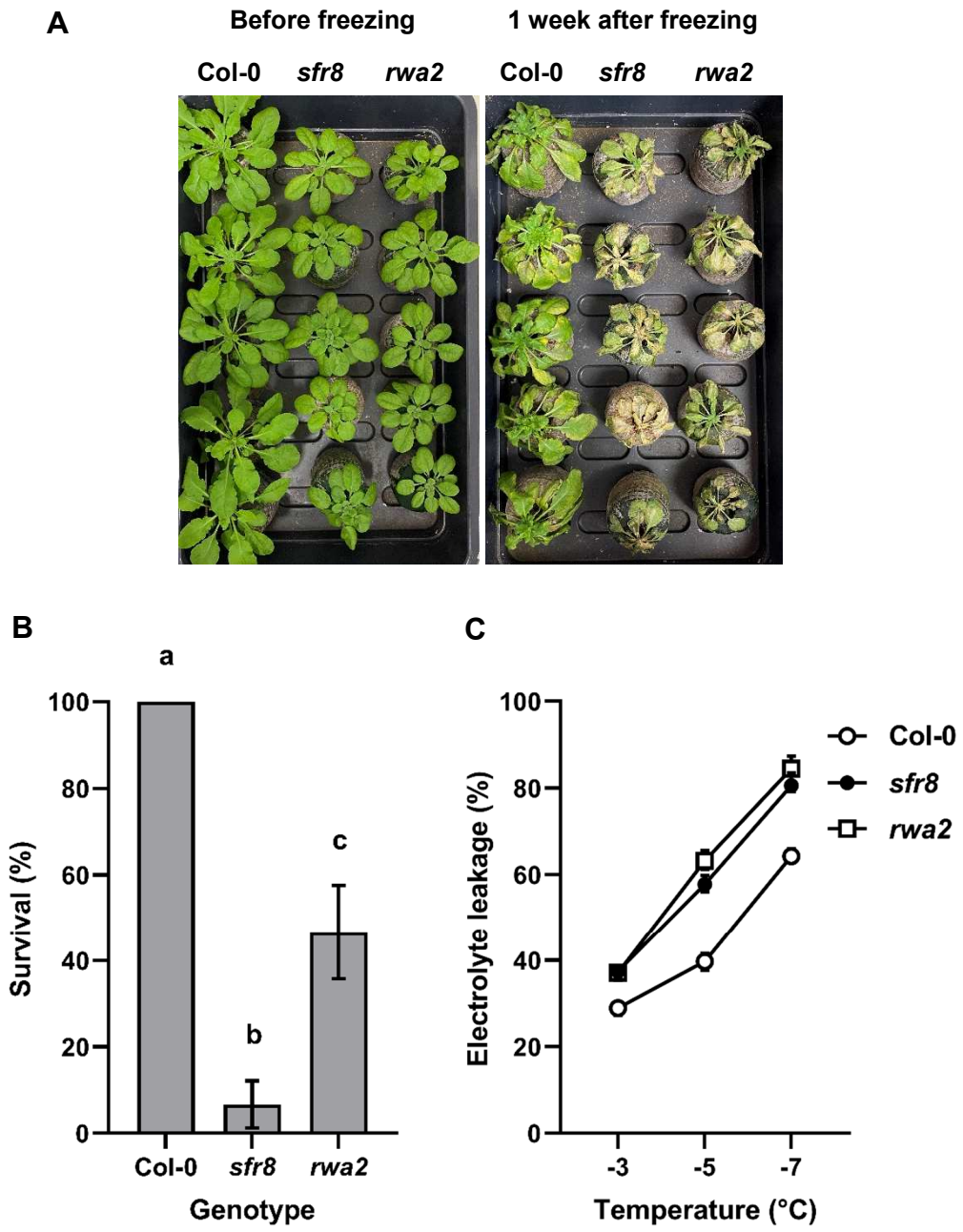

Figure 5.24: Freezing tolerance of the *rwa2* mutant. A) Freezing recovery assay of mature wild-type (Col-0), *sfr8*, and *rwa2* plants. Plants were subjected to freezing at -3°C for 24 h and recovered for one week. Photographed is one representative assay showing plants immediately before (left) and one week after (right) freezing. **B)** Survival analysis of plants from freezing recovery assays. Plants were scored on survival based on whether regrowth had occurred. Bars represent mean percentage survival of plants from three biological replicate experiments; five plants per genotype were used per experiment (n=15). Error bars represent one standard error of the mean of arcsine-transformed data. Means that do not share a letter are significantly different. **C)** Electrolyte leakage of mature leaf tissue from wild-type (Col-0), *sfr8,* and *rwa2.* Tissue was subjected to freezing at -3, -5 or -7°C and electrolyte leakage measured. Points represent mean percentage electrolyte leakage from three biological replicate experiments; each experiment used tissue from six plants per genotype per temperature (n=18 at each point). Error bars represent one standard error of the mean of arcsine-transformed data.

lower mean survival rates of 47% and 5%, respectively (**Figure 5.24B**). For electrolyte leakage assays, a linear mixed effects model confirmed that experiment number had no significant impact on data variation ($p>0.2$) so the data from three biological replicate experiments were pooled for analysis. Mean percentage electrolyte leakage of plants of each genotype was calculated at each temperature from pooled data (**Figure 5.24C**). At all three temperatures, genotype had a significant impact on electrolyte leakage ($p<0.001$ for each temperature). At all three temperatures, both *rwa2* and *sfr8* had significantly higher electrolyte leakage than that of wild-type.

5.3 Discussion

The results in this chapter provide further evidence for the multifaceted contribution that the plant cell wall makes to freezing tolerance as multiple, seemingly unrelated cell-wall defects were able to cause increased sensitivity to freezing. Two plants with genetically-altered cellulose phenotypes, and one with a chemically-altered cellulose phenotype, were all shown to have reduced freezing tolerance. Chen *et al.* (2016) demonstrated that phosphorylation of S211 of CESA3 is critical to proper CESA3 function, and an alanine substitution at S211 (as in $cesa3^{S211A}$) results in a less active protein. Given that much of the data in **Chapters 3 & 4** established a correlation between increased freezing sensitivity, increased cell-wall porosity and/or compromised cell-wall mechanical properties, it was somewhat surprising to find that $cesa3^{S211A}$ not only had unaffected mechanical properties, but even had reduced cell-wall porosity. The organisation and density of the cellulose microfibrils are the primary determinants of the mechanical properties and load-bearing capacity of plant cell walls (Probine & Preston 1961, Whitney *et al.* 1999). Given that $cesa3^{S211A}$ has significantly reduced cell-wall cellulose content and thinner cellulose microfibrils (Chen *et al.* 2016), the lack of mechanical impairment was especially surprising. On the other hand, Liu *et al.* (2019b) reported that, while $cesa3^{S211A}$ had cell-wall thickness comparable to wild-type, atomic force microscopy (AFM) imaging suggested that its cell wall is more dense, with a more extensive network of thinner cellulose microfibrils. The authors also used a similar fluorescence quenching assay to demonstrate that $cesa3^{S211A}$ has

a peculiar porosity phenotype: with trypan blue (TB), quenching efficiency was found to be reduced (indicative of reduced cell-wall porosity), which is in agreement with the present study. A similar result was found when a quencher with an even larger molecular mass, Black Hole Quencher 3 (BHQ3), was applied. However, when a quencher with a comparatively smaller molecular mass, malachite green (MG), was used, there was an increase in quenching efficiency compared to wild-type, indicative of increased cell-wall porosity. Chen *et al.* (2016) also noted the possible appearance of more cross-links between the microfibrils. Therefore, the following is a possibility: the small (but significant) reduction in cell-wall cellulose content in *cesa3*^{S211A} is not enough to impair its mechanical properties, and it may be compensated by a more dense, cross-linked cell wall. This increase in density and cross-linking may have restricted access of the relatively large quenchers, TB and BHQ3, to the plasma membrane, but not the smaller MG. Indeed, Liu *et al.* (2019b) speculated that a larger number of smaller pores facilitated the movement of MG through the cell wall to the plasma membrane. This may also explain the increased freezing sensitivity of *cesa3*^{S211A}, with ice crystals able to propagate more efficiently through its cell wall which, despite the results of the porosity assay in the present study, may be more porous to smaller molecules.

Freezing sensitivity and porosity were increased in both *prc1* mutants and ISX-treated plants. Whereas *prc1* had a subtle impairment of its cell-wall mechanical properties, ISX-treated plants had substantially reduced mechanical stiffness and strength. Fagard *et al.* (2000) reported that *prc1*, which has a mutation in *CESA6*, has a major cellulose deficiency, giving rise to incomplete, "gapped" cell walls. ISX inhibits the incorporation of glucose into the cellulose-rich fraction of cell walls and is classified as a specific inhibitor of cellulose biosynthesis (Heim *et al.* 1990, Corio-Costet *et al.* 1991). Liu *et al.* (2019b) described the cell walls of ISX-treated *Arabidopsis* seedlings as having a lower density of cellulose with larger spaces between microfibrils. Accordingly, they also reported an enormous increase in cell-wall porosity for ISX-treated seedlings with all three quenching agents, in line with the results of the present study. This suggests that a significant genetically- or chemically-induced reduction in cellulose content gives rise to a more porous, weaker cell wall, which can negatively impact freezing tolerance.

In the hemicellulose mutants, the present study was unable to establish a consistent correlation between freezing tolerance, cell-wall porosity and mechanical properties. All four mutants appeared to have compromised mechanical stiffness and strength, consistent with previous work which suggests that, after the cellulose microfibrils themselves, the cellulose-hemicellulose network is the major determinant of cell-wall load-bearing capacity (McCann *et al.* 1990, Levy *et al.* 1997, Nishiyama 2009). However, only *xxt1 xxt2* and *mur3* were found to have reduced freezing tolerance; Panter *et al.* (2019) also demonstrated that the freezing tolerance of *mur2* mutants is unaffected. Furthermore, *xxt1 xxt2*, *mur2* and *mur3* actually had reduced cell-wall porosity, whereas the freezing tolerance and cell-wall porosity of *msr1-2* was unaffected. As with $cesa3^{S211A}$, these results may be explained by examining the specific effects that each of the mutations have on the abundance and organisation of other cell-wall polymers.

It should first be noted that *xxt1 xxt2* has already been shown to have both decreased cell-wall porosity (Liu *et al.* 2019b) and impaired cell-wall mechanical properties (Cavalier *et al.* 2008), so the data presented here are supported by existing studies. The cell wall of *xxt1 xxt2* completely lacks xyloglucan, a major hemicellulose (Cavalier *et al.* 2008). It has repeatedly been suggested that the cellulose-xyloglucan network is a major load-bearing component of the cell wall with xyloglucan forming hydrogen bonds with cellulose microfibrils, either to cross-link adjacent microfibrils, facilitating the formation of an extensive, three-dimensional, load-bearing framework, or to coat them, acting as spacers to prevent them associating with adjacent microfibrils and helping to form crystalline structures (Fry & Miller 1989, Hayashi 1989, McCann & Roberts 1991, Passioura & Fry 1992, Carpita & Gibeaut 1993, Veytsman & Cosgrove 1998, Cosgrove 2000, 2001, 2005, 2015, Somerville *et al.* 2004). Either way, it is unsurprising that cell walls lacking detectable xyloglucan show significant mechanical weakness. Indeed, Cavalier *et al.* (2008) also used *xxt1* and *xxt2* single knock-outs to reveal the existence of a threshold of xyloglucan content required for normal mechanical functioning. Liu *et al.* (2019b) noted that the cell wall of *xxt1 xxt2* had a denser appearance than that of wild-type, and reported a decreased quenching efficiency with TB (in agreement with the present study) and BHQ3 but an increased

efficiency (albeit non-significant) with MG. These results are comparable to those of *cesa3*^{S211A} and may also reflect the presence of a larger number of smaller cell-wall pores which would, presumably, facilitate ice propagation.

Both *mur2* and *mur3* have also been shown to have defective cell-wall mechanical properties, though *mur3* cell walls are thought to be more impaired than those of *mur2* (Vanzin *et al.* 2002, Ryden *et al.* 2003, Peña *et al.* 2004). This would suggest that galactosylation of xyloglucan side-chains is more important in maintaining mechanical integrity than fucosylation, though both make important contributions. This pattern was not reflected in the present study, as both *mur2* and *mur3* appeared to have equally large reductions in cell-wall stiffness and strength, unlike previous studies which found more modest reductions in *mur2*. However, in the present study, the two mutants were not assessed in the same assay so direct comparisons are not appropriate. In the case of *mur2*, the existence of mechanisms to compensate for a lack of xyloglucan fucosylation have been proposed to explain the more subtle changes in its mechanical properties; for instance, changes in the conformation of the xyloglucan residues or modifications to their acetylation patterns (Ryden *et al.* 2003). It is likely that the true mechanical properties of *mur2* are less severely impaired than is suggested by the data in the present study, perhaps as a result of the relatively low sample size, or the differences in tissue type and developmental stage between this study and others. This could also explain the absence of any apparent freezing sensitivity in this mutant. Peña *et al.* (2004) demonstrated that the loss of galactose residues in *mur3* causes its xyloglucan to become less accessible to xyloglucan endotransglucosylases/hydrolases (XTHs), which normally function to remodel xyloglucans during growth and promote cell-wall stiffening (Nishitani & Tominaga 1992, Cosgrove 2022). Mutants that lack expression of a particular *XTH* gene, *XTH21*, are freezing-sensitive, whereas overexpression of *XTH21* results in increased freezing tolerance in *Arabidopsis* (Shi *et al.* 2014). Furthermore, knock-out of *XTH19*, which encodes a cold-inducible XTH, causes a reduction in freezing tolerance after cold acclimation (Takahashi *et al.* 2021a). The severe impairment of freezing tolerance and cell-wall mechanics in *mur3*, therefore, may be attributable to a reduction in XTH activity and subsequent absence of normal xyloglucan remodelling during growth. The apparent decrease in

porosity in *mur2* and *mur3* may be due to the fact that their cell walls are more abundant in cellulose, pectin and xyloglucan, giving rise to a "swollen" phenotype in hypocotyls which may be indicative of a denser cell wall (Peña *et al.* 2004).

Although widespread throughout land plants, mannans make up a relatively small proportion of polysaccharides present in the cell wall (Bacic *et al.* 1988). The mannan family of polysaccharides includes glucomannan and galactomannan, in which the mannosyl backbones are interspersed with glucose residues or anchor galactose side-chains, respectively (Matheson 1990, Melton *et al.* 2009). Mannan polysaccharides are thought to contribute to the structural rigidity of the cell wall by cross-linking adjacent cellulose microfibrils (Whitney *et al.* 1998). The 40% reduction in cell-wall mannan content in *msr1-2* could lead to its cellulose microfibrils being less tightly cross-linked, causing the observed decrease in mechanical stiffness and strength. This decrease, however, clearly was not large enough to cause any measurable difference in the freezing tolerance of *msr1-2*, and it is unknown whether any compensatory mechanisms exist for its depleted cell-wall mannan content.

PGX2^{AT}, *pmr5* and *rwa2* were all shown to have decreased freezing tolerance compared to wild-type controls. It remains to be seen if this sensitivity to freezing is correlated with any impairment in cell-wall porosity or mechanics; these parameters were not able to be measured in the present study due to difficulties with seed germination (there were no germination issues with the freezing assays as these were carried out together at an earlier point). However, given the results with other cell-wall mutants, the existence of such a correlation seems likely. *PGX2*^{AT} overexpresses a PG enzyme and, as a result, its pectin has a significantly lower average molecular mass than pectin from wild-type controls, indicating that it has been partially or fully digested (Xiao *et al.* 2016). Given the central role pectin plays in determining cell-wall porosity and mechanical properties (see **Sections 1.3.2.1 & 1.3.2.2**), it is not unreasonable to speculate that *PGX2*^{AT} may be compromised in one or both of these. In fact, Xiao *et al.* (2016) reported that the stems of *PGX2*^{AT} plants displayed a lodging phenotype, indicative of some degree of mechanical failure. However, the authors used extensometry to determine

that *PGX2*^{AT} stems actually have increased mechanical stiffness and attributed the lodging phenotype to the fact that they are thinner. On the other hand, they also concluded that *PGX2* overexpression promotes lignin polymerisation which is known to provide tissues with mechanical support (Frei 2013). This, rather than degradation of the pectin network, may be the reason for the apparent increase in mechanical stiffness. A modest reduction in freezing tolerance was also detected in *pmr5*, which has a dramatically altered pectin monosaccharide composition as well as a 23% reduction in cellulose content in 5-week old rosette leaves (Chiniquy *et al.* 2019). Further study of this mutant is required to ascertain whether its freezing sensitivity is due to these changes in its cell wall. As *rwa2* has reduced pectin acetylation, which should be conducive to increased pectin cross-linking (Harholt *et al.* 2010), it was initially thought that *rwa2* may have improved freezing tolerance due to the changes to its cell-wall physical properties this would presumably confer. However, the opposite proved to be true: *rwa2* exhibited a clear freezing-sensitive phenotype. Nafisi *et al.* (2015) reported that leaves of *rwa2* have increased surface permeability and attributed this to an impaired cuticle layer. The physiological properties of the cuticle layer are largely defined by the presence and composition of cuticular waxes within the cuticular matrix (Kunst & Samuels 2003). Due to their propensity to repel water droplets and prevent surface penetration, it has been suggested that cuticular waxes may act as a barrier to ice formation by preventing its propagation into subtending tissues (Jenks & Ashworth 1999, Workmaster *et al.* 1999, Wisniewski *et al.* 2002a,b, Griffith *et al.* 2005, Verslues *et al.* 2006). Despite Nafisi *et al.* (2015) noting that cuticle wax composition was largely unchanged in *rwa2*, the appearance of a more "diffused" cuticle layer leading to increased leaf surface permeability is still the most plausible explanation for the reduced freezing tolerance observed in this mutant.

5.4 Summary

In this chapter, plants with various aberrant cellulose, hemicellulose and pectin phenotypes were screened for freezing sensitivity and defective cell-wall physical properties. Although some degree of freezing sensitivity was confirmed in almost every one, the effects on cell-wall porosity and mechanical properties were varied

and not straightforward. Contrary to the correlations observed in *pme41*, *sfr8*, *ext18*, and cold-acclimated wild-type, increased porosity was not typically associated with increased freezing sensitivity, though this may reflect a shortcoming of the methodology rather than the absence of a true correlation. Interestingly, mechanical defects were more pronounced in hemicellulose mutants than cellulose mutants, although chemical inhibition of cellulose synthesis resulted in plants with severely impaired mechanical properties. These results open up new avenues in which to explore cell-wall mediated freezing tolerance, including the structure of the cellulose-hemicellulose framework, cell-wall density, and leaf permeability.

Chapter 6

Discussion & Conclusions

There is already a considerable body of evidence supporting a role for the plant cell wall in cold acclimation. Cold treatment has been shown to induce changes in the structure, composition or abundance of pectins, hemicelluloses, extensins (EXTs) and cell-wall modifying enzymes (Weiser *et al.* 1990, Wisniewski & Davis 1995, Kubacka-Zębalska & Kacperska 1999, Kozbial *et al.* 2002, Thonar *et al.* 2006, Solecka *et al.* 2008, Qu *et al.* 2011, Carvalho *et al.* 2013, Domon *et al.* 2013, Baldwin *et al.* 2014, Tenhaken 2015, Zhao *et al.* 2016, Lee *et al.* 2017, Chen *et al.* 2018, Willick *et al.* 2018, Takahashi *et al.* 2019, Takahashi *et al.* 2021a, Liu *et al.* 2022), as well as changes to the mass, thickness, stiffness, strength or porosity of the cell wall (Huner *et al.* 1981, Griffith & Brown 1982, Griffith *et al.* 1985, Wisniewski *et al.* 1987, Tanino *et al.* 1990, Weiser *et al.* 1990, Rajashekar & Lafta 1996, Kubacka-Zębalska & Kacperska 1999, Stefanowska *et al.* 1999, Solecka *et al.* 2008, Scholz *et al.* 2012, Carvalho *et al.* 2013, Domon *et al.* 2013, Tanino *et al.* 2013, Arias *et al.* 2015, Takahashi *et al.* 2019, Liu *et al.* 2022). Additionally, a number of cell-wall modifications or defects have been associated with altered freezing tolerance, including changes to pectin structure, porosity, or mechanical properties (Chen *et al.* 1977, Anderson *et al.* 1983, Sakai & Larcher 1987, Larcher *et al.* 1991, Wisniewski *et al.* 1991, Wisniewski & Davis 1995, Rajashekar & Burke 1996, Rajashekar & Lafta 1996, Solecka *et al.* 2008, Kuprian *et al.* 2017, Chen *et al.* 2018, Panter 2018, Panter *et al.* 2019, Takahashi *et al.* 2019, Steiner *et al.* 2020, Bertel *et al.* 2022, Liu *et al.* 2022, Stegner *et al.* 2022). These experiments are supported by an abundance of theoretical and *in vitro* models suggesting that the cell wall is an intrinsic barrier to ice nucleation and propagation, facilitating

supercooling through reduced porosity, and protecting against freezing-induced cellular dehydration and collapse by providing mechanical reinforcement (Mazur 1963, Olien 1974, Homshaw 1980, Ashworth & Abeles 1984, Rajashekar & Burke 1986, Hansen & Beck 1988, Pearce 1988, Zhu *et al.* 1989, Zhu & Beck 1991, Wisniewski 1995, Rajashekar 1997, Fujikawa *et al.* 1999, Yamada *et al.* 2002, McCully *et al.* 2004, Yang *et al.* 2017). Collectively, the data in this study add to this growing evidence supporting a role for the plant cell wall in cold acclimation and freezing tolerance.

From the large number of studies referenced above, several were key in formulating the hypotheses, and selecting genotypes and treatments to test said hypotheses, in the present investigation. Developing an assay to measure cell-wall porosity was an early priority as porosity has been repeatedly correlated with freezing tolerance in the literature. For instance, deep-supercooling woody perennials have tissues lacking extensive extracellular spaces, instead developing a continuous network of cell walls with relatively small pores (Sakai & Larcher 1987). In suspension-cultured apple and grape cells, cold acclimation was associated with both a significant reduction in cell-wall pore size and, during subsequent freezing, a large reduction in the presence of intracellular ice compared to non-acclimated cells (Rajashekar & Lafta 1996). In flowering dogwood and peach xylem ray parenchyma cells, increased porosity was linked to an impaired supercooling capacity (Wisniewski *et al.* 1991, Wisniewski & Davis 1995), and cold acclimation was associated with both increased freezing tolerance and reduced tissue permeability in Japanese bunching onion (Liu *et al.* 2022).

Several studies made it clear that it would also be useful to have a method of measuring mechanical properties. It has been proposed that increasing the mass and thickness of the cell wall during cold acclimation is a means of increasing its mechanical stiffness, leaving it better able to resist freezing-induced dehydration and less prone to subsequent deformation or collapse (Pearce 1988, Rajashekar & Burke 1996, Fujikawa *et al.* 1999, Yamada *et al.* 2002). A freezing-tolerant potato cultivar has a significantly thicker cell wall than a freezing-sensitive one (Chen *et al.* 1977). Increased cell-wall stiffness was thought to contribute to freezing

tolerance in *Citrus* leaves by resisting dehydration and collapse during freezing (Anderson *et al.* 1983). In suspension-cultured apple and grape cells, cold acclimation was associated with significant increases to resistance to breaking pressure (mechanical strength) due to an accumulation of cell-wall mass (Rajashekar & Lafta 1996). In oilseed rape, cold acclimation resulted in increased freezing tolerance, cell-wall mass and leaf tensile stiffness (Solecka *et al.* 2008). In *Arabidopsis*, both cold acclimation and sub-zero acclimation were associated with increased freezing tolerance and an increase in cell-wall mass, which was interpreted as an enhancement to cell-wall mechanical properties to resist deformation during extracellular ice formation (Takahashi *et al.* 2019).

The genotypes and treatments used to test the relationship between freezing tolerance and cell-wall physical properties were then selected on the basis of either having known alterations to freezing tolerance, porosity or mechanical properties, or being defective in a cell-wall component that is considered to be important in controlling one or more of those properties. For instance, porosity is thought to be heavily dependent on pectin structure, particularly the extent of homogalacturonan (HG) or rhamnogalacturonan-II (RG-II) cross-linking (Baron-Epel *et al.* 1988, Ehwald *et al.* 1991, 1992, Fleischer *et al.* 1999, Liu *et al.* 2022). Although pectin can also contribute to the mechanical properties of the cell wall, cellulose microfibrils, and their interactions with hemicelluloses, are considered to be the primary determinants of its load-bearing capacity (Probine & Preston 1961, Reiter *et al.* 1993, Whitney *et al.* 1999, Ryden *et al.* 2003, Peña et al. 2004, Cavalier *et al.* 2008, Nishiyama 2009, Hongo *et al.* 2012). Some of the mutant genes studied, such as *PME31*, *PME41*, *MSR1*, *GGLT1*, *CESA3*, *CESA6*, *XXT1*, *MUR3* and *PMR5*, show evidence of upregulation in response to cold according to the AtRTD2 dashboard, which can be used to visualise gene and transcript expression profiles of RNA-seq data from *Arabidopsis* (Calixto *et al.* 2018). Each of the genotypes and treatments, therefore, had sound justification for their inclusion in the study: they each had either confirmed alterations to their freezing tolerance, porosity or mechanics, or suspected alterations based on their specific cell-wall defects as supported by the literature, and could therefore help address specific hypotheses about the relationship between plant freezing tolerance and the cell wall. It was

also important to select a diverse range of cell-wall genotypes and treatments, such as those with aberrant cellulose, hemicellulose, pectin or EXT phenotypes, so that any changes to freezing tolerance could be more easily attributable to compromised physical properties and not the specific defective component. Furthermore, the results of certain experiments directed the selection of other mutants and the design of further experiments. For instance, the results of the comprehensive microarray polymer profiling (CoMPP) screen were an early indicator of the possible importance of pectin cross-linking in cold acclimation and freezing tolerance. More notably, the collective *sfr8* data provided even stronger evidence for the role of pectin cross-linking: restoration of RG-II dimerisation coinciding with increased freezing tolerance, reduced cell-wall porosity, and improved mechanical properties. Paired with the existing literature discussed above, this suggests that it is highly likely that RG-II cross-linking is central to controlling all three properties. Together, the data provided the impetus to further explore the degree to which pectin cross-linking, and indeed the physical properties which they influence, contributes to basal or acquired freezing tolerance.

6.1 Linking Cold Acclimation to the Plant Cell Wall

In this study, a cold acclimation protocol that significantly increased freezing tolerance in wild-type *Arabidopsis*, the genetic model plant, also brought about several physical, structural and compositional changes to its cell wall. The cell-wall porosity of cold-acclimated leaf tissue was found to be significantly lower than that of non-acclimated control tissue. Similarly, cold-acclimated leaf tissue was found to have both significantly increased mechanical stiffness and strength compared to non-acclimated tissue, thus it was concluded that cold acclimation enhances the mechanical properties of the cell wall. A cell-wall profiling assay revealed several cell-wall polysaccharides and proteins that changed in abundance during cold acclimation, and thus were thought to be of potential importance to freezing tolerance. Most notably, cold acclimation was shown to increase the abundance of cell-wall EXTs, rhamnogalacturonan-I (RG-I), heteroxylan, and arabinogalactan proteins (AGPs). Cold-acclimated tissue was also shown to have a higher proportion of the demethylesterified form of HG, which is thought to be more

conducive to calcium cross-linking and, hence, reducing porosity (Willats *et al.* 2001a). As EXTs and pectin cross-linking have already been implicated in freezing tolerance and maintaining the physical properties of the cell wall (see above), these findings were of particular interest and led to the assessment of their respective mutants. EXTs are structural glycoproteins that form a scaffold essential for the formation of the plant cell wall (Cannon *et al.* 2008, Lamport *et al.* 2011, Velasquez *et al.* 2011, Marzol *et al.* 2018). It is thought that tyrosine residues on adjacent EXTs form cross-links that strengthen the cell wall and provide a barrier to pathogen ingress (Esquerré-Tugayé *et al.* 1979, Showalter *et al.* 1985, Schnabelrauch *et al.* 1996, Merkouropoulos *et al.* 1999, Castilleux *et al.* 2021). In this study, a mutant lacking expression of an integral member of the *EXT* gene family, *EXT18*, was found to have significantly reduced freezing tolerance, while its cell wall was found to be significantly porous and mechanically impaired. The freezing tolerance of a mutant of another *EXT18* allele was also found to be reduced (see **Appendix Q**). This data was relegated to the appendices as there was insufficient time to complete the full dataset with freezing recovery data. However, its significance should not be understated: both sets of electrolyte leakage data confirm that it is knock-out of *EXT18* expression, and its knock-on effects on the expression of other *EXT* genes (Choudhary *et al.* 2015), that causes increased sensitivity to freezing (this would also likely be reflected in recovery assays, as every mutation or treatment that caused increased electrolyte leakage in this study also caused reduced survival after freezing). Similarly, a pectin methylesterase (PME; an enzyme responsible for removing methyl-ester groups from HG backbones to facilitate calcium cross-linking) knock-out mutant, *pme41*, was also found to have significantly reduced freezing tolerance and increased cell-wall porosity, though the mechanical properties of its cell wall showed only modest impairment. *PME41* is induced by chilling stress at 0°C and the mutant has been shown to be chilling-sensitive (Qu *et al.* 2011). The fact that these mutants were shown to be freezing-sensitive supports the idea that plants accumulate EXTs and demethylesterified HG in their cell walls to enhance their freezing tolerance, possibly by decreasing its porosity and improving its mechanical capacity. The second point is itself supported by the finding that cold-acclimated tissue was found

to be less porous and mechanically stiffer and stronger. Taken together, these data provide compelling evidence for the cell wall undergoing substantial modification to its structure, composition and physical properties during cold acclimation, enabling it to offer a greater degree of protection to the cell from freezing stress.

6.2 Linking Freezing Tolerance to the Plant Cell Wall

In total, 16 defective cell walls were screened for an association with freezing sensitivity in the form of mutants, transgenic lines, and chemically treated wild-type plants (this does not include cold-acclimated plants or boron-supplemented *sfr8*). Of these 16 phenotypes, 11 were associated with a statistically significant reduction in freezing tolerance, and 3 were associated with a slight, non-significant reduction in freezing tolerance (**Table 6.1**). None of the cell-wall impairments resulted in significantly improved freezing tolerance. In isolation, this is yet more evidence for the cell wall playing a crucial role in plant freezing tolerance, as numerous defects in a variety of largely unrelated cell-wall components were able to cause increased sensitivity to freezing. These included reduced cellulose content or altered microfibril structure, an absence of xyloglucan or altered xyloglucan side-chain composition, increased pectin degradation, reduced PME activity, decreased dimerisation of RG-II, and reduced EXT content. Out of the 11 plant groups that had significantly reduced freezing tolerance, 8 had their cell-wall physical properties assessed. Five of these 8 groups had significantly increased cell-wall porosity, while 3 had significantly decreased cell-wall porosity. Out of the 5 groups that did not have significantly reduced freezing tolerance, 1 had significantly increased porosity, 1 had significantly decreased porosity, and 3 had porosity not significantly different to that of controls. On its face, this would suggest that changes in cell-wall porosity alone are not strongly correlated with changes in freezing tolerance. However, it probably reflects a specific limitation in the methodology rather than the absence of a true correlation. Liu *et al.* (2019b) demonstrated that a potential larger number of smaller cell-wall pores (representative of a cell wall that is, overall, more porous to small molecules) cannot be detected with the quenching agent used in the present study.

Table 6.1: Semi-quantitative summary of the changes to freezing tolerance and cell-wall physical properties measured in each genotype or treated plant throughout the study. "Plant" refers to the complete selection of mutants, transgenics, cold- and chemically-treated plants used throughout the study. CA: cold-acclimated; B+: boron-supplemented; ISX: isoxaben treatment. The next three columns indicate whether differences in their freezing tolerance, porosity, and mechanical properties were measured relative to their respective controls. ns indicates no statistically significant difference and measurements were virtually indistinguishable from controls. ↑/↓ ns indicates a slight but statistically insignificant difference. For freezing tolerance, one arrow was given for each temperature there was a significant difference in electrolyte leakage, plus another for a significant difference in survival after freezing. For porosity, one arrow: $p<0.05$; two arrows: $p<0.01$; three arrows: $p<0.001$. For mechanical properties, one arrow was given for a noticeable difference in stiffness, and additional arrows were given for increasing statistical significance in measurements of strength ($p<0.05$, $p<0.01$, $p<0.001$). ? indicates measurements were not carried out.

Plant	Freezing tolerance	Porosity	Mechanical properties
Col-0 (CA)	↑↑↑↑	↓	↑↑↑↑
pme17	ns	ns	↓↓↓
pme31	↓ ns	ns	ns
pme41	↓↓	↑	↓
ext18	↓↓↓↓	↑	↓↓
sfr8	↓↓↓↓	↑↑	↓↓↓↓
sfr8 (B+)	↑↑↑↑	↓	↑↑
Col-0 (B+)	ns	ns	ns
hp*GGLT1*	↓ ns	↑↑	ns
$cesa3^{S211A}$	↓↓↓	↓↓	ns
prc1	↓↓↓	↑	↓
Col-0 (ISX)	↓↓↓	↑↑↑	↓↓↓↓
xxt1 xxt2	↓↓↓	↓	↓↓↓↓
mur2	ns	↓↓	↓↓↓↓
mur3	↓↓↓↓	↓	↓↓↓↓
msr1-2	ns	↓ ns	↓↓
$PGX2^{AT}$	↓↓↓	?	?
pmr5	↓↓	?	?
rwa2	↓↓↓↓	?	?

The data may only show that some cell walls are less permeable to the relatively large quenching agent trypan blue (TB), but not necessarily less permeable to molecules smaller than this (ice crystals, for example). This was perhaps the case with *cesa3*^{S211A} and *xxt1 xxt2*, which were freezing-sensitive but had an apparent reduction in cell-wall porosity. Indeed, Liu *et al.* (2019b) demonstrated that cell-wall porosity was significantly increased in *cesa3*^{S211A}, and non-significantly increased in *xxt1 xxt2*, when a smaller quenching agent was used. Although their respective mutations produce considerably different effects on their cell walls, both cell walls were described as having a similar "denser" appearance. The presence of a correlation between properties should also not be ruled out on the basis that there can be an apparent increase in porosity but no concomitant change in freezing tolerance, as there was with hp*GGLT1*. There may be a threshold in porosity that must be surpassed before any measurable changes in freezing tolerance are observed and, in the case of hp*GGLT1*, porosity may be highly sensitive to changes in RG-II cross-linking (which, according to Sechet *et al.* (2018), is slightly reduced in these plants), but freezing tolerance may not. In other words, the reduction in RG-II cross-linking may be sufficient to alter wall porosity but insufficient to impair freezing tolerance. Finally, two other lines of evidence support the proposed correlation between freezing tolerance and cell-wall porosity. First is the finding that cold acclimation significantly increases freezing tolerance while significantly decreasing cell-wall porosity. Second, and perhaps more importantly, is the finding that the freezing sensitivity and impaired porosity of *sfr8* are both partially rescued with the same boron-supplementation protocol. Both represent treatments that improve freezing tolerance while reducing cell-wall porosity.

For measurements of mechanical stiffness, it was difficult to determine which, if any, are significantly different, as no statistical analysis was carried out on force curve gradient values (this was because gradient values were taken from average force curves after the data from individual samples had been combined; to allow for statistical analysis, gradient values should have been taken from force curves from individual samples). Therefore, some subjective judgement was required. If a genotype or treatment was associated with a clear reduction in mechanical stiffness or strength, but not both, it was still considered to have significantly impaired

mechanical properties. Out of the same 8 groups that had reduced freezing tolerance, 5 had significantly impaired mechanical properties, 2 had modest impairments, and 1 had mechanical properties comparable its control. Out of the 5 groups that did not have significantly reduced freezing tolerance, 3 had significantly impaired mechanical properties, 1 had modest impairments, and 1 had properties comparable to its control. This is indicative of a somewhat precarious correlation between freezing tolerance and cell-wall mechanical properties but, as with porosity, some of the deviations may be explained on an individual basis. For instance, existing evidence in the literature indicates that *mur2* is not as drastically compromised in its cell-wall strength as the data here would suggest, perhaps as a result of the small sample size, differences in tissue selection and developmental stage, or growth conditions (Vanzin *et al.* 2002, Ryden *et al.* 2003, Peña *et al.* 2004). This could explain the absence of any reduced freezing tolerance in this mutant. For *cesa3*^{S211A}, the lack of mechanical impairment (despite reduced cell-wall cellulose and thinner cellulose microfibrils) may be due to a cell wall that is more dense overall, with a more extensive network of thinner microfibrils (Chen *et al.* 2016, Liu *et al.* 2019b). In other cases, as with porosity, a threshold of mechanical impairment may need to be surpassed before it produces a measurable change in freezing tolerance. Again, as with porosity, cold-acclimated wild-type plants and boron-supplemented *sfr8* had increased or restored freezing tolerance, respectively, that was correlated with improved or restored mechanical properties, respectively, further strengthening the correlation. Despite almost certainly being linked, changes in cell-wall porosity may not always be associated with changes in mechanical properties (as was the case in several mutants), and plants may only need to be significantly impaired in one or the other to exhibit sensitivity to freezing. The literature discussed above suggests that reducing porosity is important for supercooling and reducing the initial spread of ice, whereas mechanical integrity is important for resisting significant dehydration and cell collapse in the presence of extracellular ice. In theory, a porous cell wall may allow for the nucleation and propagation of such quantities of extracellular ice that even a mechanically strong cell wall cannot tolerate; equally, a mechanically weak cell

wall may not be able to cope with even small quantities of ice that has been limited by a wall with relatively low porosity.

6.3 Experimental Limitations & Future Prospects

As discussed in **Sections 3.3**, **4.3 & 5.3**, there are numerous improvements to experimental design and supplementary experiments that are recommended, along with new avenues of enquiry to pursue. An obvious place to begin would be completing the experiments in **Section 5.2.3** by measuring the cell-wall physical properties of *PGX2*^{AT}, *pmr5* and *rwa2*. Each of these exhibited a degree of freezing sensitivity, presumably because of their respective cell-wall defects, so assessment of cell-wall porosity and mechanics could strengthen the proposed correlation between them and freezing tolerance. It is not known which out of the full list of mutants, if any, only have reduced basal freezing tolerance and which lack the ability to fully cold-acclimate (or both). It may be worth the endeavour of repeating the experiments in each mutant after cold acclimation, as has been done for *sfr8, ext18* and *msr1-2*, as it is likely that some mutants only exhibit reduced freezing tolerance after cold acclimation. This may be especially warranted for *pme* mutants, as some *PME* genes are specifically induced by cold treatment (Qu *et al.* 2011), and the present study demonstrated that cold acclimation was associated with an increase in demethylesterified pectin.

There was a promising start to the infrared video thermography (IRVT) experiments which hinted at some interesting patterns in freezing behaviour in *sfr8* and cold-acclimated plants. More data is needed, with more replicate experiments and more biological replicates per experiment. If different patterns in freezing behaviour were to still be observed after this (for instance, differences in freezing points or supercooling temperatures), it would be worth expanding the experiments to include some of the other cell-wall mutants with compromised freezing tolerance and, of course, boron-supplemented *sfr8*. This could provide data supporting the idea that modifications to the cell wall alter a plant's capacity to supercool, and may help to resolve some of the inconsistencies in correlations between the three properties of interest.

The fluorescence-quenching assay proved to be a useful tool for measuring porosity in most of the cell walls that were analysed. However, in cases where there were complex alterations to cell-wall structure (e.g. the *cesa3*^{S211A} and *xxt1 xxt2* mutants), the use of TB as a lone quenching agent was insufficient to accurately quantify cell-wall porosity. Liu *et al.* (2019b) showed that use of multiple quenching agents of varying molecular weights could provide a more complete picture of wall porosity in these cases: they showed that the cell walls of *cesa3*^{S211A} and *xxt1 xxt2* were more permeable to a smaller quencher, malachite green (MG), but less permeable to the larger TB, possibly because of a denser wall with a larger number of smaller pores. The present study should have also made use of MG in each of the experiments to overcome this limitation. Of course, supplementing these data with an inherently different method of measuring cell-wall porosity would be ideal. Other methods that have been applied successfully include determining the size-exclusion limit of solutes from the cell wall by observing plasmolysis or cytorrhysis (Carpita *et al.* 1979), transmission electron microscopy (Cohen & Voyle 1987), fluorescence redistribution after photobleaching (FRAP; Baron-Epel *et al.* 1988), size-exclusion chromatography (SEC; Woehlecke & Ehwald 1995, Titel *et al.* 1997, Fleischer *et al.* 1999), cryo-electron microscopy (Derken *et al.* 2011), and gas adsorption assays (Adani *et al.* 2011). Though these techniques involve either harsh sample preparation, potentially introducing artefacts, or have low resolving power, they would still be worth pursuing if it meant measuring the same changes in porosity using multiple established methods.

Although plotting average force curves allowed for rough measurements of cell-wall mechanical stiffness by comparison of curve gradients, it lacked sufficient resolving power in cases where gradients were not overly different between genotypes or treatments (e.g. Col-0 and *cesa3*^{S211A}, which had average gradients of 0.317 and 0.299, respectively). It would have been more useful to plot individual force curves for each sample, allowing for statistical comparisons of average gradients between genotypes or treatments, in the same way that comparisons of mechanical strength were made by plotting individual peak values. It is also possible to calibrate the load cell with known weights to carry out direct measurements of absolute force with meaningful units. This would eliminate the need for data normalisation and

calculation of a crude percentage increase in force in arbitrary units, and allow for direct comparison of different mutants or treatments between experiments. The extensometer is also compatible with confocal microscopes, opening up the possibility to carry out measurements of mechanical properties with cellular resolution, allowing for live visualisation of cell-wall deformations upon application of tensile forces (Robinson *et al.* 2017).

CoMPP elucidated numerous components of the cell wall that change in abundance during cold acclimation and was therefore a productive means of identifying specific cell-wall polysaccharides and proteins that potentially contribute to increased freezing tolerance. A logical next step would be to apply the assay to each of the defective cell walls that made up the present study, both before and after cold acclimation. This would not only be helpful in confirming suspected cell-wall phenotypes (e.g. directly measuring the proportions of methyl- and de-methylesterified pectins in *pme* mutants), but also determining the presence of any unsuspected knock-on effects or compensatory mechanisms (e.g. knock-out of *EXT18* causing reduced expression of ten other *EXT* genes (Choudhary *et al.* 2015) or, in the case of *mur2* and *mur3*, truncation of xyloglucan side-chains causing alterations to cellulose and pectin content (Peña *et al.* 2004)). Antibodies that can detect monomerised and dimerised forms of RG-II could be a useful addition to the assay, but no such antibodies currently exist. As it is thought that RG-II and HG (along with RG-I) can be covalently linked to form a complex pectic layer (Caffall & Mohnen 2009), it would be interesting to find out changes in the degree of cross-linking in one pectic domain affects the degree of cross-linking in another. This would help to determine if the changes in, for instance, the porosity of *sfr8* are entirely due to differences in RG-II cross-linking or pectin cross-linking in general.

The collective data provide compelling evidence for the reduction in RG-II dimerisation in *sfr8* being reversible by boron treatment, but this was not able to be confirmed by polyacrylamide gel electrophoresis (PAGE) analysis. As discussed in **Section 4.3**, this was probably due to the unstable mutant dimer being unable to undergo the extraction process while remaining structurally intact. It would be useful, therefore, to establish an alternative method of precisely quantifying RG-II

dimerisation to remove all doubt. SEC has been successfully used to measure RG-II dimerisation in *mur1* and hp*GGLT1*, both of which are believed to also have the less stable form of the dimer (O'Neill *et al.* 2001, Sechet *et al.* 2018). Alternatively, the emergence of direct stochastic optical reconstruction microscopy (dSTORM) provides an exciting opportunity to image plant cell-wall polysaccharides *in vivo* with nanometre precision and intact molecular ultrastructure (Haas *et al.* 2020, Peaucelle *et al.* 2020). Not only could this enable comparisons of wild-type and *sfr8* RG-II structure and *in vivo* determination of the degree of dimerisation, but imaging of other cell-wall structures of interest in the other mutants; for example, the EXT network in the *ext18* mutant, the HG network in the *pme* mutants, or the cellulose-hemicellulose framework in any of the cellulose or xyloglucan mutants. The role of RG-II cross-linking in freezing tolerance could be solidified further through assessment of other plants that are deficient in RG-II dimerisation but not due to a lack of fucose causing a truncated side-chain A. Through research into human gut bacteria, enzymes that degrade specific bonds in RG-II have been characterised (Ndeh *et al.* 2017). Finding reduced freezing tolerance in *Arabidopsis* expressing these enzymes would be the ideal evidence to supplement the data from *sfr8* and *mur1*. It would also be interesting to see if total RG-II content, or RG-II dimerisation, increases with cold acclimation. This could be achieved using any of the methods described above, or through analysis of the expression of RG-II-specific biosynthesis genes such as the *RGXTs* (Egelund *et al.* 2006).

IRVT has also been used to show that *sfr8* has increased stomatal conductance, in line with the results of leaf water-loss assays and measurements of guard cell morphology (Panter 2018). Both this and the measurements of guard cell morphology could be repeated on boron-supplemented plants to determine if the defects are due to reduced RG-II dimerisation. The analysis of stomatal conductance via IRVT could also be repeated with ABA- and MES-treated plants to see if *sfr8* stomata still exhibit the same impaired responsiveness in live plants that was observed in epidermal peels in the present study. The results of these experiments could help fully determine if the water-loss phenotype of *sfr8* is caused by a lack of RG-II cross-linking which causes stomata to be unresponsive, perhaps

because of some mechanical impairment in the guard cell walls. Finally, the hp*GGLT1* leaf water-loss assays should be repeated with Col-0 and *sfr8* controls for full confirmation that no water-loss phenotype exists in these plants.

There are a plethora of other mutants and transgenic *Arabidopsis* lines that were not included in the present study but are still worthy of investigation. These include plants overexpressing an extensin gene, *EXT1,* which have reduced susceptibility to pathogen invasiveness (Wei & Shirsat 2006); overexpressors and knock-outs of other *PMEs* and *PMEIs* (Peaucelle *et al.* 2008, Guénin *et al.* 2011, Peaucelle *et al.* 2011, Hongo *et al.* 2012, Huang *et al.* 2017, Lionetti *et al.* 2017); mutants of *RGXT* genes, which encode xylosyltransferases involved in RG-II synthesis (Egelund *et al.* 2006); *pmr6*, a pathogen-susceptible cell-wall mutant with altered cellulose and pectin compositions (Chiniquy *et al.* 2019); *arad1*, which is deficient in pectic arabinose content (Harholt *et al.* 2006); *esk1*, which has increased basal freezing tolerance (Xin & Browse 1998, Xin *et al.* 2007); *kor1*, which has a severe cellulose-deficient phenotype (Zuo *et al.* 2000, Lei *et al.* 2014); and *bor* mutants, which lack boron transporter proteins and have been shown to have reduced RG-II dimerisation and freezing tolerance (Panter *et al.* 2019). As isoxaben (ISX) proved to be a useful tool for studying the effect of cellulose synthesis on freezing tolerance, other chemical treatments could be employed to the same end to complement plants with genetically altered cell walls. Plants treated with an inhibitor of fucosylation, peracetylated 2-fluoro-2-deoxy-L-fucose, have been shown to have both reduced RG-II dimerisation and freezing tolerance (Dumont *et al.* 2015, Panter 2018). Inhibitors of xyloglucan biosynthesis have also been developed (Chormova *et al.* 2015). Applying the same systematic assessments of freezing tolerance and cell-wall dynamics to plants receiving these treatments could prove to be a productive line of enquiry.

It should be acknowledged that all of the data presented here are only representative of *Arabidopsis* plants of a particular developmental stage. The degree of injury incurred by a plant undergoing cold or freezing stress can vary depending on its developmental stage (Li *et al.* 1981, Ye *et al.* 2009, da Cruz *et al.* 2013, Zhao *et al.* 2022). The cell wall also undergoes significant structural and

compositional remodelling as the plant progresses through its stages of development (Albersheim *et al.* 2010). Therefore, these experiments should ideally be repeated for various developmental stages to get a more complete picture of the relationship between the cell wall and freezing tolerance or cold acclimation.

6.4 Concluding Remarks

Although it was important to synthesise a large body of evidence in the plant genetic model, *Arabidopsis*, systematic studies in other species are still lacking, and have only been carried out sporadically using varied methodology. This does not allow for easy, direct comparisons between species. It will be pertinent, therefore, to establish the same links in important crop plants, which can have appreciably different cell-wall compositions. This must be achieved by carrying out similar studies that are systematic and thorough in their approach and utilise consistent methods of measuring freezing tolerance and the physical properties of the cell wall. However, cell-wall mutants are not as readily available in crop plants as they are in *Arabidopsis*, so it will be important to develop more pharmacological approaches to manipulate the cell wall.

In a changing climate, the severity of frost-induced crop losses will become more pronounced as spring and autumn frosts become harsher and more frequent. Understanding the molecular mechanisms underpinning both basal and acquired freezing tolerance is a necessary first step towards the development of more durable crops. The data presented here provide compelling support for the growing consensus of a link between plant freezing tolerance and the structure, composition, and physical properties of the cell wall. To the best of my knowledge, this is the first time that a broad profile of the compositional changes of cell-wall polymers that occur during cold acclimation in a single species has been reported. Their influence over freezing tolerance and the physical properties of the cell wall were found to be significant. Though RG-II has emerged as one of the key components controlling plant freezing tolerance and the full extent of its involvement remains to be seen, other cell-wall polymers and networks appear to make their own important contributions. Thus, the three central aims of this study set out in **Section 1.4** have been achieved.

Bibliography

ABDEL-MOTAGALLY F, EL-ZOHRI M. 2018. Improvement of wheat yield grown under drought stress by boron foliar application at different growth stages. *Journal of the Saudi Society of Agricultural Sciences* 17: 178–185.

ABRÀMOFF MD, MAGALHĀES PJ, RAM SJ. 2004. Image processing with ImageJ. *Biophotonics International* 11: 36–42.

ACHARD P, CHENG H, DE GRAUWE L, DECAT J, SCHOUTTETEN H, MORITZ T, VAN DER STRAETEN D, PENG J, HARBERD NP. 2006. Integration of plant responses to environmentally activated phytohormonal signals. *Science* 331: 91–94.

ACHARD P, GONG F, CHEMINANT S, ALIOUA M, HEDDEN P, GENSCHIK P. 2008. The cold-inducible CBF1 factor-dependent signalling pathway modulates the accumulation of the growth-repressing DELLA proteins via its effect on gibberellin metabolism. *The Plant Cell* 20: 2117–2129.

ACUÑA-RODRÍGUEZ IS, NEWSHAM KK, GUNDEL PE, TORRES-DÍAZ C, MOLINA-MONTENEGRO MA. 2020. Functional roles of microbial symbionts in plant cold tolerance. *Ecology Letters* 23: 1034–1048.

ADANI F, PAPA G, SCHIEVANO A, CARDINALE G, D'IMPORZANO G, TAMBONE F. 2011. Nanoscale structure of the cell wall protecting cellulose from enzyme attack. *Environmental Science & Technology* 45: 1107–1113.

AGARWAL M, HAO Y, KAPOOR A, DONG CH, FUJI H, ZHENG X, ZHU J-K. 2006. A R2R3 type MYB transcription factor is involved in the cold regulation of *CBF* genes and in acquired freezing tolerance. *Journal of Biological Chemistry* 281: 37636–37645.

ALBERSHEIM P, DARVILL AG, O'NEILL MA, SCHOLS HA, VORAGEN AGJ. 1996. An hypothesis: the same six polysaccharides are components of the primary cell walls of all higher plants. IN: VISSER J, VORAGEN AGJ. *Pectins and Pectinases* 47–55. Elsevier Science, Amsterdam.

ALBERSHEIM P, DARVILL AG, ROBERTS K, SEDEROFF R, STAEHELIN A. 2010. *Plant Cell Walls.* Garland Science, New York.

ALLEN RD. 1995. Dissection of oxidative stress tolerance using transgenic plants. *Plant Physiology* 107: 1049.

AMSBURY S, HUNT L, ELHADDAD N, BAILLIE A, LUNDGREN M, VERHERTBRUGGEN Y, SCHELLER HV, KNOX JP, FLEMING AJ, GRAY JE.

2016. Stomatal function requires pectin de-methyl-esterification of the guard cell wall. *Current Biology* 26: 1–8.

ANCHORDOGUY TJ, RUDOLPH AS, CARPENTER JF, CROWE JH. 1987. Modes of interaction of cryoprotectants with membrane phospholipids during freezing. *Cryobiology* 24: 324–331.

ANDERSON JA, GUSTA LV, BUCHANAN DW, BURKE MJ. 1983. Freezing of water in *Citrus* leaves. *Journal of the American Society for Horticultural Science* 108: 397–400.

AQUEA F, FEDERICI F, MOSCOSO C, VEGA A, JULLIAN P, HASELOFF J, ARCE-JOHNSON P. 2012. A molecular framework for the inhibition of *Arabidopsis* root growth in response to boron toxicity. *Plant, Cell & Environment* 35: 719–734.

ARIAS NS, BUCCI SJ, SCHOLZ FG, GOLDSTEIN G. 2015. Freezing avoidance by supercooling in *Olea europaea* cultivars: the role of apoplastic water, solute content and cell wall rigidity. *Plant, Cell & Environment* 38: 2061–2070.

ARIOLI T, PENG L, BETZNER AS, BURN J, WITTKE W, HERTH W, CAMILLERI C, HÖFTE H, PLAZINSKI J, BIRCH R, CORK A, GLOVER J, REDMOND J, WILLIAMSON RE. 1998. Molecular analysis of cellulose biosynthesis in *Arabidopsis. Science* 279: 717–720.

ASAHINA E. 1956. The freezing process of the plant cell. *Contribution from the Institute of Low Temperature Science Hokkaido University* 10: 83–126.

ASHWORTH EN, ABELES FB. 1984. Freezing behaviour of water in small pores and the possible role in the freezing of plant tissues. *Plant Physiology* 76: 201–204.

ASHWORTH EN, DAVIS GA. 1986. Ice formation in woody plants under field conditions. *HortScience* 21: 1233–1234.

ATMODJO MA, HAO Z, MOHNEN D. 2013. Evolving views of pectin biosynthesis. *Annual Review of Plant Biology* 64: 747–779.

BABA K, SONE Y, MISAKI A, HAYASHI T. 1994. Localization of xyloglucan in the macromolecular complex composed of xyloglucan and cellulose in pea stems. *Plant & Cell Physiology* 35: 439–444.

BACIC A, HARRIS PJ, STONE BA. 1988. Structure and function of plant cell walls. IN: PREISS J. *The Biochemistry of Plants — A Comprehensive Treatise* 14: 297–371. Academic Press, New York.

BAEK K-H, SKINNER DZ. 2012. Production of reactive oxygen species by freezing stress and the protective roles of antioxidant enzymes in plants. *Journal of Agricultural Chemistry and Environment* 1: 34–40.

BAKER SS, WILHELM SS, THOMASHOW MF. 1994. The 5'-region of *Arabidopsis thaliana* cor15a has cis-acting elements that confer cold-, drought- and ABA-regulated gene expression. *Plant Molecular Biology* 24: 701–713.

BALDWIN L, DOMON J-M, KLIMEK JF, FOURNET F, SELLIER H, GILLET F, PELLOUX J, LEJEUNE-HÉNAUT I, CARPITA NC, RAYON C. 2014. Structural alteration of cell wall pectins accompanies pea development in response to cold. *Phytochemistry* 104: 37–47.

BARLOW K, CHRISTY B, O'LEARY G, RIFFKIN P, NUTTALL J. 2015. Simulating the impact of extreme heat and frost events on wheat crop production: a review. *Field Crops Research* 171: 109–119.

BARON-EPEL O, GHARYAL PK, SCHINDLER M. 1988. Pectins as mediators of wall porosity in soybean cells. *Planta* 175: 389–395.

BECK EH, FETTIG S, KNAKE C, HARTIG K, BHATTARAI T. 2007. Specific and unspecific responses of plants to cold and drought stress. *Journal of Biosciences* 32: 501–510.

BERTEL C, KAPLENIG D, RALSER M, ARC E, KOLÁŘ F, WOS G, HÜLBER K, HOLZINGER A, KRANNER I, NEUNER G. 2022. Parallel differentiation and plastic adjustment of leaf anatomy in alpine *Arabidopsis arenosa* ecotypes. *Plants* 11: 2626.

BETHKE G, GRUNDMAN RE, SREEKANTA S, TRUMAN W, KATAGIRI F, GLAZEBROOK J. 2014. *Arabidopsis* pectin methylesterases contribute to immunity against *Pseudomonas syringae. Plant Physiology* 164: 1093–1107.

BIDHENDI AJ, GEITMANN A. 2016. Relating the mechanics of the primary plant cell wall to morphogenesis. *Journal of Experimental Botany* 67: 449–461.

BIDHENDI AJ, GEITMANN A. 2019. Methods to quantify primary cell wall mechanics. *Journal of Experimental Botany* 70: 3615–3648.

BLEVINS DG, LUKASZEWSKI KM. 1998. Boron in plant structure and function. *Annual Review of Plant Biology* 49: 481–500.

BOANARES D, FERREIRA BG, KOZOVITS AR, SOUSA AC, ISAIAS RMS, FRANÇA MGC. 2018. Pectin and cellulose cell wall composition enables different strategies to leaf water uptake in plants from tropical fog mountain. *Plant Physiology and Biochemistry* 122: 57–64.

BONIN CP, POTTER I, VANZIN GF, REITER W-D. 1997. The *MUR1* gene of *Arabidopsis thaliana* encodes an isoform of GDP-$_{D}$-mannose-4,6-dehydratase, catalyzing the first step in the *de novo* synthesis of GDP-$_{L}$-fucose. *Proceedings of the National Academy of Sciences* 94: 2085–2090.

BOUTON S, LEBOEUF E, MOUILLE G, LEYDECKER M-T, TALBOTEC J, GRANIER F, LAHAYE M, HÖFTE H, TRUONG HN. 2002. *QUASIMODO1* encodes a putative membrane-bound glycosyltransferase required for normal pectin synthesis and cell adhesion in *Arabidopsis*. *The Plant Cell* 14: 2577–2590.

BRADLEY DJ, KJELLBOM P, LAMB CJ. 1992. Elicitor- and wound-induced oxidative crosslinking of a proline-rich plant cell wall protein: a novel, rapid defense response. *Cell* 70: 21–30.

BRAYBROOK SA, PEAUCELLE A. 2013. Mechano-chemical aspects of organ formation in *Arabidopsis thaliana*: the relationship between auxin and pectin. *PLoS ONE* 8: e57813.

BROWN I, MANSFIELD J, BONAS U. 1995. *hrp* genes in *Xanthomonas campestris* pv vesicatoria determine ability to suppress papilla deposition in pepper mesophyll cells. *Molecular Plant-Microbe Interactions* 8: 825–836.

BROWN MS, PEREIRA ESB, FINKLE BJ. 1974. Freezing of non-woody plant tissues: II. Cell damage and the fine structure of freezing curves. *Plant Physiology* 53: 709–711.

BROWN MS, REUTER FW. 1974. Freezing of non-woody plant tissues: III. Videotape micrography and the correlation between individual cellular freezing events and temperature changes in the surrounding tissue. *Cryobiology* 11: 185–191.

BRUMMELL DA. 2006. Cell wall disassembly in ripening fruit. *Functional Plant Biology* 33: 103–119.

BURKE D, KAUFMAN P, MCNEIL M, ALBERSHEIM P. 1974. The structure of plant cell walls. VI. A survey of the walls of suspension-cultured monocots. *Plant Physiology* 54: 109–115.

BURKE MJ, GUSTA LV, QUAMME HA, WEISER CJ, LI PH. 1976. Freezing and injury in plants. *Annual Review of Plant Physiology* 27: 507–528.

BURN JE, HOCART CH, BIRCH RJ, CORK AC, WILLIAMSON RE. 2002. Functional analysis of the cellulose synthase genes *CesA1*, *CesA2*, and *CesA3* in *Arabidopsis*. *Plant Physiology* 129: 797–807.

CAFFALL KH, MOHNEN D. 2009. The structure, function, and biosynthesis of plant cell wall pectic polysaccharides. *Carbohydrate Research* 344: 1879–1900.

CALIXTO CPG, GUO W, JAMES AB, TZIOUTZIOU NA, ENTIZNE JC, PANTER PE, KNIGHT H, NIMMO HG, ZHANG R, BROWN JWS. 2018. Rapid and dynamic alternative splicing impacts the *Arabidopsis* cold response transcriptome. *The Plant Cell* 30: 1424—1444.

CANNON MC, TERNEUS K, HALL Q, TAN L, WANG Y, WEGENHART BL, CHEN L, LAMPORT DTA, CHEN Y, KIELISZEWSKI MJ. 2008. Self-assembly of the plant cell wall requires an extensin scaffold. *Proceedings of the National Academy of Sciences* 105: 2226–2231.

CARPITA NC, GIBEAUT DM. 1993. Structural models of primary cell walls in flowering plants: consistency of molecular structure with the physical properties of the walls during growth. *The Plant Journal* 3: 1–30.

CARPITA NC, SABULARSE D, MONTEZINOS D, DELMER DP. 1979. Determination of the pore size of cell walls of living plant cells. *Science* 205: 1144–1147.

CARPITA NC, TIERNEY M, CAMPBELL M. 2001. Molecular biology of the plant cell wall: searching for the genes that define structure, architecture, and dynamics. *Plant Molecular Biology* 47: 1–5.

CARROLL A, SPECHT CD. 2011. Understanding plant cellulose synthases through a comprehensive investigation of the cellulose synthase family sequences. *Frontiers in Plant Science* 2: 5.

CARVALHO CP, HAYASHI AH, BRAGA MR, NIEVOLA CC. 2013. Biochemical and anatomical responses related to the *in vitro* survival of the tropical bromeliad *Nidularium minutum* to low temperatures. *Plant Physiology and Biochemistry* 71: 144–154.

CASTILLEUX R, PLANCOT B, ROPITAUX M, CARRERAS A, LEPRINCE J, BOULOGNE I, FOLLET-GUEYE M-L, POPPER ZA, DRIOUICH A, VICRÉ M.

2018. Cell wall extensins in root-microbe interactions and root secretions. *Journal of Experimental Botany* 69: 4235–4247.

CASTILLEUX R, PLANCOT B, VICRÉ M, NGUEMA-ONA E, DRIOUCH A. 2021. Extensin, an underestimated key component of cell wall defence? *Annals of Botany* 127: 709–713.

CATOIRE L, PIERRON M, MORVAN C, HERVÉ DU PENHOAT C, GOLDBERG R. 1998. Investigation of the action patterns of pectin methylesterase isoforms through kinetic analyses and NMR spectroscopy. Implications in cell wall expansion. *Journal of Biological Chemistry* 273: 33150–33156.

CAVALIER DM, LEROUXEL O, NEUMETZLER L, YAMAUCHI K, REINECKE A, FRESHOUR G, ZABOTINA OA, HAHN MG, BURGERT I, PAULY M, RAIKHEL NV, KEEGSTRA K. 2008. Disrupting two *Arabidopsis thaliana* xylosyltransferase genes results in plants deficient in xyloglucan, a major primary cell wall component. *The Plant Cell* 20: 1519–1537.

CHAMBERLAIN CJ, WOLKOVICH EM. 2021. Late spring freezes coupled with warming winters alter temperate tree phenology and growth. *New Phytologist* 231: 987–995.

CHAMBERS R, HALE HP. 1932. The formation of ice in protoplasm. *Proceedings of the Royal Society* B110: 337–352.

CHEBLI Y, KANEDA M, ZERZOUR R, GEITMANN A. 2012. The cell wall of the *Arabidopsis* pollen tube—spatial distribution, recycling, and network formation of polysaccharides. *Plant Physiology* 160: 1940–1955.

CHEN J, CHEN X, ZHANG Q, ZHANG Y, OU X, AN L, FENG H, ZHAO Z. 2018. A cold-induced pectin methyl-esterase inhibitor gene contributes negatively to freezing tolerance but positively to salt tolerance in *Arabidopsis*. *Journal of Plant Physiology* 222: 67–78.

CHEN P, LI PH, CUNNINGHAM WP. 1977. Ultrastructural differences in leaf cells of some *Solanum* species in relation to their frost resistance. *Botanical Gazette* 138: 276–285.

CHEN S, JIA H, ZHAO H, LIU D, LIU Y, LIU B, BAUER S, SOMERVILLE CR. 2016. Anisotropic cell expansion is affected through bidirectional mobility of cellulose synthase complexes and phosphorylation at two critical residues on CESA3. *Plant Physiology* 171: 242–250.

CHINIQUY D, UNDERWOOD W, CORWIN J, RYAN A, SZEMENYEI H, LIM CC, STONEBLOOM SH, BIRDSEYE DS, VOGEL J, KLIEBENSTEIN DJ, SCHELLER HV, SOMERVILLE S. 2019. PMR5, an acetylation protein at the intersection of pectin biosynthesis and defense against fungal pathogens. *The Plant Journal* 100: 1022–1035.

CHORMOVA D, FRANKOVÁ L, DEFRIES A, CUTLER SR, FRY SC. 2015. Discovery of small molecule inhibitors of xyloglucan endotransglucosylase (XET) activity by high-throughput screening. *Phytochemistry* 117: 220–236.

CHORMOVA D, MESSENGER DJ, FRY SC. 2014. Rhamnogalacturonan-II cross-linking of plant pectins via boron bridges occurs during polysaccharide synthesis and/or secretion. *Plant Signalling & Behaviour* 9: 8–10.

CHOUDHARY P, SAHA P, RAY T, TANG Y, YANG D, CANNON MC. 2015. *EXTENSIN18* is required for full male fertility as well as normal vegetative growth in *Arabidopsis*. *Frontiers in Plant Science* 22: 553.

CLARKE SH. 1938. Fine structure of the plant cell wall. *Nature* 142: 899–904.

CLAUSEN MH, WILLATS WGT, KNOX JP. 2003. Synthetic methyl hexagalacturonate hapten inhibitors of anti-homogalacturonan monoclonal antibodies LM7, JIM5 and JIM7. *Carbohydrate Research* 338: 1797–1800.

COENEN GJ, BAKX EJ, VERHOEF RP, SCHOLS HA, VORAGEN AGJ. 2007. Identification of the connecting linkage between homo- or xylogalacturonan and rhamnogalacturonan type I. *Carbohydrate Polymers* 70: 224–235.

COHEN SH, VOYLE CA. 1987. Internal porosity of corn extrudate air cell wall. *Food Microstructure* 6: 209–211.

COOPER WC, YOUNG RH, TURRELL F. 1964. Microclimate and physiology of citrus: their relation to cold protection. *Agricultural Science Review* 2: 38–50.

CORIO-COSTET M-F, DALL'AGNESE M, SCALLA R. 1991. Effects of isoxaben on sensitive and tolerant plant cell cultures: I. Metabolic fate of isoxaben. *Pesticide Biochemistry and Physiology* 40: 246–254.

CORNUAULT V, BUFFETTO F, RYDAHL MG, MARCUS SE, TORODE TA, XUE J, CRÉPEAU M-J, FARIA-BLANC N, WILLATS WGT, DUPREE P, RALET M-C, KNOX JP. 2015. Monoclonal antibodies indicate low-abundance links between heteroxylan and other glycans of plant cell walls. *Planta* 242: 1321–1334.

CORPET F. 1988. Multiple sequence alignment with hierarchical clustering. *Nucleic Acids Research* 16: 10881–10890.

COSGROVE DJ. 2000. Expansive growth of plant cell walls. *Plant Physiology and Biochemistry* 38: 109–124.

COSGROVE DJ. 2001. Wall structure and wall loosening. A look backwards and forwards. *Plant Physiology* 125: 131–134.

COSGROVE DJ. 2005. Growth of the plant cell wall. *Nature Reviews Molecular Cell Biology* 6: 850.

COSGROVE DJ. 2015. Plant cell wall extensibility: connecting plant cell growth with cell wall structure, mechanics, and the action of wall modifying enzymes. *Journal of Experimental Botany* 67: 663–676.

COSGROVE DJ. 2022. Building an extensible cell wall. *Plant Physiology* 189: 1246–1277.

CUMMING CM, RIZKALLAH HD, MCKENDRICK KA, ABDEL-MASSIH RM, BAYDOUN EA-H, BRETT CT. 2005. Biosynthesis and cell-wall deposition of a pectin-xyloglucan complex in pea. *Planta* 222: 546–555.

DA CRUZ RP, SPEROTTO RA, CARGNELUTTI D, ADAMSKI JM, DE FREITASTERRA T, FETT JP. 2013. Avoiding damage and achieving cold tolerance in rice plants. *Food and Energy Security* 2: 96—119.

DALMANNSDOTTIR S, JORGENSEN M, RAPACZ M, OSTREM L, LARSEN A, RODVEN R, ROGNLI OA. 2017. Cold acclimation in warmer extended autumns impairs freezing tolerance of perennial ryegrass (*Lolium perenne*) and timothy (*Phleum pratense*). *Physiologia Plantarum* 160: 266–281.

DARVILL AG, MCNEIL M, ALBERSHEIM P. 1978. Structure of plant cell walls: VIII. A new pectic polysaccharide. *Plant Physiology* 62: 418–427.

DAVIES HA, DANIELS MJ, DOW JM. 1997. Induction of extracellular matrix glycoproteins in *Brassica* petioles by wounding and in response to *Xanthomonas campestris*. *Molecular Plant-Microbe Interactions* 10: 812–820.

DE NOBEL JG, KLIS FM, MUNNIK T, PRIEM J, VAN DEN ENDE H. 1990. An assay of relative cell wall porosity in *Saccharomyces cerevisiae*, *Kluyveromyces lactis* and *Schizosaccharomyces pombe*. *Yeast* 6: 483–490.

DEL CORPO D, FULLONE MR, MIELE R, LAFOND M, PONTIGGIA D, GRISEL S, KIEFFER-JAQUINOD S, GIARDINA T, BELLINCAMPI D, LIONETTI V. 2020. AtPME17 is a functional *Arabidopsis thaliana* pectin methylesterase regulated by its PRO region that triggers PME activity in the resistance to *Botrytis cinerea*. *Molecular Plant Pathology* 21: 1620–1633.

DERKSEN J, JANSSEN G-J, WOLTERS-ARTS M, LICHTSCHEIDL I, ADLASSNIG W, OVECKA M, DORIS F, STEER M. 2011. Wall architecture with high porosity is established at the tip and maintained in growing pollen tubes of *Nicotiana tabacum*. *The Plant Journal* 68: 495–506.

DESNOS T, ORBOVIC V, BELLINI C, KRONENBERGER J, CABOCHE M, TRAAS J, HÖFTE, H. 1996. *Procuste1* mutants identify two distinct genetic pathways controlling hypocotyl cell elongation, respectively, in dark- and light-grown *Arabidopsis* seedlings. *Development* 122: 683–693.

DESPREZ T, JURANIEC M, CROWELL EF, JOUY H, POCHYLOVA Z, PARCY F, HÖFTE H, GONNEAU M, VERNHETTES S. 2007. Organization of cellulose synthase complexes involved in primary cell wall synthesis in *Arabidopsis thaliana*. *Proceedings of the National Academy of Sciences* 104: 15572–15577.

DING JP, PICKARD BG. 1993. Modulation of mechanosensitive calcium-sensitive cation channels by temperature. *The Plant Journal* 3: 713–720.

DOBBERST B, KIERMAYE O. 1972. Occurrence of a special type of golgi-vesicles during secondary wall formation in *Micrasterias denticulata* Breb. *Protoplasma* 75: 185–194.

DOBLIN MS, KUREK I, JACOB-WILK D, DELMER DP. 2002. Cellulose biosynthesis in plants: from genes to rosettes. *Plant & Cell Physiology* 43: 1407–1420.

DOMON J-M, BALDWIN L, ACKET S, CAUDEVILLE E, ARNOULT S, ZUB H, GILLET F, LEJEUNE-HÉNAUT I, BRANCOURT-HULMEL M, PELLOUX J, RAYON C.

2013. Cell wall compositional modifications of *Miscanthus* ecotypes in response to cold acclimation. *Phytochemistry* 85: 51–61.

DOMOZYCH DS, STEWART KD, MATTOX KR. 1980. The comparative aspects of cell wall chemistry in the green algae (*Chlorophyta*). *Journal of Molecular Evolution* 15: 1–12.

DONG CH, AGARWAL M, ZHANG Y, XIE Q, ZHU J-K. 2006. The negative regulator of plant cold responses, HOS1, is a RING E3 ligase that mediates the ubiquitination and degradation of ICE1. *Proceedings of the National Academy of Sciences* 103: 8281–8286.

DONG MA, FARRE EM, THOMASHOW MF. 2011. CIRCADIAN CLOCK-ASSOCIATED 1 and LATE ELONGATED HYPOCOTYL regulate expression of the C-repeat binding factor (CBF) pathway in *Arabidopsis*. *Proceedings of the National Academy of Sciences* 108: 7241–7246.

DOROKHOV YL, KOMAROVA TV, PETRUNIA IV, FROLOVA OY, POZDYSHEV DV, GLEBA YY. 2012. Airborne signals from a wounded leaf facilitate viral spreading and induce antibacterial resistance in neighboring plants. *PLoS Pathogens* 8: e1002640.

DUMONT F, MARECHAL P-A, GERVAIS P. 2004. Cell size and water permeability as determining factors for cell viability after freezing at different cooling rates. *Applied and Environmental Microbiology* 70: 268–272.

EDWARDS K, JOHNSTONE C, THOMPSON C. 1991. A simple and rapid method for the preparation of plant genomic DNA for PCR analysis. *Nucleic Acids Research* 19: 1349.

EGELUND J, PETERSEN BL, MOTAWIA MS, DAMAGER I, FAIK A, OLSEN CE, ISHII T, CLAUSEN H, ULVSKOV P, GESHI N. 2006. *Arabidopsis thaliana RGXT1* and *RGXT2* encode golgi-localized (1,3)-α-D-xylosyltransferases involved in the synthesis of pectic rhamnogalacturonan-II. *The Plant Cell* 18: 2593–2607.

EHWALD R, HEESE P, KLEIN U. 1991. Determination of the size limits of membrane separation in vesicle chromatography by fractionation of polydisperse dextran. *Journal of Chromatography A* 542: 239–245.

EHWALD R, WOEHLECKE H, TITEL C. 1992. Cell wall microcapsules with different porosity from suspension cultured *Chenopodium album*. *Phytochemistry* 31: 3033–3038.

EINHORN-STOLL U, HATAKEYAMA H, HATAKEYAMA T. 2012. Influence of pectin modifications on water binding properties. *Food Hydrocolloids* 27: 494–502.

ELLSWORTH PV, ELLSWORTH PZ, KOTEYEVA NK, COUSINS AB. 2018. Cell wall properties in *Oryza sativa* influence mesophyll CO_2 conductance. *New Phytologist* 219: 66–76.

ESQUERRÉ-TUGAYÉ M-T, LAFITTE C, MAZAU D, TOPPAN A, TOUZÉ A. 1979. Cell surfaces in plant–microorganism interactions. II. Evidence for the accumulation of hydroxyproline-rich glycoproteins in the cell wall of diseased plants as a defence mechanism. *Plant Physiology* 64: 320–326.

ETEMADI M, ZUTHER E, MÜLLER H, HINCHA DK, BERG G. 2018. Ecotype-dependent response of bacterial communities associated with *Arabidopsis* to cold acclimation. *Phytobiomes* 2: 3–13.

FAGARD M, DESNOS T, DESPREZ T, GOUBET F, REFREGIER G, MOUILLE G, MCCANN MC, RAYON C, VERNHETTES S, HÖFTE H. 2000. *PROCUSTE1* encodes a cellulose synthase required for normal cell elongation specifically in roots and dark-grown hypocotyls of *Arabidopsis*. *The Plant Cell* 12: 2409–2424.

FENG W, KITA D, PEAUCELLE A, CARTWRIGHT HN, DOAN V, DUAN Q, LIU M-C, MAMAN J, STEINHORST L, SCHMITZ-THOM I, YVON R, KUDLA J, WU H-M, CHEUNG AY, DINNENY JR. 2018. The FERONIA receptor kinase maintains cell-wall integrity during salt stress through Ca^{2+} signaling. *Current Biology* 28: 666–675.

FINDEKLEE P, GOLDBACH HE. 1996. Rapid effects of boron deficiency on cell wall elasticity modulus in *Cucurbita pepo* roots. *Botanica Acta* 109: 463–465.

FINDEKLEE P, WIMMER M, GOLDBACH HE. 1997. Early effects of boron deficiency on physical cell wall parameters, hydraulic conductivity and plasmalemma-bound reductase activities in young *C. pepo* and *V. faba* roots. IN: BELL RW, RERKASEM B. *Boron in Soils and Plants* 221–222. Kluwer Academic Publishers.

FINKA A, CUENDET AFH, MAATHIUS FJ, SAIDI Y, GOLOUBINOFF P. 2012. Plasma membrane cyclic nucleotide gated calcium channels control land plant thermal sensing and acquired thermotolerance. *Plant Cell* 24: 3333–3348.

FLEISCHER A, O'NEILL MA, EHWALD R. 1999. The pore size of non-graminaceous plant cell walls is rapidly decreased by borate ester cross-linking of the pectic polysaccharide rhamnogalacturonan II. *Plant Physiology* 121: 829–838.

FORAND AD, FINFROCK YZ, LAVIER M, STOBBS J, QIN L, WANG S, KARUNAKARAN C, WEI Y, GHOSH S, TANINO KK. 2022. With a little help from my cell wall: structural modifications in pectin may play a role to overcome both dehydration stress and pathogens. *Plants* 11: 385.

FOURRIER N, BÉDARD J, LOPEZ-JUEZ E, BARBROOK A, BOWYER J, JARVIS P, WARREN G, THORLBY G. 2008. A role for SENSITIVE TO FREEZING2 in protecting chloroplasts against freeze-induced damage in *Arabidopsis*. *The Plant Journal* 55: 734–745.

FRANKOVÁ L, FRY SC. 2013. Biochemistry and physiological roles of enzymes that 'cut and paste' plant cell-wall polysaccharides. *Journal of Experimental Botany* 64: 3519–3550.

FRANKS F. 1985. Biophysics and biochemistry at low temperatures. Cambridge University Press, Cambridge.

FREI M. 2013. Lignin: characterization of a multifaceted crop component. *The Scientific World Journal* 2013: 1–25.

FRIDOVICH I. 1991. Molecular oxygen: friend and foe. IN: PELL EJ, STEFFEN KL. *Active Oxygen/Oxidative Stress and Plant Metabolism*. American Society of Plant Physiologists, Rockville.

FRY SC. 1989. Cellulases, hemicelluloses and auxin-stimulated growth: a possible relationship. *Physiologia Plantarum* 75: 532–536.

FRY SC, MILLER J. 1989. Towards a working model of the growing plant cell wall. Phenolic cross-linking reactions in the primary cell wall of dicotyledons. IN: LEWIS N, PAICE M. *Plant Cell Wall Polymers: Biogenesis and Biodegradation* 33–46. American Chemical Society, Washington, D.C.

FUJIKAWA S. 1995. A freeze-fracture study designed to clarify the mechanisms of freezing injury due to the freezing-induced close apposition of membranes in cortical parenchyma cells of mulberry. *Cryobiology* 32: 444–454.

FUJIKAWA S, JITSUYAMA Y, KURODA K. 1999. Determination of the role of cold acclimation-induced diverse changes in plant cells from the viewpoint of avoidance of freezing injury. *Journal of Plant Research* 112: 237–244.

FUJITA M, FUJITA Y, NOUTOSHI Y, TAKAHASHI F, NARUSAKA Y, YAMAGUCHI-SHINOZAKI K, SHINOZAKI K. 2006. Crosstalk between abiotic and biotic stress responses: a current view from the points of convergence in the stress signalling networks. *Current Opinion in Plant Biology* 9: 436–442.

FULLER MP, WISNIEWSKI M. 1998. The use of infrared thermal imaging in the study of ice nucleation and freezing of plants. *Journal of Thermal Biology* 23: 81–89.

GASPAR Y, JOHNSON KL, MCKENNA JA, BACIC A, SCHULTZ CJ. 2001. The complex structures of arabinogalactan-proteins and the journey towards understanding function. *Plant Molecular Biology* 47: 161–176.

GEORGE MF, BURKE MJ. 1977. Cold hardiness and deep supercooling in xylem of shagbark hickory. *Plant Physiology* 59: 319–325.

GERSHLAK JR, HERNANDEZ S, FONTANA G, PERREAULT LR, HANSEN KJ, LARSON SA, BINDER BYK, DOLIVO DM, YANG T, DOMINKO T, ROLLE MW, WEATHERS PJ, MEDINA-BOLIVAR F, CRAMER CL, MURPHY WL, GAUDETTE GR. 2017. Crossing kingdoms: using decellularized plants as perfusable tissue engineering scaffolds. *Biomaterials* 125: 13–22.

GILMOUR SJ, FOWLER SG, THOMASHOW MF. 2004. *Arabidopsis* transcriptional activators *CBF1, CBF2,* and *CBF3* have matching functional activities. *Plant Molecular Biology* 54: 767–781.

GILMOUR SJ, HAJELA RK, THOMASHOW MF. 1988. Cold acclimation in *Arabidopsis thaliana. Plant Physiology* 87: 745–750.

GILMOUR SJ, ZARKA DG, STOCKINGER EJ, SALAZAR MP, HOUGHTON JM, THOMASHOW MF. 1998. Low temperature regulation of the *Arabidopsis* CBF family of AP2 transcriptional activators as an early step in cold-induced *COR* gene expression. *The Plant Journal* 16: 433–443.

GONÇALVES B, MAUGARNY-CALÈS A, ADROHER B, CORTIZO M, BORREGA N, BLEIN T, HASSON A, GINEAU E, MOUILLE G, LAUFS P, ARNAUD N. 2017. GDP-$_{L}$-fucose is required for boundary definition in plants. *Journal of Experimental Botany* 68: 5801–5811.

GONZALES-GUZMAN M, PIZZIO GA, ANTONI R, VERA-SIRERA F, MERILO E, BASSEL GW, FERNÁNDEZ MA, HOLDSWORTH MJ, PEREZ-AMADOR MA, KOLLIST H, RODRIGUEZ PL. 2012. *Arabidopsis* PYR/PYL/RCAR receptors play a major role in quantitative regulation of stomatal aperture and transcriptional response to abscisic acid. *The Plant Cell* 24: 2483–2496.

GORDON-KAMM WJ, STEPONKUS PL. 1984. Lamellar-to-hexagonal-II phase transitions in the plasma membrane of isolated protoplasts after freeze-induced dehydration. *Proceedings of the National Academy of Sciences* 81: 6373–6377.

GRIFFITH M, ALA P, YANG DSC, HON W, MOFFATT BA. 1992. Antifreeze protein produced endogenously in winter rye leaves. *Plant Physiology* 100: 593–596.

GRIFFITH M, BROWN GN. 1982. Cell wall deposits in winter rye *Secale cereale* L. "Puma" during cold acclimation. *Botanical Gazette* 143: 486–490.

GRIFFITH M, HUNER NPA, ESPELIE KE, KOLATTUKUDY PE. 1985. Lipid polymers accumulate in the epidermis and mestome sheath cell walls during low temperature development of winter rye leaves. *Protoplasma* 125: 53–64.

GRIFFITH M, LUMB C, WISEMAN SB, WISNIEWSKI M, JOHNSON RW, MARANGONI AG. 2005. Antifreeze proteins modify the freezing process in Planta. *Plant Physiology* 138: 330–340.

GUÉNIN S, MARECK A, RAYON C, LAMOUR R, NDONG YA, DOMON J-M, SÉNÉCHAL F, FOURNET F, JAMET E, CANUT H, PERCOCO G, MOUILLE G, ROLLAND A, RUSTÉRUCCI C, GUERINEAU F, WUYTSWINKEL OV, GILLET F, DRIOUICH A, LEROUGE P, GUTIERREZ L, PELLOUX J. 2011. Identification of pectin methylesterase 3 as a basic pectin methylesterase isoform involved in adventitious rooting in *Arabidopsis thaliana*. *New Phytologist* 192: 114–126.

GUSTA LV, BURKE MJ, KAPOOR AC. 1975. Determination of unfrozen water in winter cereals at subfreezing temperatures. *Plant Physiology* 56: 707–709.

GUY CL, HASKELL D, LI Q-B. 1998. Association of proteins with the stress 70 molecular chaperones at low temperature: evidence for the existence of cold labile proteins in spinach. *Cryobiology* 36: 301–314.

GUY CL, LI Q-B. 1998. The organization and evolution of the spinach stress 70 molecular chaperone gene family. *The Plant Cell* 10: 539–556.

HAAKE V, COOK D, RIECHMANN JL, PINEDA O, THOMASHOW MF, ZHANG JZ. 2002. Transcription factor CBF4 is a regulator of drought adaptation in *Arabidopsis*. *Plant Physiology* 130: 639–648.

HAAS KT, WIGHTMAN R, MEYEROWITZ EM, PEAUCELLE A. 2020. Pectin homogalacturonan nanofilament expansion drives morphogenesis in plant epidermal cells. *Science* 367: 1003–1007.

HAGIWARA T, HARTEL RW, MATSUKAWA S. 2006. Relationship between recrystallization rate of ice crystals in sugar solutions and water mobility in freeze-concentrated matrix. *Food Biophysics* 1: 74–82.

HALL Q, CANNON MC. 2002. The cell wall hydroxyproline-rich glycoprotein RSH is essential for normal embryo development in *Arabidopsis*. *The Plant Cell* 14: 1161–1172.

HALLIWELL B, GUTTERIDGE JMC. 2007. Free radicals in biology and medicine. Oxford University Press, New York.

HANN CT, BEQUETTE CJ, DOMBROWSKI JE, STRATMANN JW. 2014. Methanol and ethanol modulate responses to danger- and microbe-associated molecular patterns. *Frontiers in Plant Science* 5: 550.

HANNAH MA, HEYER AG, HINCHA DK. 2005. A global survey of gene regulation during cold acclimation in *Arabidopsis thaliana*. *PLoS Genetics* 1: 172–196.

HANSEN J, BECK E. 1988. Evidence for ideal and non-ideal equilibrium freezing of leaf water in frost-hardy ivy (*Hedera helix*) and winter barley (*Hordeum vulgare*). *Botanica Acta* 101: 76–82.

HARHOLT J, JENSEN JK, SØRENSEN SO, ORFILA C, PAULY M, SCHELLER HV. 2006. ARABINAN DEFICIENT 1 is a putative arabinosyltransferase involved in biosynthesis of pectin arabinan in *Arabidopsis*. *Plant Physiology* 140: 49–58.

HARHOLT J, SUTTANGKAKUL A, SCHELLER HV. 2010. Biosynthesis of pectin. *Plant Physiology* 153: 384–395

HAYASHI T. 1989. Xyloglucans in the primary cell wall. *Annual Review of Plant Physiology and Plant Molecular Biology* 2: 1–19.

HAYASHI T, OGAWA K, MITSUISHI Y. 1994. Characterization of the adsorption of xyloglucan to cellulose. *Plant & Cell Physiology* 35: 1199–1205.

HEIM DR, SKOMP JR, TSCHABOLD EE, LARRINUA IM. 1990. Isoxaben inhibits the synthesis of acid insoluble cell wall materials in *Arabidopsis thaliana*. *Plant Physiology* 93: 695–700.

HEMSLEY PA, HURST CH, KALIYADASA E, LAMB R, KNIGHT MR, DE COTHI EA, STEELE JF, KNIGHT H. 2014. The *Arabidopsis* Mediator complex subunits MED16, MED14, and MED2 regulate Mediator and RNA polymerase II recruitment to CBF-responsive cold-regulated genes. *The Plant Cell* 26: 465–84.

HERBURGER K, XIN A, HOLZINGER A. 2019. Homogalacturonan accumulation in cell walls of the green alga *Zygnema* sp. (Charophyta) increases desiccation resistance. *Frontiers in Plant Science* 10: 540.

HERMAN EM, ROTTER K, PREMAKUMAR R, ELWINGER G, BAE R, EHLER-KING L, CHEN S, LIVINGSTON DP. 2006. Additional freeze hardiness in wheat acquired by exposure to −3°C is associated with extensive physiological, morphological, and molecular changes. *Journal of Experimental Botany* 57: 3601–3618.

HILL PW, BROUGHTON R, BOUGOURE J, HAVELANGE W, NEWSHAM KK, GRANT H, JONES DL. 2019. Angiosperm symbioses with non-mycorrhizal fungal partners enhance N acquisition from ancient organic matter in a warming maritime Antarctic. *Ecology Letters* 22: 2111–2119.

HIMMEL ME, DING SY, JOHNSON DK, ADNEY WS, NIMLOS MR, BRADY JW, FOUST TD. 2007. Biomass recalcitrance: engineering plants and enzymes for biofuels production. *Science* 315: 804–807.

HINCHA DK, ESPINOZA C, ZUTHER E. 2012. Transcriptomic and metabolomic approaches to the analysis of plant freezing tolerance and cold acclimation. IN: TUTEJA N, GILL SS, TOBURCIO AF, TUTEJA R. *Improving Crop Resistance to Abiotic Stress* 255–287. Wiley-Blackwell, Berlin.

HINCHA DK, ZUTHER E. 2014. Plant cold acclimation and freezing tolerance. *Methods in Molecular Biology* 1166: 1–6.

HOMSHAW LG. 1980. Freezing and melting temperature hysteresis of water in porous materials: application to the study of pore form. *European Journal of Soil Science* 31: 399–414.

HONGO S, SATO K, YOKOYAMA R, NISHITANI K. 2012. Demethylesterification of the primary wall by PECTIN METHYLESTERASE35 provides mechanical support to the *Arabidopsis* stem. *The Plant Cell* 24: 2624–2634.

HOUSTON K, TUCKER MR, CHOWDHURY J, SHIRLEY N, LITTLE A. 2016. The plant cell wall: a complex and dynamic structure as revealed by the responses of genes under stress conditions. *Frontiers in Plant Science* 7: 984.

HUANG YC, WU HC, WANG YD, LIU CH, LIN CC, LUO DL, JINN TL. 2017. PECTIN METHYLESTERASE34 contributes to heat tolerance through its role in promoting stomatal movement. *Plant Physiology* 174: 748–763.

HUBEL A, DARR TB, CHANG A, DANTZIG J. 2007. Cell partitioning during directional solidification of trehalose solutions. *Cryobiology* 55: 182–188.

HUGGENBERGER F, JENNINGS EA, RYAN PJ, BUROW KW. 1982. Isoxaben, a new selective herbicide for use in cereals. *Weeds* 1: 47.

HUNDERTMARK M, HINCHA DK. 2008. LEA (late embryogenesis abundant) proteins and their encoding genes in *Arabidopsis thaliana*. *BMC Genomics* 9: 1–22.

HUNER N, PALTA J, LI P, CARTER J. 1981. Anatomical changes in leaves of Puma rye in response to growth at cold-hardening temperatures. *Botanical Gazette* 142: 55–62.

IBATA H, NAGATANI A, MOCHIZUKI N. 2013. Perforated-tape Epidermal Detachment (PED): a simple and rapid method for isolating epidermal peels from specific areas of *Arabidopsis* leaves. *Plant Biotechnology* 30: 497–502.

IRAKI NM, BRESSAN RA, HASEGAWA PM, CARPITA NC. 1989. Alteration of the physical and chemical structure of the primary wall of growth-limited plant cells adapted to osmotic stress. *Plant Physiology* 91: 39–47.

ISHII T, MATSUNAGA T, PELLERIN P, O'NEILL MA, DARVILL A, ALBERSHEIM P. 1999. The plant cell wall polysaccharide rhamnogalacturonan II self-assembles into a covalently cross-linked dimer. *Journal of Biological Chemistry* 274: 13098–13104.

ISHIZAKI-NISHIZAWA O, FUJI, T, AZUMA M, SEKIGUCHI K, MURATA N, OHTANI T, TOGURI T. 1996. Low-temperature resistance of higher plants is significantly

enhanced by a nonspecific cyanobacterial desaturase. *Nature Biotechnology* 14: 1003–1006.

JAGLO-OTTOSEN KR, GILMOUR SJ, ZARKA DG, SCHABENBERGER O, THOMASHOW MF. 1998. *Arabidopsis CBF1* overexpression induces *COR* genes and enhances freezing tolerance. *Science* 280: 104–106.

JARVIS MC. 1984. Structure and properties of pectin gels in plant cell walls. *Plant, Cell & Environment* 7: 153–164.

JENKS MA, ASHWORTH EN. 1999. Plant epicuticular waxes: function, production, and genetics. IN: JANICK J. *Horticultural Reviews* 1–68. John Wiley & Sons, New York.

JIA Y, DING Y, SHI Y, ZHANG X, GONG Z, YANG S. 2016. The *cbfs* triple mutants reveal the essential functions of *CBFs* in cold acclimation and allow the definition of CBF regulons in *Arabidopsis*. *New Phytologist* 212: 345–353.

JIA Z, DAVIES PL. 2002. Antifreeze proteins: an unusual receptor-ligand interaction. *Trends in Biochemical Sciences* 27: 101–106.

JIANG B, SHI Y, ZHANG X, XIN X, QI L, GUO H, LI J, YANG S. 2017. PIF3 is a negative regulator of the CBF pathway and freezing tolerance in *Arabidopsis*. *Proceedings of the National Academy of Sciences* 114: E6695–E6702.

JONES L, SEYMOUR GB, KNOX JP. 1997. Localization of pectic galactan in tomato cell walls using a monoclonal antibody specific to (1>4)-β-D-galactan. *Plant Physiology* 113: 1405—1412.

JUURAKKO CL, BREDOW M, NAKAYAMA T, IMAI H, KAWAMURA Y, DICENZO GC, UEMURA M, WALKER VK. 2021. The *Brachypodium distachyon* cold-acclimated plasma membrane proteome is primed for stress resistance. *Genes Genomes Genetics* 11: 1—15.

KACZMARSKA A, PIECZYWEK PM CYBULSKA J, ZDUNEK A. 2022. Structure and functionality of rhamnogalacturonan I in the cell wall and in solution: a review. *Carbohydrate Polymers* 278: 118909.

KARIM MR, ZHANG YQ, ZHAO RR, CHEN XP, ZHANG FS, ZOU CQ. 2012. Alleviation of drought stress in winter wheat by late foliar application of zinc, boron, and manganese. *Journal of Plant Nutrition and Soil Science* 175: 142–151.

KAUFMANN MR. 1976. Water transport through plants: current perspectives. IN: WARDLAW IF, PASSIOURA JB. *Transport and Transfer Processes in Plants* 313—327. Academic Press, New York.

KHAN MN, AHMED I, DIN IU, NOURELDEEN A, DARWISH H, KHAN M. 2022. Proteomic insight into soybean response to flooding stress reveals changes in energy metabolism and cell wall modifications. *PLoS ONE* 17: e0264453.

KIDOKORO S, MARUYAMA K, NAKASHIMA K, IMURA Y, NARUSAKA Y, SHINWARI ZK, OSAKABE Y, FUJITA Y, MIZOI J, SHINOZAKI K, YAMAGUCHI-SHINOZAKI K. 2009. The phytochrome-interacting factor PIF7 negatively regulates *DREB1* expression under circadian control in *Arabidopsis*. *Plant Physiology* 151: 2046–2057.

KIERZKOWSKI D, NAKAYAMA N, ROUTIER-KIERZKOWSKA A-L, WEBER A, BAYER E, SCHORDERET M, REINHARDT D, KUHLEMEIER C, SMITH RS. 2012. Elastic domains regulate growth and organogenesis in the plant shoot apical meristem. *Science* 335: 1096–1099.

KIMURA S, ITOH T. 1995. Evidence for the role of the glomerulocyte in cellulose synthesis in the tunicate, *Metandrocarpa uedai*. *Protoplasma* 186: 24–33.

KIMURA S, LAOSINCHAI W, ITOH T, CUI X, LINDER CR, BROWN Jr. RM. 1999. Immunogold labeling of rosette terminal cellulose-synthesizing complexes in the vascular plant *Vigna angularis*. *The Plant Cell* 11: 2075–2085.

KNIGHT H, TREWAVAS AJ, KNIGHT MR. 1996. Cold calcium signalling in *Arabidopsis* involves two cellular pools and a change in calcium signature after acclimation. *The Plant Cell* 8: 489–503.

KNIGHT H, ZARKA DG, OKAMOTO H, THOMASHOW MF, KNIGHT MR. 2004. Abscisic acid induces *CBF* gene transcription and subsequent induction of cold-regulated genes via the CRT promoter element. *Plant Physiology* 135: 1710–1717.

KNIGHT MR, KNIGHT H. 2012. Low-temperature perception leading to gene expression and cold tolerance in higher plants. *New Phytologist* 195: 737–751.

KONNO H, YAMASAKI Y, SUGIMOTO M, TAKEDA K. 2008. Differential changes in cell wall matrix polysaccharides and glycoside-hydrolyzing enzymes in developing wheat seedlings differing in drought tolerance. *Journal of Plant Physiology* 165: 745–754.

KOSOVÁ K, VÍTÁMVÁS P, PRÁŠIL IT. 2007. The role of dehydrins in plant response to cold. *Biologia Plantarum* 51: 601–617.

KOVI MR, ERGON Å, ROGNLI OA. 2016. Freezing tolerance revisited: effects of variable temperatures on gene regulation in temperate grasses and legumes. *Current Opinion in Plant Biology* 33: 140–146.

KOZBIAL P, JERZMANOWSKI A, SHIRSAT AH, KACPERSKA A. 2002. Transient freezing regulates expression of extensin-type genes in winter oilseed rape. *Physiologia Plantarum* 103: 264–270.

KRZESŁOWSKA M. 2011. The cell wall in plant cell response to trace metals: polysaccharide remodeling and its role in defense strategy. *Acta Physiologiae Plantarum* 33: 35–51.

KUBACKA-ZĘBALSKA M, KACPERSKA A. 1999. Low temperature-induced modifications of cell wall content and polysaccharide composition in leaves of winter oilseed rape (*Brassica napus* L. var. *oleifera* L.). *Plant Science* 148: 59–67.

KUNST L, SAMUELS AL. 2003. Biosynthesis and secretion of plant cuticular wax. *Progress in Lipid Research* 42: 51–80.

KUPRIAN E, MUNKLER C, RESNYAK A, ZIMMERMANN S, TUONG TD, GIERLINGER N, MÜLLER T, LIVINGSTON DP, NEUNER G. 2017. Complex bud architecture and cell-specific chemical patterns enable supercooling of *Picea abies* bud primordia. *Plant, Cell & Environment* 40: 3101–3112.

KUREK I, KAWAGOE Y, JACOB-WILK D, DOBLIN M, DELMER D. 2002. Dimerization of cotton fiber cellulose synthase catalytic subunits occurs via oxidation of the zinc-binding domains. *Proceedings of the National Academy of Sciences* 99: 11109–11114.

KURODA K, KASUGA J, ARAKAWA K, FUJIKAWA S. 2003. Xylem ray parenchyma cells in boreal hardwood species respond to subfreezing temperatures by deep supercooling that is accompanied by incomplete desiccation. *Plant Physiology* 131: 736–744.

LAMPORT DTA. 1986. The primary cell wall: a new model. IN: YOUNG RA, ROWELL RM. *Cellulose: Structure, Modification and Hydrolysis* 77–90. John Wiley, New York.

LAMPORT DTA, KIELISZEWSKI MJ, CHEN Y, CANNON MC. 2011. Role of the extensin superfamily in primary cell wall architecture. *Plant Physiology* 156: 11–19.

LARCHER W, MEINDL U, RALSER E, ISHIKAWA M. 1991. Persistent supercooling and silica deposition in cell walls of palm leaves. *Journal of Plant Physiology* 139: 146—154.

LARSEN FH, BYG I, DAMAGER I, DIAZ J, ENGELSEN SB, ULVSKOV P. 2011. Residue-specific hydration of primary cell wall potato pectin identified by solid-state C-13 single-pulse MAS and CP/MAS NMR spectroscopy. *Biomacromolecules* 12: 1844–1850.

LE GALL H, PHILIPPE F, DOMON J-M, GILLET F, PELLOUX J, RAYON C. 2015. Cell wall metabolism in response to abiotic stress. *Plants* 4: 112–166.

LEE CM, THOMASHOW MF. 2012. Photoperiodic regulation of the C-repeat binding factor (CBF) cold acclimation pathway and freezing tolerance in *Arabidopsis thaliana*. *Proceedings of the National Academy of Sciences* 109: 15054–15059.

LEE Y, KARUNAKARAN C, LAHLALI R, LIU X, TANINO KK, OLSEN JE. 2017. Photoperiodic regulation of growth-dormancy cycling through induction of multiple bud–shoot barriers preventing water transport into the winter buds of Norway spruce. *Frontiers in Plant Science* 8: 2109.

LEI L, ZHANG T, STRASSER R, LEE CM, GONNEAU M, MACH L, VERNHETTES S, KIM SH, COSGROVE DJ, LI S, GU Y. 2014. The *jiaoyao1* mutant is an allele of *korrigan1* that abolishes endoglucanase activity and affects the organization of both cellulose microfibrils and microtubules in *Arabidopsis*. *The Plant Cell* 26: 2601–2616.

LEVITT J. 1980. Responses of plants to environmental stresses I: chilling, freezing and high temperature stresses. 2. Academic Press.

LEUCCI MR, LENUCCI MS, PIRO G, DALESSANDRO G. 2008. Water stress and cell wall polysaccharides in the apical root zone of wheat cultivars varying in drought tolerance. *Journal of Plant Physiology* 165: 1168–1180.

LEVY S, MACLACHLAN G, STAEHELIN LA. 1997. Xyloglucan sidechains modulate binding to cellulose during *in vitro* binding assays as predicted by conformational dynamics simulations. *The Plant Journal* 11: 373–386.

LI C, TAO J, ZHAO D, YOU C, GE J. 2012. Effect of calcium sprays on mechanical strength and cell wall fractions of herbaceous peony (*Paeonia lactiflora* Pall.) inflorescence stems. *International Journal of Molecular Sciences* 13: 4704–4713.

LI TG, VISPERAS RM, VERGARA BS. 1981. Correlation of cold tolerance at different growth stages in rice. *Acta Botanica Sinica* 23: 203—207.

LIDFORSS B. 1896. Zur physiologie und biologie der wintergrünen flora. *Botanisches Centralblatt* 68: 33–44.

LIDFORSS B. 1907. Die wintergrüne flora. *Lunds Universitets Årsskrift* 2: 76.

LIN CC, ARONSON JM. 1970. Chitin and cellulose in cell walls of oomycete, *Apodachlya* sp. *Archiv fur Mikrobiologie* 72: 111–114.

LINDOW SE, ARNY DC, UPPER CD. 1982. Bacterial ice nucleation: a factor in frost injury to plants. *Plant Physiology* 70: 1084–1089.

LIONETTI V, CERVONE F, BELLINCAMPI D. 2012. Methyl esterification of pectin plays a role during plant-pathogen interactions and affects plant resistance to diseases. *Journal of Plant Physiology* 169: 1623–1630.

LIONETTI V, FABRI E, DE CAROLI M, HANSEN AR, WILLATS WGT, PIRO G, BELLINCAMPI D. 2017. Three pectin methylesterase inhibitors protect cell wall integrity for *Arabidopsis* immunity to *Botrytis*. *Plant Physiology* 173: 1844–1863.

LIONETTI V, RAIOLA A, CAMARDELLA L, GIOVANE A, OBEL N, PAULY M, FAVARON F, CERVONE F, BELLINCAMPI D. 2007. Overexpression of pectin methylesterase inhibitors in *Arabidopsis* restricts fungal infection by *Botrytis cinerea*. *Plant Physiology* 143: 1871–1880.

LIU H, BRETTELL LE, QIU Z, SINGH BK. 2020. Microbiome-mediated stress resistance in plants. *Trends in Plant Science* 25: 733–743.

LIU J, WILLICK IR, HIRAKI H, FORAND AD, LAWRENCE JR, SWERHONE GDW, WEI Y, GHOSH S, LEE YK, OLSEN JE, USADEL B, WORMIT A, GÜNL M, KARUNAKARAN C, DYNES JJ, TANINO KK. 2022. Cold and exogenous calcium alter *Allium fistulosum* cell wall pectin to depress intracellular freezing temperatures. *Journal of Experimental Botany* 73: 3807–3822.

LIU Q, KASUGA M, SAKUMA Y, ABE H, MIURA S, YAMAGUCHI-SHINOZAKI Y. 1998. Two transcription factors, DREB1 and DREB2, with an EREBP/AP2 DNA binding domain separate two cellular signal transduction pathways in drought- and low-temperature-responsive gene expression, respectively, in *Arabidopsis*. *The Plant Cell* 10: 1391–1406.

LIU X, GÜNTHER-POMORSKI T, LIESCHE J. 2019a. Non-invasive quantification of cell wall porosity by fluorescence quenching microscopy. *Bio-Protocol* 9: e3344.

LIU X, LI J, ZHAO H, LIU B, GÜNTHER-POMORSKI T, CHEN S, LIESCHE J. 2019b. Novel tool to quantify cell wall porosity relates wall structure to cell growth and drug uptake. *Journal of Cell Biology* 218: 1407–1420.

LIU X, ZHOU Y, XIAO J, BAO F. 2018. Effects of chilling on the structure, function and development of chloroplasts. *Frontiers in Plant Science* 9: 1715.

LIU Y, DANG P, LIU L, HE C. 2019c. Cold acclimation by the CBF-*COR* pathway in a changing climate: lessons from *Arabidopsis thaliana*. *Plant Cell Reports* 38: 511–519.

LIVINGSTON DP. 1996. The second phase of cold hardening: freezing tolerance and fructan isomer changes in winter cereal crowns. *Crop Science* 36: 1568–1573.

LIVINGSTON DP, TUONG TD, MURPHY JP, GUSTA LV, WILLICK I, WISNIEWSKI M. 2018. High-definition infrared thermography of ice nucleation and propagation in wheat under natural frost conditions and controlled freezing. *Planta* 247: 791–806.

LUCAU-DANILA A, TOITOT C, GOULAS E, BLERVACQ AS, HOT D, BAHRMAN N, SELLIER H, LEJEUNE-HÉNAUT I, DELBREIL B. 2012. Transcriptome analysis in pea allows to distinguish chilling and acclimation mechanisms. *Plant Physiology and Biochemistry* 58: 236–244.

LUSENA CV, COOK WH. 1953. Ice propagation in systems of biological interest. I. Effect of membranes and solutes in a model cell system. *Archives of Biochemistry and Biophysics* 46: 232–240.

LUYET BJ, GEHENIO PM. 1937. The double freezing point of living tissues. *Biodynamica* 1: 1–23.

LYONS JM. 1973. Chilling injury in plants. *Annual Review of Plant Physiology* 24: 445–466.

MA Y, DAI X, XU Y, LUO W, ZHENG X, ZENG D, PAN Y, LIN X, LIU H, ZHANG D, XIAO J, GUO X, XU S, NIU Y, JIN J, ZHANG H, XU X, LI L, WANG W, QIAN Q, GE S, CHONG K. 2015. *COLD1* confers chilling tolerance in rice. *Cell* 160: 1209–1221.

MADSON M, DUNAND C, LI X, VERMA R, VANZIN GF, CAPLAN J, SHOUE DA, CARPITA NC, REITER W-D. 2003. The *MUR3* gene of *Arabidopsis thaliana* encodes a xyloglucan galactosyltransferase that is evolutionarily related to animal exostosins. *Plant Cell* 15: 1662–1670.

MAERCKER U. 1965. Mikroautoradiographischer nachweis tritiumhaltigen transpirationswassers. *Naturwissenschaften* 52: 15–16.

MAJEWSKA-SAWKA A, MU A, RODRIGUEZ-GARCIA MI. 2002. Guard cell wall: immunocytochemical detection of polysaccharide components. *Journal of Experimental Botany* 53: 1067–1079.

MARCUS SE, BLAKE AW, BENIANS TAS, LEE KJD, POYSER C, DONALDSON L, LEROUX O, ROGOWSKI A, PETERSEN HL, BORASTON A, GILBERT HJ, WILLATS WGT, KNOX JP. 2010. Restricted access of proteins to mannan polysaccharides in intact plant cell walls. *The Plant Journal* 64: 191–203.

MARCUS SE, VERHERTBRUGGEN Y, HERVÉ C, ORDAZ-ORTIZ JJ, FARKAS V, PEDERSEN HL, WILLATS WGT, KNOX JP. 2008. Pectic homogalacturonan masks abundant sets of xyloglucan epitopes in plant cell walls. *BMC Plant Biology* 8: 6.

MARTSOLF JD, GERBER JF, CHEN EY, JACKSON JL, ROSE AJ. 1984. What do satellite and other data suggest about past and future Florida freezes? *Proceedings of the Florida Horticultural Society* 97: 17–21.

MARZOL E, BORASSI C, BRINGAS M, SEDE A, GARCIA DRR, CAPECE L, ESTEVEZ JM. 2018. Filling the gaps to solve the extensin puzzle. *Molecular Plant* 11: 645–658.

MATHESON MK. 1990. Mannose-based polysaccharides. *Methods in Plant Biochemistry* 12: 371–413.

MATOH T, KAWAGUCHI S, KOBAYASHI M. 1996. Ubiquity of a borate-rhamnogalacturonan II complex in the cell walls of higher plants. *Plant & Cell Physiology* 37: 636–640.

MAURYA JP, BHALERAO RP. 2017. Photoperiod- and temperature-mediated control of growth cessation and dormancy in trees: a molecular perspective. *Annals of Botany* 120: 351–360.

MAZAU D, RUMEAU D, ESQUERRÉ-TUGAYÉ M-T. 1987. Molecular approaches to understanding cell–surface interactions between plants and fungal pathogens. *Plant Physiology and Biochemistry* 25: 337–343.

MAZEAU K, PEREZ S. 1998. The preferred conformations of the four oligomeric fragments of rhamnogalacturonan II. *Carbohydrate Research* 311: 203–217.

MAZUR P. 1963. Kinetics of water ions from cells at sub-zero temperatures and the likelihood of intracellular freezing. *Journal of General Physiology* 47: 347–369.

MAZUR P. 1984. Freezing of living cells: mechanisms and implications. *American Journal of Physiology* 247: 125–142.

MAZUR P, KOSHIMOTO C. 2002. Is intracellular ice formation the cause of death of mouse sperm frozen at high cooling rates? *Biology of Reproduction* 66: 1485–1490.

MCCANN MC, ROBERTS K. 1991. Architecture of the primary cell wall. IN: LLOYD CW. *The Cytoskeletal Basis of Plant Growth* 109–129. Academic Press, London.

MCCANN MC, WELLS B, ROBERTS K. 1990. Direct visualisation of cross-links in the primary plant cell wall. *Journal of Cell Science* 96: 323–334.

MCCARTNEY L, MARCUS SE, KNOX JP. 2005. Monoclonal antibodies to plant cell wall xylans and arabinoxylans. *The Journal of Histochemistry and Cytochemistry* 53: 543–546.

MCCARTNEY L, ORMEROD AP, GIDLEY MJ, KNOX JP. 2000. Temporal and spatial regulation of pectic (1→4)-β-d-galactan in cell walls of developing pea cotyledons: implications for mechanical properties. *The Plant Journal* 22: 105–113.

MCCULLY ME, CANNY MJ, HUANG CX. 2004. The management of extracellular ice by petioles of frost-resistant herbaceous plants. *Annals of Botany* 94: 665–674.

MCNEIL M, DARVILL AG, FRY SC, ALBERSHEIM P. 1984. Structure and function of the primary cell walls of plants. *Annual Review of Biochemistry* 53: 625–663.

MCQUEEN-MASON SJ, DURACHKO DM, COSGROVE DJ. 1992. Two endogenous proteins that induce cell wall extension in plants. *The Plant Cell* 4: 1425–1433.

MELTON LD, SMITH BG, IBRAHIM R, SCHRÖDER R. 2009. Mannans in primary and secondary plant cell walls. *New Zealand Journal of Forestry Science* 39: 153–160.

MERKOUROPOULOS G, BARNETT DC, SHIRSAT AH 1999. The *Arabidopsis* extensin gene is developmentally regulated, is induced by wounding, methyl jasmonate, abscisic and salicylic acid, and codes for a protein with unusual motifs. *Planta* 208: 212–219.

MERKOUROPOULOS G, SHIRSAT AH. 2003. The unusual *Arabidopsis* extensin gene *EXT1* is expressed throughout plant development and is induced by a variety of biotic and abiotic stresses. *Planta* 217: 356–366.

MERLOT S, MUSTILLI A-C, GENTY B, NORTH H, LEFEBVRE V, SOTTA B, VAVASSEUR A, GIRAUDAT J. 2002. Use of infrared thermal imaging to isolate *Arabidopsis* mutants defective in stomatal regulation. *The Plant Journal* 30: 601–609.

MEYERHOFF O, MÜLLER K, ROELFSEMA MRG, LATZ A, LACOMBE R, HEDRICH R, BECKER D. 2005. *At*GLR3.4, a glutamate receptor channel-like gene is sensitive to touch and cold. *Planta* 222: 418–427.

MILANI P, GHOLAMIRAD M, TRAAS J, ARNÉODO A, BOUDAOUD A, ARGOUL F, HAMANT O. 2011. *In vivo* analysis of local wall stiffness at the shoot apical meristem in *Arabidopsis* using atomic force microscopy. *The Plant Journal* 67: 1116–1123.

MIURA K, JIN JB, LEE J, YOO CY, STIRM V, MIURA T, ASHWORTH EN, BRESSAN RA, YUN D-J, HASEGAWA PM. 2007. SIZ1-mediated sumoylation of ICE1 controls *CBF3/DREB1A* expression and freezing tolerance in *Arabidopsis*. *The Plant Cell* 19: 1403–1414.

MOELLERING ER, MUTHAN B, BENNING C. 2010. Freezing tolerance in plants requires lipid remodelling at the outer chloroplast membrane. *Science* 330: 226–228.

MOFFAT CS, INGLE RA, WATHUGALA DL, SAUNDERS NJ, KNIGHT H, KNIGHT MR. 2012. ERF5 and ERF6 play redundant roles as positive regulators of JA/Et-mediated defense against *Botrytis cinerea* in *Arabidopsis*. *PLoS ONE* 7: e35995.

MOHNEN D. 1999. Biosynthesis of pectins and galactomannans. IN: BARTON D, NAKANISHI K, METH-COHN O. *Comprehensive Natural Products Chemistry* 3: 497–527. Elsevier Science, Amsterdam.

MOHNEN D. 2008. Pectin structure and biosynthesis. *Current Opinion in Plant Biology* 11: 266–277.

MOLLER I, MARCUS SE, HAEGER A, VERHERTBRUGGEN Y, VERHOEF R, SCHOLS H, ULVSKOV P, MIKKELSEN JD, KNOX JP, WILLATS WGT. 2008. High-throughput screening of monoclonal antibodies against plant cell wall glycans by hierarchical clustering of their carbohydrate microarray binding profiles. *Glycoconjugate Journal* 25: 37–48.

MOLLER I, SØRENSEN I, BERNAL AJ, BLAUKOPF C, LEE K, ØBRO J, PETTOLINO F, ROBERTS A, MIKKELSEN JD, KNOX JP, BACIC A, WILLATS WGT. 2007.

High-throughput mapping of cell-wall polymers within and between plants using novel microarrays. *The Plant Journal* 50: 1118–1128.

MONK LS, FAGERSTEDT KV, CRAWFORD RM. 1989. Oxygen toxicity and superoxide dismutase as an antioxidant in physiological stress. *Physiologia Plantarum* 76: 456–459.

MOOR H. 1960. Reaktionsweisen der Pflanzen auf Kälteeinflüsse. *Z. Schweiz. Forstv* 30: 211–222.

MOORE JP, FARRANT JM, DRIOUICH A. 2008a. A role for pectin-associated arabinans in maintaining the flexibility of the plant cell wall during water deficit stress. *Plant Signalling & Behaviour* 3: 102–104.

MOORE JP, VICRÉ-GIBOUIN M, FARRANT JM, DRIOUICH A. 2008b. Adaptations of higher plant cell walls to water loss: drought vs desiccation. *Physiologia Plantarum* 134: 237–245.

MOUILLE G, RALET M-C, CAVELIER C, ELAND C, EFFROY D, HÉMATY K, MCCARTNEY L, TRUONG HN, GAUDON V, THIBAULT J-F, MARCHANT A, HÖFTE H. 2007. Homogalacturonan synthesis in *Arabidopsis thaliana* requires a Golgi-localized protein with a putative methyltransferase domain. *The Plant Journal* 50: 605–614.

MOULY A, RUMEAU D, ESQUERRÉ-TUGAYÉ M-T. 1992. Differential accumulation of hydroxyproline-rich glycoprotein transcripts in sunflower plants infected with *Sclerotinia sclerotiorum* or treated with oxalic acid. *Plant Science* 85: 51–59.

MUELLER SC, BROWN RM. 1980. Evidence for an intramembrane component associated with a cellulose microfibril-synthesizing complex in higher-plants. *Journal of Cell Biology* 84: 315–326.

MÜLLER GV, REPINALDO CRR, ARANEO DC. 2017. Extreme cold events in South America analysed from a GFDL model perspective: comparison between CMIP3 and CMIP5 climate scenarios. *Theoretical and Applied Climatology* 134: 453–466.

MURAI M, YOSHIDA S. 1998. Evidence for the cell wall involvement in temporal changes in freezing tolerance of Jerusalem artichoke (*Helianthus tuberosus* L.) tubers during cold acclimation. *Plant & Cell Physiology* 39: 97–105.

MURASHIGE T, SKOOG F. 1962. A revised medium for rapid growth and bio assays with tobacco tissue cultures. *Physiologia Plantarum* 15: 473–497.

MURATA N, ISHIZAKI-NISHIZAWA O, HIGASHI S, HAYASHI H, TASAKA Y, NISHIDA I. 1992. Genetically engineered alteration in the chilling sensitivity of plants. *Nature* 356: 710–713.

MURATA N, LOS DA. 1997. Membrane fluidity and temperature perception. *Plant Physiology* 115: 875.

NAFISI M, STRANNE M, FIMOGNARI L, ATWELL S, MARTENS HJ, PEDAS PR, HANSEN SF, NAWRATH C, SCHELLER HV, KLIEBENSTEIN DJ, SAKURAGI Y. 2015. Acetylation of cell wall is required for structural integrity of the leaf surface and exerts a global impact on plant stress responses. *Frontiers in Plant Science* 6: 550.

NANJO T, KOBAYASHI M, YOSHIBA Y, KAKUBARI Y, YAMAGUCHI-SHINOZAKI K, SHINOZAKI K. 1999. Antisense suppression of proline degradation improves tolerance to freezing and salinity in *Arabidopsis thaliana*. *FEBS Letters* 461: 205–210.

NDEH D, ROGOWSKI A, CARTMELL A, LUIS AS, BASLÉ A, GRAY J, VENDITTO I, BRIGGS J, ZHANG X, LABOUREL A, TERRAPON N, BUFFETTO F, NEPOGODIEV S, XIAO Y, FIELD RA, ZHU Y, O'NEILL MA, URBANOWICZ BR, YORK WS, DAVIES GJ, ABBOTT DW, RALET M-C, MARTENS EC, HENRISSAT B, GILBERT HJ. 2017. Complex pectin metabolism by gut bacteria reveals novel catalytic functions. *Nature* 544: 65–70.

NEUNER G. 2014. Frost resistance in alpine woody plants. *Frontiers in Plant Science* 5: 654.

NISHITANI K, TOMINAGA R. 1992. Endoxyloglucan transferase, a novel class of glycosyltransferase that catalyzes transfer of a segment of xyloglucan molecule to another xyloglucan molecule. *Journal of Biological Chemistry* 267: 21058–21064.

NISHIYAMA Y. 2009. Structure and properties of the cellulose microfibril. *Journal of Wood Science* 55: 241–249.

NOVILLO F, ALONSO JM, ECKER JR, SALINAS J. 2004. CBF2/DREB1C is a negative regulator of *CBF1/DREB1B* and *CBF3/DREB1A* expression and plays a central role in stress tolerance in *Arabidopsis*. *Proceedings of the National Academy of Sciences* 101: 3985–3990.

NOVILLO F, MEDINA J, SALINAS J. 2007. *Arabidopsis* CBF1 and CBF3 have a different function than CBF2 in cold acclimation and define different gene classes in the *CBF* regulon. *Proceedings of the National Academy of Sciences* 104: 21002–21007.

NUÑEZ A, FISHMAN ML, FORTIS LL, COOKE PH, HOTCHKISS AT Jr. 2009. Identification of extensin protein associated with sugar beet pectin. *Journal of Agricultural and Food Chemistry* 57: 10951–10958.

OAKENFULL RJ, BAXTER R, KNIGHT MR. 2013. A C-repeat binding factor transcriptional activator (CBF/DREB1) from European bilberry (*Vaccinium myrtillus*) induces freezing tolerance when expressed in *Arabidopsis thaliana*. *PLoS ONE* 8: e54119.

ODEPA (Oficina de Estudios y Políticas Agrarias). 2013. Effect of September frosts on fruit trees and vegetables between the Coquimbo and Maule regions. *Chilean Government Agricultural Ministry* 39.

OKIE W, BECKMAN T, REIGHARD G, NEWALL W, GRAHAM C, WERNER D, POWELL A, KREWER G. 1998. Spring freeze damage to the 1996 peach and nectarine crop in the southeastern United States. *HortTechnology* 8: 381–386.

OLIEN CR. 1974. Energies of freezing and frost desiccation. *Plant Physiology* 53: 764–767.

OLIEN CR. 1984. An adaptive response of rye to freezing. *Crop Science* 24: 51–54.

OLIVEIRA DM, MOTA TR, SALATTA FV, SINZKER RC, KONČITÍKOVÁ R, KOPEČNÝ D, SIMISTER R, SILVA M, GOEMINNE G, MORREEL K, RENCORET J, GUTIÉRREZ A, TRYFONA T, MARCHIOSI R, DUPREE P,

DEL RÍO JC, BOERJAN W, MCQUEEN-MASON SJ, GOMEZ LD, FERRARESE-FILHO O, DOS SANTOS WD. 2020. Cell wall remodeling under salt stress: insights into changes in polysaccharides, feruloylation, lignification, and phenolic metabolism in maize. *Plant, Cell & Environment* 43: 2171–2191.

O'NEILL MA, ALBERSHEIM P, DARVILL A. 1990. The pectic polysaccharides of primary cell walls. IN: DEY PM. *Methods in Plant Biochemistry* 2: 415–441. Academic Press, London.

O'NEILL MA, EBERHARD S, ALBERSHEIM P, DARVILL AG. 2001. Requirement of borate cross-linking of cell wall rhamnogalacturonan II for *Arabidopsis* growth. *Science* 294: 846–849.

O'NEILL MA, WARRENFELTZ D, KATES K, PELLERIN P, DOCO T, DARVILL AG, ALBERSHEIM P. 1996. Rhamnogalacturonan-II, a pectic polysaccharide in the walls of growing plant cell, forms a dimer that is covalently cross-linked by a borate ester. *In vitro* conditions for the formation and hydrolysis of the dimer. *Journal of Biological Chemistry* 271: 22923–22930.

ÖRVAR BL, SANGWAN V, OMANN F, DHINDSA R. 2000. Early steps in cold sensing by plant cells: the role of actin cytoskeleton and membrane fluidity. *The Plant Journal* 23: 785–794.

OSORIO S, CASTILLEJO C, QUESADA MA, MEDINA-ESCOBAR N, BROWNSEY GJ, SUAU R, HEREDIA A, BOTELLA MA, VALPUESTA V. 2008. Partial demethylation of oligogalacturonides by pectin methyl esterase 1 is required for eliciting defence responses in wild strawberry (*Fragaria vesca*). *The Plant Journal* 54: 43–55.

PABST M, FISCHL RM, BRECKER L, MORELLE W, FAULAND A, KÖFELER H, ALTMANN F, LÉONARD R. 2013. Rhamnogalacturonan II structure shows variation in the side chains monosaccharide composition and methylation status within and across different plant species. *The Plant Journal* 76: 61–72.

PAGTER M, ARORA R. 2013. Winter survival and deacclimation of perennials under warming climate: physiological perspectives. *Physiologia Plantarum* 147: 75–87.

PALIN R, GEITMANN A. 2012. The role of pectin in plant morphogenesis. *Biosystems* 109: 397–402.

PANTER PE. 2018. Exploring the role of cell-wall pectin cross-linking in freezing tolerance and guard cell dynamics in *Arabidopsis thaliana*. PhD Thesis, Durham University.

PANTER PE, KENT O, DALE M, SMITH SJ, SKIPSEY M, THORLBY G, CUMMINS I, RAMSAY N, BEGUM RA, SANHUEZA D, FRY SC, KNIGHT MR, KNIGHT H. 2019. MUR1-mediated cell-wall fucosylation is required for freezing tolerance in *Arabidopsis thaliana*. *New Phytologist* 224: 1518–1531.

PAPAGIANNAKI K, LAGOUVARDOS K, KOTRONI V, PAPAGIANNAKIS G. 2014. Agricultural losses related to frost events: use of the 850 hPa level temperature as an explanatory variable of the damage cost. *Natural Hazards and Earth System Sciences* 14: 2375–2386.

PARK S, LEE CM, DOHERTY CJ, GILMOUR SJ, KIM Y, THOMASHOW MF. 2015. Regulation of the *Arabidopsis* CBF regulon by a complex low-temperature regulatory network. *The Plant Journal* 82: 193–207

PARKER L, PATHAK T, OSTOJA S. 2021. Climate change reduces frost exposure for high-value California orchard crops. *Science of The Total Environment* 762: 143971.

PARROTTA L, FALERI C, GUERRIERO G, CAI G. 2019. Cold stress affects cell wall deposition and growth pattern in tobacco pollen tubes. *Plant Science* 329–342.

PASSIOURA J, FRY SC. 1992. Turgor and cell expansion: beyond the Lockhart equation. *Journal of Functional Plant Biology* 19: 565–576.

PAULY M, GILLE S, LIU L, MANSOORI N, DE SOUZA A, SCHULTIK A, XIONG G. 2013. Hemicellulose biosynthesis. *Planta* 238: 627–642.

PAULY M, KEEGSTRA K. 2016. Biosynthesis of the plant cell wall matrix polysaccharide xyloglucan. *Annual Review of Plant Biology* 67: 235–259.

PAULY M, SCHELLER HV. 2000. *O*-Acetylation of plant cell wall polysaccharides: identification and partial characterization of a rhamnogalacturonan *O*-acetyl-transferase from potato suspension-cultured cells. *Planta* 210: 659–667.

PEAR JR, KAWAGOE Y, SCHRECKENGOST WE, DELMER DP, STALKER DM. 1996. Higher plants contain homologs of the bacterial *celA* genes encoding the catalytic subunit of cellulose synthase. *Proceedings of the National Academy of Sciences* 93: 12637–12642.

PEARCE RS. 1988. Extracellular ice formation and cell shape in frost-stressed cereal leaves: a low-temperature scanning-electron-microscopy study. *Planta* 175: 313–324.

PEARCE RS. 2001. Plant freezing and damage. *Annals of Botany* 87: 417–424.

PEARCE RS, ASHWORTH EN. 1992. Cell shape and localisation of ice in leaves of overwintering wheat during frost stress in the field. *Planta* 188: 324–331.

PEARCE RS, FULLER MP. 2001. Freezing of barley studied by infrared video thermography. *Plant Physiology* 125: 227–240.

PEARCE RS, WILLISON J. 1985. A freeze-etch study of the effects of extracellular freezing on cellular membranes of wheat. *Planta* 163: 304-316

PEAUCELLE A, BRAYBROOK SA, LE GUILLOU L, BRON E, KUHLEMEIER C, HÖFTE H. 2011. Pectin-induced changes in cell wall mechanics underlie organ initiation in *Arabidopsis*. *Current Biology* 21: 1720–1726.

PEAUCELLE A, LOUVET R, JOHANSEN JN, HÖFTE H, LAUFS P, PELLOUX J, MOUILLE G. 2008. *Arabidopsis* phyllotaxis is controlled by the methyl-esterification status of cell-wall pectins. *Current Biology* 18: 1943–1948.

PEAUCELLE A, WIGHTMAN R, HAAS KT. 2020. Multicolor 3D-dSTORM reveals native-state ultrastructure of polysaccharides' network during plant cell wall assembly. *iScience* 23: 101862.

PELLOUX J, RUSTÉRUCCI C, MELLEROWICZ EJ. 2007. New insights into pectin methylesterase structure and function. *Trends in Plant Science* 12: 267–277.

PEÑA MJ, CARPITA NC. 2004. Loss of highly branched arabinans and debranching of rhamnogalacturonan I accompany loss of firm texture and cell separation during prolonged storage of apple. *Plant Physiology* 135: 1305–1313.

PEÑA MJ, RYDEN P, MADSON M, SMITH AC, CARPITA NC. 2004. The galactose residues of xyloglucan are essential to maintain mechanical strength of the primary cell walls in *Arabidopsis* during growth. *Plant Physiology* 134: 443–451.

PERRIN RM. 2003. Analysis of xyloglucan fucosylation in *Arabidopsis*. *Plant Physiology* 132: 768–778.

PERSSON S, PAREDEZ A, CARROLL A, PALSDOTTIR H, DOBLIN M, POINDEXTER P, KHITROV N, AUER M, SOMERVILLE CR. 2007. Genetic evidence for three unique components in primary cell-wall cellulose synthase complexes in *Arabidopsis*. *Proceedings of the National Academy of Sciences* 104: 15566–15571.

PHILIPPE F, PELLOUX J, RAYON C. 2017. Plant pectin acetylesterase structure and function: new insights from bioinformatic analysis. *BMC Genomics* 18: 1–18.

PHYO P, WANG T, KIEMLE SN, O'NEILL H, PINGALI SV, HONG M, COSGROVE DJ. 2017. Gradients in wall mechanics and polysaccharides along growing inflorescence stems. *Plant Physiology* 175: 1593–1607.

PIRO G, LEUCCI MR, WALDRON K, DALESSANDRO G. 2003. Exposure to water stress causes changes in the biosynthesis of cell wall polysaccharides in roots of wheat cultivars varying in drought tolerance. *Plant Science* 165: 559–569.

PLIETH C, HANSEN U-P, KNIGHT H, KNIGHT MR. 1999. Temperature sensing by plants: the primary characteristics of signal perception and calcium response. *The Plant Journal* 18: 491–497.

PROBINE MC, PRESTON RD. 1961. Cell growth and the structure and mechanical properties of the wall in internodal cells of *Nitella opaca*: I. Wall structure and growth. *Journal of Experimental Botany* 12: 261–282.

QI X, BEHRENS BX, WEST PR, MORT AJ. 1995. Solubilization and partial characterization of extensin fragments from cell walls of cotton suspension cultures: evidence for a covalent cross-link between extensin and pectin. *Plant Physiology* 108: 1691–1701.

QU T, LIU R, WANG W, AN L, CHEN T, LIU G, ZHAO Z. 2011. Brassinosteroids regulate pectin methylesterase activity and *AtPME41* expression in *Arabidopsis* under chilling stress. *Cryobiology* 63: 111-117.

RAIOLA A, LIONETTI V, ELMAGHRABY I, IMMERZEEL P, MELLEROWICZ EJ, SALVI G, CERVONE F, BELLINCAMPI D. 2011. Pectin methylesterase is induced in *Arabidopsis* upon infection and is necessary for a successful colonization by necrotrophic pathogens. *Molecular Plant-Microbe Interactions* 24: 432–440.

RAJASHEKAR CB. 1997. Cell tension and cavitation in plants during freezing. IN: LI PH, CHEN THH. *Plant Cold Hardiness* 271–280. Springer, New York.

RAJASHEKAR CB, BURKE MJ. 1986. Methods to study the freezing process in plants. *Methods in Enzymology* 127: 761–771.

RAJASHEKAR CB, BURKE MJ. 1996 Freezing characteristics of rigid plant tissues (development of cell tension during extracellular freezing). *Plant Physiology* 111: 597–603.

RAJASHEKAR CB, LAFTA A. 1996. Cell-wall changes and cell tension in response to cold acclimation and exogenous abscisic in leaves and cell cultures. *Plant Physiology* 111: 605–612.

RAPACZ M, ERGON A, HOGLIND M, JORGENSEN M, JURCZYK B, OSTREM L, ROGNLI OA, TRONSMO AM. 2014. Overwintering of herbaceous plants in a changing climate: still more questions than answers. *Plant Science* 225: 34–44.

REDDY A, CALER EV, ANDREWS NW. 2001. Plasma membrane repair is mediated by Ca^{2+}-regulated exocytosis of lysosomes. *Cell* 106: 157–169.

REID JSG. 1985. Cell-wall storage carbohydrates in seeds – biochemistry of the seed 'gums' and 'hemicelluloses'. *Advances in Botanical Research* 11: 125–155.

REITER W-D, CHAPPLE CC, SOMERVILLE CR. 1993. Altered growth and cell walls in a fucose-deficient mutant of *Arabidopsis*. Science 261: 1032–1035.

REITER W-D, CHAPPLE CC, SOMERVILLE CR. 1997. Mutants of *Arabidopsis thaliana* with altered cell-wall polysaccharide composition. *The Plant Journal* 12: 335—345.

REYES-DÍAZ M, ULLOA N, ZÚÑIGA-FEEST A, GUTIÉRREZ A, GIDEKEL M, ALBERDI M, CORCUERA LJ, BRAVO LA. 2006. *Arabidopsis thaliana* avoids freezing by supercooling. *Journal of Experimental Botany* 57: 3687–3696.

RICHMOND TA, SOMERVILLE CR. 2000. The cellulose synthase superfamily. *Plant Physiology* 124: 495–498.

RIDLEY BL, O'NEILL MA, MOHNEN D. 2001. Pectins: structure, biosynthesis, and oligogalacturonide-related signalling. *Phytochemistry* 57: 929–967.

ROBINSON S, HUFLEJT M, DE REUILLE PB, BRAYBROOK SA, SCHORDERET M, REINHARDT D, KUHLEMEIER C. 2017. An automated confocal micro-extensometer enables *in vivo* quantification of mechanical properties with cellular resolution. *The Plant Cell* 29: 2959–2973.

RÖMLING U. 2002. Molecular biology of cellulose production in bacteria. *Research in Microbiology* 153: 205–212.

ROUND AN, RIGBY NM, MACDOUGALL AJ, MORRIS VJ. 2010. A new view of pectin structure revealed by acid hydrolysis and atomic force microscopy. *Carbohydrate Research* 345: 487–497.

RUI Y, ANDERSON CT. 2016. Functional analysis of cellulose and xyloglucan in the walls of stomatal guard cells of *Arabidopsis*. *Plant Physiology* 170: 1398–1419.

RUI Y, XIAO C, YI H, KANDEMIR B, WANG JZ, PURI VM, ANDERSON CT. 2017. POLYGALACTURONASE INVOLVED IN EXPANSION3 functions in seedling development, rosette growth, and stomatal dynamics in *Arabidopsis thaliana*. *The Plant Cell* 29: 2413– 2432.

RUI Y, YI H, KANDEMIR B, WANG JZ, PURI VM, ANDERSON CT. 2016. Integrating cell biology, image analysis, and computational mechanical modeling to analyze the

contributions of cellulose and xyloglucan to stomatal function. *Plant Signalling & Behaviour* 11: e1183086.

RYDEN P, SUGIMOTO-SHIRASU K, SMITH AC, FINDLAY K, REITER W-D, MCCANN MC. 2003. Tensile properties of *Arabidopsis* cell walls depend on both a xyloglucan cross-linked microfibrillar network and rhamnogalacturonan II-borate complexes. *Plant Physiology* 132: 1033–1040.

SAKAI A, LARCHER W. 1987. Frost survival of plants. Springer, Berlin.

SAKAMOTO A, MURATA N. 2002. The role of glycine betaine in the protection of plants from stress: clues from transgenic plants. *Plant, Cell & Environment* 25: 163–171.

SARAGUSTY J, GACITUA H, ROZENBOIM I, ARAV A. 2009. Do physical forces contribute to cryodamage? *Biotechnology and Bioengineering* 104: 719–728.

SCANDALIOS JG. 1993. Oxygen stress and superoxide dismutases. *Plant Physiology* 101: 7.

SCHERRER R, GERHARDT P. 1971. Molecular sieving by the *Bacillus megaterium* cell wall and protoplast. *Journal of Bacteriology* 107: 718–735.

SCHINDELIN J, ARGANDA-CARRERAS I, FRISE E, KAYNIG V, LONGAIR M, PIETZSCH T, PREIBISCH S, RUEDEN C, SAALFELD S, SCHMID B, TINEVEZ J-Y, WHITE DJ, HARTENSTEIN V, ELICEIRI K, TOMANCAK P, CARDONA A. 2012. Fiji: an open-source platform for biological-image analysis. *Nature Methods* 9: 676–682.

SCHNABELRAUCH LS, KIELISZEWSKI MJ, UPHAM BL, ALIZEDEH H, LAMPORT DTA. 1996. Isolation of pl 4.6 extensin peroxidase from tomato cell suspension cultures and identification of Val-Tyr-Lys as putative intermolecular cross-link site. *The Plant Journal* 9: 477–489.

SCHOLZ FG, BUCCI SJ, ARIAS NS, MEINZER FC, GOLDSTEIN G. 2012. Osmotic and elastic adjustments in cold desert shrubs differing in rooting depth: coping with drought and subzero temperatures. *Oecologia* 170: 885–897.

SCHROEDER JI, KWAK JM, ALLEN GJ. 2001. Guard cell abscisic acid signalling and engineering drought hardiness in plants. *Nature* 410: 327–330.

SECHET J, HTWE S, URBANOWICZ B, AGYEMAN A, FENG W, ISHIKAWA T, COLOMES M, KUMAR KS, KAWAI-YAMADA M, DINNENY JR, O'NEILL MA, MORTIMER JC. 2018. Suppression of *Arabidopsis* GGLT1 affects growth by reducing the L-galactose content and borate cross-linking of rhamnogalacturonan-II. *The Plant Journal* 96: 1036–1050.

SEIFERT GJ, ROBERTS K. 2007. The biology of arabinogalactan proteins. *Annual Review of Plant Biology* 58: 137–161.

SEKI S, MAZUR P. 2012. Ultra-rapid warming yields high survival of mouse oocytes cooled to -196°C in dilutions of a standard vitrification solution. *PLoS ONE* 7: e36058.

SÉNÉCHAL F, GRAFF L, SURCOUF O, MARCELO P, RAYON C, BOUTON S, MARECK A, MOUILLE G, STINTZI A, HÖFTE H, LEROUGE P, SCHALLER A, PELLOUX J. 2014. *Arabidopsis* PECTIN METHYLESTERASE17

is co-expressed with and processed by SBT3.5, a subtilisin-like serine protease. *Annals of Botany* 114: 1161–1175.

SHAO HB, LI-YE C, MING-AN S, SHI-QING L, JI-CHENG Y. 2008. Bioengineering plant resistance to abiotic stresses by the global calcium signal system. *Biotechnology Advances* 26: 503–510.

SHI H, YE T, ZHONG B, LIU X, JIN R, CHAN Z. 2014. AtHAP5A modulates freezing stress resistance in *Arabidopsis* through binding to CCAAT motif of AtXTH21. *New Phytologist* 203: 554–567.

SHI Y, DING Y, YANG S. 2015. Cold signal transduction and its interplay with phytohormones during cold acclimation. *Plant & Cell Physiology* 56: 7–15.

SHI Y, HUANG J, SUN T, WANG X, ZHU C, AI Y, GU H. 2017. The precise regulation of different *COR* genes by individual CBF transcription factors in *Arabidopsis thaliana*. *Journal of Integrative Plant Biology* 59: 118–133.

SHOWALTER AM, BELL JN, CRAMER CL, BAILEY JA, VARNER JE, LAMB CJ. 1985. Accumulation of hydroxyproline-rich glycoprotein mRNAs in response to fungal elicitor and infection. *Proceedings of the National Academy of Sciences* 82: 6551–6555.

SHOWALTER AM, KEPPLER BD, LICHTENBERG J, GU D, WELCH LR. 2010. A bioinformatics approach to the identification, classification, and analysis of hydroxyproline-rich glycoproteins. *Plant Physiology* 153: 485–513.

SIMINOVITCH D. 1979. Protoplasts surviving freezing to -196°C and osmotic dehydration in 5 molar salt solutions prepared from the bark of winter black locust trees. *Plant Physiology* 63: 722–725.

SINGH J. 1979. Freezing of protoplasts isolated from cold-hardened and non-hardened winter rye. *Plant Science Letters* 16: 195–201.

SINGLE WV, MARCELLOS H. 1981. Ice formation and freezing injury in actively growing cereals. IN: OLIEN CR, SMITH MN. *Analysis and Improvement of Plant Cold Hardiness*. CRC Press, Boca Raton.

SMALLWOOD M, BEVEN A, DONOVAN N, NEILL SJ, PEART J, ROBERTS K, KNOX JP. 1994. Localization of cell wall proteins in relation to the developmental anatomy of the carrot root apex. *The Plant Journal* 5: 237–246.

SMALLWOOD M, MARTIN H, KNOX JP. 1995. An epitope of rice threonine- and hydroxyproline-rich glycoprotein is common to cell wall and hydrophobic plasma-membrane glycoproteins. *Planta* 196: 510–522.

SMITH JJ, MULDOON EP, LAMPORT DTA. 1984. Isolation of extensin precursors by direct elution of intact tomato cell suspension cultures. *Phytochemistry* 23: 1233–1239.

SOLECKA D, ŻEBROWSKI J, KACPERSKA A. 2008. Are pectins involved in cold acclimation and de-acclimation of winter oil-seed rape plants? *Annals of Botany* 101: 521–530.

SOMERVILLE CR, BAUER S, BRININSTOOL G, FACETTE M, HAMANN T, MILNE J, OSBORNE E, PAREDEZ A, PERSSON S, RAAB T, VORWERK S, YOUNGS

H. 2004. Towards a systems approach to understanding plant cell walls. *Science* 306: 2206–2211.

STEFANOWSKA M, KURAŚ M, KUBACKA-ZEBALSKA M, KACPERSKA A. 1999. Low temperature affects pattern of leaf growth and structure of cell walls in winter oilseed rape (*Brassica napus* L., var. *oleifera* L.). *Annals of Botany* 84: 313–319.

STEGNER M, FLÖRL A, LINDNER J, PLANGGER S, SCHAEFERNOLTE T, STRASSER A-L, THOMA V, WALDE J, NEUNER G. 2022. Freeze dehydration vs. supercooling of mesophyll cells: impact of cell wall, cellular and tissue traits on the extent of water displacement. *Physiologia Plantarum* 174: e13793.

STEINER P, OBWEGESER S, WANNER G, BUCHNER O, LÜTZ-MEINDL U, HOLZINGER A. 2020. Cell wall reinforcements accompany chilling and freezing stress in the streptophyte green alga *Klebsormidium crenulatum. Frontiers in Plant Science* 11: 873.

STEPONKUS PL. 1984. Role of the plasma membrane in freezing injury and cold acclimation. *Annual Review of Plant Physiology* 35: 543–584.

STEPONKUS PL, GARBER MP, MYERS SP, LINEBERGER RD. 1977. Effects of cold acclimation and freezing on structure and function of chloroplast thylakoids. *Cryobiology* 14: 303.

STEPONKUS PL, LYNCH DV. 1989. Freeze/thaw-induced destabilization of the plasma membrane and the effects of cold acclimation. *Journal of Bioenergetics and Biomembranes* 21: 21–41.

STEPONKUS PL, UEMURA M, JOSEPH RA, GILMOUR SJ, THOMASHOW MF. 1998. Mode of action of the *COR15a* gene on the freezing tolerance of *Arabidopsis thaliana. Proceedings of the National Academy of Sciences* 95: 14570–14575.

STEPONKUS PL, UEMURUA M, WEBB MS. 1993. The contrast of cryostability of the plasma membrane of winter rye and spring oat - two species that widely differ in their freezing tolerance and plasma membrane lipid composition. IN: STEPONKUS PL. *Advances in Low Temperature Biology* 2: 211–312. JAI Press, London.

STERLING JD, ATMODJO MA, INWOOD SE, KOLLI VSK, QUIGLEY HF, HAHN MG, MOHNEN D. 2006. Functional identification of an *Arabidopsis* pectin biosynthetic homogalacturonan galacturonosyltransferase. *Proceedings of the National Academy of Sciences* 103: 5236–5241.

STERLING JD, QUIGLEY HF, ORELLANA A, MOHNEN D. 2018. The catalytic site of the pectin biosynthetic enzyme α-1,4-galacturonosyltransferase is located in the lumen of the Golgi. *Plant Physiology* 127: 360–371.

STICKLEN M. 2008. Plant genetic engineering for biofuel production: towards affordable cellulosic ethanol. *Nature Reviews Genetics* 9: 433.

STITT M, HURRY V. 2002. A plant for all seasons: alterations in photosynthetic carbon metabolism during cold acclimation in *Arabidopsis. Current Opinion in Plant Biology* 5: 199–206.

STOCKINGER EJ, GILMOUR SJ, THOMASHOW MF. 1997. *Arabidopsis thaliana CBF1* encodes an AP2 domain-containing transcriptional activator that binds to the C-

repeat/DRE, a *cis*-acting DNA regulatory element that stimulates transcription in response to low temperature and water deficit. *Proceedings of the National Academy of Sciences* 94: 1035–1040.

STOUT DG, MAJAK W, REANEY M. 1980. *In vivo* detection of membrane injury at freezing temperatures. *Plant Physiology* 66: 74–77.

STRANNE M, REN Y, FIMOGNARI L, BIRDSEYE D, YAN J, BARDOR M, MOLLET J-C, KOMATSU T, KIKUCHI J, SCHELLER HV, SAKURAGI Y. 2018. *TBL10* is required for *O*-acetylation of pectic rhamnogalacturonan-I in *Arabidopsis thaliana*. *The Plant Journal* 96: 772–785.

STRAUSS G, HAUSER H. 1986. Stabilization of lipid bilayer vesicles by sucrose during freezing. *Proceedings of the National Academy of Sciences* 83: 2422–26.

SU F, JACQUARD C, VILLAUME S, MICHEL J, RABENOELINA F, CLÉMENT C, BARKA EA, DHONDT-CORDELIER, VAILLANT-GAVEAU N. 2015. *Burkholderia phytofirmans PsJN* reduces impact of freezing temperatures on photosynthesis in *Arabidopsis thaliana*. *Frontiers in Plant Science* 6: 810.

SUBRAMANIAN P, MAGESWARI A, KIM K, LEE Y, SA T. 2015. Psychrotolerant endophytic *Pseudomonas* sp. strains OB155 and OS261 induced chilling resistance in tomato plants (*Solanum lycopersicum* Mill.) by activation of their antioxidant capacity. *Molecular Plant-Microbe Interactions* 28: 1073–1081.

TAJI T, OHSUMI C, IUCHI S, SEKI M, KASUGA M, KOBAYASHI M, YAMAGUCHI-SHINOZAKI K, SHINOZAKI K. 2002. Important roles of drought- and cold-inducible genes for galactinol synthase in stress tolerance in *Arabidopsis thaliana*. *The Plant Journal* 29: 417–426.

TAKAHASHI D, GORKA M, ERBAN A, GRAF A, KOPKA J, ZUTHER E, HINCHA DK. 2019. Both cold and sub-zero acclimation induce cell wall modification and changes in the extracellular proteome in *Arabidopsis thaliana*. *Scientific Reports* 9: 2298.

TAKAHASHI D, JOHNSON KL, HAO P, TUONG T, ERBAN A, SAMPATHKUMAR A, BACIC A, LIVINGSTON DP, KOPKA J, KUROHA T, YOKOYAMA R, NISHITANI K, ZUTHER E, HINCHA DK. 2021a. Cell wall modification by the xyloglucan endotransglucosylase/hydrolase XTH19 influences freezing tolerance after cold and sub-zero acclimation. *Plant, Cell & Environment* 44: 915–930.

TAKAHASHI D, LI B, NAKAYAMA T, KAWAMURA Y, UEMURA M. 2013. Plant plasma membrane proteomics for improving cold tolerance. *Frontiers in Plant Science* 4: 90.

TAKAHASHI D, WILLICK IR, KASUGA J, LIVINGSTON DP. 2021b. Responses of the plant cell wall to sub-zero temperatures: a brief update. *Plant & Cell Physiology* 62: 1858–1866.

TANINO KK, CHEN THH, FUCHIGAMI LH, WEISER CJ. 1990. Metabolic alterations associated with abscisic acid-induced frost hardiness in bromegrass suspension culture cells. *Plant & Cell Physiology* 31: 505–511.

TANINO KK, KOBAYASHI S, HYETT C, HAMILTON K, LIU J, LI B, BORONDICS F, PEDERSEN T, TSE J, ELLIS T, KAWAMURA Y, UEMURA M. 2013. *Allium fistulosum* as a novel system to investigate mechanisms of freezing resistance. *Physiologia Plantarum* 147: 101–111.

TAO D-L, LI PH, CARTER JV. 1983. Role of cell wall in freezing tolerance of cultured potato cells and their protoplasts. *Physiologia Plantarum* 58: 527–532.

TAO D-L, ÖQUIST G, WINGSLE G. 1998. Active oxygen scavengers during cold acclimation of Scots pine seedlings in relation to freezing tolerance. *Cryobiology* 37: 38–45.

TAYLOR NG, HOWELLS RM, HUTTLY AK, VICKERS K, TURNER SR. 2003. Interactions among three distinct CesA proteins essential for cellulose synthesis. *Proceedings of the National Academy of Sciences* 100: 1450–1455.

TENHAKEN R. 2015. Cell wall remodeling under abiotic stress. *Frontiers in Plant Science* 5: 771.

THIBAULT J-F, RENARD CMGC, AXELOS MAV, ROGER P, CREPEAU MJ. 1993. Studies of the length of homogalacturonic regions in pectins by acid-hydrolysis. *Carbohydrate Research* 238: 271–286.

THOMASHOW MF. 1999. Plant cold acclimation: freezing tolerance genes and regulatory mechanisms. *Annual Review of Plant Physiology and Plant Molecular Biology* 50: 571–599.

THOMPSON JE, FRY SC. 2000. Evidence for covalent linkage between xyloglucan and acidic pectins in suspension-cultured rose cells. *Planta* 211: 275–286.

THONAR C, LINERS F, VAN CUTSEM P. 2006. Polymorphism and modulation of cell wall esterase enzyme activities in the chicory root during the growing season. *Journal of Experimental Botany* 57: 81–89.

THORLBY G, VEALE E, BUTCHER K, WARREN G. 1999. Map positions of *SFR* genes in relation to other freezing-related genes of *Arabidopsis thaliana*. *The Plant Journal* 17: 445–452.

TITEL C, WOEHLECKE H, AFIFI I, EHWALD R. 1997. Dynamics of limiting cell wall porosity in plant suspension cultures. *Planta* 203: 320–326.

TYREE MT, DIXON MA. 1986. Water stress induced cavitation and embolism in some woody plants. *Physiologia Plantarum* 66: 397–405.

TYREE MT, SPERRY JS. 1989. Vulnerability of xylem to cavitation and embolism. *Annual Review of Plant Physiology and Plant Molecular Biology* 40: 19–38.

UEMURA M, JOSEPH RA, STEPONKUS PL. 1995. Cold acclimation of *Arabidopsis thaliana* (effect on plasma membrane lipid composition and freeze-induced lesions). *Plant Physiology* 109: 15–30.

ULVSKOV P, WIUM H, BRUCE D, JØRGENSEN B, QVIST KB, SKJØT M, HEPWORTH D, BORKHARDT B, SØRENSEN SO. 2005. Biophysical consequences of remodeling the neutral side chains of rhamnogalacturonan I in tubers of transgenic potatoes. *Planta* 220: 609–620.

UNTERGASSER A, NIJVEEN H, RAO X, BISSELING T, GEURTS R, LEUNISSEN JAM. 2007. Primer3Plus, an enhanced web interface to Primer3. *Nucleic Acids Research* 35: W71–W74.

VANZIN GF, MADSON M, CARPITA NC, RAIKHEL NV, KEEGSTRA K, REITER W-D. 2002. The *mur2* mutant of *Arabidopsis thaliana* lacks fucosylated xyloglucan because of a lesion in fucosyltransferase *AtFUT1*. *Proceedings of the National Academy of Sciences* 99: 3340–3345.

VARKI A, CUMMINGS RD, AEBI M, PACKER NH, SEEBERGER PH, ESKO JD, STANLEY P, HART G, DARVILL A, KINOSHITA T. 2015. Symbol nomenclature for graphical representations of glycans. *Glycobiology* 25: 1323–1324.

VELASQUEZ SM, RICARDI MM, DOROSZ JG, FERNANDEZ PV, NADRA AD, POL-FACHIN L, EGELUND J, GILLE S, CIANCIA M, VERLI H, PAULY M, BACIC A, OLSEN CE, ULVSKOV P, PETERSEN BL, SOMERVILLE CR, IUSEM ND. 2011. *O*-glycosylated cell wall extensins are essential in root hair growth. *Science* 332: 1401–1403.

VERGER S, CHABOUT S, GINEAU E, MOUILLE G. 2016. Cell adhesion in plants is under the control of putative *O*-fucosyltransferases. *Development* 143: 2536–2540.

VERHERTBRUGGEN Y, MARCUS SE, HAEGER A, ORDAZ-ORTIZ JJ, KNOX JP. 2009a. An extended set of monoclonal antibodies to pectic homogalacturonan. *Carbohydrate Research* 344: 1858–1862.

VERHERTBRUGGEN Y, MARCUS SE, HAEGER A, VERHOEF R, SCHOLS HA, MCCLEARY BV, MCKEE L, GILBERT HJ, KNOX JP. 2009b. Developmental complexity of arabinan polysaccharides and their processing in plant cell walls. *The Plant Journal* 59: 413–425.

VERSLUES PE, AGARWAL M, KATIYAR-AGARWAL S, ZHU JH, ZHU J-K. 2006. Methods and concepts in quantifying resistance to drought, salt and freezing, abiotic stresses that affect plant water status. *The Plant Journal* 45: 523–539.

VEYTSMAN BA, COSGROVE DJ. 1998. A model of cell wall expansion based on thermodynamics of polymer networks. *Biophysical Journal* 75: 2240–2250.

VILLOUTA C, WORKMASTER BA, LIVINGSTON DP, ATUCHA A. 2022. Acquisition of freezing tolerance in *Vaccinium macrocarpon* Ait. is a multi-factor process involving the presence of an ice barrier at the bud base. *Frontiers in Plant Science* 13: 891488.

VINCKEN JP, SCHOLS HA, OOMEN RJFJ, MCCANN MC, ULVSKOV P, VORAGEN AGJ, VISSER RGF. 2003. If homogalacturonan were a side chain of rhamnogalacturonan I. Implications for cell wall architecture. *Plant Physiology* 132: 1781–1789.

VOGLER H, DRAEGER C, WEBER A, FELEKIS D, EICHENBERGER C, ROUTIER-KIERZKOWSKA A-L, BOISSON-DERNIER A, RINGLI C, NELSON BJ, SMITH RS. 2013. The pollen tube: a soft shell with a hard core. *The Plant Journal* 73: 617–627.

VOGLER H, FELEKIS D, NELSON BJ, GROSSNIKLAUS U. 2015. Measuring the mechanical properties of plant cell walls. *Plants* 4: 167–182.

VON SCHAEWEN A, STURM A, O'NEILL J, CHRISPEELS MJ. 1993. Isolation of a mutant *Arabidopsis* plant that lacks N-acetyl glucosaminyl transferase I and is unable to synthesize Golgi-modified complex N-linked glycans. *Plant Physiology* 102: 1109–1118.

VYSE K, PAGTER M, ZUTHER E, HINCHA DK. 2019. Deacclimation after cold acclimation—a crucial, but widely neglected part of plant winter survival. *Journal of Experimental Botany* 70: 4595–4604.

WADA H, COMBOS Z, MURATA N. 1990. Enhancement of chilling tolerance of a cyanobacterium by genetic manipulation of fatty acid desaturation. *Nature* 347: 200–203.

WAKABAYASHI K, HOSON T, HUBER DJ. 2003. Methyl de-esterification as a major factor regulating the extent of pectin depolymerization during fruit ripening: a comparison of the action of avocado (*Persea americana*) and tomato (*Lycopersicon esculentum*) polygalacturonases. *Journal of Plant Physiology* 160: 667–673.

WALTERS KR, SERIANNI AS, SFORMO T, BARNES BM, DUMAN JG. 2009. A nonprotein thermal hysteresis-producing xylomannan antifreeze in the freeze-tolerant Alaskan beetle *Upis ceramboides*. *Proceedings of the National Academy of Sciences* 106: 20210–20215.

WANG Y, HOLROYD G, HETHERINGTON AM, NG CK-Y. 2004. Seeing "cool" and "hot" - infrared thermography as a tool for non-invasive, high-throughput screening of *Arabidopsis* guard cell signalling mutants. *Journal of Experimental Botany* 55: 1187–1193.

WANG Y, MORTIMER JC, DAVIS J, DUPREE P, KEEGSTRA K. 2013. Identification of an additional protein involved in mannan biosynthesis. *The Plant Journal* 73: 105–117.

WARINGTON K. 1923. The effect of boric acid and borax on the broad bean and certain other plants. *Annals of Botany* 37: 629–672.

WARREN G, MCKOWN R, MARIN A, TEUTONICO R. 1996. Isolation of mutations affecting the development of freezing tolerance in *Arabidopsis thaliana* (L.) Heynh. *Plant Physiology* 111: 1011–1019.

WEBB MS, UEMURA M, STEPONKUS PL. 1994. A comparison of freezing injury in oat and rye: two cereals at the extremes of freezing tolerance. *Plant Physiology* 104: 467–478.

WEI G, SHIRSAT AH. 2006. Extension over-expression in *Arabidopsis* limits pathogen invasiveness. *Molecular Plant Pathology* 7: 579–592.

WEISER CJ. 1970. Cold resistance and injury in woody plants: knowledge of hardy plant adaptations to freezing stress may help us to reduce winter damage. *Science* 169: 1269-1278.

WEISER CJ, WHITE W. 1964. The relation of tissue desiccation, extreme cold, and rapid temperature fluctuations to winter injury of American arborvitae. *Journal of the American Society for Horticultural Science* 85: 554.

WEISER RL, WALLNER SJ, WADDELL JW. 1990. Cell wall and extensin mRNA changes during cold acclimation of pea seedlings. *Plant Physiology* 93: 1021–1026.

WESLEY-SMITH J, BERJAK P, PAMMENTER NW, WALTERS C. 2014. Intracellular ice and cell survival in cryo-exposed embryonic axes of recalcitrant seeds of *Acer saccharinum*: an ultrastructural study of factors affecting cell and ice structures. *Annals of Botany* 113: 695–709.

WHITNEY SEC, BRIGHAM JE, DARKE AH, REID JSG, GIDLEY MJ 1998. Structural aspects of the interaction of mannan-based polysaccharides with bacterial cellulose. *Carbohydrate Research* 307: 299–309.

WHITNEY SEC, GOTHARD MGE, MITCHELL JT, GIDLEY MJ. 1999. Role of cellulose and xyloglucan in determining the mechanical properties of primary plant cell walls. *Plant Physiology* 121: 657–663.

WIEST SC, STEPONKUS PL. 1978. Freeze-thaw injury to isolated spinach protoplasts and its simulation at above freezing temperatures. *Plant Physiology* 62: 699–705.

WILLATS WGT, MCCARTNEY L, MACKIE W, KNOX JP. 2001a. Pectin: cell biology and prospects for functional analysis. *Plant Molecular Biology* 47: 9–27.

WILLATS WGT, ORFILA C, LIMBERG G, BUCHHOLT HC, VAN ALEBEEK GJ, VORAGEN AG, MARCUS SE, CHRISTENSEN TM, MIKKELSEN JD, MURRAY BS, KNOX JP. 2001b. Modulation of the degree and pattern of methyl-esterification of pectic homogalacturonan in plant cell walls. Implications for pectin methyl esterase action, matrix properties, and cell adhesion. *Journal of Biological Chemistry* 276: 19404–19413.

WILLATS WGT, STEELE-KING CG, MARCUS SE, KNOX JP. 1999. Side chains of pectic polysaccharides are regulated in relation to cell proliferation and cell differentiation. *The Plant Journal* 20: 619–628.

WILLICK IR, TAKAHASHI D, FOWLER DB, UEMURA M, TANINO KK. 2018. Tissue-specific changes in apoplastic proteins and cell wall structure during cold acclimation of winter wheat crowns. *Journal of Experimental Botany* 69: 1221–1234.

WIMMER MA, EICHERT T. 2013. Mechanisms for boron deficiency-mediated changes in plant water relations. *Plant Science* 203: 25–32.

WISNIEWSKI M. 1995. Deep supercooling in woody plants and the role of cell wall structure. IN: LEE RE, WARREN GJ, GUSTA LV. *Biological Ice Nucleation and Its Applications* 163–181. APS Press, Minneapolis.

WISNIEWSKI M, ASHWORTH EN, SCHAFFER K. 1987. The use of lanthanum to characterize cell wall permeability in relation to deep supercooling and extracellular freezing in woody plants. *Protoplasma* 139: 105–116.

WISNIEWSKI M, DAVIS G. 1995. Immunogold localization of pectins and glycoproteins in tissues of peach with reference to deep supercooling. *Trees* 9: 253–260.

WISNIEWSKI M, DAVIS G, SCHAFFER K. 1991. Mediation of deep supercooling of peach and dogwood by enzymatic modifications in cell-wall structure. *Planta* 184: 254–260.

WISNIEWSKI M, FULLER MP. 1999. Ice nucleation and deep supercooling in plants: new insights using infrared thermography. IN: MARGESIN R, SCHINNER F. *Cold-Adapted Organisms: Ecology, Physiology, Enzymology and Molecular Biology* 105–118. Springer, Berlin.

WISNIEWSKI M, FULLER MP, GLENN D, GUSTA L, DUMAN J, GRIFFITH M. 2002a. Extrinsic ice nucleation in plants: what are the factors involved and can they be manipulated? IN: LI PH, PALVA ET. *Plant Cold Hardiness: Gene Regulation and Genetic Engineering*. Kluwer Academic/Plenum Publishers, New York.

WISNIEWSKI M, GLENN DM, FULLER MP. 2002b. Use of a hydrophobic particle film as a barrier to extrinsic ice nucleation in tomato plants. *Journal of the American Society for Horticultural Science* 127: 358–364.

WISNIEWSKI M, GUSTA L, NEUNER G. 2014. Adaptive mechanisms of freeze avoidance in plants: a brief update. *Environmental and Experimental Botany* 99: 133–140.

WISNIEWSKI M, LINDOW SE, ASHWORTH EN. 1997. Observation of ice nucleation and propagation in plants using infrared video thermography. *Plant Physiology* 113: 327–334.

WOEHLECKE H, EHWALD R. 1995. Characterization of size-permeation limits of cell walls and porous separation materials by high-performance size-exclusion chromatography. *Journal of Chromatography A* 708: 263–271.

WOLF R. 2008. The Easter freeze of April 2007: a climatological perspective and assessment of impacts and services. *NOAA Technical Report* 2008-01.

WOLF S, GREINER S. 2012. Growth control by cell wall pectins. *Protoplasma* 249: 169–175.

WORKMASTER BA, PALTA JP, WISNIEWSKI M. 1999. Ice nucleation and propagation in cranberry uprights and fruit using infrared video thermography. *Journal of the American Society for Horticultural Science* 124: 619–625.

WORMIT A, USADEL B. 2018. The multifaceted role of pectin methylesterase inhibitors (PMEIs). *International Journal of Molecular Sciences* 19: 2878.

WU H-C, BULGAKOV VP, JINN T-L. 2018. Pectin methylesterases: cell wall remodeling proteins are required for plant response to heat stress. *Frontiers in Plant Science* 9: 1612.

XI X, KIM SH, TITTMANN B. 2015. Atomic force microscopy based nanoindentation study of onion abaxial epidermis walls in aqueous environment. *Journal of Applied Physics* 117: 024703.

XIAO C, BARNES WJ, ZAMIL MS, YI H, PURI VM, ANDERSON CT. 2016. Activation tagging of *Arabidopsis POLYGALACTURONASE INVOLVED IN EXPANSION2* promotes hypocotyl elongation, leaf expansion, stem lignification, mechanical stiffening, and lodging. *The Plant Journal* 89: 1159–1173.

XIN Z, BROWSE J. 1998. *eskimo1* mutants of *Arabidopsis* are constitutively freezing-tolerant. *Proceedings of the National Academy of Sciences* 95: 7799–7804.

XIN Z, MANDAOKAR A, CHEN J, LAST RR, BROWSE J. 2007. *Arabidopsis ESK1* encodes a novel regulator of freezing tolerance. *The Plant Journal* 49: 786–799.

YAMADA T, KURODA K, JITSUYAMA Y, TAKEZAWA D, ARAKAWA K, FUJIKAWA S. 2002. Roles of the plasma membrane and the cell wall in the responses of plant cells to freezing. *Planta* 215: 770–778.

YAMAZAKI T, KAWAMURA Y, MINAMI A, UEMURA M. 2008. Calcium-dependent freezing tolerance in *Arabidopsis* involves membrane resealing via synaptotagmin SYT1. *The Plant Cell* 20: 3389–3404.

YAN J, HE H, FANG L, ZHANG A. 2018. Pectin methylesterase31 positively regulates salt stress tolerance in *Arabidopsis*. *Biochemical and Biophysical Research Communications* 496: 497–501.

YANG D, LI J, DING Y, TYREE MT. 2017. Experimental evidence for negative turgor pressure in small leaf cells of *Robinia pseudoacacia* L. versus large cells of *Metasequoia glyptostroboides* Hu et W.C. Cheng. 2. Höfler diagrams below the volume of zero turgor and the theoretical implication for pressure-volume curves of living cells. *Plant, Cell & Environment* 40: 340–350.

YANG KA, LIM CJ, HONG JK, PARK CY, CHEONG YH, CHUNG WS, LEE KO, LEE SY, CHO MJ, LIM CO. 2006. Identification of cell wall genes modified by a permissive high temperature in Chinese cabbage. *Plant Science* 171: 175–182.

YATES EA, VALDOR JF, HASLAM SM, MORRIS HR, DELL A, MACKIE W, KNOX JP. 1996. Characterization of carbohydrate structural features recognized by anti-arabinogalactan-protein monoclonal antibodies. *Glycobiology* 6: 131–139.

YE H, DU H, TANG N, LI X, XIONG L. 2009. Identification and expression profiling analysis of TIFY family genes involved in stress and phytohormone responses in rice. *Plant Molecular Biology* 71: 291—305.

YOOYONGWECH S, PHAUKINSANG N, CHA-UM S, SUPAIBULWATANA K. 2013. Arbuscular mycorrhiza improved growth performance in *Macadamia tetraphylla* L. grown under water deficit stress involves soluble sugar and proline accumulation. *Plant Growth Regulation* 69: 285–293.

ZABLACKIS E, HUANG J, MÜLLER B, DARVILL AG, ALBERSHEIM P. 1995. Characterization of the cell-wall polysaccharides of *Arabidopsis thaliana* leaves. *Plant Physiology* 107: 1129–1138.

ZABLACKIS E, YORK WS, PAULY M, HANTUS S, REITER W-D, CHAPPLE CC, ALBERSHEIM P, DARVILL A. 1996. Substitution of L-fucose by L-galactose in cell walls of *Arabidopsis mur1*. *Science* 272: 1808–1810.

ZARAGOTAS D, LIOLIOS NT, ANASTASSOPOULOS E. 2016. Supercooling, ice nucleation and crystal growth: a systematic study in plant samples. *Cryobiology* 72: 239–243.

ZARKA DG, VOGEL JT, COOK D, THOMASHOW MF. 2003. Cold induction of *Arabidopsis CBF* genes involves multiple ICE (inducer of CBF expression) promoter

elements and a cold-regulatory circuit that is desensitised by low temperature. *Plant Physiology* 133: 910–918.

ZELKO IN, MARIANI TJ, FOLZ RJ. 2002. Superoxide dismutase multigene family: a comparison of the CuZn-SOD (SOD1), Mn-SOD (SOD2) and EC-SOD (SOD3) gene structures, evolution and expression. *Free Radical Biology and Medicine* 33: 337–349.

ZERZOUR R, KROEGER J, GEITMANN A. 2009. Polar growth in pollen tubes is associated with spatially confined dynamic changes in cell mechanical properties. *Developmental Biology* 334: 437–446.

ZHANG J, KIRKHAM MB. 1994. Drought-stress-induced changes in activities of superoxide dismutase, catalase, and peroxidase in wheat species. *Plant & Cell Physiology* 35: 785–791.

ZHANG L, PAASCH BC, CHEN J, DAY B, HE SY. 2018. An important role of $_{L}$-fucose biosynthesis and protein fucosylation genes in *Arabidopsis* immunity. *New Phytologist* 222: 981–994.

ZHANG T, TANG H, VAVYLONIS D, COSGROVE DJ. 2019. Disentangling loosening from softening: insights into primary cell wall structure. *The Plant Journal* 100: 1101–1117.

ZHAO C, ZHANG Z, XIE S, SI T, LI Y, ZHU JK. 2016. Mutational evidence for the critical role of CBF transcription factors in cold acclimation in *Arabidopsis*. *Plant Physiology* 171: 2744–2759.

ZHAO J, SHI M, YU J, GUO C. 2022. SPL9 mediates freezing tolerance by directly regulating the expression of *CBF2* in *Arabidopsis thaliana*. *BMC Plant Biology* 22:59.

ZHENG B, CHENU K, FERNANDA DRECCER M, CHAPMAN SC. 2012. Breeding for the future: what are the potential impacts of future frost and heat events on sowing and flowering time requirements for Australian bread wheat (*Triticum aestivium*) varieties? *Global Change Biology* 18: 2899–2914.

ZHOU A, LIU E, LI H, LI Y, FENG S, GONG S, WANG J. 2018. *Ps*Cor413pm2, a plasma membrane-localized, cold-regulated protein from *Phlox subulata*, confers low temperature tolerance in *Arabidopsis*. *International Journal of Molecular Sciences* 19: 2579.

ZHU JJ, BECK E. 1991. Water relations of *Pachysandra* leaves during freezing and thawing: evidence for a negative pressure potential alleviating freeze-dehydration stress. *Plant Physiology* 97: 1146–1153.

ZHU JJ, STEUDLE E, BECK E. 1989. Negative pressures produced in an artificial osmotic cell by extracellular freezing. *Plant Physiology* 91: 1454–1459.

ZHU Y, LI L. 2021. Multi-layered regulation of plant cell wall thickening. *Plant & Cell Physiology* 62: 1867–1873.

ZUO J, NIU Q-W, NISHIZAWA N, WU Y, KOST B, CHUA N-H. 2000. KORRIGAN, an *Arabidopsis* endo-1,4-β-glucanase, localizes to the cell plate by polarized targeting and is essential for cytokinesis. *The Plant Cell* 12: 1137–1153.

ZURLO G, TRUSKINOVSKY L. 2017. Printing non-euclidean solids. *Physical Review Letters* 119: 048001.

APPENDIX A

Genomic primer list.

Name	Gene (accession)	Sequence (5'-3')	Use
PME17-F	*PME17* (AT2G45220)	AGCTGGGTTCTTAGAGCTTGG	Confirming T-DNA insertion in *pme17*
PME17-R		CGACCCGGATCTTAGAGCTAC	
PME31-LP	*PME31* (AT3G29090)	TCAAATTTCACCTAGGTGATTTG	Confirming T-DNA insertion in *pme31*
PME31-RP		CACAACCAAACGTACCAGTCC	
PME41-RT-F	*PME41* (AT4G02330)	TGGACCACTTTCAACTCCG	Measuring gene expression in *pme41* (RT-PCR)
PME41-RT-R		GGTTCAACAACCTCGTCTATG	
EXT18-LP	*EXT18* (AT1G26250)	ATATGTTTACAAGTCCCCGCC	Confirming T-DNA insertion in *ext18*
EXT18-RP		CAACATCAAAAGCAAAAAGCC	
MUR1-F	*MUR1* (AT3G51160)	GGATCAACTCCTCCTCCACA	Confirming nucleotide substitution in *sfr8*
MUR1-R		CCTCTGTTGCCACAACGTAA	
GGLT1-RT-F	*GGLT1* (AT1G76340)	GGAAACGCTTTTCTTGCATC	Measuring gene expression in hp*GGLT1* (qPCR)
GGLT1-RT-R		ACGCAAGAGCCCAGCTATAA	
CESA3-F	*CESA3* (AT5G05170)	GCTAATCGTAATACCGTGTTCTTTGAT	Confirming cDNA insertion in $cesa3^{S211A}$
CESA3-R		AGCGTCGTTGGCGGAATCAGAAGTGTT	
CESA6-F	*CESA6* (AT5G64740)	TTCAGGAGGCAAGCGCTTTA	Confirming nucleotide substitution in *prc1*
CESA6-R		GCTGATCCTTTGAAAGCCGC	
XXT1-LP	*XXT1* (AT3G62720)	GAAATCTCGAGACCGGACTAATAAACCT	Confirming T-DNA insertions in *xxt1* *xxt2*
XXT1-RP		ATCCCCCAATAACCGTGCAAGTAATAA	
XXT2-LP	*XXT2* (AT4G02500)	CCAAAGAGCTTTACGCCAAT	
XXT2-RP		CGCTTGTTAGGTCCGATGAA	
FUT1-F	*FUT1* (AT2G03220)	TCTTGTGACAAGTGCTTGGTCT	Confirming nucleotide substitution in *mur2*
FUT1-R		TGAGACTTTGGTAATAAAAACTCAACC	
MUR3-F	*MUR3* (AT2G20370)	ATGCGATTTTGGGGAGAGCA	Confirming nucleotide substitution in *mur3*
MUR3-R		CGGCCCTCGATCATGTTCTT	
MSR1-LP	*MSR1* (AT3G21190)	CAAGACCTTCCATTTTTGGATC	Confirming T-DNA insertion in *msr1-2*
MSR1-RP		TACAGGATCAGTTTCGCCATC	
PMR5-CAPS-F	*PMR5* (AT5G58600)	CCGTTCTTGGTGGACATAG	Confirming nucleotide substitution in *pmr5*
PMR5-CAPS-R		AGTCACTCGGGCTGATCAAT	
RWA2-F	*RWA2* (AT3G06550)	CACCCTGAATTTCATCTCAGC	Confirming T-DNA insertion in *rwa2*
RWA2-R		TTGAATAGGCATCAAACCGAG	

APPENDIX B

T-DNA and reference gene primer list.

Name	Gene (accession)	Sequence (5'-3')	Use
SALK-LB	T-DNA	CGATTTCGGAACCACCATCAAACAGGA	Confirming T-DNA insertion in *pme17*
LBb1.3		ATTTTGCCGATTTCGGAAC	Confirming T-DNA insertion in *pme31*, *ext18*
LB_3		TAGCATCTGAATTTCATAACCAATCTCGATACAC	Confirming T-DNA insertions in *xxt1 xxt2*
LBb1		GCGTGGACCGCTTGCTGCAACT	
LBa1		TGGTTCACGTAGTGGGCCATCG	Confirming T-DNA insertion in *msr1-2*
LB		ATATTGACCATCATACTCATTGC	Confirming T-DNA insertion in *rwa2*
ACT-F	*ACT-2* (AT3G18780)	GGCTCCTCTTAACCCAAAGG	Reference gene
ACT-R		TTCTCGATGGAAGAGCTGGT	
UBC-F	*UBC30* (AT1G14400)	CAAATCCAAAACCCTAGAAACCGAA	
UBC-R		ATCTCCCGTAGGACCTGCACTG	

APPENDIX C

Genotyping the *pme17* mutant. Genomic DNA was extracted from 10-day old wild-type (Col-0) and *pme17* (SALK_055909) seedlings. PCR and agarose gel electrophoresis were then used to confirm the presence of a T-DNA insertion in *PME17-2* in the mutant.

L: HyperLadder 1kb. 1: Col-0 genomic primers. 2: Col-0 T-DNA primers (F + SALK-LB). 3: Col-0 reference gene primers (*ACT-2*). 4: *pme17* genomic primers. 5: *pme17* T-DNA primers (F + SALK-LB). 6: *pme17* reference gene primers (*ACT-2*).

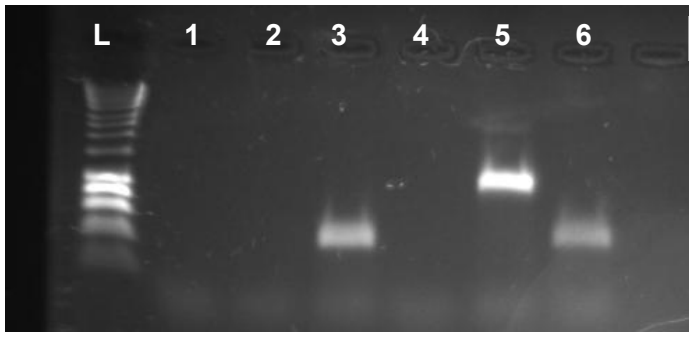

As the reactions in lanes 2 and 3 failed they were repeated separately:

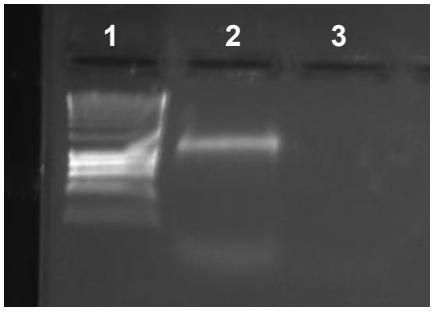

This is confirmation of the correct T-DNA insertion present in the *PME17* coding region in the *pme17* mutant: the T-DNA band is present but the genomic band is not.

APPENDIX D

Genotyping the *pme31* mutant. Genomic DNA was extracted from 10-day old wild-type (Col-0) and *pme31* (SALK_074820) seedlings. PCR and agarose gel electrophoresis were then used to confirm the presence of a T-DNA insertion in *PME31* in the mutant. As the direction of the insertion was unknown, every primer combination was used.

L: HyperLadder 1kb. 1: Col-0 genomic primers. 2: Col-0 T-DNA primers (RP + LBb1.3). 3: Col-0 T-DNA primers (LP + LBb1.3). 4: *pme31* genomic primers. 5: *pme31* T-DNA primers (RP + LBb1.3). 6: *pme31* T-DNA primers (LP + LBb1.3).

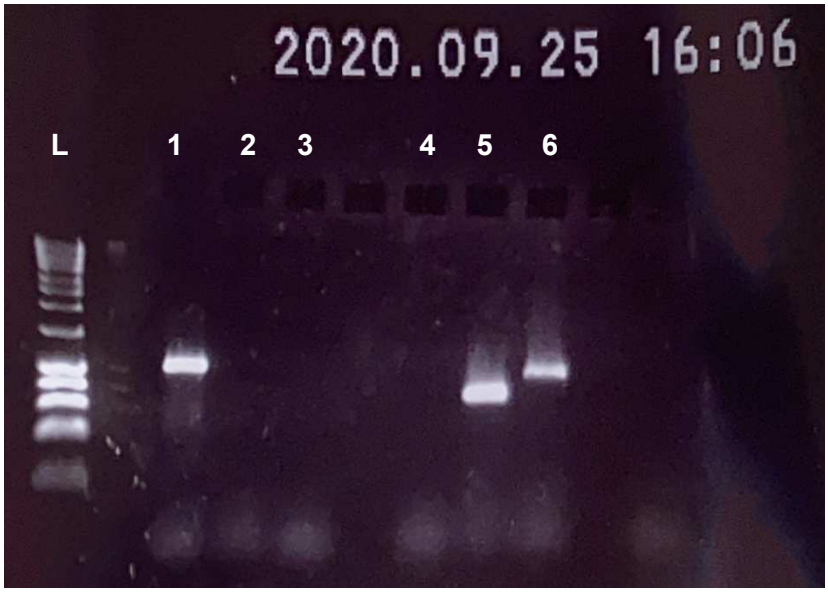

This is confirmation of the correct T-DNA insertion present in the *PME31* coding region in the *pme31* mutant: the T-DNA band is present but the genomic band is not. Both genomic/T-DNA primer combinations worked.

APPENDIX E

Genotyping the *pme41* mutant. Total RNA was extracted from 7-day old wild-type (Col-0) and *pme41* (SALK_008958C). cDNA was synthesised from 1 µg RNA using MMLV reverse transcriptase. PCR and agarose gel electrophoresis was used to confirm knock-out of *PME41* in the mutant; *UBIQUITIN-CONJUGATING ENZYME 30* (*UBC30*) was used as a reference gene.

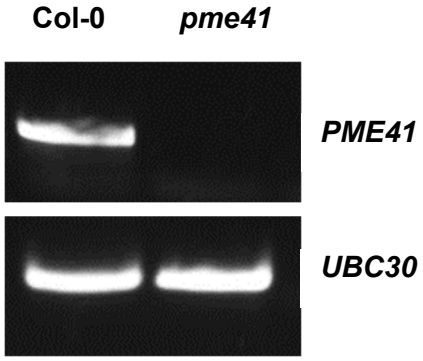

This is confirmation that expression of *PME41* has been knocked out in the *pme41* mutant.

APPENDIX F

Genotyping the *ext18* mutant. Genomic DNA was extracted from 7-day old wild-type (Col-0) and *ext18* (SALK_201747) seedlings. PCR and agarose gel electrophoresis were then used to confirm the presence of a T-DNA insertion in *EXT18* in the mutant.

L: HyperLadder 1kb. 1-3: Col-0 genomic primers temperature gradient. 4-6: *ext18* genomic primers temperature gradient. 7: Col-0 T-DNA primers (RP + LBb1.3). Lane 10: *ext18* T-DNA primers (RP + LBb1.3).

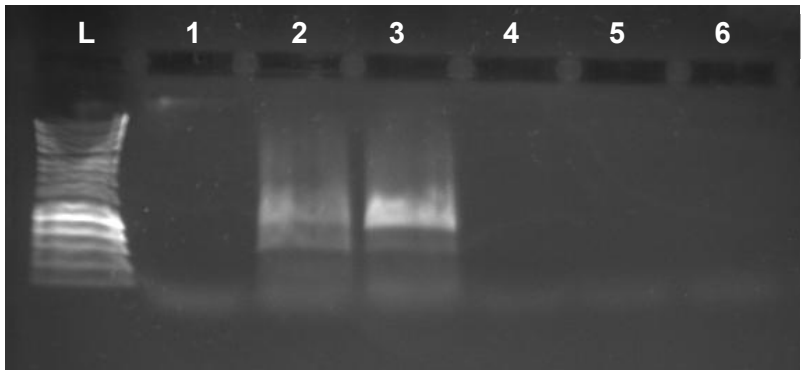

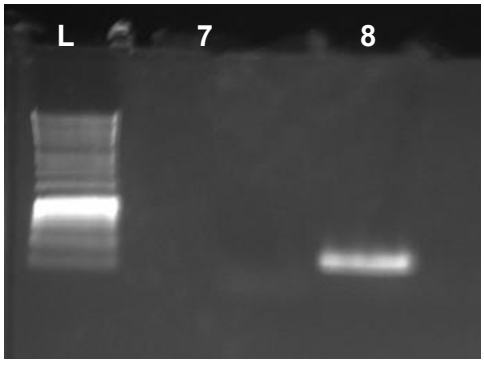

This is confirmation of the correct T-DNA insertion present in the *EXT18* coding region in the *ext18* mutant: the T-DNA band is present but the genomic band is not.

APPENDIX G

Genotyping the *sfr8* mutant. Genomic DNA was extracted from 7-day old wild-type (Col-0) and *sfr8* seedlings. PCR was used to amplify the *MUR1* gene in both samples before sequencing.

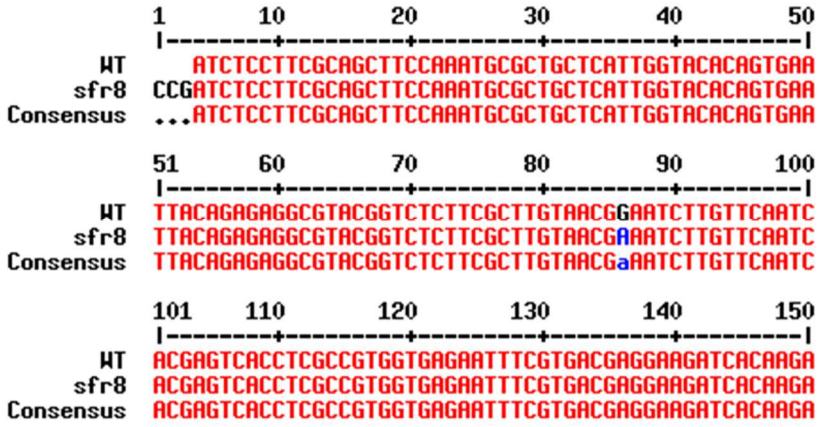

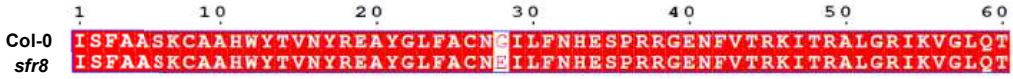

DNA sequence alignment shows the correct substitution in *sfr8*:
G629A (G86A in this cropped alignment).

Peptide sequence alignment shows the resultant amino acid substitution:
Glycine > Glutamic Acid.

APPENDIX H

Genotyping hp*GGLT1*. Total RNA was extracted from 10-day old empty-vector (EV) control and hp*GGLT1* seedlings. cDNA was synthesised from 1 µg RNA using MMLV reverse transcriptase. qPCR was used to measure the expression of *GGLT1* in both samples.

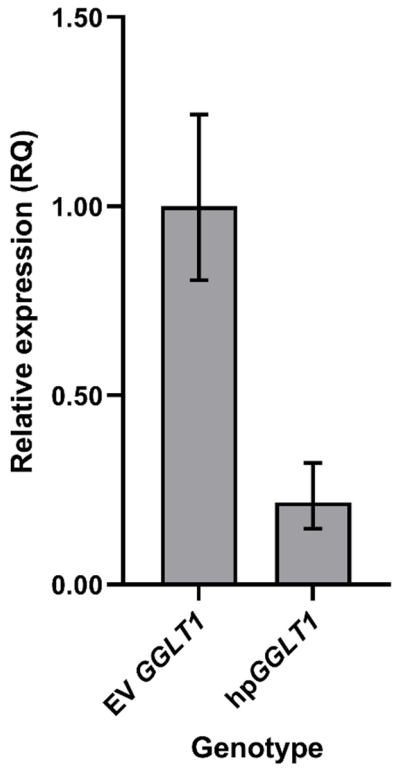

This is confirmation that expression of *GGLT1* has been reduced in hp*GGLT1*.

APPENDIX I

Genotyping the *cesa3*^{S211A} mutant. Genomic DNA was extracted from 7-day old wild-type (Col-0) and *cesa3*^{S211A} seedlings. PCR and agarose gel electrophoresis were then used to confirm the presence of the cDNA insert causing the S211A mutation in the mutant. The primers were designed to amplify the genomic *CESA3* gene in Col-0 (amplicon size 1679 bp) and the cDNA insertion in *cesa3*^{S211A} (amplicon size 1139 bp). The mutant amplicon is smaller as it lacks introns. The primers do not amplify the mutant's genomic copy of *CESA3* as they have been designed around the T-DNA insertion. A separate genotyping experiment confirmed the presence of the T-DNA insertion in the mutant (data not shown). A temperature gradient was used during PCR as the ideal annealing temperature was unknown.

Outer lanes: HyperLadder 1kb. Left-most lane in each pair: Col-0. Right-most lane in each pair: *cesa3*^{S211A}.

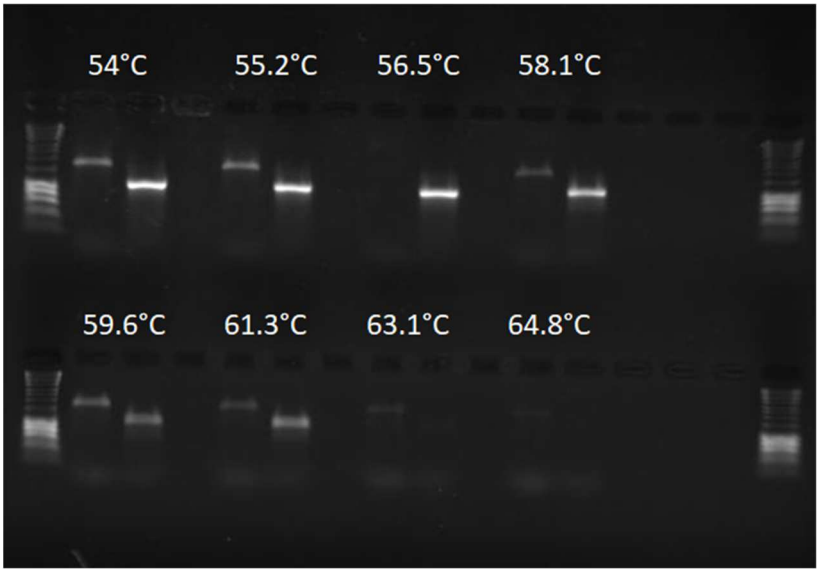

This is confirmation that the cDNA insertion is present in the mutant: both amplicons are the correct size.

APPENDIX J

Genotyping the *prc1* mutant. Genomic DNA was extracted from 7-day old wild-type (Col-0) and *prc1* seedlings. PCR was used to amplify the *CESA6* gene in both samples before sequencing.

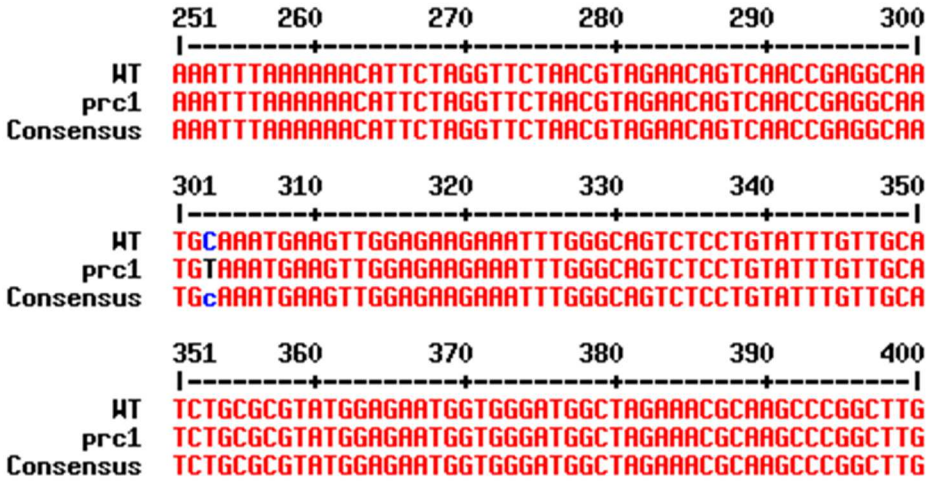

DNA sequence alignment shows the correct substitution in *prc1*:
C2158T (C303T in this cropped alignment).

According to TAIR, the resultant amino acid substitution is:
Glutamine > STOP.

APPENDIX K

Genotyping the *xxt1 xxt2* mutant. Genomic DNA was extracted from 10-day old wild-type (Col-0) and *xxt1 xxt2* (SAIL_785-E02/SALK_101308) seedlings. As *xxt1 xxt2* is a double knock-out, PCR and agarose gel electrophoresis were used to confirm the presence of T-DNA insertions in both *XXT1* and *XXT2* in the mutant. The below diagram from Cavalier *et al.* (2008) illustrates where the T-DNA insertions are in each gene with respect to the primer regions.

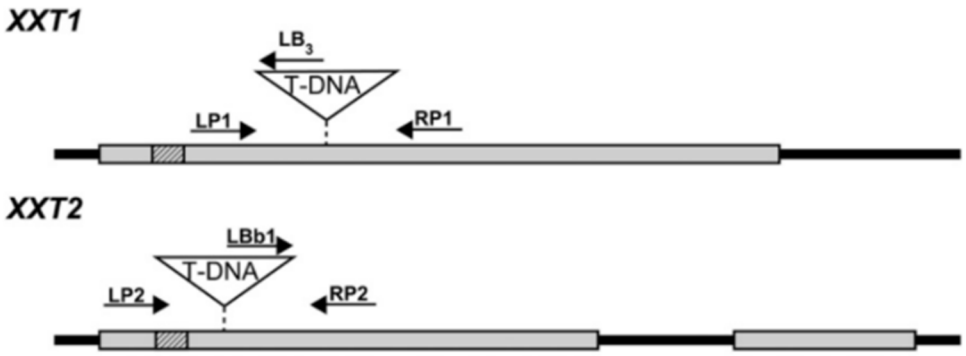

L: HyperLadder 1kb. 1: Col-0 *XXT1* genomic primers. 2: Col-0 *XXT2* genomic primers. 3: Col-0 *XXT1* T-DNA primers (LP + LB_3). 4: Col-0 *XXT2* T-DNA primers (RP + LBb1). 5: *xxt1 xxt2 XXT1* genomic primers. 6: *xxt1 xxt2 XXT2* genomic primers. 7: *xxt1 xxt2 XXT1* T-DNA primers (LP + LB_3). 8: *xxt1 xxt2 XXT2* T-DNA primers (RP + LBb1).

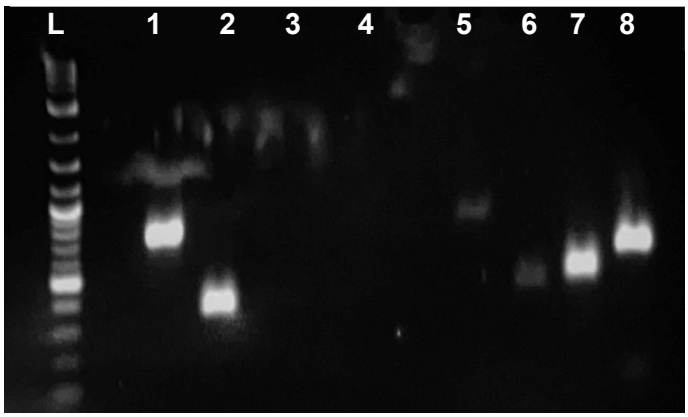

Despite the very faint genomic bands for *xxt1 xxt2*, this is confirmation of the correct T-DNA insertions in both *XXT1* and *XXT2* in the mutant.

APPENDIX L

Genotyping the *mur2* mutant. Genomic DNA was extracted from 7-day old wild-type (Col-0) and *mur2* seedlings. PCR was used to amplify the *FUT1* gene in both samples before sequencing.

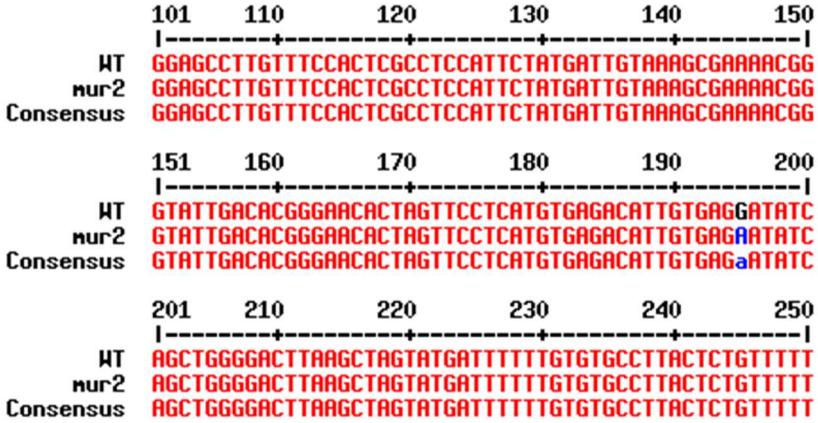

DNA sequence alignment shows the correct substitution in *mur2*:
G1712A (G195A in this cropped alignment).

According to Vanzin *et al.* (2002), the resultant amino acid substitution is:
Aspartic Acid > Asparagine.

APPENDIX M

Genotyping the *mur3* mutant. Genomic DNA was extracted from 7-day old wild-type (Col-0) and *mur3* seedlings. PCR was used to amplify the *MUR3* gene in both samples before sequencing.

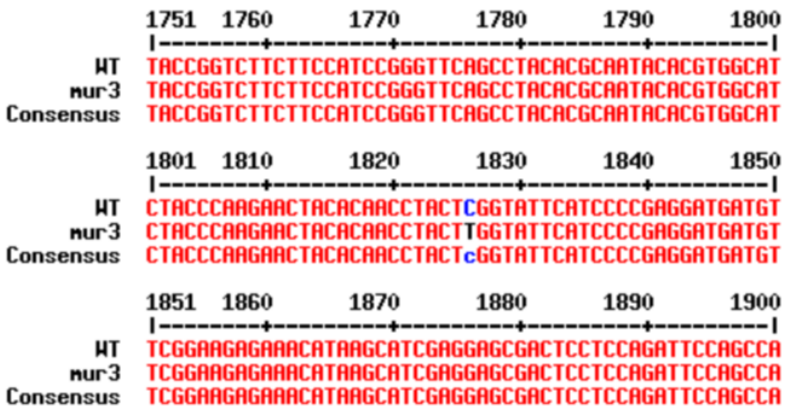

DNA sequence alignment shows the correct substitution in *mur3*:
C1411T (C1826T in this cropped alignment).

According to Madson *et al.* (2003), the resultant amino acid substitution is:
Serine > Leucine.

APPENDIX N

Genotyping the *msr1-2* mutant. Genomic DNA was extracted from 7-day old wild-type (Col-0) and *msr1-2* (SALK_075245C) seedlings. PCR and agarose gel electrophoresis were then used to confirm the presence of a T-DNA insertion in *MSR1* in the mutant.

L: HyperLadder 1kb. 1: Col-0 genomic primers. 2: Col-0 T-DNA primers (RP + LBa1). 3: *msr1-2* genomic primers. 4: *msr1-2* T-DNA primers (RP + LBa1).

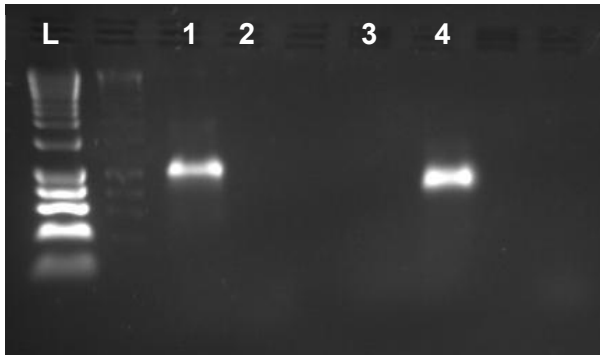

This is confirmation of the correct T-DNA insertion present in the *MSR1* coding region in the *msr1-2* mutant: the T-DNA band is present but the genomic band is not.

APPENDIX O

Genotyping the *pmr5* mutant. Genomic DNA was extracted from 7-day old wild-type (Col-0) and *pmr5* seedlings. PCR was used to amplify the *PMR5* gene in both samples before sequencing.

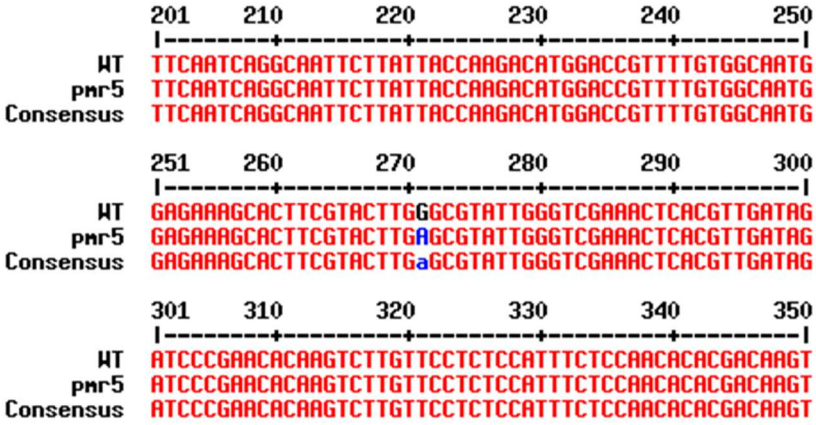

Chiniquy *et al.* (2019) state that restriction enzymes SmoI/SM1I are able to cut the mutant amplicon in a CAPS assay. RestrictionMapper.org showed that the *pmr5* sequence would be cut at position 271, where there is a G>A substitution.

This is confirmation that the mutant is *pmr5*.

APPENDIX P

Genotyping the *rwa2* mutant. Genomic DNA was extracted from 7-day old wild-type (Col-0) and *rwa2* (GK-571F07) seedlings. PCR and agarose gel electrophoresis were then used to confirm the presence of a T-DNA insertion in *RWA2* in the mutant. As the direction of the insertion was unknown, every primer combination was used.

L: HyperLadder 1kb. 1: Col-0 genomic primers. 2: Col-0 T-DNA primers (F + LB). 3: Col-0 T-DNA primers (R + LB). 4: *rwa2* genomic primers. 5: *rwa2* T-DNA primers (F + LB). 6: *rwa2* T-DNA primers (R + LB).

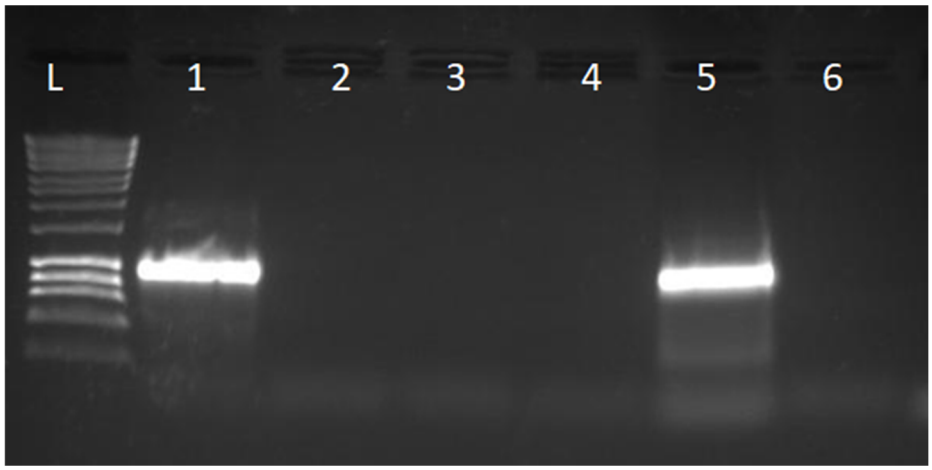

This is confirmation of the correct T-DNA insertion present in the *RWA2* coding region in the *rwa2* mutant: the T-DNA band is present but the genomic band is not.

APPENDIX Q

Freezing tolerance of a second mutant *EXT18* allele. Electrolyte leakage of mature leaf tissue from non-acclimated wild-type (Col-0), *sfr8,* and SALK_082257, which has a T-DNA insertion in *EXT18* (the original *ext18* mutant used in the main thesis is SALK_201747). Tissue was subjected to freezing at -3, -5 or -7°C and electrolyte leakage measured. Points represent mean percentage electrolyte leakage from three biological replicate experiments; each experiment used tissue from six plants per genotype per temperature (n=18 at each point). Error bars represent one standard error of the mean of arcsine-transformed data.

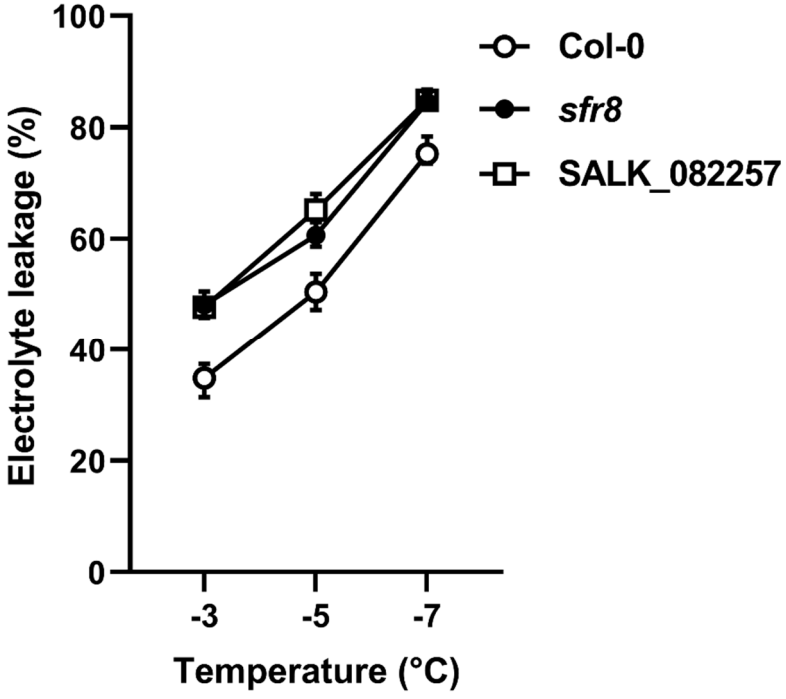

APPENDIX R

Potential mannan accumulation during cold acclimation. An early comprehensive microarray polymer profiling (CoMPP) experiment detected modest accumulation of mannan with the LM21 probe. In this pilot experiment, three experimental groups were used: 5-week non-acclimated (5 NA; grown under ambient conditions for 5 weeks before cell-wall extractions were prepared), 7-week non-acclimated (7 NA; grown under ambient conditions for 7 weeks before cell-wall extractions were prepared), and 7-week cold-acclimated (7 CA; grown under ambient conditions for 5 weeks, followed by 2 weeks of cold acclimation, before cell-wall extractions were prepared). The finalised CoMPP experiment reported in **Section 3.2.3** used an improved experimental design but did not detect significant changes in mannan abundance. Means which do not share a letter are significantly different.

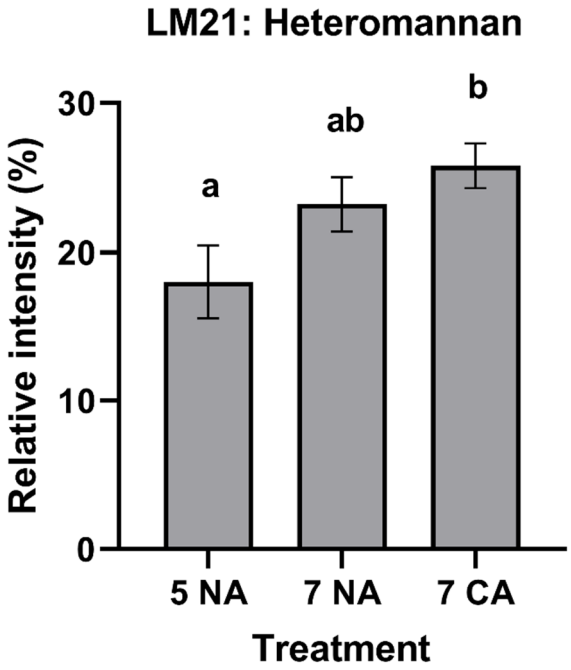

APPENDIX S

Software accessibility.

- This thesis was written in Microsoft Word, data management was largely carried out in Microsoft Excel, and some figures were created or modified in Microsoft PowerPoint. All three can be accessed here: https://www.microsoft.com/en-gb/microsoft-365/buy/compare-all-microsoft-365-products?tab=1&rtc=1
- Graphs were made in GraphPad Prism 9: https://www.graphpad.com/scientific-software/prism/
- Statistical analysis was carried out using Minitab Statistical Software: https://www.minitab.com/en-us/
- Confocal image capture was carried out using ZEISS ZEN Blue Edition version 2.6: https://www.zeiss.com/microscopy/en/products/software/zeiss-zen.html
- Micrograph analysis was carried out using Fiji, a version of ImageJ which includes plugins to facilitate scientific image analysis (Schindelin *et al.* 2012). It can be found here: https://imagej.net/software/fiji/
- Movement of the extensometer actuator was controlled using Zaber Console version 2.7.4.5975: https://www.zaber.com/software
- Force readings from the extensometer load cell were obtained using Lord MicroStrain SensorConnect version 15.0.8: https://www.microstrain.com/software/sensorconnect
- Infrared video thermography was carried out using FLIR Research Studio: https://www.flir.co.uk/products/flir-research-studio/
- CoMPP microarrays were analysed using Media Cybernetics Array-Pro Analyzer version 6.3.1: https://www.mediacy.com/
- Primers were designed using Primer3Plus (Untergasser *et al.* 2007): https://www.primer3plus.com/

- T-DNA primers were designed using the SIGnAL Salk Institute Genomic Analysis Laboratory T-DNA Primer Design Tool: http://signal.salk.edu/tdnaprimers.2.html
- Primers were synthesised using Integrated DNA Technologies: https://eu.idtdna.com/pages
- DNA sequence alignment was carried out using MultAlin (Corpet 1988): http://multalin.toulouse.inra.fr/multalin/
- Cold-responsive genes were identified using the AtRTD2 dashboard (Calixto *et al.* 2018): https://wyguo.shinyapps.io/atrtd2_profile_app/